STUDIA

UNIVERSITATIS BABEŞ-BOLYAI

Chemia

CLUJ-NAPOCA 1998

1-2

Anul XLIII **1998**

STUDIA
UNIVERSITATIS BABEŞ-BOLYAI
CHEMIA

1-2

EDITORIAL OFFICE: Gh. Bilaşcu no. 24, 3400 Cluj-Napoca ✦ Phone 064-40.53.52

SUMAR - SOMMAIRE - CONTENTS - INHALT

STUDIA UNIVERSITATIS BABEŞ-BOLYAI, CHEMIA, XLIII, 1-2, 1998

IN MEMORIAM

EMIL CHIFU (1925-1997)

The eminent Romanian scientist Professor Emil Chifu died on April 1, 1997, at age 72. He was a great physicochemist and a world-renowned scientist in the field of the modern science of colloid, surfaces and membrane phenomena.

Born on 17 July 1925 in Herţa, Dorohoi, belonging then to Romania, Emil Chifu is originate from a modest family of craftsworker.

In 1949, after graduating with merit diploma from Faculty of Chemistry, specialty physical chemistry, at the University of Cluj, he began his scientific and academic career in the Department of Physical Chemistry at this University, occupying all the didactic degrees: assistant professor, reader, lecturer and since 1970 professor. Concurrently, from 1951 to 1953, Emil Chifu worked in the Institute of Chemistry, a branch of the Romanian Academy of Sciences in Cluj. He received his PH.D. from the University of Cluj.

He gained scholarships in Russia at the University "M. V. Lomonosov", Moscow (1966), in Italy at the University of Florence (1967), in Germany at the University of Tübingen (1976).

Dean of the Faculty of Chemistry at the V. Babeş University, Cluj (1958-1959), substitute dean of the Faculty of Chemistry at the Babeş-Bolyai University, Cluj (1959-1962), head of the Chair of Physical Chemistry (1970-1977), head of the Chair of Physical, Organic and Technological Chemistry (1985-1990).

Since1973 he was a doctorate supervisor in the following specialties physical chemistry, biophysics and biochemical physics.

Professor Chifu was awarded the first Prize for his outstanding scientific achievements in the field of chemistry (1967) and appointed to the Distinguished Professor (1980), by the Romanian Ministry of Education. In 1983, he was awarded the Gheorghe Spacu Prize by the Academy of Science in Romania for his theory and novel experiments on colloidal systems and thin films. He was specially invited to the Workshop "In memoriam R. Defay", at the Université Libre de Bruxelles, Belgium (1990) and at the Université de Provence, Institut Universitaire Systémes Thermiques Industriels, UA CNRS, France (1991).

He was a member of the New York Academy of Sciences, the Planetary Society of Pasadena, USA, the Italian Society of Chemistry, Rome, Italy, and the Romanian Society of Colloids and Surface Science and the Thermodynamic Division of the Romanian Academy of Sciences.

Professor Chifu made essential contributions to the teaching of colloid science by lecturing over 30 years on this subject and with his book "Colloidal Chemistry", published in 1969. Recently, he finished a fully revised and updated edition of this book (in press) including his standard work on modern surface science and new approaches to the thermodynamics and hydrodynamics of thin films. This new edition features several new chapters on extended treatment of films at liquid-air and liquid-liquid interfaces, molecular interactions in mixtures of surfactants, micellization processes, macromolecular films and optical properties of Langmuir-Blodgett films, which reflect his pioneering work in the field. Unfortunately, he did not live to see the publication of this updated and extended Colloidal Chemistry edition.

Emil Chifu became world-wide known for his work on the physical and chemical properties of liquids and thin films, which examined hydrodynamics and surface mobility of surfactant solutions. This work, particularly the original research towards the stability of thin films, their properties in microgravity conditions, the behaviour of liquids under the action of surface tension gradients caused by various surfactants or by temperature differences in both normal and microgravity conditions, surface flow of liquids in the absence of gravity, gained international recognition and was selected and approved in 1978 by National Aeronautics and Space Administration (NASA) of the USA for the international cooperation between NASA and the University of Cluj-Napoca. This work has important applications in the space technology of liquids, and in the modeling of deformations at biological surfaces.

In pioneering work, he initiated studies of the biophysical properties of biologically active compounds, such as lecithins, fatty acids, carotenoids, vitamins, and drugs, developing new experimental methods and ingenious techniques based on original ideas. From 1981, part of this work has been accomplished in collaboration with King's College, University of London, UK, and has important applications to food and pharmaceutical industries, and to biomedical research. From 1989, important contributions on biophysical properties of drugs, nucleation and relaxation phenomena, collapse mechanism and stability of thin films were developed in cooperation with the State University of New York at Buffalo, USA, and have significant applications in biosensors and biomedical technology. His studies on mineral processing, flotation, mass transfer through interfaces are widely appreciated.

In recent years, he devoted his time to study the adsorption of biosurfactants at fluid interfaces and the molecular interactions among drugs and natural membrane constituents, with the major goal to evaluate their structure and function relationships. In all these areas he developed theories and experimental methods and techniques based on his original ideas.

The research efforts of Professor Chifu have been characterized by originality of his theoretical developments, based on physical, chemical and mathematical concepts, and the great consistency in solving scientific problems, and ingenuity in setting experiments to analyze complex phenomena.

The activities of Professor Chifu in the organization of scientific meetings have been extensive. Since 1980, he organized and supervised conferences on colloidal chemistry, surface and membrane science and interfacial phenomena. These conferences were attended by leading scientists in the field and enjoyed international recognition.

Professor Chifu performed great service to the creation and development of the international cooperation on colloid, surface and membrane science and contributed very much to useful and friendly relations between scientist.

The authors thank Alexandra Chifu and Aurora Mocanu for valuable discussion and information during the preparation of this obituary.

LIST OF PUBLICATIONS

BOOKS

1. E. Chifu, T. Goina, G. Niac, L. Oniciu and E. Schönberger, "Manual de lucrări practice de Chimie fizică şi coloidală", Litografia Învăţământului, Ministerul Învăţământului şi Culturii, Universitatea "V.Babeş", Cluj-Napoca, 1957.
2. E. Chifu, "Curs de chimie coloidală", Litografia Învăţământului, Ministerul Învăţământului şi Culturii, Universitatea "V.Babeş", Cluj-Napoca, 1958.
3. L. Oniciu and E. Chifu, "Chimie Fizică", Ed. Didactică şi Pedagogică", Bucharest, 1967.
4. E. Chifu, "Chimie coloidală", Ed. Didactică şi Pedagogică, Bucharest, 1969.
5. E. Chifu (în Colectivul de redacţie), "Enciclopedia de Chimie", **vol. 1,** Ed. Ştiinţifică şi Enciclopedică, Bucharest, 1983.
6. E. Chifu (în Colectivul de redacţie), "Enciclopedia de Chimie", **vol. 2,** Ed. Ştiinţifică şi Enciclopedică, Bucharest, 1986.
7. E. Chifu (în Colectivul de redacţie), "Enciclopedia de Chimie", **vol. 3,** Ed. Ştiinţifică şi Enciclopedică, Bucharest, 1986.
8. E. Chifu (în Colectivul de redacţie), "Enciclopedia de Chimie", **vol. 5,** Ed. Ştiinţifică şi Enciclopedică, Bucharest, 1988.
9. E. Chifu (în Colectivul de redacţie), "Enciclopedia de Chimie", **vol. 6,** Ed. Ştiinţifică şi Enciclopedică, Bucharest, 1989.
10. E. Chifu, "Chimie Coloidală", 1999, în curs de apariţie.

PAPERS

1. E. Chifu and G. Niac, "Despre o metodă de microdozare a acidului clorhidric gazos", *Rev. Chim. (Bucureşti),* **6** (11), 609 (1955).
2. E. Chifu and L. Stănescu, "Aspecte din teoria supratensiunii hidrogenului", *Bul. Univ. Cluj*, **2** (1-2), 185-202 (1957).
3. E. Chifu and I. Cădariu, "Despre mobilitatea superficială a soluţiilor de substanţe tensioactive. I. Scurgerea superficială împotriva presiunii hidrostatice", *Stud. Univ. Babeş-Bolyai, Chem.*, **6** (2), 19-24 (1961).

4. E. Chifu and G. Hager, "Despre unele aspecte ale precipitării periodice în geluri", *St. Cerc. Chim. Cluj*, **13** (1), 41-48 (1962).
5. E. Chifu, "Despre mobilitatea superficială a soluţiilor de substanţe tensioactive. II. Echilibrul presiune superficială – presiune hidrostatică", *Stud. Univ. Babeş-Bolyai, Chem.*, **8** (1), 49-56 (1963).
6. E. Chifu and L. Oniciu, "Despre mobilitatea superficială a soluţiilor de substanţe tensioactive. III. Determinare cu radioizotopi a echilibrului presiune superficială–presiune hidrostatică", *Stud. Univ. Babeş-Bolyai, Chem.*, **9** (1), 95-99 (1964).
7. R. Deutsch and E. Chifu, "Despre mobilitatea superficiala a soluţiilor de substanţe tensioactive. IV. Hidrodinamica scurgerii împotriva presiunii hidrostatice", *Stud. Univ. Babeş-Bolyai, Chem.*, **9** (1), 101-110 (1964).
8. E. Chifu, "Studiu asupra mobilităţii superficiale a soluţiilor", Lucrare de disertaţie, *Univ. Babeş-Bolyai, Cluj-Napoca, Facultatea de Chimie*, 1964, 139 pp.
9. E. Chifu, "Despre mobilitatea superficială a soluţiilor de substanţe tensioactive. V. Debit superficial şi de volum", *Stud. Univ. Babeş-Bolyai, Chem.*, **10** (2), 85-89 (1965).
10. R. Deutsch, P. Sandru and E. Chifu, "Despre mobilitatea superficială a soluţiilor de substanţe tensioactive. VI. Scurgerea superficială prin canale orizontale cu secţiune triungiulară şi dreptunghiulară", *Stud. Univ. Babeş-Bolyai, Chem.*, **10** (2), 91-98 (1965).
11. R. Deutsch, H. Szöcs and E. Chifu, "Despre mobilitatea superficială a soluţiilor de substanţe tensioactive. VII. Scurgerea superficială prin canale înclinate cu secţiune triunghiulară şi dreptunghiulară cînd stratul superficial devine imobil", *Stud. Univ. Babeş-Bolyai, Chem.*, **10** (2), 99-105 (1965);
12. E. Chifu and R. Deutsch, "L'hydrodynamique de l'écoulement superficiel des solutions contre la pression hydrostatique", *Rev. Roumaine Chim.*, **11** (7), 873-889 (1966).
13. E. Chifu and I. Albu, "Despre mobilitatea superficială a soluţiilor de substanţe tensioactive. VIII. Măsurători de debit", *Stud. Univ. Babeş-Bolyai, Chem.*, **13** (1), 99-109 (1968).
14. E. Chifu and G. Gabrielli, "Formazione e stabilità dell'associato tributilfosfato-nitrato di litio", *Gazz. Chim. Ital.*, **98** (10), 1213-1223 (1968)
15. E. Chifu, Cronică la "Al X-lea Congres al Societăţii Italiene de Chimie", Padova, 17-21 iunie, 1968, *Stud. Univ. Babeş-Bolyai, Chem.,* **14** (1), 151-152 (1969).
16. E. Chifu, I. Albu and M. L. Huszár, "Tensiunea superficială a soluţiilor de acid mandelic-aluminiu(III)", *Stud. Univ. Babeş-Bolyai, Chem.*, **16** (2), 15-18 (1971).
17. E. Chifu, "Sur un problème d'activité superficielle et équilibre chimique", *Stud. Univ. Babeş-Bolyai, Chem.*, **17** (2), 143-145 (1972).

18. E. Chifu and I. Albu, "La tension superficielle des solutions d'acide lactique-azotate d'aluminium", *Stud. Univ. Babeş-Bolyai, Chem.*, **18** (1), 81-87 (1973).
19. M. Tomoaia, Z. Andrei and E. Chifu, "Tension interfaciale dans le système solution benzénique de tributylphosphate/solution aqueuse de nitrate cuivrique", *Rev. Roumaine Chim.*, **18** (9), 1547-1554 (1973).
20. E. Chifu and I. Albu, "Variation de la tension interfaciale pendant l'extraction liquide-liquide. I. Extraction de quelques acides aliphatiques mono-carboxiliques dans le système acétate de butyl/eau", *Stud. Univ. Babeş-Bolyai, Chem.*, **19** (2), 83-88.
21. E. Chifu, Z. Andrei and M. Tomoaia, "Interfacial tension in the benzene-tributylphosphate / aqueous nitric acid system", *Ann. Chim. (Rome)*, **64** (11-12), 869-871 (1974).
22. M. Cîndea and E. Chifu, "Tensiunea superficială şi capacitatea de spumare în testarea biodegradabilităţii detergenţilor anion-activi" *Rev. Chim. (Bucureşti)*, **26** (11), 905-907 (1975).
23. L. Szabó, I. Mathé, E. Chifu, N.Almási, Z. Finta, F. Kacsó, E. Cîmpeanu, I. Bâldea and I. Albu, "Obţinerea pulberilor de nichel din carbonil de nichel", în *Conferinţa Naţională de Metalurgia Pulberilor, Com. Şt.*, **1**, pp. 67-72 (1975).
24. N. Almási, I. Mathé, F. Kacsó, E. Cîmpianu, E. Chifu, Z. Finta, I. Bâldea, A. Otea, M. Tomoaia and L. Szábo, "Despre metalizarea unor materiale nemetalice prin descompunerea termică a carbonililor metalici", în *Conferinţa Naţională de Metalurgia Pulberilor*, **1**, (1975), pp. 97-102.
25. E. Chifu and I. Albu, "Interfacial tension variation in the course of liquid-liquid extraction. II. Molecular associations on extracting some monocarboxylic aliphatic acids", *Ann. Chim. (Rome)*, **65** (9-10), 519-531 (1975).
26. E. Chifu, M. Tomoaia, and A. Ioanette, "Behaviour of cantaxanthin at the benzene/water and air/water interfaces", *Gazz. Chim. Ital.*, **105** (11-12), 1225-1232 (1975).
27. M. Tomoaia, A. Ioanette and E. Chifu, "Behaviour of β-apo-8'-carotenal at the oil/water interfaces and air/water interfaces", *Proceedings of the International Conference on Colloid and Surface Science*, **1**, Akadémiai Kiadó, Budapest, 15-20 September 1975, pp. 559-566.
28. Z. Andrei and E. Chifu, "Interfacial tension in the benzene-tributylphosphate /aqueous alkaline-earth nitrate systems", *Stud. Univ. Babeş-Bolyai, Chem.*, **21**, 10-12 (1976).
29. M. Mioşcu, I. Albu, E. Chifu and M. Mureşan, "Behaviour of cyclohexanol-water interface in acid-base titrations", *Chem. Analit. (Warszawa)*, **21**(2), 255-261 (1976).

30. E. Chifu, "Surface flow of liquids in the absence of gravity", Proposal selected by NASA's Office of Aeronautics and Space Technology, 1977.
31. E. Chifu and Z. Andrei, "Interfacial tension and interfacial polycondensation of polyethyilene terephtalate", *Gazz. Chim. Ital.*, **107** (11-12), 569-571 (1977).
32. E. Chifu and Z. Finta, "Capacitatea de spumare a unor spumanţi folosiţi în flotaţia minereurilor neferoase", *Stud. Univ. Babeş-Bolyai, Chem.*, **23** (2), 38-42 (1978).
33. E. Chifu, M. Tomoaia, E. Nicoară, and A. Olteanu, "Isozeaxanthin films at the oil/water and air/water interfaces", *Rev. Roumaine Chim.*, **23** (8), 1163-1169 (1978).
34. E. Chifu, and M. Tomoaia-Cotişel, "Insoluble monolayers of lecithin and carotenoid pigments", *Rev. Roumaine Chim.*, **24** (7), 979-986 (1979).
35. E. Chifu, M. Tomoaia-Cotişel and Z. Andrei, "Mixed monolayers of cantaxanthin with lipids", *Stud. Univ. Babeş-Bolyai, Chem.*, **24** (2), 63-67 (1979).
36. M. Tomoaia-Cotişel, I. Albu and E. Chifu, "Adsorbtion of carotene and albumin at the oil/water interface", *Stud.Univ.Babeş-Bolyai*, Chem., **24** (2), 68-73 (1979).
37. E. Chifu and I. Albu, "Variaţia tensiunii interfaciale şi a potenţialului chimic în timpul extracţiei lichid-lichid", *Rev. Chim.,* (Bucureşti), **30** (10), 1004-1008 (1979).
38. Stan and E. Chifu, "Hidrodinamica picăturii libere acţionată de gradienţi de tensiune interfacială", în *Colocviul de Mecanica Fluidelor şi Aplicaţiile ei Tehnice*, Galaţi, 12-13 oct. 1979, pp.88-91.
39. E. Chifu, M. Tomoaia-Cotişel, Z. Andrei and E. Bonciu, "β-apo-8'-carotenoic acid ethyl ester films at fluid interfaces", *Gazz. Chim. Ital.*, **109** (6-7), 365-369 (1979).
40. M. Tomoaia-Cotişel and E. Chifu, "Mixed insoluble monolayers with el and E. Chifu, "Mixed insoluble mono*Gazz." Chim. Ital.*, **109** (6-7), 371-375 (1979).
41. E. Chifu, M. Tomoaia-Cotişel and A. Ioanette, "Mixed insoluble monolayers of cholesterol and ćel and A. Ioanette", *Gazz. Chim. Ital.*, **109** (6-7), 397-398 (1979).
42. J. Zsakó, E. Chifu and M. Tomoaia-Cotişel, "Rotating rigid-plate model of carotenoid molecules and the behaviour of their monolayers at the air/water interfaces", *Gazz. Chim. Ital.*, **109** (11-12) 663-668 (1979).
43. M. Tomoaia-Cotişel, E. Chifu, V. Tămaş and V. Mărculeţiu, "Behaviour of some apocarotenoid derivatives at the air/water interface", *Rev. Roumaine Chim.*, **25** (2), 175-180 (1980).
44. I.Albu and E. Chifu, "Interfacial tension variation in the course of liquid-liquid extraction. III. The extraction of butyric acid by different solvents", *Rev. Roumaine Chim.*, **25** (4), 459-466 (1980).
45. E. Chifu and I. Stan, "The flow of fluids in weightlessness under the action of interfacial tension gradients", in "Einstein's Centenary in Romania, General Relativity and Gravitation" *Proceedings of the First Experimental Gravitation*

Symposium and the National Colloquium on the Theory of Relativity, I.C.P.E. Bucharest, 1980, pp. 413-418.

46. E. Chifu, I. Stan, Z. Finta and E. Gavrilă, "Efectul Marangoni şi translaţia picăturii libere nedeformabile", *Rev. Chim. (Bucureşti),* **31** (8), 765-771 (1980).
47. E. Chifu and I. Stan, "Model for the undeformable free drop acted by interfacial tension gradients", *Rev. Roumaine Chim.*, **25** (11-12), 1449-1459 (1980).
48. E. Chifu and M. Tomoaia-Cotişel, "Carotene and protide films at the oil/water interface", *Stud. Univ. Babeş-Bolyai, Chem.*, **26** (2), 3-8 (1981).
49. I.Stan, E. Chifu and Z. Finta, "Efectul Marangoni şi difuziunea convectivă pe o interfaţa sferică", *Rev. Chim. (Bucureşti)*, **32** (9), 916-917 (1981).
50. M. Tomoaia-Cotişel and E. Chifu, "Filme de pigmenţi carotenoidici la interfeţe fluide", *Rev. Chim. (Bucureşti)*, **32** (11), 1063-1069 (1981).
51. E. Chifu, Z. Finta, M. Sălăjan and E. Gavrilă, "Surface mobility of surfactant solutions. IX. Surface and capillary flow between drops linked by surface canals", *Rev. Roumaine Chim.*, **26** (11-12), 1345-1354 (1981).
52. M. Tomoaia-Cotişel, J. Zsakó and E. Chifu, "Dipalmitoyl lecithin and egg lecithin monolayers at an air/water interface", *Ann. Chim. (Rome)*, **71** (3-4), 189-200 (1981).
53. E. Chifu and M. Tomoaia-Cotişel, "Mixed films of retinyl palmitate with lipids at the air/water interface", *Rev. Roumaine Chim.*, **27** (1), 27-35 (1982).
54. Z. Finta, E. Chifu, E. Gavrilă and M. Sălăjan, "Surface oxidation of some sulphurous minerals by the hypochlorite ion", *Rev. Roumaine Chim.*, **27** (2), 191-198 (1982).
55. E. Chifu and M. Tomoaia-Cotişel, "Filme mixte de pigmenţi carotenoidici şi lipide la interfaţa aer/apă", *Rev. Chim. (Bucureşti)*, **33** (2), 125-131 (1982).
56. E. Chifu and I. Stan, "Surface mobility of surfactant solutions. X. Marangoni flow against gravity forces", *Rev. Roumaine Chim.*, **27** (6), 703-711 (1982).
57. M. Tomoaia-Cotişel, E. Chifu, A. Sen and P. J. Quinn, "Galactolipid and lecithin monolayers at the air/water interface", in *Biochemistry and Metabolism of Plant Lipids*, (J.F.G.M.Wintermans and P.J.C.Kuiper, Eds.), Elsevier Biomedical, Amsterdam, 1982, pp. 393-396 .
58. I.Albu and E. Chifu, "Interfacial tension variations in the course of liquid-liquid extraction. IV. The extraction of some aliphatic acids", *Stud. Univ. Babeş-Bolyai, Chem.*, **28**, 46-51 (1983).
59. M. Tomoaia-Cotişel, E. Chifu and I. Albu, "Critical micelle concentration of egg lecithin in the presence of some carotenoids", *Stud. Univ. Babeş-Bolyai, Chem.*, **28**, 42-45 (1983).

60. M. Tomoaia-Cotişel and E. Chifu, "Albumin and carotenoid films at the benzene/water interface", in *IUPAC Macro'93, Section IV Structure and Properties*, Bucharest-Romania, September 5-9, 1983, pp. 636-639.

61. M. Tomoaia-Cotişel, J. Zsakó, E. Chifu and P.J.Quinn, "Filme mono-moleculare de galactolipide - modele de membrană - şi histereza în ciclurile compresiune-expansiune", în *Al XVI-lea Simpozion Naţional de Biofizică*, Iaşi 20-21 octombrie 1983, pp. 45-49.

62. E. Chifu, I. Stan, Z. Finta and E. Gavrilă, "Marangoni type surface flow on an undeformable free drop", *J. Colloid Interface Sci.*, **93** (1), 140-150 (1983).

63. E. Chifu, J. Zsakó, and M. Tomoaia-Cotişel, "Xantophyll films. I. Single-component monolayers at the air/water interface", *J. Colloid Interface Sci.*, **95** (2), 346-354 (1983).

64. M. Tomoaia-Cotişel and E. Chifu, "Xantophyll films. II. Two-component monolayers of some xantophylls and egg lecithin at the air/water interface", *J. Colloid Interface Sci.*, **95** (2), 355-361 (1983).

65. M. Tomoaia-Cotişel, J. Zsakó, E. Chifu and P. J. Quinn, "Influence of electrolytes on the monolayers properties of saturated galactolipids at the air/water interface", *Chem. Phys. Lipids*, **34** (1), 55-64 (1983).

66. E. Chifu, C. Gheorghiu and I. Stan, "Surface mobility of surfactant solutions. XI. Numerical analysis for the Marangoni and gravity flow in a thin liquid layer of triangular section", *Rev. Roumaine Chim.*, **29** (1), 31-42 (1984).

67. M. Tomoaia-Cotişel, M. Sălăjan, I. Albu, E. Chifu and J. Zsakó, "Monomolecular films of carotenoids-membrane models- and mechanism of collaps", in *Proceedings of the 2nd National Symposium on Methods, Models and Techniques in Physics and Related Fields*, (V. Mercea, V. Znamirovschi, M. Vasiu, O. Cozar, Eds.), Cluj-Napoca, 1984, pp. 175-179.

68. M. Tomoaia-Cotişel, J. Zsakó, E. Chifu and P. J. Quinn, "Structure of galactolipid monolayers", in *Proceedings of the 2nd National Symposium on Methods, Models and Techniques in Physics and Related Fields*, (V. Mercea, V. Znamirovschi, M. Vasiu, O. Cozar, Eds.), Cluj-Napoca, 1984, pp.190-194.

69. E. Chifu and C. I. Gheorgiu, "Mişcarea fluidelor sub acţiunea gradienţilor de tensiune superficiala. Metode de analiză numerică", în *Lucrările Colocviului de Mecanica Fluidelor şi Aplicaţiile ei Tehnice*, Iaşi, 12-13 octombrie 1984, pp.312-315.

70. E. Chifu and M. Tomoaia-Cotişel, "Carotenoid films at the air/water interface", in *Surfactants in Solution, Proceedings of International Symposium on Surfactants in Solution*, (K. L. Mittal, C. Lindman, Eds.), **vol.2**, Plenum Press, New-York, 1984, pp. 1349-1364.

71. J. Zsakó, M. Tomoaia-Cotişel and E. Chifu, "Insoluble mixed monolayers. I. phase equilibria at the collaps of binary monolayers at gas/liquid interfaces", *J. Colloid Interface Sci.*, **102** (1), 186-205 (1984).

72. M. Tomoaia-Cotişel, J. Zsakó, E. Chifu and P. J. Quinn, "Mixed monolayers of 1,2-distearoyl digalactosyl glycerol and astaxanthin", in *Structure, Function and Metabolism of Plant Lipids*, (P. A. Siegenthaler, W. Eichenberger, Eds.), Elsevier Science Publishets, BV, 1984, pp. 421-424.

73. M. Tomoaia-Cotişel, J. Zsakó, M. Sălăjan and E. Chifu, "Interaction of unimolecular films of some carotenoids with electrolytes at the air/water interface", in *Water and Ions in Biological Systems, Proceedings of the Third International Conference*, (A. Pullman, V. Vasilescu, L. Packer, Eds.), Union of Societies for Medical Sciences, Bucharest, 1985, pp. 371-381.

74. E. Chifu, J. Zsakó, M. Tomoaia-Cotişel, A. Mocanu, M. Sălăjan, J. Demeter-Vodnár and I. Albu, "Filme interfaciale de interes biologic", în *A III-a Conferinţă Naţională de Biofizică*, Iaşi, 27-29 august 1985, USSM, pp. 16-23.

75. J. Zsakó, M. Tomoaia-Cotişel, I. Stan, V. Coman, V. Tămaş and E. Chifu, "Colapsul unor monostraturi de carotenoide la interfaţa aer/apă", în *A III-a Conferinţă Naţională de Biofizică*, Iaşi, 27-29 august 1985, USSM, pp. 63-68.

76. M. Tomoaia-Cotişel, E. Chifu and J. Zsakó, "The structure of some lecithin monolayers at the air/water interface", in *Water and Ions in Biological Systems, Proceedings of the Second International Conference*, (A. Pullman, V. Vasilescu, L. Packer, Eds.), Plenum Press, New-York, London, 1985, pp. 243-250.

77. M. Tomoaia-Cotişel, E. Chifu and J. Zsakó, "Mixed monolayers of egg lecithin and carotenoids", *Colloids & Surface*, **14**, 239-246 (1985).

78. E. Chifu, I. Albu, C. I. Gheorghiu, E. Gavrilă, M. Sălăjan and M. Tomoaia-Cotişel, "Marangoni flow-induced by temperature gradients-against gravity forces", *Rev.Roumaine Chim.*, **31** (1), 105-112 (1986).

79. E. Chifu, M. Tomoaia-Cotişel, A. Mocanu, L. Andrei and J. Zsakó, "Protolytic equilibria in monolayers of biological significance", *Stud. Univ. Babeş-Bolyai, Chem.*, **31** (1), 74-79 (1986).

80. G. Oprea and E. Chifu, "Infrared spectroscopic investigation of the adsorption products of 8-hydroxyquinoline onto malachite", *Stud. Univ. Babeş-Bolyai, Chem.*, **31** (2), 65-68 (1986).

81. S. Jitian, E. Chifu, "The ellipsometric study of polymer films on metals", *Stud. Univ. Babeş-Bolyai, Chem.*, **31** (2), 69-75 (1986).

82. E. Chifu, J. Zsakó and M. Tomoaia-Cotişel, "Insoluble mixed monolayers. IV. Ejection curves of β-cryptoxanthin palmitate–egg lecithin films at the air/water interface", *Stud. Univ. Babeş-Bolyai, Chem.*, **31** (2), 90-96 (1986).

83. M. Tomoaia-Cotişel, E. Chifu and J. Zsakó, "Xantophill films. III. Two-component monolayers of some xantophills and L-α-dipalmitoyl lecithin at the air/water interface", *Stud. Univ. Babeş-Bolyai, Chem.*, **31** (2), 80-89 (1986).

84. J. Zsakó, M. Tomoaia-Cotişel, A. Mocanu and E. Chifu, "Insoluble mixed monolayers. II. Protolytic equilibria and the influence of the pH on the collapse pressure", *J. Colloid Interface Sci.*, **110** (2), 317-334 (1986).

85. E. Chifu, J. Zsakó, M. Tomoaia-Cotişel, M. Sălăjan and I. Albu, "Xantophyll films. IV. Interaction of zeaxanthin and astaxanthin with electrolytes at the air/water interface", *J. Colloid Interface Sci.*, **112** (1), 241-251 (1986).

86. E. Chifu, A. Chifu, M. Tomoaia-Cotişel and J. Zsakó, "Specific interactions in monomolecular membranes of biological interest", *Rev. Roumaine Chim.*, **32** (7), 627-636 (1987).

87. M. Tomoaia-Cotişel, J. Zsakó and E. Chifu, "Ejection curves and miscibility of egg lecithin with some carotenoid derivatives", *Rev. Roumaine Chim.*, **32** (7), 663-670 (1987).

88. E. Chifu, M. Sălăjan, I. Demeter-Vodnár and M. Tomoaia-Cotişel, "Fatty acid films at the benzene/water interface", *Rev. Roumaine Chim.*, **32** (7), 683-691 (1987).

89. E. Chifu and M. Tomoaia-Cotişel, "Thin liquid layers", in *Seminars in Biophysics*, **Vol.4** (P. T. Frangopol, V. V. Morariu, Eds.), CIP Press, Bucharest, 1987, pp. 163-184.

90. J. Zsakó, V. Neagu, M. Tomoaia-Cotişel and E. Chifu, "Molecular structure and monolayer properties", *Rev. Roumaine Chim.*, **32** (8), 739-748 (1987).

91. E. Chifu and C. I. Gheorghiu, "Surface mobility of surfactant solutions. XII. Remarks concerning the Marangoni flow through an inclined surface canal", *Rev. Roumaine Chim.*, **32** (9-10), 945-951 (1987).

92. E. Chifu, M. Tomoaia-Cotişel, "Report of Meeting: The II-nd Symposium on Colloid and Surface Chemistry", *Stud. Univ. Babeş-Bolyai, Chem.,* **32** (1), 3-4, 1987.

93. E. Chifu, "Some topics of present interest in the chemistry of liquid interfaces", *Stud. Univ. Babeş-Bolyai, Chem.*, **32** (1), 5-16 (1987).

94. M. Tomoaia-Cotişel, J. Zsakó, E. Chifu and P. J. Quinn, "Monomolecular films and collaps structures as biomembrane models", *Stud. Univ. Babeş-Bolyai, Chem.*, **32** (1), 35-49 (1987).

95. E. Chifu, M. Sălăjan, M. Tomoaia-Cotişel, I. Demeter-Vodnár and J. Zsakó, "Interaction of some biologically active compound monolayers with electrolytes at the air/water interface", *Stud. Univ. Babeş-Bolyai, Chem.*, **32** (1), 50-57 (1987).

96. M. Tomoaia-Cotişel, J. Zsakó, A. Mocanu, I. Albu and E. Chifu, "Relaxation phenomena in fatty acid monolayers", *Stud. Univ. Babeş-Bolyai, Chem.*, **32** (1), 58-67 (1987).

97. S. Gocan, L. Olenic, M. Tomoaia-Cotişel and E. Chifu, "Adsorption mechanism of some carotenoid derivatives at the liquid/silica gel interface", *Stud. Univ. Babeş-Bolyai, Chem.*, **32** (1), 83-91 (1987).

98. J. Demeter-Vodnár, M. Sălăjan, M. Tomoaia-Cotişel, J. Zsakó and E. Chifu, "Complex formation at the benzene/water interface", *Stud. Univ. Babeş-Bolyai, Chem.*, **32** (1), 92-98 (1987).

99. M. Sălăjan, J. Demeter-Vodnár, E. Gavrilă and E. Chifu, "Studiul coalescenţei unei picături la o interfaţă lichid-lichid plană. I. Timpi de coalescenţă", *Rev. Chim. (Bucureşti)*, **38** (10), 882-886 (1987).

100. E. Chifu, J. Zsakó, M. Tomoaia-Cotişel, M. Sălăjan, J. Demeter-Vodnár and Cs.Várhely, "Adsorbed films at the benzen/water interface", *Stud. Univ. Babeş-Bolyai, Chem.*, **32** (2), 90-97 (1987).

101. J. Zsakó, M. Tomoaia-Cotişel, V. Tămaş, V. Coman and E. Chifu, "Monomolecular films of some apocarotenoid derivatives", *Rev. Roumaine Chim.*, **32** (11-12), 1193-1202 (1987).

102. E. Chifu, C. I. Gheorghiu and I. Stan, "Some remarks concerning the Marangoni flow on an inclined plane", in *VI. Intenationale Tagung über Grenzflächenaktive Stoffe*, Akademie Verlag, Berlin, 1987, pp. 211-217.

103. M. Tomoaia-Cotişel, J. Zsakó, A. Mocanu, M. Lupea and E. Chifu, "Insoluble mixed monolayers. III. The ionization characteristics of some fatty acids at the air/water interface", *J. Colloid Interface Sci.*, **117** (2), 464-476 (1987).

104. M. Tomoaia-Cotişel, J. Zsakó, E. Chifu and P. J.Quinn, "Molecular association in lipid-carotenoid monolayers", in *The Metabolism, Structure and Function of Plant Lipids*, (Paul K. Stumpf, J. Brian Mudd, W. David Ness, Eds.), Plenum Press, New-York, 1987, pp.131-133.

105. M. Tomoaia-Cotişel, J. Zsakó, E. Chifu, D. A. Cadenhead and H. E. Ries Jr., "Collapse mechanism of some carotenoid monomolecular films – membrane model", in *Progress in Photosyntesis Research*, (J. Biggins, Ed.), **vol. II** (4), Martinus Nijhoff Publ., Dordrecht, The Netherlands, 1987. pp. 333-337.

106. M. Tomoaia-Cotişel, J. Zsakó, E. Chifu and P. J. Quinn, "Intermolecular interactions in lipid/carotenoid monolayers", *Biochem. J.*, **248**, 877-662 (1987).

107. M. Sălăjan, J. Demeter-Vodnár, E. Gavrilă and E. Chifu, "Studiul coalescenţei unei picături la o interfaţă lichid-lichid plană. II. Drenajul şi ruperea filmului", *Rev. Chim. (Bucureşti)*, **39** (2), 138-142 (1988);

108. M. Tomoaia-Cotişel, J. Zsakó and E. Chifu, "State equations of fatty acid monolayers", *Stud. Univ. Babeş-Bolyai,Chem.*, **33** (2), 54-60 (1988).

109. M. Tomoaia-Cotişel, E. Chifu, A. Mocanu, J. Zsakó, M. Sălăjan and P.T. Frangopol, "Stearic acid monolayers on procaine containing subphases", *Rev. roum.Biochim.*, **25** (3), 227-237 (1988).

110. M. Tomoaia-Cotişel, J. Zsakó, A. Mocanu, E. Chifu and P.J.Quinn, "Monolayer properties of membrane lipids of the extreme Halophile Halobacterium Cutirubrum, at the air/water interface", *Biochim. Biophys. Acta*, **942**, 295-304 (1988).

111. M. Tomoaia-Cotişel, J. Zsakó, E. Chifu, P. T. Frangopol, W.A.P.Luck, and E.Osawa, "Interaction of procaine with uncharged stearic acid monolayers at the air/water interface", *Rev. roum. Biochim.*, **26** (4), 305-313 (1989).

112. M. Tomoaia-Cotişel, J. Zsakó, M. Sălăjan and E. Chifu, "Surface complexes of xanthophyll films with transition metal ions", *Rev. roum. Morphol. Embryol. Physiol.,* **26** (4), 341-347 (1989).

113. E. Chifu, I. Stan, M. Sălăjan and E. Gavrilă, "Surface mobility of surfactant solutions. XIII. Influence of the magnetic field", *Rev. Roumaine Chim.*, **34** (1), 79-85 (1989).

114. E. Chifu, J. Zsakó, M. Tomoaia-Cotişel and A. Mocanu, "A comparative study of some fatty acid monolayers at the air/water interface", *Stud. Univ. Babeş-Bolyai, Chem.*, **34** (2), 3-9 (1989).

115. E. Chifu, M. Tomoaia-Cotişel, M. Sălăjan, A. Chifu and J. Zsakó, "Xanthophylls. V. Dynamics of xanthophyll monolayers at the liquid/air interface", *Stud. Univ. Babeş-Bolyai, Chem.*, **34** (2), 28-34 (1989).

116. I.Stan, E. Chifu, Z. Finta and E. Gavrilă, "Marangoni translational motion of a free drop initially at rest", *Rev. Roumaine Chim.*, **34** (2), 603-615 (1989).

117. M. Sălăjan, E. Gavrilă and E. Chifu, "Coalescenţa picăturilor în condiţii de microgravitaţie simulată", *Rev. Chim. (Bucureşti)*, **40** (7), 576-580 (1989).

118. E. Chifu, I. Stan and E. Gavrilă, "Marangoni flow and mass transport on a spherical liquid-liquid interface in microgravity conditions", in *Proceedings of the 4th Intercosmos Seminar on Cosmic Materials and Technologies*, (V. Lupei, D. Toma, Eds.), Poiana Braşov, 11-19 November, 1988, Bucharest, November 1989, pp. 203-214.

119. M. Tomoaia-Cotişel, J. Zsakó, E. Chifu and P. J. Quinn, "Hysteresis in compression-expansion cycles of distearoylmonogalactosylglycerol monolayers", *Chem. Phys. Lipids*, **50**, 127-133 (1989).

120. J. Zsakó, M. Tomoaia-Cotişel and E. Chifu, "Discussion of compression isotherms of some carotenoid monolayers on the basis of HMO calculations", in *Surfactants in Solution*, (K. L. Mittal, Ed.), **vol.9**, Plenum Press, New-York, 1989, pp. 311-324.

121. E. Chifu, M. Tomoaia-Cotişel, J. Zsakó, A. Mocanu, M. Sălăjan, M. Neag and P. T. Frangopol, "Procaine penetration into uncharged stearic acid monolayers in terms of Gibbs adsorbtion equation", in *Seminars in Biophysics*, **vol. 6** (P. T. Frangopol, V. V. Morariu, Eds.), IAP Press, Bucharest, 1990, pp.117-128.

122. E. Chifu, J. Zsakó, M. Tomoaia-Cotişel and I. Albu, "Interfacial tension extrema at the adsorption from polycomponent systems", *Rev. Roumaine Chim.*, **35** (7-9), 843-851 (1990).

123. J. Zsakó, M. Tomoaia-Cotişel, E. Chifu, I. Albu and P.T. Frangopol, "Protolytic equilibria in surface solutions of stearic acid, procaine and benzoic acid at the air/water interface", *Rev. Roumaine Chim.*, **35** (7-9), 867-877 (1990).

124. E. Chifu, M. Tomoaia-Cotişel, J. Zsakó, I. Albu, A. Mocanu and P.T. Frangopol, "Penetration of procaine hydrochloride into stearic acid monolayers from underlying aqueous solutions", *Rev. Roumaine Chim.*, **35** (7-9), 879-889 (1990).

125. E. Chifu, E. Gavrilă and M. Sălăjan, "Surface mobility of surfactant solutions. XIV. Marangoni flow through square sectioned horizontal "surface" canals", *Stud. Univ. Babeş-Bolyai, Chem.*, **35** (1), 50-53 (1990).

126. J. Zsakó, M. Tomoaia-Cotişel, A. Mocanu and E. Chifu, "Surface equation of state for oleic acid monolayers on acidic aqueous solutions", *Stud. Univ. Babeş-Bolyai, Chem.*, **35** (1), 74-84 (1990).

127. M. Tomoaia-Cotişel, E. Chifu, S. Jitian, I. Bratu, S. Bran, P. T. Frangopol and A. Mocanu, "The study of stearic acid films by ellypsometry and absorption-reflection IR spectroscopy", *Stud. Univ. Babeş-Bolyai, Chem.*, **35** (2), 17-24 (1990).

128. M. Tomoaia-Cotişel, J. Zsakó, E. Chifu and D. A. Cadenhead, "Relaxation phenomena in apocarotenoid monolayers", *Langmuir*, **6** (1), 191-197 (1990).

129. J. Zsakó, M. Tomoaia-Cotişel, E. Chifu, A. Mocanu and P. T. Frangopol, "Influence of stearic acid monolayers upon the procaine adsorption from underlying alkaline aqueous solutions", *Biochim. Biophys. Acta*, **1024**, 227-232 (1990).

130. J. Zsakó, M. Tomoaia-Cotişel, I. Albu, A. Mocanu, E. Chifu and P. T. Frangopol, "Acid-base properties of some local anesthetics", *Rev. roum. Biochim.*, **28** (1-2), 33-40 (1991).

131. G. Oprea and E. Chifu, "Studiul adsorbţiei 8-hidroxichinolinei pe sulfură de plumb precipitată, prin spectroscopie IR", *Bul. Univ. Baia-Mare*, *Seria B*, **vol. VIII**, 239-241 (1991).

132. J. Zsakó, M. Tomoaia-Cotişel and E. Chifu, "Insoluble mixed monolayers. V. Molecular association in binary films: The regular association approach", *J. Colloid Interface Sci.*, **146** (2), 353-362 (1991).

133. G. Oprea and E. Chifu, "Studiul produşilor de adsorbţie a 8-hidroxichinolinei pe smitsonit prin spectroscopie IR", *Bul. Univ. Baia-Mare*, *Seria B*, **vol. IX**, 149-153 (1992).

134. M. Tomoaia-Cotişel, E. Chifu, J. Zsakó, A. Mocanu, P. J. Quinn and M. Kates, "Monolayer properties of archaenol and caldarchaenol polar lipids of a methanogenic archaebacterium, Methanospirillum Hungatei, at the air/water Interface", *Chem. Phys. Lipids*, **63**, 131-138 (1992).

135. E.Gavrilă, E.Chifu, M.Sălăjan and C.I.Gheorghiu, "Influenţa vâscozităţii fluidelor asupra scurgerii Marangoni", în *Lucrările Conferinţei Naţionale de Chimie şi Inginerie Chimică*, **Vol. 1**, Universitatea Politehnică Bucureşti, 29-30 octombrie 1993, pp. 139-142.

136. E.Chifu, "Some Features of the Hydrodynamics and thermodynamics of surface films", *Roum.Chem.Quart.Rev.*, **1** (1), 33-45 (1993).

137. M. Tomoaia-Cotişel, E. Chifu, J. Zsakó, P. T. Frangopol, P. J. Quinn and A. Mocanu, "Interaction of some drugs with monomolecular membranes at the fluid interfaces", *Stud. Univ. Babeş-Bolyai, Chem.*, **38** (1-2), 81-85 (1993).

138. J. V. Demeter, M. Sălăjan and E. Chifu, "Fatty acids at benzene/water interface", in *Proceedings of the 6th Conference on Colloid Chemistry*, (F. Csempesz, Z. Horvölgyi, I. Paszli, Eds.), MKE, Budapest, 16-19 september 1993, pp. 87-90.

139. J. Zsakó, E. Chifu, M. Tomoaia-Cotişel, A. Mocanu and P. T. Frangopol, "Procaine penetration into mixed monomolecular films of cholesterol and dipalmitoylphosphatidylcholine", *Rev. Roumaine Chim.*, **39** (7), 777-786 (1994).

140. E.Chifu, E.Gavrilă and M.Sălăjan, "Surface mobility of surfactant solutions. XV. Marangoni mobility of liquid layers under extreme values of surface tension", *Rev.Roumaine Chim.*, **39** (6), 697-704 (1994).

141. J. Zsakó, M. Tomoaia-Cotişel, E. Chifu, A. Mocanu and P. T. Frangopol, "Procaine interactions with phospholipid monolayers at the air/water interface", *Gazz. Chim. Ital.*, **124**, 5-9, (1994).

142. E.Chifu, C.I.Gheorghiu, M.Sălăjan and E.Gavrilă, "Marangoni and gravity flows in thin liquid layers", *Proceedings of the Second International Thermal Energy Congress*, Agadir, Morocco, 5-8 June 1995, **Vol. II**, (E. Bilgen, A. Mir, T. H. Nguyen, P. Vasseur, Eds.), Ecole Polytechnique de Montreal Publ., 1995, pp. 832-837.

143. Stan, E. Chifu and Z. Kása, "Convective diffusion of a soluble surfactant from a free drop", *Zamm*, **75**, 369-370 (1995).

144. E. Chifu, E. Gavrilă, M. Sălăjan and C. I. Gheorghiu, "Surface mobility of surfactant solutions. XVII. Determination of Marangoni rate of flow in simulated zero gravity conditions", *J. Rom. Colloid Surface Chem. Assoc.*, **2** (3-4), 25-29, (1997).

145. E. Chifu, "Mixed films – biomembrane models", *J. Colloid & Surf. Chem. Assoc.*, **2** (3-4), 25-29, (1997).

146. M. Tomoaia-Cotişel, I. Zsakó, E. Chifu, A. Mocanu, P. T. Frangopol and P. J. Quinn, "Procaine binding to stearic acid monolayers spread at the air/buffer interface. The influence of pH and surface pressures", *J. Colloid & Surf. Chem. Assoc.*, **2** (3-4), 30-36 (1997).

147. I.Zsakó, M. Tomoaia-Cotişel, A. Mocanu, Cs. Racz and E. Chifu, "Thermodynamics of adsorption and micelle formation of sodium cholate in two-phase systems", *J. Colloid & Surf. Chem. Assoc.*, **2** (3-4), 37-40 (1997).

148. J. Zsakó, A. Mocanu, Cs. Racz, K. Racz and E. Chifu, "Critical micelle concentration of sodium cholate solutions", *Stud. Univ. Babeş-Bolyai, Chem.*, **42**, (1-2), 37-41 (1997).

149. E. Chifu, J. Zsakó, M. Tomoaia-Cotişel, A. Mocanu and A. Voina, "Interaction of cholesterol with bile salts at the CCl_4 /water interface, *Stud. Univ. Babeş-Bolyai, Chem.*, **42** (1-2), 129-133, (1997).

STUDIA UNIVERSITATIS BABEŞ-BOLYAI, CHEMIA, XLIII, 1-2, 1998

THE KINETICS OF METHYLENE BLUE – ASCORBIC ACID REACTION

ALEXANDRA RUSTOIU – CSAVDARI, IOAN BÂLDEA and COSMINA CORA[1]

ABSTRACT. The clock reaction between methylene blue and ascorbic acid has been investigated over a large variety of experimental conditions. Kinetic parameters are reported. The overall rate equation has been obtained and the Arrhenius activation energy is calculated. The effect of dielectric constant on the rate is explained. A reaction sequence is suggested and discussed in relation to previous studies.

INTRODUCTION

The reduction of methylene blue, a basic thiazinic dye used as a redox indicator, may be performed with different reducing agents. L-ascorbic acid, vitamin C - a biologically important compound is among them. Snehalatha, Rajanna and Saiprakash [1] have demonstrated a clock reaction involving methylene blue (MB) and ascorbic acid (H_2A). Many advanced concepts of chemical kinetics could be explained by this clock reaction, having the stoechiometry:

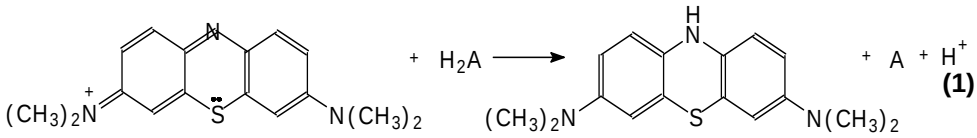

(1)

Blue colored Colorless

[1] *Facultatea de Chimie şi Inginerie Chimică, Universitatea "Babeş-Bolyai", Catedra de Chimie Fizică; Str. Arany Janos 11, 3400 Cluj-Napoca, România,* ***E-mail: arustoiu@chem.ubbcluj.ro***

The colored cation can exist in three mezomeric forms:

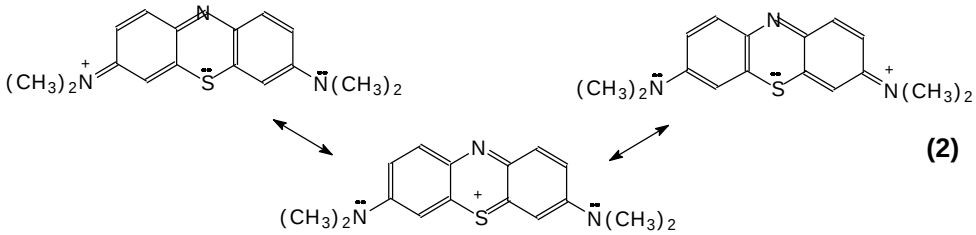

(2)

having para quinoid structure of extended conjugation.

A biequivalent reduction of the cation, which formally means the attachment of a hydride to the central nitrogen atom, breaks the conjugation and a neutral leuco-compound is formed. Half-reduction, when a neutral free radical is formed, yields also to a colored species [2] with the formation of a colorless reduced compound and dehydroascorbic acid (A).

Such clock reaction studies have been undertaken with Landolt-type reactions [3], bromate-bromide [4], persulfate-iodide [5], bromination of phenols [6], hydrogen peroxide – bromide [7] or iodide [8] systems, to achieve kinetic or analytical.

It seems that Snehalatha and his co-workers [1] made some misinterpretation concerning the methylene blue - ascorbic acid reaction, in both the rate equation and rate-determining steps in their proposed mechanism.

In the present work, this reaction has been studied in a wide condition range of reactants and hydrogen ion concentrations, choosing those conditions that ensure time measurements less affected by the experimental errors.

EXPERIMENTAL

Aqueous or 1,4-dioxane-water and acetone-water solutions of the reagents were freshly prepared before each set of measurements. Analytical grade reagents were used without further purification. Methylene blue chloride and sodium ascorbate (Merck) were weighted, dissolved with twice distilled water and made up to the mark in volumetric flasks of 250 ml. Hydrocloric, sulfuric and phosphoric acids were used as sources for hydrogen ions. The solutions were standardized by usual procedures.

Two solutions were prepared for each kinetic experiment, so that after mixing the total volume was 25 ml. One solution contained ascorbic acid, HCl (or other) and KCl while the other contained methylene blue. Solutions were kept at controlled temperature, the first one in a double wall glass vessel connected to a precision circulation bath. It was placed on a magnetic stirrer. The solution of methylene blue was added to the first one under stirring and a stop-watch was started. The reaction time (t) for blue color to change colorless was recorded.

Three to four replicate runs were carried out for the same experimental conditions. Time measurements do not differ with more than ± 1.5 %.

Free radical involvement was checked by the polymerization of vinyl-acetate.

RESULTS AND DISCUSSION

The effect of reactants and hydrogen ion concentrations as well as the effect of ionic strength, solvent composition and temperature on the reaction rate are presented in tables 1 - 6.

Table 1.

The effect of ascorbic acid concentration on the reaction rate at T = 293 K, $[MB]_o = 1.78 \bullet 10^{-5}$ mole.l^{-1}, $[KCl]_o = 0.12$ mole.l^{-1}, in aqueous solution.

Medium	10^3 $[H_2A]_o$ (mole.l^{-1})	t (s)	t_{mean} (s)	10^7 r (mole.l^{-1}.s^{-1})
HCl $[H^+]_o = 0.75$ mole.l^{-1} j = 0.87 mole.l^{-1}	2	408, 408, 411, 412	410	0.43
	4	216, 215, 219, 215	216	0.82
	6	147, 150, 147, 148	148	1.20
	8	119, 120, 120, 118	119	1.49
	10	100, 100, 101, 101	100	1.78
	12	81, 81, 81, 82	81	2.19
	13	68, 68, 68	68	2.61
H_2SO_4 $[H^+]_o = 0.44$ mole.l^{-1} j = 0.65 mole.l^{-1}	2	448, 450, 447, 449,	448.5	0.39
	4	233, 234, 230, 229	231.5	0.76
	6	157, 160, 158, 156	158	1.12
	8	125, 126, 125, 125	125	1.42
	10	99, 99, 102, 101	100	1.78
	12	82, 84, 83, 85	83.5	2.13
	13	70, 71	70.5	2.52
H_3PO_4 $[H^+]_o = 0.04$ mole.l^{-1} j = 0.16 mole.l^{-1}	2	892, 891, 888	890	0.20
	4	541, 542, 543	542	0.32
	6	387, 385, 388	387	0.45
	8	332, 333, 333	333	0.53
	10	256, 259, 258	258	0.68
	12	242, 243, 245	243	0.73
	13	226, 228	227	0.78

Table 2.

The effect of methylene blue concentration on the reaction rate at T = 293 K, $[H_2A]_o = 6 \bullet 10^{-3}$ mole.l^{-1}, $[KCl]_o = 0.12$ mole.l^{-1}, in aqueous solution.

Medium	10^5 $[MB]_o$ (mole.l^{-1})	t_{mean} (s)	10^7 r (mole.l^{-1}.s^{-1})
HCl $[H^+]_o = 0.75$ mole.l^{-1} j = 0.87 mole.l^{-1}	0.36	59	0.61
	1.07	110	0.97
	1.78	148	1.20
	2.49	164	1.51
	3.20	184	1.73
	3.91	199	1.96
H_2SO_4 $[H^+]_o = 0.44$ mole.l^{-1} j = 0.65 mole.l^{-1}	0.36	59	0.61
	1.07	112	0.95
	1.78	157	1.13
	2.49	180.5	1.37
	3.20	106.5	1.54
	3.91	220	1.77
H_3PO_4 $[H^+]_o = 0.04$ mole.l^{-1} j = 0.16 mole.l^{-1}	0.36	172	0.20
	1.07	288	0.37
	1.78	386	0.46
	2.49	511	0.49
	3.20	550	0.58
	3.91	619	0.63

Reaction orders:

Using a differential method for determining the reaction order with respect to various species, the following conclusions were drawn:

a.) The process obeys first-order dependence with respect to ascorbic acid for all experimental conditions employed. The plots of *lg (r)* versus *lg ($[H_2A]_o$)* were linear with slopes of 1.00 ± 0.03. Figure 1 presents the dependence of rate on $[H_2A]_o$. Points lie on the line, with good correlation coefficients (0.9956 – 0.9982). Slopes in figure 1 are different because of different hydrogen ion concentrations when using HCl, H_2SO_4 or H_3PO_4.

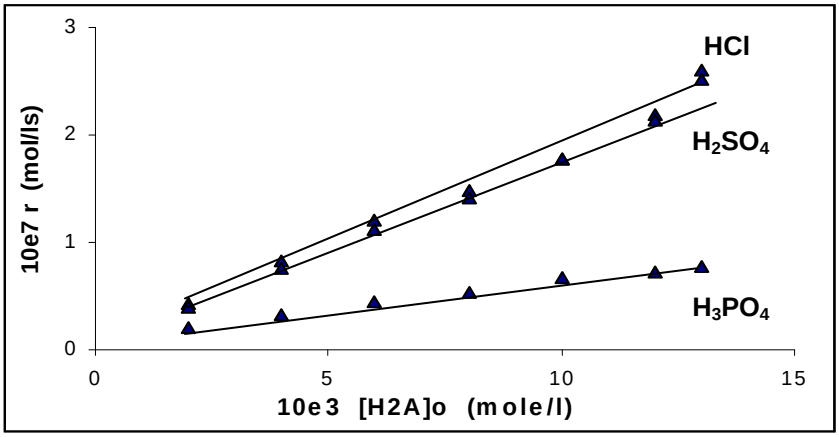

Figure 1. Reaction rate versus ascorbic acid initial concentration at T = 293 K, $[MB]_o = 1.78 \bullet 10^{-5}$ mole.l^{-1}, $[KCl]_o = 0.12$ mole.l^{-1}, in aqueous solution.

b.) The process obeys a 0.5 order with respect to methylene blue as shown in figure 2 which presents the rate versus $[MB]_o^{1/2}$. Points lie on lines with good correlation coefficients (0.9925 – 0.9957) irrespective of the acid used. The slopes vary because of the same reasons as explained above.

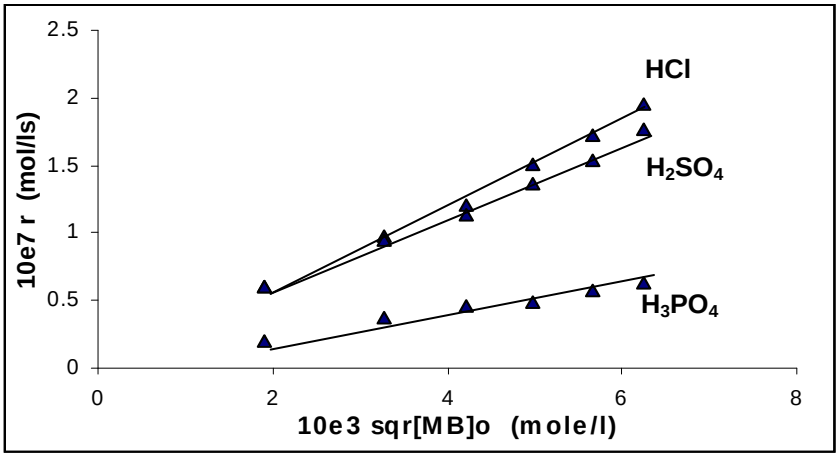

Figure 2. Reaction rate versus the square root of initial methylene blue concentration at T = 293 K, $[H_2A]_o = 6 \bullet 10^{-3}$ mole.l^{-1}, $[KCl]_o = 0.12$ mole.l^{-1}, in aqueous solution.

c.) The fractional order on H^+ ion found by Snehalatha and his co-workers [1], was confirmed by us by plotting *lg (r)* versus *lg ($[H^+]_o$)*. Lines with good correlation coefficients, 0.9938 and 0.9898 were found. Orders of 0.47 and 0.5 were calculated in HCl and H_2SO_4 respectively. These values are comparable with the ones reported previously [1], of 0.68 and 0.76.

From the above-presented findings, it may be concluded that for a constant H^+ concentration, the rate law is:

$$r = \frac{[MB]_o}{t} = -\frac{d\,[MB]}{dt} = k_{obs}\,[H_2A]\,[MB]^{1/2} \qquad (3)$$

Using the above relationship, rate coefficients k_{obs}, expressed in $l^{1/2}.mole^{-1/2}.s^{-1}$, were calculated for various hydrogen ion concentrations and presented in table 3.
\

Table 3.

The effect of hydrogen ion concentration on the reaction rate and observed rate coefficient at T = 293 K, $[H_2A]_o = 6\bullet10^{-3}$ mole.l^{-1}, $[MB]_o = 1.78\bullet10^{-5}$ mole.l^{-1}, $[KCl]_o$ = 0.12 mole.l^{-1}, in aqueous solution.

Medium	$[H^+]_o$ (mole.l^{-1})	t_{mean} (s)	10^7 r (mole.$l^{-1}.s^{-1}$)	10^3 k_{obs} ($l^{1/2}.mole^{-1/2}.s^{-1}$)
HCl	0.15	325	0.54	2.14
	0.45	178	1.00	3.96
	0.75	146	1.21	4.79
	1.05	123	1.44	5.70
	1.35	118	1.50	5.94
H_2SO_4	0.10	354	0.50	1.98
	0.27	230	0.77	3.05
	0.44	157	1.13	4.47
	0.60	140	1.27	4.03
	0.76	135	1.31	5.19

Observed rate constants depend upon hydrogen ion concentration, with a fractional and less than unity order. A trend to level off is also observed. This can be described by the following equation:

$$k_{obs} = \frac{a\,[H^+]}{1 + b\,[H^+]} \qquad (4)$$

To obtain parameters a and b, a linear, double reciprocal, form of equation (4) could be used:

$$\frac{1}{k_{obs}} = \frac{b}{a} + \frac{1}{a} \bullet \frac{1}{[H^+]} \qquad (5)$$

The linearity (correlation coefficient of 0.9930) holds with all the data obtained with hydrochloric and sulfuric acid. It is presented in figure 3. From the intercept and the slope b/a = 127.0 ± 7.0 $mole^{1/2}.l^{-1/2}.s$ and 1/a = 51.5 ± 2.3 $mole^{3/2}.l^{-3/2}.s$ were calculated.

Figure 3. The plot $1/k_{obs}$ versus $1/[H^+]$ at T = 293 K, $[H_2A]_o = 6 \bullet 10^{-3}$ $mole.l^{-1}$, $[KCl]_o = 0.12$ $mole.l^{-1}$, in aqueous solution.

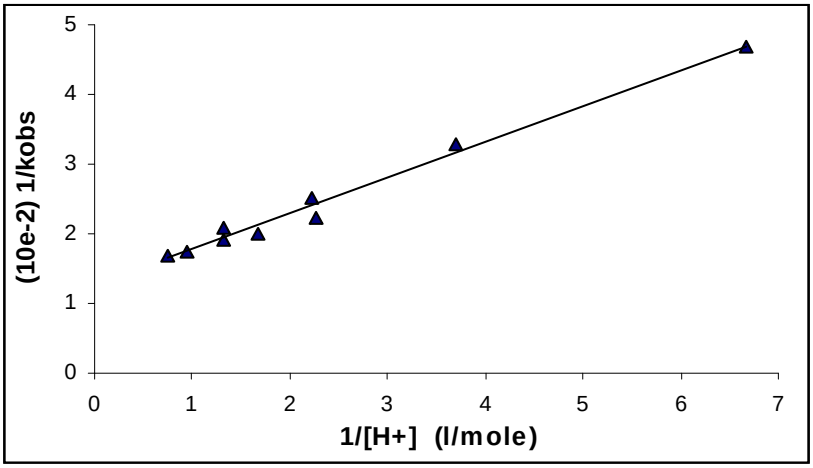

Finally, the rate law including all the species involved is:

$$r = \frac{[MB]_o}{t} = -\frac{d\,[MB]}{dt} = \frac{a\,[H_2A]\,[MB]^{1/2}\,[H^+]}{1 + b\,[H^+]} \qquad (6)$$

Effect of ionic strength

Using constant acidity and initial concentrations of reagents, but varying the concentration of potassium chloride, it was found that salt did not affect the reaction rate. Its value is practically unmodified over a large range of ionic strength, as one can conclude from table 4.

Table 4.

The effect of ionic strength on the reaction rate at T = 293 K, $[H_2A]_o = 6 \bullet 10^{-3}$ mole.l^{-1}, $[MB]_o = 1.78 \bullet 10^{-5}$ mole.l^{-1}, $[H^+]_o = 0.45$ mole.l^{-1}, aqueous solution.

Medium	j (mole.l^{-1})	t (s)	t_{mean} (s)	10^7 r (mole.l^{-1}.s^{-1})
HCl	0.45	174, 173, 170	172	1.03
	0.57	173, 174, 174, 172	173	1.02
	0.69	170, 170, 171	170	1.04
	0.93	170, 171, 170	170	1.04

This indicates either compensation of primary salt effect by the secondary one, if two ions are concerned, or the interaction of an uncharged species with an ion (an ion-dipole interaction).

Effect of solvent

Binary solvent mixtures of water-acetone and water-1,4 dioxane were used to search for the effect of dielectric constant on the rate. The reaction was performed in mixtures containing 8 - 32 % vol acetone and 8 – 24 % vol 1,4-dioxane. The kinetic results presented in table 5 indicate that, the higher the contents of organic solvent, the slower the reaction rate. Figures 4.a and 4.b present the plot of *lg (k_{obs})* versus *1/D* [9], characteristic to ion-dipole interaction, and the plot of *lg (k_{obs})* versus *(D-1)/(2D+1)*, characteristic to interaction between polar molecules [10], respectively.

Table 5.

The effect of dielectric constant (D) on the reaction rate and observed rate coefficient at T = 293 K, $[MB]_o = 1.78 \bullet 10^{-5}$ mole.l^{-1}, $[H^+]_o = 1.93$ mole.l^{-1} (source HCl), $[KCl]_o = 0.12$ mole.l^{-1}, j = 2.05 mole.l^{-1}.

Medium	D	t_{mean} (s)	10^8 r (mole.l^{-1}.s^{-1})	10^3 k_{obs} (l$^{1/2}$.mole$^{-1/2}$.s^{-1})
water $[H_2A]_o = 4 \bullet 10^{-3}$ mole.l^{-1}	78.5	231	7.72	4.57
water – acetone mixture $[H_2A]_o = 4 \bullet 10^{-3}$ mole.l^{-1}	30.1	307	5.80	3.44
	16.95	440	4.09	2.42
	12.62	605	2.97	1.76
	8.28	882	2.04	1.21
water – 1,4 dioxane mixture $[H_2A]_o = 6 \bullet 10^{-3}$ mole.l^{-1}	30.95	389.5	4.62	1.83
	18.32	478	3.76	1.49
	13.09	626.5	2.87	1.13

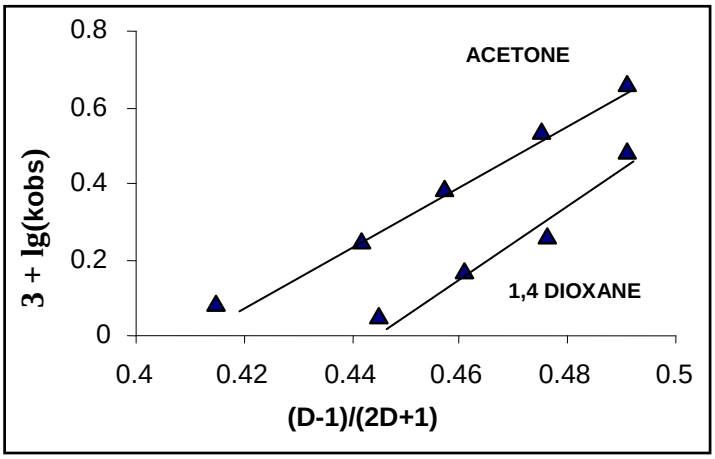

Figure 4.a.

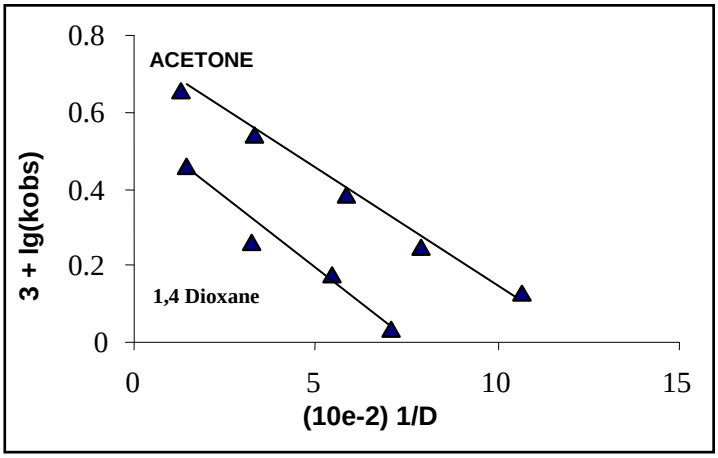

Figure 4.b.

Figure 4. The effect of dielectric constant (D) on the observed rate coefficient at T = 293 K, $[MB]_o = 1.78 \bullet 10^{-5}$ mole.l^{-1}, $[H^+]_o = 1.93$ mole.l^{-1} (source HCl), $[KCl]_o = 0.12$ mole.l^{-1}, j = 2.05 mole.l^{-1}, in a.) water - acetone and b.) water – 1,4 dioxane mixtures.

Points lie on lines for both plots. If the rate-determining step consists of an ion-polar molecule interaction, the attraction, assuming correct orientation of the dipole, will be somewhat greater and the rate of reaction should be larger in a medium of lower dielectric constant. The experimental results show the reverse. On the other hand, the substrate is a cationic dye, and the validity of a relation applying to interaction between polar molecules is fortuitous.

These equivocal findings show that the effect of the solvent is mainly determined by the influence on the pre-equilibrium, rather than on the rate-determining step.

Free radical involvement

The system MB – H_2A was used to initiate polymerization of vinyl-acetate. The reaction was performed in a small calorimeter and the increase of temperature was measured. Significant difference was noticed in the presence of monomer as compared to the initial mixture, due to the cumulative thermal effect of radical polymerization.

Effect of temperature

Various temperatures in the range of 289.4 – 303.6 K were used to determine experimental activation energy. Table 6 contains rate data and observed rate coefficients. A value of E_a = 45.4 ± 6.7 KJ.mole^{-1} was obtained, in good agreement with the one previously determined [1].

Table 6.

The effect of temperature (T) on the reaction rate and observed rate coefficient at $[H_2A]_o = 6 \bullet 10^{-3}$ mole.l^{-1}, $[MB]_o = 1.78 \bullet 10^{-5}$ mole.l^{-1}, $[H^+]_o$ = 0.75 mole.l^{-1} (source HCl), $[KCl]_o$ = 0.12 mole.l^{-1}, j = 0.87 mole.l^{-1}, in aqueous solution.

T (K)	t_{mean} (s)	10^7 r (mole.l^{-1}.s^{-1})	10^3 k_{obs} (l$^{1/2}$.mole$^{-1/2}$.s^{-1})
289.4	185	0.96	3.79
293	146	1.21	4.78
297.5	96	1.85	7.31
303.6	79	2.25	8.89

If the rate determining step were the interaction HB^+ - H_3A^+ as suggested by Snehalatha [1] (who omitted the charge on the cationic dye in explaining the mechanism), the activation energy should be larger because of charge repulsion.

Reaction mechanism

In the acid medium used (pH far less than pK_1), ascorbic acid exists as undissociated species H_2A [11]. The redox indicator methylene blue presents a dimerisation equilibrium [11]:

$$(MB^+)_2 \Leftrightarrow 2\ MB^+ \qquad (K_1) \qquad (7)$$

which should be considered as a pre-equilibrium.

First-order dependence on H_2A, square root dependence on methylene blue and fractional-order dependence on hydrogen ion, in connection with the effect of ionic strength and dielectric constant on the rate are consistent with the following mechanism:

$MB^+ + H^+ \Leftrightarrow MBH^{2+}$ (K_2) (8)

$MBH^{2+} + H_2A \rightarrow MBH^+\bullet + HA\bullet + 2\,H^+$ (k_1) (9)

$MBH^{2+} + H_2A \rightarrow MBH + A + 2\,H^+$ (k_2) (10)

$MBH^+\bullet + HA\bullet \rightarrow MBH + A + H^+$ (k_3, fast) (11)

The species $MBH^+\bullet$ and $HA\bullet$ stand for protonated half-reduced and half-oxidized free radicals respectively, MBH for the reduced and colorless form of MB and A for dehydroascorbic acid.

Steps (9) and (11) should be taken into consideration for the redox process, because of the involvement of some free radicals, proved by the initialization of polymerization of vinyl-acetate. Snehalatha reported the same finding [1].

On the other hand we consider that the proton attaches to methylene blue cation which bears basic positions, rather than to ascorbic acid, which should loose protons during the oxidation. Such a process has been proposed [1] as an alternative mechanism, but the dimerization equilibrium was misinterpreted. Since the free radical $MBH^+\bullet$ is a reactive species, process (11) should proceed with the rate of process (9). Free radical $MBH^+\bullet$ is also a colored species as the dimeric $(MB^+)_2$ and monomeric MB^+ species. The rate was measured by the decay of the mixture's color and process (11) has here a certain contribution. Discrimination between the two redox processes could not be made with the data available. Therefore only their sum is taken into consideration.

The slower rate in the presence of an organic solvent in the reaction mixture as compared to the one in aqueous media can be explained by favoring equilibrium (7) towards the dimeric species, at lower dielectric constants of the environment.

The imperceptible influence of the ionic strength is obvious by the involvement of an ion-dipole interaction in the rate-determining step.

From the above mechanism, the rate law could be derived as:

$$r = -\frac{d\,[MB]}{dt} = (k_1 + k_2)\,[MBH^{2+}]\,[H_2A] = k\,[MBH^{2+}]\,[H_2A] \qquad (12)$$

Taking into account the protonation pre-equilibrium, the material balance for the monomeric species is:

$$[MB^+]_{total} = [MB^+]_{free} + [MBH^{2+}] = [MB^+]_{free}\left\{1 + K_2[H^+]\right\} \quad (13)$$

A correlation between dimeric and monomeric species is done by means of the dimerization equilibrium (7) so that the concentration of the protonated species is:

$$[MBH^{2+}] = \frac{K_1^{1/2} K_2 [(MB^+)_2]^{1/2} [H^+]}{1 + K_2[H^+]} \qquad (14)$$

Therefore, the rate law becomes:

$$r = -\frac{d\,[MB]}{dt} = \frac{kK_1^{1/2}K_2[(MB^+)_2]^{1/2}[H^+][H_2A]}{1+K_2[H^+]} \qquad (15)$$

of the form (6).

The observed rate constant ($l^{1/2}.mole^{-1/2}.s^{-1}$) is

$$k_{obs} = \frac{kK_1^{1/2}K_2\,[H^+]}{1+K_2\,[H^+]} \qquad (16)$$

showing the trend to level off with the hydrogen ion concentration. Its linear form is

$$\frac{1}{k_{obs}} = \frac{1}{kK_1^{1/2}} + \frac{1}{kK_1^{1/2}K_2} \bullet \frac{1}{[H^+]} \qquad (17)$$

with $b/a = (k\,K_1^{1/2})^{-1}$ and $a = k\,K_1^{1/2}K_2$. Thus, the following values could be calculated:

$k\,K_1^{1/2} = (7.9 \pm 0.4) \bullet 10^{-3}\ l^{1/2}.mole^{-1/2}.s^{-1}$ and $K_2 = 2.5 \pm 0.5\ l.mole^{-1}$.

The rate law deduced from the suggested mechanism is in accordance with all observed kinetic features. The effect of ionic strength and dielectric constant are also explained by the proposed mechanism, giving us confidence that it is operative.

REFERENCES

1. T. Snehalatha, K.C. Rajanna, P.K. Saiprakash, *J. Chem Educ.*, ***1997***, *74(2)*, 228.
2. M. Avram, *Chimie Organica*, Ed. Zecasin, Bucuresti, ***1995***, 201-202, 441-442.
3. I.Bognar, O. Jettinec, *Mikrochim. Acta. (* Wien), ***1970***, 1017.
4. I.Bognar, L. Sipos, *Z. Physik. Chem. (Leipzig)*, ***1969***, *55*, 99.
5. B.P. Levitt, *Findlay's Practical Physical Chemistry*, Longman, London, ***1983***, 351.
6. J.R. Clarcke, *J. Chem. Educ.*, ***1970***, *47*, 775.
7. A.E. Burges, J.L. Latham, *Analyst*, ***1966***, *91*, 343.
8. K.B. Iatsimiskii, L.P. Raizman, *Zhur. Neorg. Khim.*, ***1960***, *5*, 593.
9. W.F.K. Wynne-Jones, H. Ehring, *J. Chem. Phys.*, ***1935***, *3*, 492; K.J. Leidler, H. Eyring, *Ann. N.Y. Acad. Sci.*, ***1940***, *39*, 303.
10. J.G. Kirkwood, *J. Chem. Phys.*, ***1934***, *2*, 351; J.W. More, R.G. Pearson, *Kinetics and Mechanism*, Jon Wiley and Sons, New York, 1981, 258-268.
11. W.J. Blaedel, V.W. Meloche, *Elementary Quantitative Analysis, Theory and Practice*, 2nd ed., Harper & Row, New York, ***1963***, 447 and 883; T. Snehalatha, K.C. Rajanna, P.K. Saiprakash, *J. Chem Educ.*, ***1997***, *74(2)*, 228.

STUDIA UNIVERSITATIS BABEŞ-BOLYAI, CHEMIA, XLIII, 1-2, 1998

SIMULTANEOUS DETERMINATION OF RATE CONSTANTS FOR FIRST ORDER CONSECUTIVE IRREVERSIBLE REACTIONS

ALEXANDRA RUSTOIU – CSAVDARI, IOAN BALDEA, DOINA PASERE[1]

ABSTRACT. A method for simultaneous experimental determination of rate constants for a first-order, two stage, irreversible process is proposed. It is based on the monitoring of a commun product.The first and second rate coefficient are determined at small and high reaction degrees, respectively. The obtained values are independent from each other.

The method is ilustrated for the acvation of trans-dibromo-bis-dymethylglyoximato-cobalt (III) acid. Its evolution was monitored by potentiometrical means. Kinetic parameters are reported for a variety of experimental conditions. Activation parameters have been calculated and a dissociative monomolecular substitution mechanism is proposed for both the stages.

INTRODUCTION

Numerous reactions of industrial importance occur consecutively or competitively, by combining at least two independent reactions. Therefore, the individual rate coefficients are important in chemical reactor design. Their simultaneous experimental determination has to take into account the individual features of each studied process. However, some general "recipes" can be developed.

When experiments provide a product distribution, ratios of rate constants can be obtained for a variety of complex reactions by superposing the experimental and calculated plots [1]. A method to determine k_1 and k_2 (when $k_1 >> k_2$) is reported for two first-order consecutive reactions, when an additive propriety of the reaction mixture is monitored [2,3] (for example the absorbance). This method is similar to the one applied for first-order parallel processes which yield the same product [4]. Determination of individual rate coefficients for competitive reactions of different orders (first and second) [5] follows the same principle as for catalyzed and uncatalyzed competitive ones [6].

This paper presents a method to determine the individual rate constants k_1 and k_2 for a sequence of two first-order consecutive irreversible reactions. One of

[1] *Facultatea de Chimie si Inginerie Chimică, Universitatea "Babeş-Bolyai", Catedra de Chimie Fizică, Str. Arany Janos 11, 3400 Cluj-Napoca, Romania, E-mail: arustoiu@chem.ubbcluj.ro.*

the products is yield in each of them. The method is based on monitoring its concentration versus reaction time.

A chemical system with these features is the acvation process of trans-dibromo-bis-dymethylglyoximato-cobalt (III) acid:

$$[Co(DH)_2Br_2]^- + H_2O \rightarrow [Co(DH)_2Br(H_2O)] + Br^- \qquad (k_1) \quad (1)$$

$$[Co(DH)_2Br(H_2O)] + H_2O \rightarrow [Co(DH)_2(H_2O)_2]^+ + Br^- \qquad (k_2) \quad (2)$$

where the commun product is bromide.

Sychev [7] and Zsako [8,11] studied the kinetics of these processes in water-dimethylformamide mixtures, at the pH of the reactant acid. They determined both k_1 and k_2: Sychev by studying reactions (1) and (2) separately and Zsako by monitoring the whole sequence. He first obtained the value of k_1 and than the one of k_2 by constantly adjusting it, till the experimental concentration plots superposed the theoretical ones. This way, value of k_2 is affected by the experimental determination of k_1.

Although Sychev and Zsako used both a potentiometric method, the ionic strength of the reaction mixture was not controlled. Neither was the pH, although experiments were carried out in acid media and it was recognized that acidity affects reaction rates.

By reconsidering these measurements, we tried not only to avoid, but also to complement the results Sychev and Zsako have arrived at [7,8,11].

EXPERIMENTAL

Analytical grade reagents, provided by "Reactivul-Bucuresti", were used without further purification. The reactant $H[Co(DH)_2Br_2]$ was syntetized by a known method [7]. HNO_3 and a CH_3COOH / CH_3COONa buffer were used to ensure a known acidity of medium. The ionic strength was adjusted to j = 1 mole.l^{-1} with KNO_3. All aqueous solutions were prepared in twice distilled water.

Two solutions were prepared for each kinetic experiment, so that after mixing the total volume became 8 ml. One solution contained the acid or the buffer and KNO_3. The other contained 70 mg of $H[Co(DH)_2Br_2]$ dissolved in N,N – dimethylformamide (DMFA) and was freshly prepared before each experiment. Both solutions were kept at controlled temperature, the first one in a double wall glass vessel connected to a precision circulation bath. It was placed on a magnetic stirrer. The second solution was added to the first one under stirring and a stop-watch was started.

A selective bromide electrode was introduced in the reaction mixture and connected together with a reference electrode to a digital RADELKIS multimeter. The salt bridge contained saturated aqueous solution of KNO_3. The electromotive force of the cell was recorded versus reaction time. Three to seven replicate runs were carried out for the same experimental conditions.

The value of acidity was verified with a glass pH electrode. Both the electrodes (bromide and pH) were calibrated at j = 1 mole.l^{-1} for each working temperature. After each experiment the bromide electrode was washed and dried.

RESULTS AND DISCUSSIONS

Determination of individual rate coefficients

For simplicity, reactions (1) and (2) are written schematically as follows:

$A \rightarrow B + D \qquad (k_1) \qquad (3)$

$B \rightarrow C + D \qquad (k_2) \qquad (4)$

where A stans for $[Co(DH)_2Br_2]^-$, B for $[Co(DH)_2Br(H_2O)]$, C for $[Co(DH)_2(H_2O)_2]^+$ and D for Br^-.

In order to study the kinetics of processes (1) and (2), the electromotive force *E* of the cell below was recorded versus reaction time *t*.

(-) Hg / Hg_2Cl_2 / Cl^- (sat) // Br^- (C_D) / EMIS – Br (+) (5)

C_D stands for the total molar concentration of released Br^- ions. Its values can be calculated by using equation (7) from the calibration lines (6):

$$E = A + B \lg C_D \qquad (mV) \qquad (6)$$

$$\lg C_D = \frac{E - A}{B} \qquad (7)$$

Relationship (6) is valid only for $10^{-3} \leq C_D \leq 10^{-1}$ mole.l^{-1}. The constants *A* and *B* were determined experimentally at j = 1 mole.l^{-1} and various temperatures. Their values, as well as the correlation coefficients of the corresponding calibration lines, are given in table 1.

Table 1.

Values of constants *A* and *B* at j = 1 mole.l^{-1}.

T (K)	298	308	320
A (mV)	- 128.71	- 121.76	-113.63
B (mV)	- 62.18	- 62.76	-65.60
r	0.9994	0.9991	0.9989

The kinetic model for two first-order consecutive irreversible reactions, provides the expressions of concentrations C_A and C_B [10]:

$$C_A = C_{Ao} \exp\left(-k_1 t\right) = C_{Ao} - C_D \qquad (8)$$

$$C_B = \frac{k_1 C_{Ao}}{k_2 - k_1}\left[\exp\left(-k_1 t\right) - \exp\left(-k_2 t\right)\right] \qquad (9)$$

Mass balances for Co(III) and Br^- written as:

$$C_{Ao} - C_A = C_B + C_C \qquad (10)$$

and $C_D = C_B + 2C_C$ (11)

will lead to the expressions of C_C and C_D. C_{A0} stands for the initial molar concentration of species A.

The linear form of equation (8) is:

$$\ln \frac{C_{Ao}}{C_{Ao} - C_D} = k_1 t \quad (12)$$

If $k_1 > k_2$, at low overall conversion (less than 8 ÷ 10 %), only reaction (3) occurs at a significant rate. Thus, k_1 can be obtained from the slope of the plot *ln* $[C_{Ao}/(C_{Ao} - C_D)]$ versus reaction time (see equation 12), as ilustrated in figure 1.

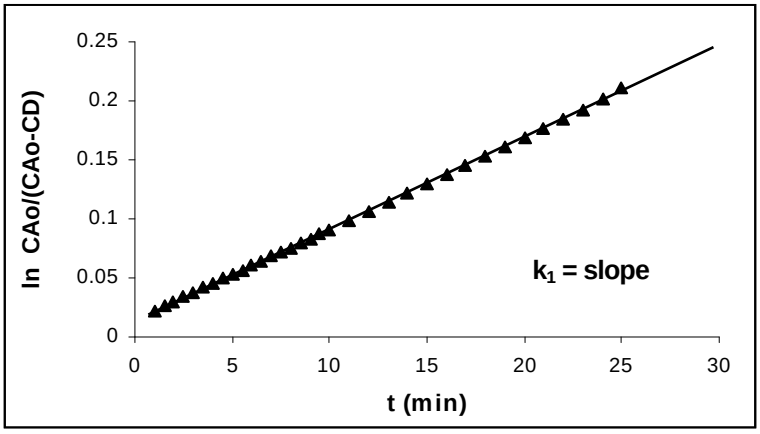

Figure 1. The plot of *ln* $[C_{Ao}/(C_{Ao} - C_D)]$ versus reaction time at T = 298 K, j = 1 mole.l^{-1}, $C_{Ao} = 1.95 \bullet 10^{-2}$ mole.l^{-1}, $[H^+] = 9.30 \bullet 10^{-3}$ mole.l^{-1} in water – 25 % vol DMFA mixture.

From equations (10) and (11), by introducing expressions (8) and (9), the result becomes:

$$C_D - C_{Ao}\left[1 - \exp\left(-k_1 t\right)\right] = C_{Ao}\left\{\frac{k_1}{k_1 - k_2}\left[\exp\left(-k_2 t\right)\right] - \frac{k_2}{k_2 - k_1}\left[\exp\left(-k_1 t\right)\right]\right\} \quad (13)$$

At high overall conversion (over70 ÷ 80 %), if $k_1 > k_2$, reaction (3) is already accomplished and variation of C_D is due only to reaction (4). Thus, at high *t*, values of *exp* $(-k_1 t)$ become negligible and equation (13) will be simplified at:

$$2C_{Ao} - C_D = C_{Ao}\frac{k_1}{k_1 - k_2}\exp\left(-k_2 t\right) \quad (14)$$

Its linear form is:

$$\ln\left(2C_{Ao} - C_D\right) = \ln\left(C_{Ao}\frac{k_1}{k_1 - k_2}\right) - k_2 t \quad (15)$$

Values of k_2 can be obtaind directly from experimental data, by using the plot of *ln* $(2C_{Ao} - C_D)$ versus reaction time (see equation 15), as ilustrated in figure 2.

Hence, individual rate coefficients k_1 and k_2 of reactions (1) and (2) respectively, can be determined ***directly*** from the experimental data:

- k_1 is calculated by using the plot of equation (12) and data collected at the beginning of the overall process
- k_2 is calculated by using the plot of equation (15) and data towards the end of the overall process.

Values of k_2 are independent of those obtained for k_1. For all experimental conditions, we found that.

- correlation coefficients of lines ilustrated in figures 1 and 2 were very good, between 0.9990 and 0.9994.
- $k_1 / k_2 \cong 2$, meaning that reaction (2) occurs aproximately twice as slow as reaction (1).

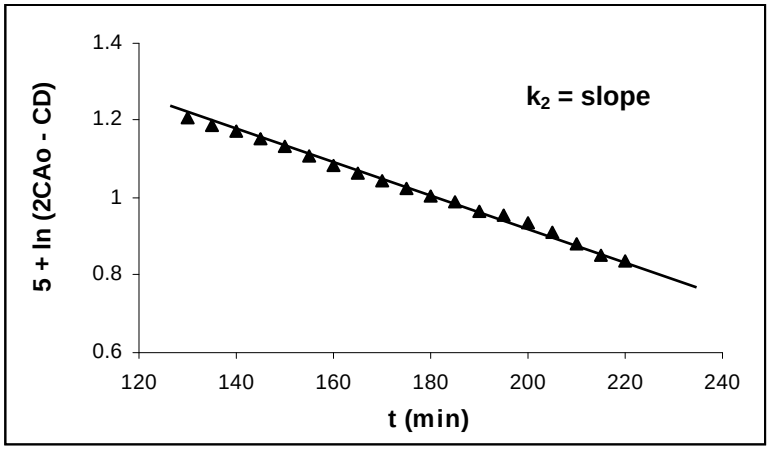

Figure 2. The plot of *ln* $(2C_{Ao} - C_D)$ versus reaction time at T = 298 K, j = 1 mole.l^{-1}, $C_{A0} = 1.95 \bullet 10^{-2}$ mole.l^{-1}, $[H^+] = 9.30 \bullet 10^{-3}$ mole.l^{-1} in water – 25 % vol DMFA mixture.

Validation of the method

Values of k_1 and k_2 obtained from experiments were used to calculate both the evolution of the electromotive force *E* of cell (5) and of the concentrations C_A, C_B, C_C and C_D during reaction time.

Figure 3 showes that the calculated plot $E = f(t)$ (see equation 6) superposes very closely the experimental one. The continuous line stands for calculated values, the circles for experimental values.

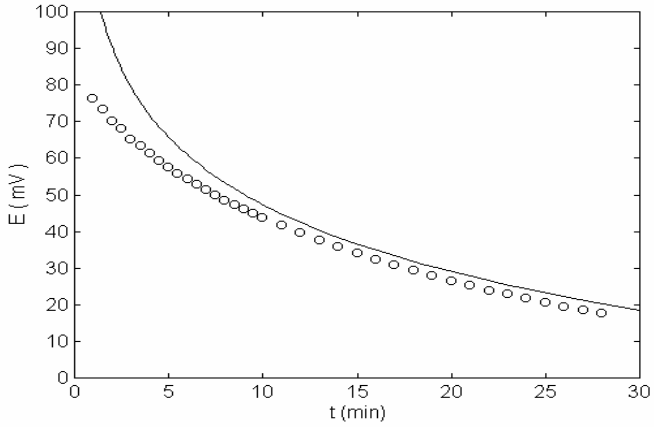

Figure 3. The calculated and experimental plots $E = f(t)$ at T = 298 K, j =1 mole.l^{-1}, $C_{A_0} = 1.95 \bullet 10^{-2}$ mole.l^{-1}, $[H^+] = 9.30 \bullet 10^{-3}$ mole.l^{-1} in water – 25 % vol DMFA mixture.

The slight difference at the beginning is due to the validity of relationship (6) only for $10^{-3} << C_D << 10^{-1}$ mole.l^{-1}, condition which is not respected during the first moments of processes (1) and (2).

The plots of equations (8) ÷ (11) are presented in figure 4. The concentration curves have tipical shapes for consecutive processes [10].

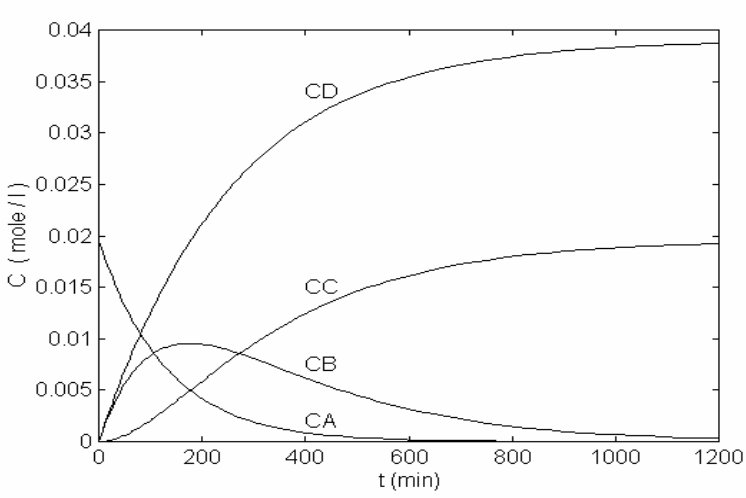

Figure 4. Calculated concentration curves at T = 298 K, j = 1 mole.l^{-1}, $C_{A_0} = 1.95 \bullet 10^{-2}$ mole.l^{-1}, $[H^+] = 9.30 \bullet 10^{-3}$ mole.l^{-1} in water – 25 % vol DMFA mixture.

Effect of acidity

The effect of hydrogen ion concentration on the reaction rate was studied at controlled temperature and ionic strength, in a water – 25 % vol DMFA mixture. Rate constants k_1 and k_2 obtained for a wide range of H^+ ion concentrations, are given in table 2 bellow.

Table 2.

Effect of hydrogen ion concentration on k_1 and k_2 at T=298 K, j =1 mole.l^{-1}, $C_{Ao} = 1.95 \bullet 10^{-2}$ mole.l^{-1} in water – 25 % vol DMFA mixture.

$[H^+]$ (mole.l^{-1})	10^4 k_1 (s^{-1})	10^5 k_2 (s^{-1})
$3.05 \bullet 10^{-5}$	62.40	51.00
$1.77 \bullet 10^{-4}$	15.50	21.80
$2.96 \bullet 10^{-3}$	3.60	9.40
$9.30 \bullet 10^{-3}$	2.36	6.75
$2.48 \bullet 10^{-2}$	1.20	5.37
$4.31 \bullet 10^{-2}$	1.34	5.15
$6.22 \bullet 10^{-2}$	1.26	4.85

The value of $[H^+] = 9.30 \bullet 10^{-3}$ mole.l^{-1} was obtained only by dissociation of the reactant acid $H[Co(DH)_2Br_2]$ itself. It was both measured as such and obtained from the dissociaton constant $K_a = 8 \bullet 10^{-3}$ mole.l^{-1} previously reported [9].

A differential method to determine reaction orders with respect to hydrogen ions, was employed. Figure 5 showes the plots of *ln* k_1 and *ln* k_2 versus *ln* $[H^+]$. Points lie on lines for both cases, with correlation coefficients of 0.9875 and 0.9888 respectively. The orders are negative and fractional (less than unity): 0.51 and 0.30 for process (1) and (2), respectively.

Rate coefficient k_1 decreases strongly when $[H^+]$ is increased and a trend to level off at $[H^+] > 10^{-2}$ mole.l^{-1} is observed. This value is an order of magnitude greater than that found previously by Zsako [8]. The dependence of k_1 on he acidity can be described by equation (16) with a corelation coefficient of 0.9980:

$$k_1 = A' + B' / [H^+] \qquad (16)$$

where A' = (2.22 ± 0.65)$\bullet 10^{-4}$ s^{-1} and B' = (1.85 ± 0.05)$\bullet 10^{-7}$ mole.l^{-1}.s^{-1} are constants.

Rate coefficient k_2 decreases strongly with increasing $[H^+]$ until aproximately $[H^+] = 10^{-2}$ mole.l^{-1}. Afterwards, its decrease slows down, but showes no trend to level off. No mathematical relationship having kinetic relevance and a good corelation coefficient, could be found with the available data, to expres the dependence of k_2 on acidity.

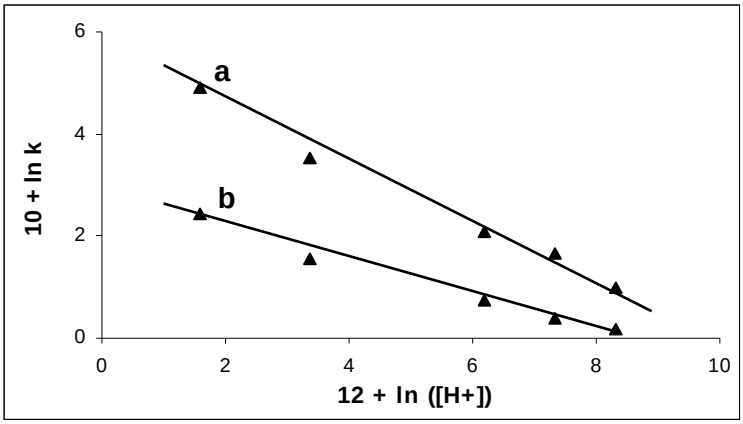

Figure 5. The plots of a.) *ln* k_1 and b.) *ln* k_2 versus *ln* $[H^+]$ at T =298 K, j =1 mole.l^{-1}, $C_{Ao} = 1.95 \bullet 10^{-2}$ mole.l^{-1} in water – 25 % vol DMFA mixture.

These findings may be explained by the existence of the following equlibria, even at the acidity of the reactant itself. Both the reactant $[Co(DH)_2Br_2]^-$ and the intermediate $[Co(DH)_2Br(H_2O)]$ are involved:

$$[Co(DH)_2Br_2]^- + H^+ \Leftrightarrow [Co(DH)(DH_2)Br_2] \quad (17)$$

$$[Co(DH)(DH_2)Br_2] + H^+ \Leftrightarrow [Co(DH_2)_2Br_2]^+ \quad (18)$$

$$[Co(DH)_2Br(H_2O)] \Leftrightarrow H^+ + [Co(DH)_2Br(OH)]^- \quad (19)$$

$$[Co(DH)_2Br(OH)]^- \Leftrightarrow H^+ \quad [Co(DH)_2Br(OH)_2]^{-2} \quad (20)$$

Equlibria (19) and (20) explain the slight decrease of k_2 for $[H^+] > 10^{-2}$ mole.l^{-1}.

The shift of equlilibria (17) and (18) towards the protonated forms is determined by te increasing hydrogen ion concentration of the mixture. The species $[Co(DH)(DH_2)Br_2]$ and $[Co(DH_2)_2Br_2]^+$ are most probably obtained by binding a hydrogen ion to the nitrogen atom of the nitrogen-oxygen groups within the dimethylglyoxime (DH). The hydrogen bridges in the DH will break and N-Co bonds will become weaker, while Co-Br bonds grow stronger. As a result, the substitution of bromide is more difficult.

The acvation process involves unprotonated as well as protonated forms. In strong acid media, the concentration of protonated forms is higher and the experimentally observed rate constants k_1 and k_2 will decrease.

Effect of solvent

The effect of solvent on reaction rates was studied by varying its dielectric constant. Experiments were performed at controlled temperature, ionic strength and hydrogen ion concentration, by adding N,N'-dimethylformamide (DMFA) to the reaction mixture. The values of rate constants k_1 and k_2 at different dielectric constants *D* of the medium are given in table 3.

Table 3 showes that k_2 is independent of *D*. Instead, k_1 slightly increases and reaction (1) becomes faster when the dielectric constant of the solvent decreases strongly. A possible explanation is based on the fact that at low *D*, hydrogen bridges within the dimethylglyoxime groups become more rigid and the Co-Br bonds are hydrolizable at an increased rate. Hence, acvation occurs easier. However, the available data are not enough to draw a doubtless conclusion.

Table 3.

Effect of solvent on k_1 and k_2 at T = 298 K, j = 1 mole.l^{-1}, C_{Ao} = 1.95•10^{-2} mole.l^{-1}, [H$^+$] = 9.30•10^{-3} mole.l^{-1}.

DMFA (% vol)	D	10^4 k_1 (s^{-1})	10^5 k_2 (s^{-1})
15	75.19	1.40	9.82
25	68.89	2.34	9.42
50	54.85	2.36	9.94

Effect of temperature

Temperature was varied within the range of 298 – 320 K, in order to study its effect on the reaction rates of processes (1) ad (2). Table 4 presents the values of k_1 and k_2 for various temperatures.

Table 4.

Effect of temperature on k_1 and k_2 at j = 1 mole.l^{-1}, C_{Ao} =1.95•10^{-2} mole.l^{-1}, [H$^+$] = 9.30•10^{-3} mole.l^{-1} in water – 25 % vol DMFA mixture.

T (K)	10^4 k_1 (s^{-1})	10^5 k_2 (s^{-1})
298	2.36	6.75
308	4.55	25.70
320	23.70	138.00

The plots of *ln k* versus *1/T* are linear for both processes, with very good corelation coefficients (0.9998 and 0.9999). The slope and the intercept provided the Arrhenius activation energy E_a and the preexponential factor *lnZ*, respectively. The activation enthalpy ΔH^* and entropy ΔS^* were obtained similary by plotting *ln (k/T)* versus *1/T*. Lines with corelation coefficients of 0.9858 and 0.9935 were found. Table 5 gives the activation parameters for reactions (1) and (2). The presented values are in good agreement with those reported previously [7,8,11].

Table 5.

Activation parameters at j = 1 mole.l^{-1}, C_{A_0} = 1.95•10^{-2} mole.l^{-1}, [H^+] = 9.30•10^{-3} mole.l^{-1} in water – 25 % vol DMFA mixture.

Reaction	E_a (KJ.mole^{-1})	ln Z	ΔH^* (KJ.mole^{-1})	ΔS^* (KJ.mole^{-1}.s^{-1})
(1)	107.9	34.5	105.3	33.4
(2)	113.8	37.0	111.2	53.5

Reaction mechanism

Because acvation of $H[Co(DH)_2Br_2]$ involves a ion-molecule interaction in both stages, the ionic strength of the medium will not affect reaction rates. Therefore, the sign and the magnitude of activation entropy ΔS^* were interpreted in order to propose a possible mechanism. Table 5 showes that for both processes, ΔS^* is positive and fairly small. This proves that solvatation of the activated complex in the rate determinig step is not different from that of the "parent" complex. Instead, the Co-Br bond is longer. This is possible only with a dissociative monomolecular substitution mechanism.

Hence, processes (1) and (2) occur as follows:

$$[Co(DH)_2Br_2]^- \Leftrightarrow [Co(DH)_2Br] + Br^- \quad \text{(Slow, } k_1\text{)} \quad (21)$$

$$[Co(DH)_2Br] + H_2O \rightarrow [Co(DH)_2Br(H_2O)] \quad \text{(Rapid)} \quad (22)$$

and

$$[Co(DH)_2Br(H_2O)] \Leftrightarrow [Co(DH)_2(H_2O)]^+ + Br^- \quad \text{(Slow, } k_2\text{)} \quad (23)$$

$$[Co(DH)_2(H_2O)] + H_2O \rightarrow [Co(DH)_2(H_2O)_2]^+ \quad \text{(Rapid)} \quad (24)$$

ACKNOWLEDGMENTS

We use this oportunity to thank Mr. Csaba Varhelyi from the Department of Analytical Chemistry of our faculty, for kindly preparing and providing the reactant $H[Co(DH)_2(H_2O)]$.

REFERENCES

1. I. Baldea, A. Rustoiu-Csavdari, *Studia Univ. "Babeş-Bolyai", Chem.*, 38(1-2), ***1993***, 31.
2. C. Mureşanu, I. Baldea, L. Oniciu, *Studia Univ. "Babeş-Bolyai", Chem.*, 40(1-2), ***1995***, 119.
3. I. Baldea, *Studia Univ. "Babes-Bolyai", Chem.*, 39(1-2), ***1994***, 138.
4. H.C. Blown, R.S. Fletcher, *J. Amer. Chem. Soc.*, 71, ***1949***, 1845.

5. B. Barnett, W.E. Wanghan, *J. Phys. Chem.*, 51, ***1947***, 926.
6. I. Cadariu, I. Baldea, *Studia Univ. "Babeş-Bolyai", Chem.*, 16(2), ***1971***, 93.
7. A. Sychev, V. Ablov, *Z. Neorg. Khim.*, 6(IV), ***1961***, 2292.
8. I. Zsako, Cs. Varhelyi, Z. Finta, *Studia Univ. "Babeş-Bolyai", Chem.*, 14(1), ***1969***, 51.
9. I. Zsako, Z. Finta, Cs. Varhelyi, *Studia Univ. "Babeş-Bolyai", Chem.*, 14(2), ***1969***, 145.
10. G. Niac, E. Schonberger, *Chimie Fizică*, Ed. Technică, Bucureşti, ***1970***, vol 3, 353-356.
11. J. Zsako, Cs. Varhelyi, *Magyar Kemiai Folyoirat*, 6, ***1994***, 257.

STUDIA UNIVERSITATIS BABEŞ-BOLYAI, CHEMIA, XLIII, 1-2, 1998

VOLTAMMETRIC RESPONSE OF FREE AND POLYMER ENTRAPPED BIS-(TRISALKOXY)-HEXAVANADATE

GRAZIELLA TURDEAN, OLIVIA SERDAN, SIMONA CURTICĂPEAN, IONEL CĂTĂLIN POPESCU[1]

ABSTRACT. The electrochemical behaviour of the dissolved and polymer entrapped trans-bis-(trisalkoxy)-hexavanadate (trans-BTHV) was studied by cyclic voltammetry performed at glassy carbon and carbon paste electrodes, in different experimental conditions (potential scan rate and pH). The free trans-BTHV showed a one pair of well defined peaks, corresponding to a 5 electrons quasi-reversible redox process. In the pH range 4.5 to 7 the voltammetric response of trans-BTHV, immobilized in AQ 55D polymer, consisted in two waves: a first one of 5 electrons at 0.15 V/SCE and a second one of 1 electron at –0.075 V/SCE (pH 6). In both cases, the dependence of peak current intensity on the potential scan rate proved that the redox process was controlled by diffusion.

INTRODUCTION

A modified electrode (ME) has been generally defined as a deliberate control of the molecular structure at the electrode surface, aimed at tailoring the electrode to meet specific applications. Thus, the IUPAC definition indicate that a ME is "an electrode made of a conducting or semiconducting material that is coated with a selected monomolecular, multimolecular, ionic or polymeric chemical film and by means of faradaic (charge-consuming) reactions exhibits chemical, electrochemical and/or optical properties of the chemical film" [1]. In the last years the CMEs became very attractive because of the wide range of their applications in electrochemical technology as well as in chemical analysis and energy conversion.

Modified electrodes can be prepared by several different techniques as follows: chemisorption, covalent binding or polymer film coating. Polymeric layers can be obtained starting from the preformed polymers (by dip coating, solvent evaporation or cross linking) or produced by *in-situ* polymerization (photo- or electrochemical polymerization) [1, 2]. Additionaly to the stability and to the long lifetime of the electrode, the most important advantage of ME with polymer matrix is that the multilayered coating provides a three dimensional reaction zone at the electrode surface, which gives rise to an increase in the flux of reactions that occur there, finally increasing the electrode sensitivity [3].

[1] *Department of Physical Chemistry, "Babes-Bolyai" University, 3400 Cluj-Napoca, Romania.*

Recently, considerable interest was focused on the preparation, investigation and development of inorganic polynuclear electrode materials, i.e. polyoxometalates. These offer large possibilities of composition variations with a direct applicability in many and various domains among electrocatalysis is the most relevant in the present context [4, 5, 6]. These mediators exhibit good stability, specific reactivity, fast redox transition leading to direct electron transfer, and facilitate the formal transfers of oxygen or hydrogen during electrode reactions [7].

Electrochemical characterization by cyclic voltammetry (CV) [6, 8, 9], cronopotentiometry [8] or UV - VIS spectroscopy [6] of some vanadium-containing heteropoly acids were reported. Muller and coworkers [10] taking in consideration that trisalkoxy-hexavanadate may be able to become an interesant redox catalyst depending on the variation of nature, position and number of trisalkoxy ligands, synthetised and characterized the cis- and trans- $(CN_3H_6)_2[V_6O_{13}\{(OCH_2)_3CCH_2OH\}_2] * H_2O$.

The aim of this paper is the electrochemical characterization, of the free and polymer entrapped trans–bis-(trisalkoxy)-hexavanadates (trans-BTHV), by cyclic voltammetry at two electrode materials: glassy carbon (GC) and carbon paste (CP) electrode. The voltammetric response, recorded in different experimental conditions (potential scan rate and pH), was analysed in order to be attributed to a redox process and to estimate the characteristic electrochemical parameters. Consequently, a comparison of the redox responses of cis- and trans- BTHV was performed.

EXPERIMENTAL

Chemicals

Pure bis-(trisalkoxy)-hexavanadate (trans-$(CN_3H_6)_2[V_6O_{13}\{(OCH_2)_3C-CH_2OH\}_2]*H_2O$) (trans-BTHV) was a kindle gift of Dr. Muller (*Bielefeld, Fakultät fûr Chemie der Universität*) and was used without further purification. The polyoxometalate solutions were freshly prepared just before using by dissolving the appropriate amounts of the salt into the supporting electrolyte. All other reagent grade chemicals were obtained from *Reactivul-Bucureşti*.

The supporting electrolyte was a 0.25 M solution of K_2SO_4. Its pH value was adjusted with 1/15 M phosphate buffer in the pH range 5.5-7 and with diluted phosphoric acid in the pH range 1-5.5. The 1/15 M phosphate buffer (pH 7) was prepared by mixing the appropriate volumes of $Na_2HPO_4*12H_2O$ and KH_2PO_4 solutions.

The poly(ester-sulphonic acid) polymer (Eastman Kodak AQ 55D) was purchased as a 28% aqueous solution from *Eastman Kodak Co., France*. The graphite powder (99.9% purity) was obtained from *Fluka, Germany* and the paraffin oil from *Fischer Oil, USA*. A glassy carbon disk (Type 16, *Hochtemperature-Werkstoffe GmbH, Thierhaupten, Germany*) (ϕ= 3.5 mm) was used as a working electrode. The carbon paste electrode CPE was obtained as previously described [11, 12].

Electrochemical measurements

The electrochemical characterization of the polyoxometalate was carried out using an undivided three electrode electrochemical cell (10 ml capacity), equipped with a saturated calomel electrode (SCE) and a platine electrode (~ 1 cm^2) as reference and counter electrode, respectively. As working electrode were employed a carbon electrode (GC) (ϕ = 3.5 mm), a carbon paste electrode (CP) (ϕ = 6 mm) and a glassy carbon modified electrode (ME). A fresh and clean surface of the GC electrode was obtained by polishing the electrode with emery paper (400-450 and 600 grit, *Buehler, Lake Bluff. Ill, USA*).

All cyclic voltammetry measurements were performed with a home made cyclic voltammetry set-up, including a low current potentiostat (Polarograph LP7e, *Czechoslovakia*), and an acquisition data module (AT MOI - 16F*, National Instruments, USA*) controlled by a AT-486-DX PC - computer (*Olivetti, Switzerland*). The software was elaborate based on LabVIEW 3.1. package [13].

All experiments were conducted at ambient temperature (20 ± 2℃) and at atmospheric pressure. All potentials are quoted with respect to the SCE.

Preparation of the modified electrode

The trans-BTHV-modified glassy carbon electrode (ME), was obtained by deposition on the electrode surface of a polymer film containing the salt of trans-BTHV. Thus, on the surface of a freshly polished and thoroughly rinsed (distilled water) GC electrode was deposited a mixture containing 100 µl AQ 55D polymer and 4 mg trans-BTHV. In order to obtain a strongly adherent trans-BTHV-AQ 55D film, the coated electrode was allowed to dry for 2 h at 45℃.

RESULTS AND DISCUSSION

The voltammetric response of the dissolved cis-BTHV on gold electrode showed two waves placed at $\varepsilon^{o'}$ = 0 V/NHE and $\varepsilon^{o'}$ = 0.57 V/NHE [10]. The first one was attributed to a 5 e^- process corresponding to the following reaction:

$$V_6^{(IV)}O_7(OH)_6\left\{(OCH_2)_3CCH_2OH\right\}_2]^{2-} \rightarrow [V^{(IV)}V_5^{(V)}O_{13}\left\{(OCH_2)_3CCH_2OH\right\}_2]^{3-} + 6H^+ + 5e^- \quad (1)$$

and the second one, involving 1 e^- transfer, was associated with:

$$[V^{(IV)}V_5^{(V)}O_{13}\left\{(OCH_2)_3CCH_2OH\right\}_2]^{3-} \rightarrow [V_6^{(V)}O_{13}\left\{(OCH_2)_3CCH_2OH\right\}_2]^{2-} + e^- \quad (2)$$

In order to compare the electrochemical behaviour of cis-BTHV and trans-BTHV the cyclic voltammograms of the trans-BTHV in solution were recorded in the pH range of 1 - 7. Contrarily to the cis-BTHV, the voltammetric response of the trans- BTHV presents one pair of well defined peaks (A1/C1, figures 1A, 1B), irrespective of the electrode materials (GC and CP). The corresponding peak currents decrease with the increase of the pH value, due to the low stability of the trans-BTHV in neutral media.

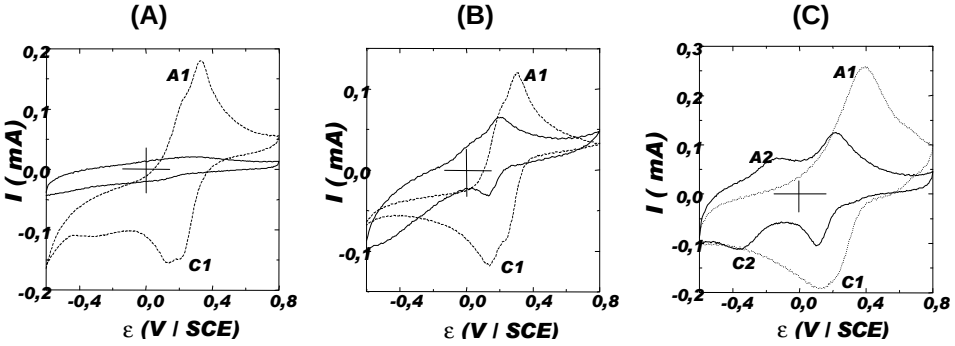

***Figure 1**. Voltammetric response of dissolved bis-(trisalkoxy)-hexavanadate at [GC (A), CPE (B)] and polymer entrapped in an Eastman AQ 55 D matrix (C). Experimental conditions: scan rate 75 mV/s; supporting electrolyte 0.25 M K_2SO_4, pH 2 (-- -- --) and pH 6 (-------); ambient temperature; starting potential - 0.6 V vs SCE.*

In the pH range 1-4, the trans-BTHV immobilized in a polymer matrix showed a similar voltammetric response to the dissolved compound. For higher pH values (4 - 7) a second wave (A2/C2) was observed (figure 1 C) in the lower potential domain, as was reported for dissolved cis-BTHV [10] at gold electrode.

The hight of A1/C1 wave suggested a 5 electrons redox process, corresponding to the reaction (1), while the A2/C2 wave was associated to an one electron transfer, described by the reaction (2).

The immobilization efficiency is proved by the following sequences of the A1/C1 peak currents: $(I)_{CP} < (I)_{GC} < (I)_{ME}$, observed at pH 2 and $(I)_{GC} < (I)_{CP} < (I)_{ME}$, noticed at pH 6. Moreover, at all pHs the redox response corresponding to the immobilized trans - BTHV was higher than that for dissolved compound.

In table 1 are presented the main electrochemical parameters of the A1/C1 voltammetric wave obtained from cyclic voltammograms recorded in the specified experimental conditions. The values of these parameters point out the redox process associate to the A1/C1 voltammetric wave as a quasi-reversible one, indifferent of the pH value or the immobilization state.

As a consequence of the immobilization, at pH 2, an increase of the electrochemical parameters ($\Delta\varepsilon_p$; $\varepsilon^{o\prime}$; $\varepsilon_p - \varepsilon_{p/2}$) was observed (table 1), suggesting the existence of some interactions between the trans-BTHV polyanion and the negatively charged polymer matrix. Contrarily, at pH 6, the decrease of $\Delta\varepsilon_p$, $\varepsilon^{o\prime}$and $(\varepsilon_p - \varepsilon_{p/2})_{anodic}$ values could be attributed to the protective effect of the polymer matrix on the polyanion stability.

Table 1.

Electrochemical parameters of the cyclic voltammetric response observed for dissolved (*) and polymer entrapped (**) trans-BTHV. Experimental conditions: see figure 1, v = 50 mV/s.

Elec-trode	pH = 2					pH = 6				
	$\Delta\varepsilon_p$ (mv)	$\varepsilon^{o'}$ (V)	Ipa/Ipc	$\varepsilon_p - \varepsilon_{p/2}$ (mV)		$\Delta\varepsilon_p$ (mv)	$\varepsilon^{o'}$ (V)	Ipa/Ipc	$\varepsilon_p - \varepsilon_{p/2}$ (mV)	
				anodic	cathodic				anodic	cathodic
GC*	221	0.111	0.92	126	-163	189	0.095	0.74	203	-
CPE*	180	0.090	1.17	139	-151	108	0.054	1.4	134	61
ME**	305	0.153	1.12	169	-217	110	0.055	0.54	69	90

As can be shown from reaction (1), the standard potential corresponding to the redox process associated to the peak A1/C1 should be pH dependent. Indeed, the cyclic voltammograms recorded at different pH values for free or immobilized trans-BTHV showed that the formal standard potential ($\varepsilon^{o'}$) (estimated as the average of the anodic and cathodic peak potentials) depends on the electrolyte pH (figure 2).

The number of protons (table 2) involved in the redox process, corresponding to the A1/C1 wave, were calculated from the slope $\varepsilon^{o'}$–pH dependence calculated for different electrodes, considering a 5 electrons transfer [10]. The obtained results revealed that in the 1 to 3.5 pH range 4 and 3 protons are involved in the redox process at GC, ME and CP electrodes, respectively. At pH > 4, the $\varepsilon^{o'}$ value became independent on the pH for all investigated electrodes.

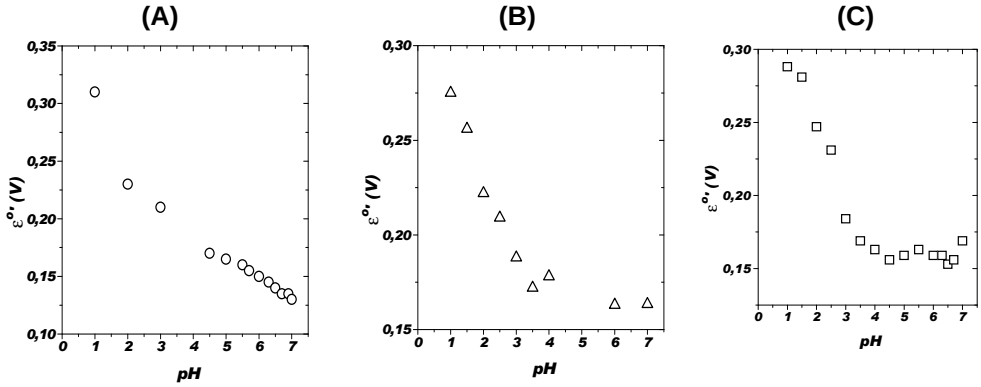

Figure 2. *pH dependence of formal potential of A1/C1 peak GC (○), CP (Δ) and ME (□). Experimental conditions: see figure 1.*

Table 2.

The protons number estimation corresponding to the A1/C1 peak process at the pH 1 - 3.5, v = 75 mV/s.

Type of electrode	GC	ME	CP
slope = 0.059 (p/n)	0.053	0.048	0.037
p/n	4.5/5	4.1/5	3.1/5
r	0.98	0.98	0.997

It is interesting to remark that the intensity of the A1/C1 peak slightly increase with the pH decrease (figure 3), proving once again the effect of pH on the trans-BTHV stability.

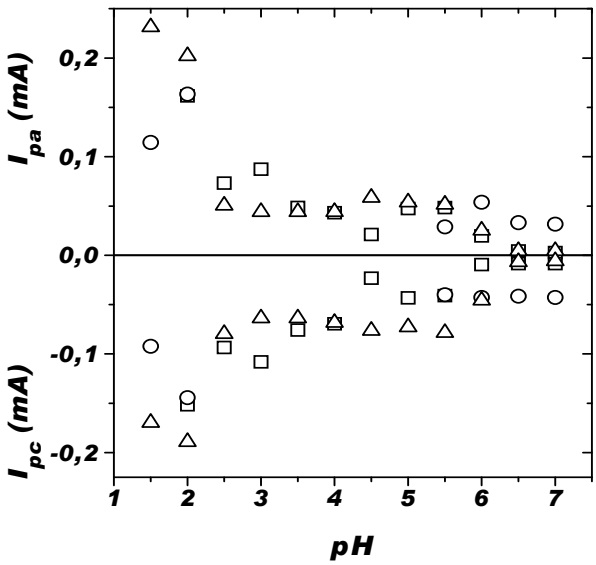

Figure 3. *Dependence the (A1/A2) peak currents on the pH: GC (❍), CP (Δ) and ME (*C). *Experimental conditions: scan rate, 75 mV/s; for other conditions see fig. 1*

As can be seen in figure 4, within the experimental errors, the peak currents corresponding to the A1/C1 wave depend linearly on $v^{1/2}$, proving a diffusion controlled process for all type of studied electrodes. This behaviour is expected for the dissolved trans-BTHV on GC and CP electrodes, while for ME proves that the trans-BTHV is freely diffusing within the AQ 55D-polymer matrix. In the same time, this finding offers a supplementary explanation for the low stability of the ME.

(A) **(B)** **(C)**

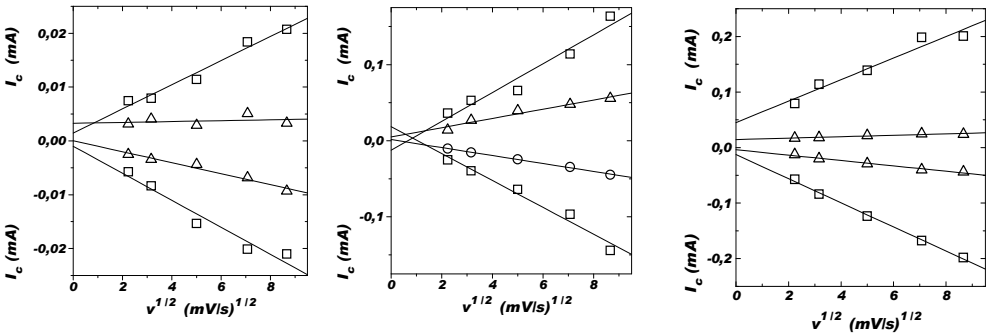

***Figure 4**. Dependence of the peak currents (A1/A2)on the potential scan rate for GC (A), CPE (B) and polymer modified electrod ME (C) at pH 2 ( ), pH 6 (Δ). Experimental conditions: see fig. 1.*

CONCLUSIONS

All the experimental results obtained converge to prove the feasibility of electrochemical characterization of trans-bis-(trisalkoxy)-hexavanadate free and immobilized on glassy carbon, carbon paste and glassy carbon, respectively. Contrarily of cis-BTHV and irrespective of the electrode materials (GC and CP), the voltammetric response of the dissolved trans- BTHV presented one pair of well defined peaks, corresponding to a 5 electrons quasi-reversible redox process.

In the pH range 4.5 to 7 the ME with polyoxometalate showed a relatively stable voltammetric response of the trans-BTHV immobilized in AQ 55D polymer, consisting in two waves: a first one of 5 electons at 0.15 V/SCE and a second one of 1 electron at –0.075 V/SCE (pH 6).

For all investigated electrodes, the influence of the potential scan rate on the peak current intensity showed that the voltammetric response was controlled by diffusion.

The effect of pH on the formal standard potential of the 5 electrons wave, placed at ~ 0.1 V/SCE, allowed to estimate the number of proton involved in the redox process, showing a participation of 4 and 3 protons for GC, ME and CP electrodes respectively.

ACKNOWLEDGEMENT

The authors thank to Dr. Achim Muller who has furnished the trans–bis-(trisalkoxy)hexavanadate as a kindly gift.

REFERENCES

1. R. A. Durst, R. W. Murray, R. P. Buck, K. M. Kadish and C. P. Andrieux – IUPAC Commision V.5, Project 19/83, 1983, 1-10.
2. A. Merz, Top. *Curr. Chem*., 1990, **152**, 49-90.
3. R. W. Murray, A. G. Ewing and R. A. Durst, *Anal. Chem*, 1987, **59(5),** 379A-390A
4. J. A. Cox, R. K. Jaworski and P. J. Kulesza, *Electroanal*., 1991, **3**, 869-877.
5. M. Sadakane and E. Steckhan, *Chem. Rev*., 1998, **98,** 219-237.
6. B. Keita, K. Essaadi, L. Nadjo and M. Desmadril, *Chem. Physics Lett,* 1995, **237**, 411-418.
7. R. W. Murray, in “Electroanalytical Chemistry", A.J. Bard ed, Marcel Dekker, New York, 1984, **13,** 191.
8. H. Wang, Z. Yu, E. Wang and E. Wang, *J. Electroanal. Chem*, 1995, **380**, 69-75.
9. A. Fodor, L. Muresan, A. Suteu and I. C. Popescu, *Studia Univ. Babeş-Bolyai. - Chemia*, 1996, **41(2)**, 247-251.
10. A. Muller, J. Meyer, H. Bogge, A. Stammler and A. Botar, *Z. Anorg Allgem Chem*., 1995**, 621**, 1818-1831.
11. G. Turdean, I. C. Popescu and L. Oniciu, *Rev. Roum. Chim*., 1998, **43(3)**, 203-208.
12. L. Gorton, Electroanalysis, 1995, **7**, 23.
13. P. Ilea, S. Dorneanu and A. Nicoara, *Rev. Roum Chim*, 1998, accepted.

STUDIA UNIVERSITATIS BABEŞ-BOLYAI, CHEMIA, XLIII, 1-2, 1998

THE LIPOPHILICITY DETERMINATION FOR SOME AMIDOESTERS OF ETHANOLAMINE WITH POTENTIAL BIOLOGICAL ACTIVITY BY REVERSED PHASE LIQUID CHROMATOGRAPHY

GABRIELA CÎMPAN[1], FLORIN IRIMIE[1], BOGUMILA MAKUCH[2], SIMION GOCAN[1], HENK A. CLAESSENS[3]

ABSTRACT. The lipophilicity of 13 derivatives, amidoesters of ethanolamine, with potential biologic activity, was studied by reversed phase liquid chromatography, on a LiChrosorb RP-18 column by using methanol-water and methanol-phosphate buffer (pH 7.0) as mobile phase. The extrapolated $\log k_W$ values, to 100% water as eluent was correlated with the calculated LogP values obtained from Pomona College database or by using Rekker's revised fragmental constant system. High correlation coefficients were obtained for the dependence $\log k = f(\varphi)$, where φ is the methanol concentration in the mobile phase, and for the relationships $\log k_W = f(\text{CLogP})$ or $\log k_W = f(\text{LogP}_{\text{Rekker}})$.

INTRODUCTION

The partition coefficient (log P) of a substance in a two-phase system consisting of n-octanol/water is often used to predict or to correlate its biological activity. Fujita et al. has proposed the n-octanol-water partition coefficient ($P_{O/W}$) as a standard measure of hydrophobicity of substances [1]. The determination of log P values of substances with potential biological activity by reversed-phase liquid chromatography (RPLC) can, in principal, overcome the difficulties of the conventional "shake-flask" method. The direct measurement of $P_{O/W}$ values by the latter method faces different problems as the necessary high purity of substances, which must be available in reasonable quantities and the fact that the method is not applicable to very hydrophilic or very hydrophobic compounds. In addition, this method is rather time consuming too. Since the first research of Meyer [2] and Overton [3], several techniques have been developed to determine substance

[1] Faculty of Chemistry and Chemical Engineering, "Babe¿-Bolyai" University, 11 Arany Janos street, 3400, Cluj-Napoca, Romania.
[2] Faculty of Chemistry, Technical University Gdansk, Poland.
[3] Department of Chemical Engineering, Technical University, P.O.Box 513, 5600, Eindhoven, The Netherlands.

lipophylicity experimentally, by the "shake-flask" method and by alternative approaches like e.g. chromatographic methods [4, 5]. In a recent review these techniques were thoroughly reviewed [6].

For some time RPLC is proposed as an alternative method for log $P_{O/W}$ determination, showing distinct advantages as speed of determination and better reproducibility compared to conventional methods. Furthermore, only small amounts of even contaminated samples are sufficient to use RPLC for this purpose [7-12]. Many researchers have discussed the use of RPLC as an attractive alternative method for the determination of log $P_{O/W}$ values using correlations between chromatographic data and the corresponding log $P_{O/W}$ values from other sources, e.g. shake-flask experiments or calculations. At present a substantial number of papers can be found in literature reporting the use of RPLC to establish octanol-water partition coefficients, with correlation coefficients between 0.5-0.999, depending on the applied columns and compounds under investigation [13-19]. Still there is debate on and to what extend the various parameters in RPLC, like e.g. nature of the reversed phase (RP) stationary phase and composition of the eluent, are of influence on log $P_{O/W}$ determination by RPLC.

13 amidoesters of ethanolamine were studied by RPLC. $Logk_W$ measurements were performed on LiChrosorb RP-18 column. LogP data were obtained from Pomona College and by using Rekker's revised fragmental constant system too [20-22]. $Logk_W$ values were obtained from the RPLC measurements by extrapolation to 100% water or buffer. The correlations between the experimentally obtained $logk_W$ values, and the log P data are discussed.

EXPERIMENTAL

The structures of the studied amidoesters of ethanolamine are shown in Figure 1. These are new compounds synthesized at Faculty of Chemistry and Chemical Engineering, and have plant growth stimulating activity, according to the Moewus test on *Lepidium Sativum* [23, 24]. The samples were prepared as methanolic solutions, 0.1 mg/ml.

All solvents were of analytical purity. Methanol was purchased from Merck (Darmstadt, Germany). Deionized water was obtained by a Milli-Q Water Purification System (Millipore, Bedford, MA, USA). Sodium phosphate ($NaH_2PO_4 \cdot H_2O$) was obtained from Vel (Leuven, Belgium) and was used for buffer solutions (pH 7.0) adjusted with NaOH 0.01M. Tricine (N-tris[hydroxymethyl]methylglycine) from Sigma (St. Louis, MO, SUA) was used as organic buffer.

Instrumentation

The instrumentation included a Beckman pump Model 100A (Beckman, Fullerton, CA, USA), a Merck-Hitachi AS-2000A autosampler (Merck, Darmstadt, Germany), an UV-VIS Philips detector (ATI Unicam, Cambridge, UK) and a PE Nelson 900 Interface (Perkin Elmer, San Jose, CA, USA). The detection

wavelength was 254 nm, the flow rate 1mL/min and the amount of sample solution was 10 μl/injection. The logk values were measured on a LiChrosorb® RP-18 column (5μm, L=119 mm, i.d. = 4 mm) (Merck, Darmstadt, Germany). The dead time, t_0, was measured for each experimental condition, using uracil as unretained compound.

Determination of $logk_W$ values

The retention factors were determined by RP-HPLC, using the following binary solvent systems as mobile phases: methanol-water, methanol-phosphate buffer (20 mM, pH 7.0) and methanol – Tricine buffer (20 mM, pH 7.0). The measurements were performed starting with 50% (v/v) methanol, gradually decreasing with increments of 10% to 30-40% organic modifier in the mobile phase. The compounds have a high degree of hydrophobicity, so that 3, maximum 4 measurements could be performed. In order to increase the reliability, every measurement was performed in triplicate and the mean value was used for calculations. The $logk_W$ values were obtained by extrapolation to 100% water as mobile phase, using the linear relationship logk = f(φ), where φ is the methanol concentration in the mobile phase.

RESULTS AND DISCUSSION

The calculated LogP values, CLogP, obtained from Pomona College database (Claremont, CA, USA), and $LogP_{Rekker}$, calculated by using Rekker's revised fragmental constant system [20, 21] are shown in Table 1.

A linear relationship is established between the calculated LogP values by using the two methods (equation 1).

$$LogP_{Rekker} = 0.083\ (\pm 0.624) + 1.078\ (\pm 0.246)\ CLogP \qquad (1)$$
$$s_{a0} = 0.083,\ s_{a1} = 0.078,\ s = 0.183,\ F = 93,\ r = 0.946,\ n = 13$$

where s_{a0}, sa1 are the standard errors for the intercept and the slope, s is the fit standard error, F is the statistic parameter for the F test, n is the number of compounds, and r is the correlation coefficient for 95% confidence limits.

The high values of correlation coefficients show that both values can be used in lipophilicity calculations. The $LogP_{Rekker}$ values have been calculated by the addition of the corresponding fragmental constants and a number of corrections, C_M=0.219, the so-called "magic constant", which were applied following Rekker's rules: 4 C_M for polar groups separated by an aliphatic carbon, 2 or 3 C_M for polar groups separated by two aliphatic carbons, 1 C_M for ortho substituents, and 1 C_M for extra chain-branching. The substitution of the pyridil fragment in para or meta position was not taken into account when calculation CLogP or $LogP_{Rekker}$ values, so that the pairs A1 – A9, A3 – A10, A4 – A11, A6 – A13 and A8 – A14 have the same LogP values.

Table 1. The calculated LogP values by using Rekker's revised fragmental constant system
($LogP_{Rekker}$), or obtained from Pomona College database (CLogP) for compounds A1-A13.

Compound	CLogP	$logP_{Rekker}$
A1	1.746	1.879
A2	2.920	3.167
A3	3.194	3.555
A4	2.599	2.607
A5	2.055	2.399
A6	2.584	3.137
A7	2.744	2.198
A8	2.245	2.617
A9	1.746	1.879
A10	3.194	3.555
A11	2.599	2.607
A12	2.584	3.137
A13	2.245	2.617

The degree of dissociation of residual silanol groups in the non-popular stationary phase, or the degree of (de)protonation of polar or ionic compounds cannot be controlled very well when using non-buffered eluents. The chromatographic behaviour of the studied amidoesters of ethanolamine was checked in buffered and in non-buffered eluents.

The linear correlations 2 for methanolwater and methanol-phosphate buffer, as well as the statistical data for 95% confidence limits are shown in Tables 2 and 3.

$$\log k = a_0 + a_1\varphi \qquad (2)$$

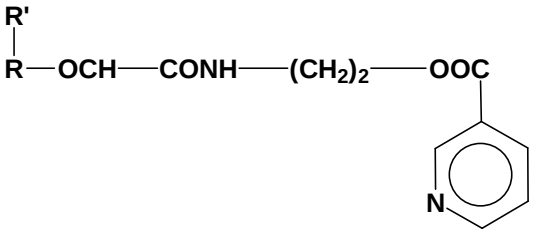

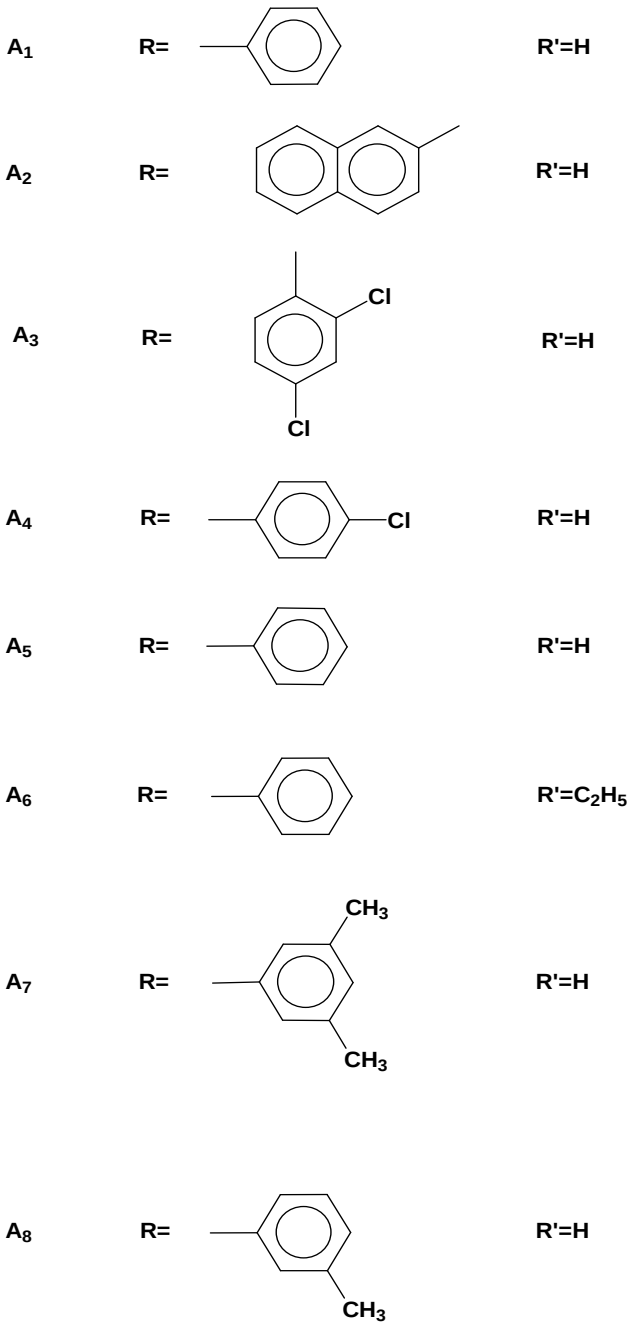

Figure 1. The structures of the studied amidoesters of ethanolamine

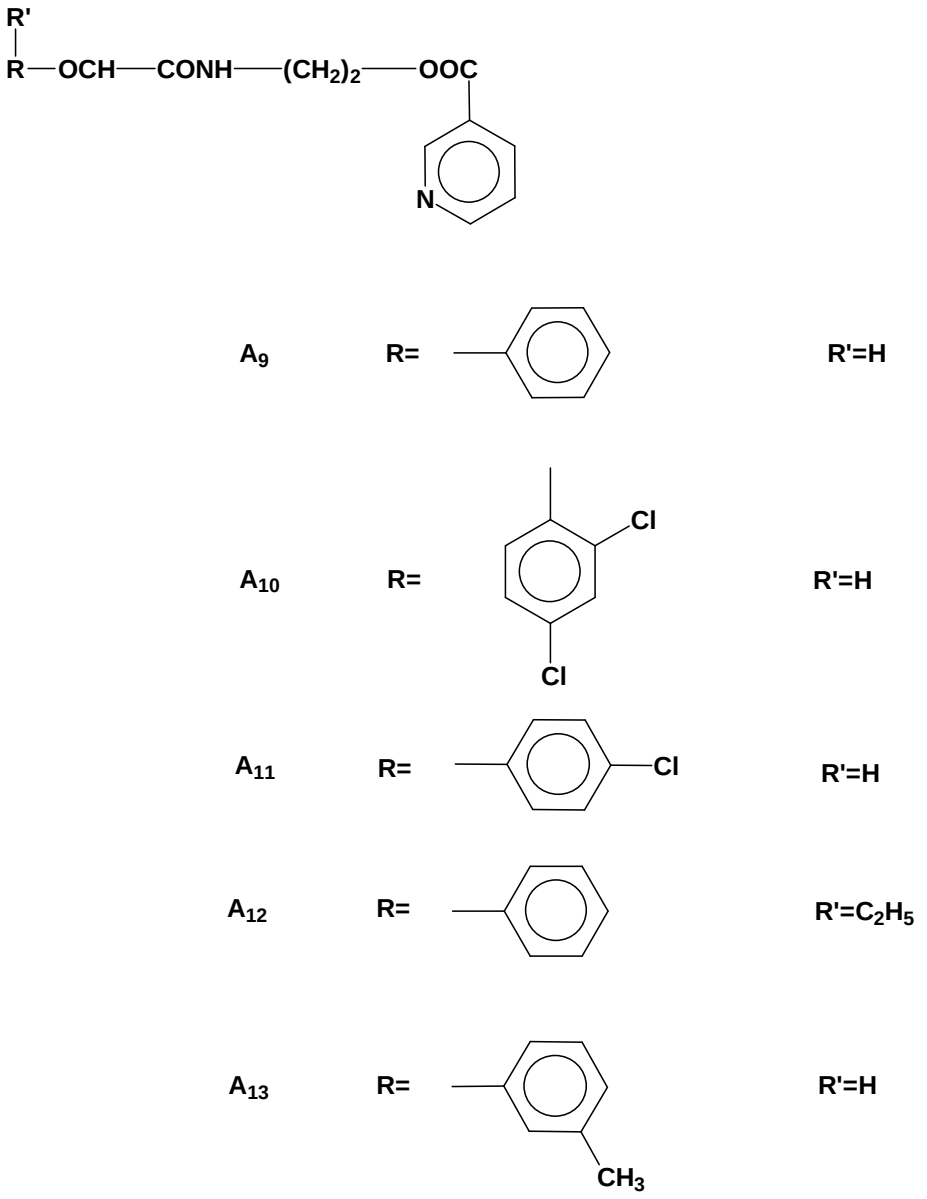

Figure 1.The structures of the studied amidoesters of ethanolamine

In order to check if the nature of buffering substance, inorganic or organic, influences the partition equilibrium of compounds between the stationary and the mobile phases, several experiments were performed with Tricine buffer (N-tris[hydroxymethyl]methylglycine], pH 7.0. The results (not shown) were in the

experimental error limits, so that the organic buffer does not influence the chromatographic behaviour of the studied compounds. This observation can be very important for compounds, which need high values of pH in order to be maintained in the neutral form. The RPLC experiments at pH>7.0 can be performed on silica-based stationary phases, only if the eluent is buffered with an organic substance.

Table 2. The $logk_w$ values obtained on LiChrosorb®RP-18 with methanol-water as mobile phase.

$a_0 = logk_w$ = the intercept of equation 2, a_1 = the slope (eq. 2)
s_{a0}, s_{a1} = standard errors for the intercept and the slope; s = fit standard error, F = the statistic parameter for F test, r = correlation coefficient, n = 13 (number of compounds); confidence limits 95%.

Compound	% (v/v) Methanol	a_0 ($logk_w$)	a_1	s_{a0}	s_{a1}	s	F	r
A1	60-30	2.882 ±0.495	-0.047 ±0.011	0.115	0.002	0.055	360	0.997
A2	60-40	3.662 ±1.932	-0.053 ±0.038	0.152	0.003	0.042	314	0.998
A3	60-40	3.989 ±1.691	-0.056 ±0.033	0.133	0.003	0.037	452	0.999
A4	60-30	3.519 ±0.417	-0.053 ±0.009	0.097	0.002	0.047	653	0.998
A5	60-30	3.051 ±0.480	-0.049 ±0.010	0.112	0.002	0.054	416	0.998
A6	60-30	3.550 ±0.459	-0.054 ±0.010	0.107	0.002	0.051	558	0.998
A7	60-40	3.615 ±1.914	-0.052 ±0.038	0.151	0.003	0.042	306	0.998
A8	60-30	3.564 ±0.509	-0.054 ±0.011	0.118	0.002	0.057	454	0.998
A9	60-30	2.965 ±0.484	-0.048 ±0.010	0.112	0.002	0.054	399	0.997
A10	60-40	3.988 ±1.486	-0.056 ±0.029	0.117	0.002	0.033	580	0.999
A11	60-30	3.590 ±0.462	-0.055 ±0.010	0.107	0.002	0.052	555	0.998
A12	60-40	3.574 ±0.465	-0.054 ±0.010	0.108	0.002	0.052	546	0.998
A13	60-40	3.557 ±0.479	-0.054 ±0.010	0.111	0.002	0.054	507	0.998

The correlation coefficients in Tables 2 and 3 are very good. Usually, the logk values for the compounds, which have the heteroatomic nitrogen in "para"

regarding the substituent, are a little higher than the corresponding values for "meta" position. Almost all logk data obtained in the buffered system are higher than the logk values obtained in methanol-water. This fact can be attributed to the neutral form of the molecule of studied compounds, which leads to a stronger retention. The small differences between the logk values obtained in buffered and non-buffered eluents shows the almost neutral character of the studied compounds.

The linear correlations between the extrapolated $logk_w$ values (to 100% water as eluent) and the calculated LogP values (CLogP and $LogP_{Rekker}$) are shown in equations 3-6.
methanol-water:

$$logk_w = 1.804(\pm 0.415) + 0.680(\pm 0.327)\ CLogP \quad (3)$$
$$s_{a0} = 0.189,\ s_{a1} = 0.074,\ s = 0.122,\ F = 84,\ r = 0.940,\ n = 13$$

$$logk_w = 1.877(\pm 0.459) + 0.585(\pm 0.162)LogP_{Rekker} \quad (4)$$
$$s_{a0} = 0.208,\ s_{a1} = 0.074,\ s = 0.138,\ F = 63,\ r = 0.922,\ n = 13$$

The statistical parameters in equations 3 - 6 have the same significance as in the legend of Table 2.

Table 3. The $logk_w$ values obtained on LiChrosorb® RP-18 with methanol-phosphate buffer (20 mM, pH 7.0) as mobile phase.
$a_0 = logk_w$ = the intercept of equation 2, a_1 = the slope (eq. 2)
s_{a0}, s_{a1} = standard errors for the intercept and the slope; s = fit standard error, F = the statistic parameter for F test, r = correlation coefficient, n = 13 (number of compounds); confidence limits 95%.

Compound	% (v/v) Methanol	a_0 ($logk_w$)	a_1	s_{a0}	s_{a1}	s	F	r
A1	60-30	2.804 ±0.397	-0.045 ±0.008	0.092	0.002	0.044	514	0.998
A2	60-40	3.591 ±1.654	-0.051 ±0.033	0.130	0.002	0.036	398	0.999
A3	60-40	3.931 ±1.375	-0.054 ±0.027	0.108	0.002	0.030	639	0.999
A4	60-30	3.364 ±0.331	-0.050 ±0.007	0.077	0.002	0.037	895	0.999
A5	60-30	2.919 ±0.331	0.046 ±0.007	0.077	0.002	0.037	769	0.999
A6	60-30	3.431 ±0.338	-0.051 ±0.007	0.079	0.002	0.038	922	0.999
A7	60-40	3.588 ±0.855	-0.051 ±0.017	0.067	0.001	0.019	1458	0.999
A8	60-30	3.461 ±0.367	-0.052 ±0.008	0.085	0.002	0.041	791	0.999

A9	60-30	2.868 ±0.352	-0.046 ±0.007	0.082	0.002	0.039	682	0.998
A10	60-40	3.926 ±1.654	-0.054 ±0.033	0.130	0.003	0.036	437	0.999
A11	60-30	3.401 ±1.282	-0.050 ±0.025	0.101	0.002	0.028	639	0.999
A12	60-40	3.513 ±0.313	-0.053 ±0.007	0.073	0.002	0.035	1130	0.999
A13	60-40	3.507 ±0.310	-0.052 ±0.007	0.072	0.001	0.035	1138	0.999

methanol-phosphate buffer (pH 7.0):

$$\log k_w = 1.659(\pm 0.464) + 0.701(\pm 0.183)\text{CLogP} \quad (5)$$
$$s_{a0} = 0.211,\ s_{a1} = 0.083,\ s = 0.136,\ F = 71,\ r - 0.931,\ n = 13$$

$$\log k_w = 1.707(\pm 0.461) + 0.613(\pm 0.163)\text{LogP}_{\text{Rekker}} \quad (6)$$
$$s_{a0} = 0.209,\ s_{a1} = 0.074,\ s = 0.139,\ F = 68,\ r = 0.928,\ n = 13$$

The differences between the linear correlations 3-6 for buffered and non-buffered eluent are smaller when $\text{LogP}_{\text{Rekker}}$ was included in the calculations, compared with CLogP. The data in Tables 2 and 3 shows that there are no significant differences between the retention parameters, logk, obtained in buffered or non-buffered mobile phases.

ACKNOWLEDGEMENTS

The autors gratefully acknowledge the Netherlands' Organization for International Cooperation in Higher Education (NUFFIC) for their financial support for a trainig scholarship in the Laboratory of Instrumental Analysis of the Eindhoven University of Technology, The Netherlands.

REFERENCES

1. T. Fujita, J. Iwasa, C. Hansch, *J. Am. Chem. Soc.*, 1964, ***86***, 5175.
2. H. Meyer, *Arch Exp. Pathol. Pharmakol.*, 1899, ***42***, 109.
3. E.Z. Overton, *Phys. Chem.*, 1897, ***22***, 189.
4. C. Hansch, T. Fujita, *J. Am. Chem Soc.*, 1964, ***86***, 1616.
5. A. Leo, C. Hansch, D. Elkins, *Chem. Rev.*, 1971, ***71***, 525.
6. L.G. Danielson, Yu-Hui Zhang, *Trends in Analytical Chemistry*, 1996, ***15***, 188.

7. A. Nahum, Cs. Horváth, *J. Chromatogr.*, 1980, ***192****i, 315.*
8. *Th. Braumann, J. Chromatogr.*, 1986, ***373***, 1981.
9. Th. Braumann, H.-G. Geniesner, C. Lüllmann, B. Jastorff, *Chromatographia*, 1987, ***24***, 777.
10. R. Kaliszan, *Anal. Chem.*, 1992, ***64***, 619A.
11. R.J.E. Grouls, E.W. Ackerman, H.H.M. Korsten, L.J. Hellebrekers, D.D. Breimer, *J. Chromatogr.B.*, 1997, ***694***, 421.
12. C. Helweg, T. Nielsen, P.E. Hanion, *Chemosphere*, 1997, ***34***, 1673.
13. C. Tanford, *The Hydrophobic Effect*, Wiley, New York, 1980.
14. N. El Tayar, H. van de Waterbeemd, B. Testa, *Qant. Struct. -Act. Relat.*, 1985, ***4***, 69.
15. C. Hansch, A. Leo, *Substituent Constants for Correlation Analysis in Chemistry and Biology*, Wiley, New York, 1979.
16. M. Harnink, H.J. Mörkel, G. Schulze, *J. Chromatogr.*, 1983, ***282***, 315.
17. J.G. Dorsey, M.G. Khaledi, *J. Chromatogr. A.*, 1993, ***656***, 485.
18. R. Kaliszan, A. Nasal, A. Bucinski, *Eur. J. Med. Chem.*, 1994, ***29***, 163.
19. M. Henczi, J. Nagy, D.F. Weaver, *J. Pham. Pharmacol.*, 1995, ***47***, 345.
20. R.F. Rekker, *The Hydrophobic Fragmental Constant* (Pharmacochemistry Library, vol. 1), Elsevier, Amsterdam, 1977.
21. R.F. Rekker, R. Mannhold, *Calculation of Drug Lipophilicity. The Hydrophobic Fragmental Constant Approach*, VCH, Weinheim, Germany, 1992.
22. A.J. Leo, *Chem Rev.*, 1993, ***93***, 4.
23. F. Irimie, *PhD. Thesis*, "Babeş-Bolyai" University, Cluj-Napoca, Romania, 1993.
24. F. Irimie, S. Mager, E. Brown, M. Horn, *Rev. Roum. Chim.*, 1995, ***40***, 369.

STUDIA UNIVERSITATIS BABEŞ-BOLYAI, CHEMIA, XLIII, 1-2, 1998

THE SYNTHESIS AND THE STUDY OF THE COORDINATION POLYMERS OBTAINED BY THE INTERACTION BETWEEN Pd(II) ACETYLACETONATE WITH DIPHENYLPHOSPHINIC, DIPHENYLTHIOPHOSPHINIC AND DIPHENYLDITHIOPHOSPHINIC ACIDS AS LIGANDS

IOAN ROŞCA, MIHAELA VIZITIU, DAN SUTIMAN, ADRIAN CĂILEAN, DOINA SIBIESCU, IULIAN RUSU

ABSTRACT. The synthesis and the study of some coordination polymers derived from the interaction of acetylacetonate of Rh(II) with diphenyl-phosphinic acid, dipheylthiophosphinic acid and diphenyldithiophosphinic acid are presented. The methods applied for the study are: chemical analysis, IR-absorption spectra, ESR, Spectroscopy, X-ray diffraction, the registration of some curves on a derivatograph and the determination of the kinetics parameters of the thermal decomposition reactions. Based on experimental data and on literature indications, the structural formulas of these compounds are assigned.

INTRODUCTION

From the synthesis of the first compound derived from the class of polymers obtained by the interaction between acetylacetonate of metals with organophosphinic acids (poly-[diμ-diphenylphosphinato-acetylacetonate Cr(III)] obtained in 1962 [1] till present days a lot of compounds were synthesized and studied. The obtained compounds presented similar structures and some important practical properties (semiconductors, birefrigence anticorrosive protection, high thermal stability, a.s.o.) [2-9]. Almost all the synthesized compounds are coordinated polymers.

In this work, a continuation of the authors research in this field is presented. The paper consists in the synthesis and the study of the obtained coordination polymers by the interaction of Pd(II) acetylacetonate with the following acids: diphenylphosphinic, diphenylthiophosphinic and diphenyldithiophosphinic.

The IR-absorption spectra, ESR and X-ray diffraction spectra were recorded and also the derivatographic curves in order to determine the kinetics parameters of the thermal decomposition were registred. The molecular weight was determined and the dispersion curves were registred by a gel-cromatograph.

RESULTS AND DISCUSSIONS

a) The synthesis, the elemental analysis, molecular weight and dispersion degree. The synthesis of the studied compounds occurred by different methods and conditions but the best results obtained through the direct reaction between Pd(II) acetylacetonate and one of the acids: diphenylphosphinic, diphenylthiophosphinic and diphenyldithiophosphinic at a molar rate of 1 : 2, by heating for two hours and a half, at a temperature of 170^0C. The heating process lasted until in the resulted gas-compounds (containing acetylacetone) the characteristic reaction for acetylacetone with the ferric ion is not observed. When the reaction was over, the final compounds were wasched with distilled water and then dried at the temperature of 150^0C at constant weight. After drying, the soluble fractions from these compounds were separated by solving them in ethanol and then in benzene. The solubility of these compounds in ethanol varied between 2-3% and in benzene between 3-5%. The most soluble compound was the polymer derived from Pd(II) acetylacetonate with diphenyldithio-phosphinic acid.

The determined chemical composition obtained by classic methods applied to the soluble and insoluble samples in the mentioned solvents is presented in Table 1. It is shown that the experimental values are almost equal to those determined by calculations. Together with the values of the chemical composition, the molecular weight determined by cryoscopic methods applied in benzene are also presented in Table 1.

Table 1.

Elemental composition (%) and molecular weight for the synthesized

The compounds derived from:	Pd^{2+}	C	P	O	H	M
	calc. exp.	calc. exp.	calc. exp.	calc. exp.	calc. exp.	
$Pd(Acac)_2$ + $2(C_6H_5)_2PO_2H$	19.69 19.80	53.29 53.50	11.47 11.65	11.84 11.92	3.70 3.82	3800
$Pd(Acac)_2$ + $2(C_6H_5)_2POSH$	18.58 18.75	50.31 50.40	10.82 10.95	5.59 5.72	3.49 3.54	5200
$Pd(Acac)_2$ + $2(C_6H_5)_2PS_2H$	17.60 17.69	47.65 47.74	10.25 10.53	- -	3.30 3.41	5.500

We considered useful to apply this method for determining the molecular weight, because some other researchers (for example, Black [1] and others [2-9]) applied it for the same type of coordination polymers, so it is interesting for comparison reasons.

All the synthesized compounds are brown solids.

From the chemical analysis and from the ratio of the reactants, it is shown that chemical reactions occur as following:

$$n\,Pd(Acac)_2 + 2n(C_6H_5)_2PO_2H \rightarrow \{Pd[(C_6H_5)_2PO_2]_2\}_n + 2n\text{HAcac}$$
$$n\,Pd(Acac)_2 + 2n(C_6H_5)_2POSH \rightarrow \{Pd[(C_6H_5)_2POS]_2\}_n + 2n\text{HAcac}$$
$$nPd(Acac)_2 + 2n(C_6H_5)_2PS_2H \rightarrow \{Pd[(C_6H_5)_2PS_2]_2\}_n + 2n\text{HAcac}$$

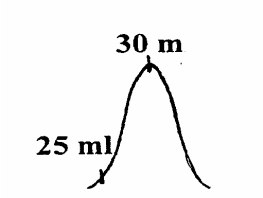

Fig. 1. The registred gel-cromatography curve for Pd-I using styrex and ciclohexanone as eluent

For an easier writing of the formulas, the following notations are used: $\{Pd[(C_6H_5)_2PO_2]_2\}_n$ is noted Pd-I, $\{Pd[(C_6H_5)_2POS]_2\}_n$ is noted Pd-II, $\{Pd[(C_6H_5)_2PS_2]_2\}_n$ is noted Pd-III.

For all the synthesized compounds the dispersion degree was determined using the gel-cromatographic method. The instrument used was a Watter type cromatograph with a column filled with styrex, using as solvent ciclohexanone.

From the registered curves it is shown that all the compounds presented a single peak not very sharp (Fig.1). As sharper the peak is as omogenous the polymer is concerning the polymerization degree and the structure. The volume of eluent (ml) where the peak appears is conversely proportional with molecular weight of the respective polymer.

b) Thermal-gravimetric-analysis and the establishing of the kinetics parameters of the thermal decomposition. For the thermal-gravimetric analysis, a derivatograph Paulik-Erdey was used; the samples used had 50 mg weight, at a heating speed of 10^0C/min and the temperature was between 20^0C and 700^0C.

Studying the registred curves obtained by derivatographic method of the synthesized compounds, it can be observed that the thermal destruction occurs in phases, by releasing gaseous products derived from the organic parts of the used acids. The final solid compounds resulting from the reaction correspond as chemical composition to Pd(II) metaphosphat.

The thermal destruction occurs in two stages for all the synthesized compounds and starts at a temperature of about 300^0C (Table 2). The reaction order and the activation energy corresponding to the thermal decomposition stages are determined using the Freeman and Carol method [10] (Table 2).

Table 2.

The two stages of the thermal decomposition, the values of the reaction order and of the activation energy [kj/mol]

The compound	Stage 1 (^{0}C)		Stage 2 (^{0}C)		Reaction order		Activation energy	
	Start	End	Start	End	Stage 1	Stage 2	Stage 1	Stage 2
Pd-I	295	390	390	560	0.83	0.88	150	175
Pd-II	285	375	375	570	0.80	0.85	135	158
Pd-III	280	370	370	570	0.80	0.85	130	150

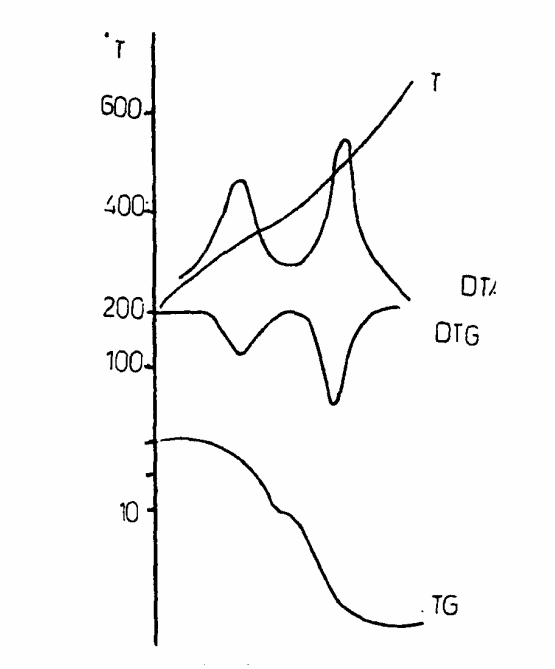

Fig. 2. The derivatographic curves of Pd-I.

From the experimental data it is shown that the beginning of the thermal decomposition for the synthesized compounds occurs at lower temperatures for the S-containing compounds than fot the similar ones without S-atoms (Table 2). This fact is justified by the exterior electronic structures of the S-atoms that is less stable more polarizable and with a greater reducing character of sulphur in comparison with the structure of O-atoms from the groups from the synthesized compounds.

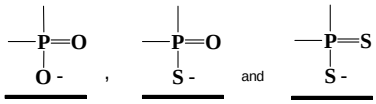

c) The IR-Absorption Spectra. The IR-absorption spectra of the studied compounds were registred using an instrument "Unicam" with a frequency band of 400-4000 cm^{-1}. Primarly, it was studied the absorption in the field of frequncy 950-1250 cm^{-1} that is characteristic for the groups PO_2 and PS_2.

Generally, the IR-absorption spectra of the synthesized compounds are similar with those of the free acids. The differences arise only in the field of absorption of the groups $>PO_2^-$, $>POS^-$ and PS_2^- due to the coordinaton to the central atom Pd(II):

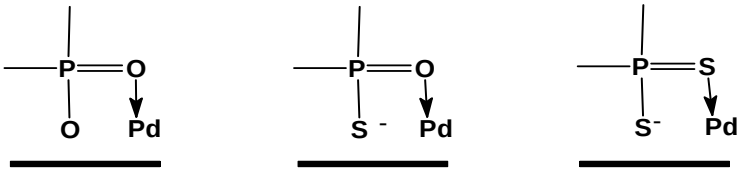

For the group P=O, the characteristic absorption spectra, $\nu_{P=0}$ is between the values 1261 cm^{-1} and 1087 cm^{-1}, for the molecules that contain hydroxilic (-OH) groups bound to the phosphorous atom [11,12].

For the acid $(C_6H_5)_2PO_2H$, were observed a diffuse band in the 3000-3100 cm^{-1} range and two usual bands in the 2200-2360 cm^{-1} and 909-932 cm^{-1} ranges.

For the compounds that contain the group, 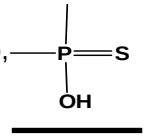 the following tautometric equilibria is observed:

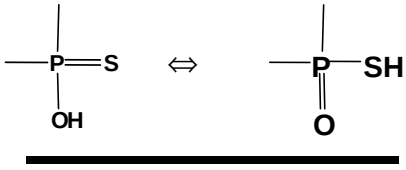

The substitutes presenting an electronic deficiency decrease the basicity of the group P=O and are favorable to the formation of the thiolic-isomer. The group P=S is less basic than the group P=O and that is why the equilibrium is favorable to the formation of the thio-isomer in benzene and chlor-benzene media. In aqueous or alcoholic solutions, the equilibrium is favorable to the thio-isomer.

For the coordinated groups and 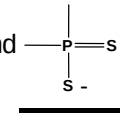 to 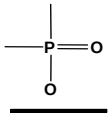 the central atom Pd(II), the frequencies of the absorption vibrations $\nu_{P=O}$, $\nu_{P=S}$ for the free acids and for the coordination compounds derived from the same acids, differences noted $\Delta\nu$, the following equation is established:

$$\Delta\nu = \frac{\nu - \nu'}{\nu} \cdot 100$$

This equation represents the percent modifications of the vibration frequencies of the same group (P=O or P=S) from free acids towards the synthesized compounds.

The values corresponding to the synthesized coordination compounds Pd-I, Pd-II, Pd-III are 3.1, 3.9, 4.5. These values show a stronger bound of the P=S groups in the coordination compounds in comparison with the P=O groups.

d) The ESR-Spectroscopy. The ESR-spectra were registred for the solid samples with a spectrometer RES-IFA Bucharest.

Studying the ESR-spectra it was shown that the central atom Pd(II) had one of the two possible electronic structures $4d^8$:

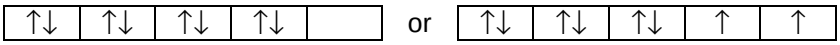

From the experimental data it is noted that all the synthesized compounds presented in this paper have a diamagnetic stucture, which means that the exterior electronic structure is formed by pairs of electrons in orbitals: 4d, 5s and 5p; the central atom Pd(II) has a planar structure as it is observed in almost all complex combinations of this metal [13-15].

e) The X-ray Diffraction Spectra. The X-ray diffraction spectra for the synthesized compounds were registred using a Kristalloflex-Siemens instrument that has a Roentgen tube with Cu(K) radiations filtred through Ni. The anode voltage is 35 kV and the intensity is 12 mA. The irradiation technique consists in transmission using the continuous exploration of the diffraction spectra with Geiger-Müller counter situated on a texture goniometer. The diffraction field was of $2\theta = 10\text{-}45^0$. From the X-ray diffraction spectra the crystallinity degree was established using the equation:

$$X_C = \frac{F_C}{F_C + F_A} \cdot 100 ,$$

where: F_C represents the crystalline halo area and F_A - the amorphous halo area.

All the synthesized compounds have a bi-phase structure: one characteristic for the amorphous state and the second with diffraction lines characteristic for the crystalline phase. The crystallinity degree for the synthesized compounds is relatively small having the values: 23% for Pd-I; 16% for Pd-II and 12% for Pd-III.

CONCLUSIONS

The proposed structure for the synthesized compounds

From the chemical analysis it is shown that for every central atom of Pd(II) correspond two anions of: diphenylphosphinic, diphenylthiophosphinic or diphenyl-dithiophosphinic acids. These data mean that the central atom Pd(II) is surroundet with four oxygen atoms or four sulphur atoms or two oxygen and two sulphur atoms or two oxygen and two sulphur atoms derived from the two anions of the respective acids:

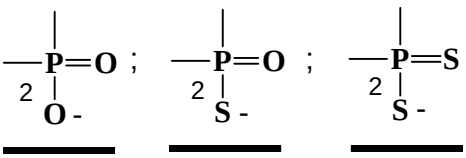

From the IR-absorption spectra it was deduced that the groups $\underline{>PO_2^-}$, $\underline{>POS^-}$ and $\underline{>PS_2^-}$, from the acids are bidentate coordinated.

Every central atom is bounded with two acid anions and tetracoordinated structures of Pd(II), result which can be tetrahedron or planar. Because of ESR-spectroscopy shows that all the synthesized compounds are diamagnetic, the conclusion is that the dsp^2 hybridization is established and the planar configuration of Pd(II) as central atom results.

From the experimental data it is shown that all the synthesized compounds are polymers having the molecular weights, for the benzene soluble fractions, between the limits 3800-5500, that correspond to a polymerization degree of 7 and 9, respectively.

Based on the mentioned facts, it results that the structures of the synthesized coordination compounds are those of a polymer derived from the concatenation of the planar structures of the central atom Pd(II) (Fig.3). This resulted structure is similar to literature indications [14,15] concerning the planar structures of almost all tetracoordinated compounds of Pd(II).

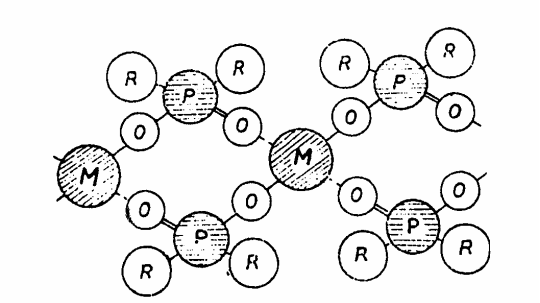

Fig. 3. The structure assigned for the synthesized compounds

REFERENCES

1. P.B. Block, J. Simkin, R.L. Ocone, *J.Am. Chem. Soc.*, 1962, ***84***, 1749.
2. A. Stone, G.A.W. Graham, *Inorganic Polymers*, Acad. Press, London, 1962.
3. V.V. Korsak, P.C. Krukovski, *Viskomolek Soed.*, 1967, ***A69***, 583.
4. T. Golotiu, I. Roşca, *Makromolek. Chem.*, 1972, ***160***, 59.
5. I. Roşca, *Viskomolek. Soed.*, 1985, ***B1***, 34.
6. I. Roşca, *Viskomolek. Soed.*, 1985, ***B10***, 735.
7. C. Silvestru, I. Haiduc, *J. Organomet. Chem.*, 1989, ***365***, 83.

8. C. Silvestru, I. Haiduc, F. Caruso, M. Rossi, B. Mahieu, M. Gielen, *J. Organomet.Chem.*, 1993, ***448***, 75.

9. I. Roşca, D. Sutiman, A. Cailean, M. Vizitiu, I. Rusu, D. Sibiescu, *Thermochim. Acta.*, 1995, ***269/270***, 295.

10. S.E. Freeman, B. Carol, *J. Phys. Chem.*, 1958, ***62***, 394.

11. I. Kossler, *Methoden der Infrarot Spectroscopie in der chemischen Analyse*, Akad. Verlog., Leipzig, 1961.

12. K. Nakamoto, *Infrared Spectra of Inorganic and Coordination Compounds*, John Wiley & Sons, Inc. New York, London, 1963.

13. A. Okaya, *Paramagnetic Resonance*, Akad. Press, New York, 1963.

14. 0J. Lewis, R.G. Wilkinson, *Modern Coordination Chemistry*, London, New York, 1988.

15. M. Brezeanu, P. Spacu, *Chimia combinațiilor complexe*, Ed. Did. Pedag., Bucharest, 1986.

STUDIA UNIVERSITATIS BABEŞ-BOLYAI, CHEMIA, XLIII, 1-2, 1998

HYDRODYNAMICS OF A NEW TYPE OF STRUCTURED PACKING

MIHAELA DRAGAN[1], A. FRIEDL[2], M. HARASEK[2], S. DRAGAN[1] and I. SIMINICEANU[3]

ABSTRACT. New bench scale measurements of the gas-side pressure drop have been carried out using columns equipped with two different packings: conventional Raschig rings, and a structured packing of Mellapak 750 Y type. The pressure drop per unit height, at the same loading, was about twenty folds smaller in the structured packing. The data have been further correlated on the basis of a new fluid-dynamics model, valid for any type of packing. It has been found that the packing constant C_p is not dependent only on the texture of the packing. It linearly increases with the liquid load.

INTRODUCTION

The main applications for packed columns are the separation processes such as absorption, desorption, rectification, and extraction. In the last few years these processes were not still confined to petroleum refineries, chemical and allied industries but they were adopted on wider scale in ecological engineering for purifying off –gas streams and for water treatment. Consequently, the demand for the necessary equipment, including packing, is growing.

A major criterion in selecting the packing for absorption process, in which the gas is forced through the column by a compressor, is the *pressure drop* in the bed. It largely governs the compressor rating and the final operating cost of the process. The pressure drop per unit height of bed depends on the gas and liquid load, as well as on the hydrodynamic characteristics of the packing.

Packing stacked in a regular pattern, also called *structured packing*, makes it possible to decrease the pressure drop per theoretical stage and is therefore most suitable for minimizing energy consumption in separations that necessitate many stages. It also permits the lowest possible temperature at the column bottom in the separation of heat – sensitive mixtures. Maldistribution, which is often observed in conventional beds and which greatly impairs the efficiency can be largely avoided with this new types of column interiors. A factor that restricts their widespread acceptance is the capital investment cost. They are considered uneconomical at pressure drops higher than 10 mm WG per theoretical stage [1]. New and cheaper, yet more effective structured packings had to be developed. Mellapak 750 Y, recently

[1] *University "Babeş-Bolyai" of Cluj- Napoca, Romania, E-mail: dmihaela@mailcity.com.*
[2] *Technical University of Vienna, Austria.*
[3] *Technical University of Iaşi, Faculty of Industrial Chemistry, 71 Bd. Mangeron, 6600 Iaşi, Romania, Fax: 40-32-211667, E-mail:isiminic@ch.tuiasi.ro.*

introduced on the market by Sulzer, is one of the most promising structured packings.

The optimum design of absorption columns equipped with such new packings requires sound mathematical models derived from comprehensive physical relationships between the packing performance, the fluid dynamics, and the properties of the system to be separated. Until now, the approach commonly followed was to use semiempirical equations with uncertain limits of application [1]. The specific models derived to predict the pressure drop in particular geometric packing [2-5] don't allow a comparison of different packings performance. Bravo et al. [6] have proposed a more comprehensive model but, because of the large number of adjustable parameters, its application in ranges outside the tested region can lead to sizable errors [1].

A more general model, including a single packing constant (C_p) is derived and tested in this work. The model, based on the Billet's fluid-dynamics assumptions [7], describes the resistance to flow in terms of column load and liquid holdup, the physical properties of the liquid -gas system, and the packing characteristics. On the basis of experimental data, the constant C_p is identified for the Mellapak 750Y type of structured packing.

EXPERIMENTAL

The flow chart of the bench-scale plant used for the absorption rate and pressure drop measurements is reproduced in the Figure 1.

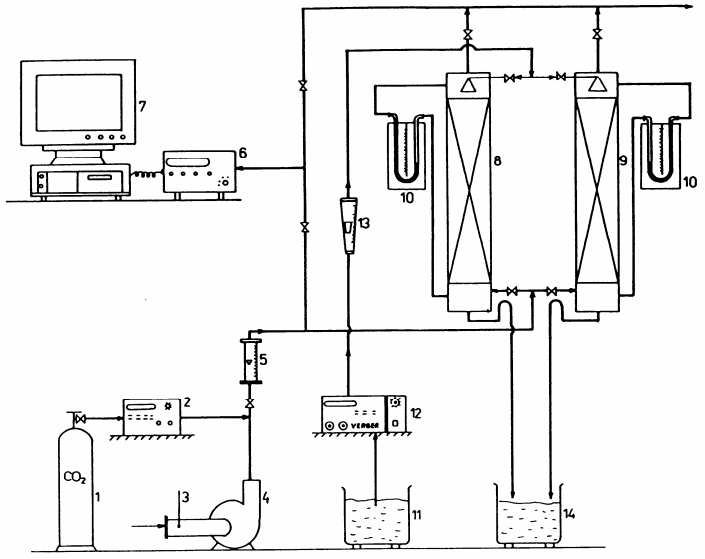

Figure 1. The experimental bench-scale plant
1- carbon dioxide cylinder, 2- carbon dioxide mass-flow meter, 3-air temperature controller, 4- air blower, 5- rotameter, 6- gas analyzer, 7- IBM compatible personal computer, 8/9- absorption columns, 10- manometer (mm WG), 11/14- solution tanks, 12- liquid pump, 13- liquid rotameter.

The first absorption column was equipped with a conventional bed of random packing: Raschig rings made of glass, with a nominal diameter of 10 mm. The second column contained an almost equal volume of Mellapak 750 Y structured packing from Sulzer SA. Geometrically, this was made of corrugated sheets arranged in parallel, successive layers having an opposite angle of corrugation as shown in Figure 2.a. The flow channels resulting from this arrangement are inclined at an angle of 45 degrees to the horizontal. The particular form of this packing makes it possible to obtain a specific surface as high as 750 m^2/m^3 in the case of Mellapak 750Y type. The picture of module of this packing is presented in Figure 2.b. The main geometric characteristics of the two absorption columns as well as the physical properties of the system used for pressure drop experiments are listed in the Table 1.

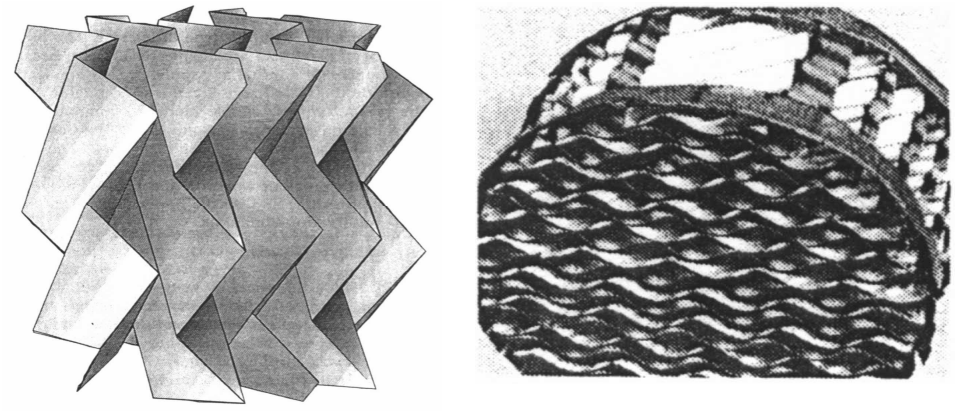

a. b.

Figure 2. Structured packing of Mellapak 750 Y type.
a- corrugated sheets, b- element of structured packing.

Table 1.

Data on the investigated systems

Packing	Raschig rings	Mellapak 750Y
Column diameter (m)	0.100	0.100
Packing height (m)	0.550	0.518
Packing volume ($10^3 m^3$)	4.3175	4.0663
Nominal packing size (mm)	10 x 8 x 10	-
Equivalent diameter (mm)	2.105	0.400
Void fraction of the bed	0.800	0.950
Geometric surface area (m^2/m^3)	570	750

Liquid density (kg/m^3)	998.2
Liquid viscosity (Pa.s)	1.01×10^{-3}
Gas density (kg/m^3)	1.182
Gas viscosity (Pa . s)	17.84×10^{-6}
Temperature (K)	298
Pressure (bar)	1.00
Liquid flow rates (L/h)	0,30,40,50,60,70,80,100,150,200,250,300
Gas flow rates (m^3/h)	0,1,2,3,4,5,6,7,8,9,10,15,20,25

Corresponding to the thirteen gas flow rates and 12 liquid loads, a number of 312 ΔP - v_G pairs have been measured for the two packings.

RESULTS AND DISCUSSION

The directly measured pressure drops (mm WG) at different gas flow rates for some values of the liquid load are presented in the Table 2 (Raschig rings) and Table 3 (Mellapak 750 Y).

Table 2.

Pressure drop (mm WG) in the experimental column packed with Raschig rings.

V_G, m^3/h	V_L (10^3 m^3/h)						
	0	30	50	100	150	200	250
0	0	0	0	0	0	0	0
1	1	4	5	12	14	17	20
2	2	10	13	20	25	26	36
3	3	21	25	30	33	34	42
4	4	27	30	35	38	39	50
5	5	29	34	40	44	47	65
6	7	33	38	46	52	57	78
7	8	37	41	53	62	69	87
8	11	40	48	60	74	85	110
9	14	50	58	72	107	130	180
10	17	55	62	78	160	185	250
15	30	122	250	390	510	610	900
20	47	350	-	-	-	-	-
25	70	-	-	-	-	--	-

Table 3.

Pressure drop (mm WG) in the experimental column equipped with structured packing Mellapak 750 Y

V_G, m^3/h	V_L (10^3 m^3/h)						
	0	50	100	150	200	250	300
0	0	0	0	0	0	0	0
1	0	1	2	2	2	3	4
2	0	1	2	2	2	3	5
3	1	2	2	2	3	4	6
4	1	2	3	3	4	6	8
5	1	2	3	3	4	8	10
6	1	2	5	7	8	15	16
7	2	3	5	8	11	18	20
8	2	4	6	8	13	20	24
9	3	5	7	9	17	23	29
10	3	6	8	10	21	26	33
15	4	9	12	18	32	45	60
20	8	13	32	36	42	60	86
25	15	22	53	62	75	88	122

The two absorption columns had the same diameter and almost the same height of packing (see Table1). Therefore, this row experimental data allow a primary comparison of the pressure drops in the two packings at identical loads. At V_L = 0.250 m^3/h and V_G = 15 m^3/h , for instance, the ratio ($\Delta P_{Raschig} / \Delta P_{\text{Mellapak}}$) is as high as 900/45 =20. The advantage of Mellapak is obvious. A more rigorous comparison can be done by representing the pressure drop per unit height of bed (mbar/m) versus the capacity factor F_v, for constant liquid load, in the two packings (Figure 3).

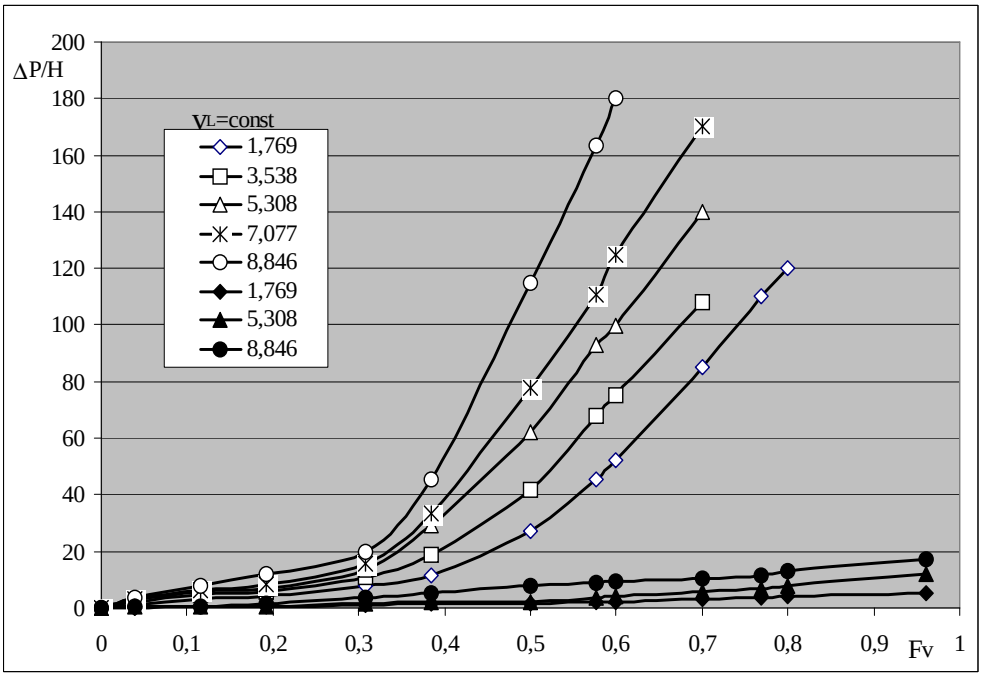

Figure 3. Pressure drop per unit height of bed (mbar/m) versus gas capacity factor at given liquid loads for the two packings (white figures: Raschig, black figures: Mellapak).

Mathematical modeling

The equations found in the literature for the prediction of gas –side pressure drop in packed columns are usually empirical or semiempirical. Moreover, they have been derived from studies on traditional packing and can not be applied unreservedly to modern, structured types. The aim of this paragraph is to present theoretical equation allowing the prediction of pressure drop for both conventional and modern types of packing. It is based on the fluid-dynamics model described by Billet [7]. The main assumption of the model is that the effective void fraction of the

bed is equivalent to a number of vertical flow channels in which the liquid flows in the form of the film of thickness x_0 at an average velocity u_G. the gravity and shear forces are held in equilibrium within the film by the frictional forces that act in the gas at the surface of the film:

$$\mu_L \left(\frac{du_L}{dx} \right)_{x=x_0} = k\mu_L - \rho_l g x_0 = \zeta \rho_G \frac{u_G^{\ 2}}{2} \tag{1}$$

The pressure drop per unit height of the bed with effective area a_e and effective void fraction $\varepsilon_e = \varepsilon - \varepsilon_L$ is:

$$\frac{\Delta P}{H} = \left(\frac{a_e}{\varepsilon - \varepsilon_L} \right) \zeta \rho_G \frac{u_G^{\ 2}}{2} \tag{2}$$

The effective area a_e is the sum of the unwetted area (a_u) and the area of the liquid surface (a_w) in the flow channels. Taking into account the definition of the gas load:

$$v_G = (\varepsilon - \varepsilon_L) u_G \tag{3}$$

and the wall factor f_w:

$$f_w = 1 + \frac{4}{aD} \tag{4}$$

the equation of the pressure drop becomes:

$$\frac{\Delta P}{H} = \zeta_L \frac{a}{(\varepsilon - \varepsilon_L)^3} \left(\frac{a}{2} + \frac{2}{D} \right) \rho_G v_G^{\ 2} \tag{5}$$

were:

$$\zeta_L = \zeta \left(\frac{a_u + a_w}{a} \right) \tag{6}$$

In the extreme case, when $\varepsilon_L = 0$, i.e. a_w=0, the equation of pressure drop through an unwetted bed of packing is derived from (5):

$$\frac{\Delta P_0}{H} = \zeta_0 \frac{a}{\varepsilon^3} \left(\frac{a}{2} + \frac{2}{D} \right) \rho_G v_G^{\ 2} \tag{5'}$$

where ζ_0 is the resistance factor for the dry bed. From (5) and (5') the extend to which the pressure drop in the gas stream within the wetted bed exceeds that within the dry bed is derived:

$$\frac{\Delta P}{\Delta P_0} = \frac{\zeta_L}{\zeta_0}\left(\frac{\varepsilon}{\varepsilon - \varepsilon_L}\right)^3 \tag{7}$$

The equation (7) states that the higher the liquid load, the higher the pressure drop. This expected conclusion is validated by our experimental results in Tables 2 and 3.

The resistance factor ζ_0 can be determined with the following equation taken from the literature [9]:

$$\zeta_0 = C_p\left(\frac{64}{\mathrm{Re}_G} + \frac{1.8}{\mathrm{Re}_G^{0.08}}\right) \tag{8}$$

where:

$$\mathrm{Re}_G = \left(\frac{v_G d_p \rho_G}{(1-\varepsilon)\mu_G}\right) f_w \tag{9}$$

$$d_p = \frac{6(1-\varepsilon)}{a} \tag{10}$$

The constant C_p characterizes the geometry and the surface of the unwetted packing and is therefore specific for any type of packing. It must be determined experimentally.

Using the equation (7) the resistance factor in the gas-liquid flow becomes:

$$\zeta_L = C_p F_w\left(\frac{64}{\mathrm{Re}} + \frac{1.8}{\mathrm{Re}_G^{0.08}}\right)\left(\frac{\varepsilon - \varepsilon_L}{\varepsilon}\right)^{1.5} \tag{11}$$

The wetting factor F_w is a function of Re_L and the liquid holdup [8]:

$$F_w = \left(\frac{\varepsilon_L}{\varepsilon_{L,S}}\right)^{0.3} .\exp\left(\frac{\mathrm{Re}_L}{200}\right) \tag{12}$$

$$\mathrm{Re}_L = \frac{\rho_L v_L}{u\mu_L} \tag{13}$$

Obviously, the ratio $\frac{\varepsilon_L}{\varepsilon_{L,S}}$ becomes unity below the loading point (S). Above this point, the shear forces acting in the gas progressively support the liquid film and the liquid holdup increases until it attains a maximum in the flood point (Fl). An empirical equation has been proposed [6] to satisfy this condition:

$$\left(\varepsilon_L\right)_{v_G>v_{G,S}} = \varepsilon_{L,S} + \left(\varepsilon_{L,Fl} - \varepsilon_L\right)\left(\frac{v_G}{v_{G,Fl}}\right)^{13} \qquad (14)$$

The system of equations (4),(5), and (9) to (14) can predict the gas-side pressure drop in *a bed of any type of packing.* Obviously, after its validation by experimental data. The packing constant (C_p) is identified on this occasion. The values of $\Delta P, v_G, v_L$ are directly measured, whereas the geometric characteristics (a, ε, D, H) and the physical properties ($\rho_L, \mu_L, \rho_G, \mu_G$) are taken from the literature (Table 1). A single but very important parameter, necessary for the solution of the equations is still unknown: the liquid holdup. The use of the equation (14) needs the coordinates of the two points (load and flood points) to be known.

Loading and flooding conditions

According to the postulated fluid-dynamics model, in steady state conditions, the geometry and the shear forces within the liquid film are in equilibrium with the frictional force exercised by the gas at the interface. At a given liquid load the liquid begins to holdup when its average velocity at the interface becomes zero, i.e.:

$$u_{L,S} = 0, \qquad \text{if} \qquad x = x_0 \qquad (15)$$

This is a load point S. The equations for liquid holdup, gas loading and resistance factor in this point are presented in the ***Appendix***.

The flood point (Fl) can be identified experimentally by representing the liquid holdup against the gas load at constant liquid load. The curves becomes vertical at the flood point, i.e.:

$$\left(\frac{dv_G}{d\varepsilon_L}\right)_{v_L=v_{L,Fl}} = 0 \qquad (16)$$

The theoretical flood point correlations are also presented in the ***Appendix***. The application of these equations (17-25) together with the equation (14) for the entire range of load point in our experiments with the structured packing has lead to the diagram in Figure 4.

Now, with the coordinates of the points S and Fl determined, the equations (4), (5), and (9-14) can be applied to correlate the experimental data on pressure drop in the structured packing. This is the model validation.

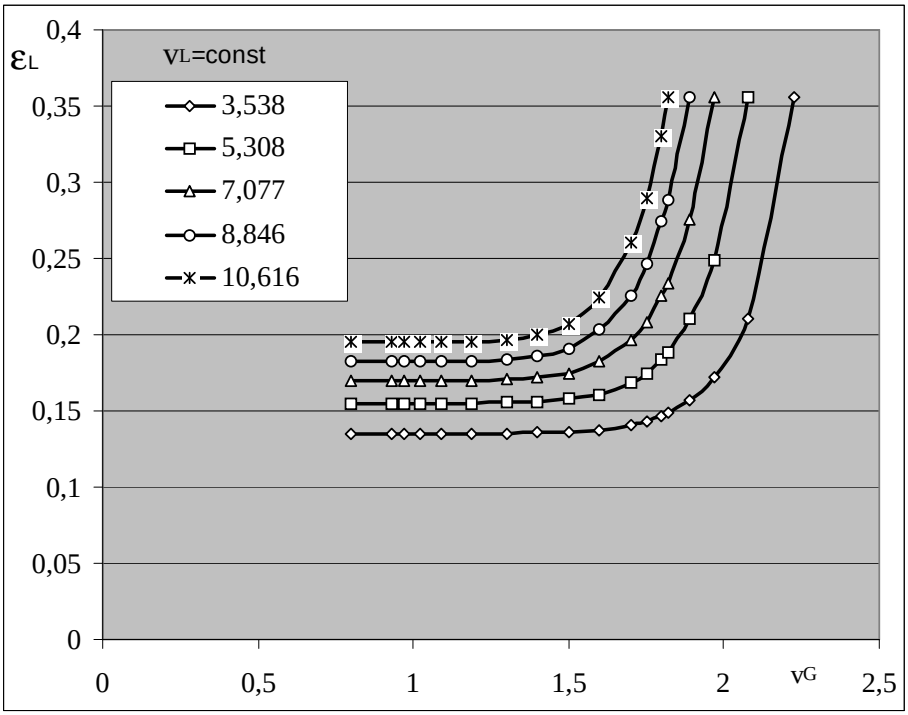

Figure 4. Relationship between the liquid holdup and the phase load in the experimental column with Mellapak 750 Y packing.

The model validation and C_p identification

The results are summarized in the Table 4. The results in Table 4 revealed that C_p is not a real constant of the packing. Its value is influenced by the liquid load. The average values of C_p for the six (I –VI) liquid loads are listed in the Table 5.

Table 4.

Calculated and experimental pressure drop at variable loading in the structured packing Mellapak 750 Y.

v_G , m/s	0.1415	0.3183	0.5305	0.7077	0.8846
Re_G	71.206	160.176	266.960	356.132	445.153
	I. V_L =50	v_L = 1.769		ε_{LS} = 0.1066	
$\Delta P / H$	30.759 C_p	106.724 C_p	257.892 C_p	430.575 C_p	643.868 C_p
$(\Delta P / H)_{exp}$	38.602	135.107	193.011	347.420	540.431
C_p	1.255	1.266	0.748	0.806	0.839
	II. V_L = 100	v_L = 3.538		$\varepsilon_{L,S}$ = 0.1353	

$\Delta P / H$	32.775C_p	113.714C_p	274.780C_p	458.781C_p	685.97C_p
$(\Delta P / H)_{exp}$	57.903	154.409	231.613	617.652	1022.961
C_p	1.767	1.357	0.841	1.346	1.491
	III. V_L = 150	v_L = 5.308		$\varepsilon_{L,S}$ = 0.1546	
$\Delta P / H$	34.471C_p	119.254C_p	288.170C_p	481.127C_p	719.461 C_p
$(\Delta P / H)_{exp}$	57.903	193.012	347.420	694.842	1196.672
C_p	1.685	1.618	1.205	1.444	1.663
	IV. V_L = 200	v_L = 7.077		$\varepsilon_{L,S}$ =0.1702	
$\Delta P / H$	35.820C_p	124.270C_p	300.060C_p	501.360C_p	749.720 C_p
$(\Delta P / H)_{exp}$	77.204	405.320	617.637	810.148	1447.586
C_p	2.155	3.262	2.058	1.616	1.931
	V. V_L = 250	v_L = 8.846		$\varepsilon_{L,S}$ = 0.1833	
$\Delta P / H$	37.171 C_p	128.970 C_p	311.650 C_p	520.380 C_p	778.080 C_p
$(\Delta P / H)_{exp}$	154.41	501.83	868.52	1158.06	1698.50
C_p	4.154	3.885	2.786	2.225	2.183
	VI. V_L = 300	v_L = 10.616		$\varepsilon_{L,S}$ = 0.1948	
$\Delta P / H$	38.458 C_p	133. 429 C_p	322.423 C_p	538.316 C_p	804.979 C_p
$(\Delta P / H)_{exp}$	193.01	636.93	1158.07	1659.90	2354.73
C_p	5.019	4.773	3.592	3.083	2.925

Table 5.

The average values of the constant C_p for the Mellapak 750Y packing.

10^3 v_L (m/s)	1.769	3.538	5.308	7.077	8.846	10.616
ε_L	0.1066	0.1353	0.1546	0.1702	0.1833	0.1948
C_p	0.983	1.360	1.522	2.204	3.046	3.878

The values of C_p in Table 5 can be correlated by the equation (26) of a straight line passing through origin:

$$C_p = 398.09\ v_L \qquad (26)$$

CONCLUSIONS

The experimental results reported here show that the pressure drop per unit height in a structured packing of Mellapak 750 Y type is much smaller than that through conventional bed of Raschig rings, as expected. The data referred to the structured packing are correlated with fluid-dynamics model containing a single adjustable parameter (C_p) specific for every type of packing. The model must be valid for any type of packing if this constant is empirically identified. It has been found, in the present work, that the constant C_p is not dependent only on the packing type but also on the liquid load. This is in contradiction with the previous conclusion of Billet who stated that C_p depends only on the packing geometry and texture.

NOTATIONS

- a total surface area per unit packed volume, m^2/m^3
- a_u area of the unwetted surface, m^2/m^3
- a_w area of the liquid surface in the flow channels, m^2/m^3
- A cross sectional area of the column, m^2
- C_{Fl} flood point constant, specific for the packing
- C_p constant of the packing
- C_S load point constant, specific for the packing
- d_p equivalent diameter of the packing, m
- D column diameter, m
- f_w wall factor
- Fl flood point
- F_v gas capacity factor, $m^{-1/2}kg^{1/2}s^{-1}$
- F_w wetting degree
- g acceleration due to gravitation, m/s^2
- H effective height of column packing, m
- K integration constant in the Eqn(1)
- m_L liquid mass flow rate, kg/s
- m_G gas flow rate, kg/s
- n exponent
- P total pressure, Pa
- ΔP pressure drop, Pa or mm WG
- Re_G Reynolds number of the gas phase, Eqn(9)
- Re_L Reynolds number of the liquid phase, Eqn(13)
- S load point
- u_G average gas velocity, m/s
- u_L average liquid velocity, m/s
- v_G gas load, m^3/m^2s
- v_L liquid load, m^3/m^2s
- V_G gas flow rate, m^3/s
- V_L liquid flow rate,m^3/s
- x thickness of the liquid film,m

Greek symbols

ε_L liquid holdup

$\varepsilon_{L,Fl}$ liquid holdup in the flood point

$\varepsilon_{L,S}$ liquid holdup in the load point

ε total void fraction of the packing

μ_G dynamic viscosity of the gas, Pa s

μ_L dynamic viscosity of the liquid, Pa s

ζ_{Fl} coefficient of resistance at the flood point

ζ_L coefficient of resistance in the irrigated packing

ζ_0 coefficient of resistance to flow in the unwetted bed

ζ_S coefficient of resistance in the load point

ρ_G gas density, kg/m^3

ρ_L liquid density, kg/m^3

Subscripts

Fl flood point
S load point
L liquid phase
G gas phase
p packing (in the constant C_p)
W wall (in wall factor), wetting (in F_v), wetted (in a_w)
v vapor or gas.

REFERENCES

1. Brunazzi, E., Paglianti, A., *A.I. Ch. E. Journal*, (1997) ***43***, 2, 317.
2. Robbins, L.A., *Chem. Eng. Prog*., (1991) ***87***, 87.
3. Spiegel, L., Meier, W.A., *Inst. Chem. Eng. Symp. Ser*., (1992) ***128***, B85.
4. Nardini, G.A., Paglianti, A., Petarca, L., Viviani, E., *Chem. Eng. Technol*., (1996) ***19***, 20.
5. Brunazzi, E., Paglianti, A., Petarca, L., *Chim. Ind*.,(1996) ***78***, 459.
6. Bravo, J.L., Rocha, J.A., Fair, J.R., *Int. Chem. Eng. Symp. Ser*, (1992) ***128***, A439.
7. Billet, R., Schultes, M., *Chem. Eng. Technol*., (1993) ***16***, 1.
8. Billet, R., *Packed Towers,* WCH, Weinheim, 1995.
9. Dutkai, E.P., *Coloane cu umplutură în tehnologia chimică,* Ed. Tehnică, Bucureşti, 1977.
10. Weimer, Th., Schaber, K., *Chemische Technik*, (1996) ***48***, 5, 241.

APPENDIX

Load point (S)

In the load point the liquid phase begins to holdup when its velocity at the interface ($x = x_0$) becomes zero. The corresponding gas velocity is the upper limit for the absolutely stable hydrodynamic range, defined by [9,10]:

$$v_{G,S} = \left(\varepsilon - \varepsilon_{L,S}\right)\sqrt{\frac{\varepsilon_{L,S}\, g \rho_L}{\zeta_S\, a \rho_G}} \qquad (17)$$

The application of the equation (17) requires the knowledge of the liquid holdup at the load point ($\varepsilon_{L,S}$) and the corresponding resistance factor(ζ_S).These can be predicted by the equations (18) and (19) respectively [10]:

$$\varepsilon_{L,S} = \left(\frac{12}{g} a^2 \frac{\mu_L}{\rho_L} v_L\right)^{1/3} \qquad (18)$$

$$\zeta_S = \frac{g}{{C_S}^2}\left[\frac{m_L}{m_G}\left(\frac{\rho_G}{\rho_L}\right)^{1/2}\left(\frac{\mu_L}{\mu_G}\right)^{0.4}\right]^{2n_S} \qquad (19)$$

It has been found that the following empirically determined numerical values of the exponent n_S usually apply for all types of packing in the loading ranges concerned [7]:

when: $\frac{m_L}{m_G}\left(\frac{\rho_G}{\rho_L}\right)^{0.5} \le 0.4$ $n_S = 0.326$ (20)

when: $\frac{m_L}{m_G}\left(\frac{\rho_G}{\rho_L}\right)^{0.5} > 0.4$ $n_S = 0.723$ (21)

Numerical values of the constant C_S for specific types of randomly dumped as well as systematically stacked packings are listed in tables [8]. A value $C_S = 3.157$, determined for Mellapak 250 Y has been adopted to predict $\varepsilon_{L,S}$ for our Mellapak 750Y. This is the weak point of the calculations in the present work.

Flood point (Fl)

The curves ε_L versus v_G become vertical at the flood point. The general equation derived from the fluid dynamic model becomes of the following form in the flood point:

$$\varepsilon^{3}{}_{L,Fl}\left(3\varepsilon_{L,Fl}-\varepsilon\right)=\frac{6}{g}\frac{m_l}{m_G}\frac{\rho_G}{\rho_L}\frac{\mu_L}{\mu_G}a^2\varepsilon v_{G,Fl} \tag{22}$$

The right hand-side of this equation must be positive. This implies that the liquid holdup at the flood point has not to be less than $\varepsilon/3$ and must lie only within the limits:

$$\frac{\varepsilon}{3}\le\varepsilon_{L,Fl}\le\varepsilon \tag{23}$$

It has been found that for liquid loading between 0.1 and 200 m^3/m^2h, $\varepsilon_{L,Fl}$ can be evaluated by:

$$\varepsilon_{L,Fl}=0.3741\varepsilon\left(\frac{\mu_L\rho_{H_2O}}{\rho_L\mu_{H_2O}}\right) \tag{24}$$

The resistance factor at the flood point is given by[1]:

$$\zeta_{Fl}=\frac{g}{C^2{}_{Fl}}\left[\frac{m_L}{m_G}\left(\frac{\rho_L}{\rho_G}\right)^{0.5}\left(\frac{\mu_L}{\mu_G}\right)^{0.2}\right]^{2n_{Fl}} \tag{25}$$

where:

n_{Fl} = 0.194 when: $\frac{m_L}{m_G}\left(\frac{\rho_G}{\rho_L}\right)\le 0.4$ (26)

n_{Fl} = 0.708 when: $\frac{m_L}{m_G}\left(\frac{\rho_G}{\rho_L}\right)> 0.4$ (27)

Similarly, the constant C_{Fl} has been adopted from the literature (C_{Fl} = 2.464) for Mellapak 250Y, the only structured packing already studied [7].
The gas load in the flood point has been determined with the equation [10]:

$$v_{g,Fl}=\sqrt{\frac{\left(\varepsilon-\varepsilon_{L,Fl}\right)^3}{\varepsilon}}\left(\frac{2g\rho_L\varepsilon_{L,Fl}}{\zeta_{Fl}a\rho_G}\right)^{1/2} \tag{28}$$

The liquid holdup at loading between the point S and the point Fl has been calculated with the empirical equation (14) using the data in Figure 4 for S and Fl.

STUDIA UNIVERSITATIS BABEŞ-BOLYAI, CHEMIA, XLIII, 1-2, 1998

BIOTRANSFORMATION OF NITROSO NAPHTOLS BIOASSISTED BY BAKER'S YEAST

R. SILAGHI-DUMITRESCU, CS. PAISZ, FL.D. IRIMIE, FR. JOO, C. MAJDIK, M. TOŞA

ABSTRACT. 1- Nitroso-2-naphtol, 2-nitroso-1-naphtol and 4-nitroso-1-naphtol were used as substrates for the reductive action of Baker's yeast. The expected amino-naphtols were not isolated, and some new products of their oxidation were identified, Sodium borohydride afforded unexpected products with 2-nitroso-1-naphtol. Ab initio were employed in elucidating the nature of the processes described.

INTRODUCTION

Baker's yeast has been shown to exhibit selectivity as far as reduction of such groups as carbonyl, nitro or C=C is concerned. We have recently found aromatic nitroso compounds to be readily reduced to the corresponding amines [1], and have succeeded in isolating the products. Of the functional groups thus far considered as yeast substrates, nitroso is the most easily transformed. The mechanism of this reaction should involve firstly hidroxilamine formation (by the same mechanism as for carbonyl reduction), and then a hidride attack on the nitrogen atom. The simple experimental procedure we have developed [1] provides a convenient route for nitroso group reduction, as no demanding experimental conditions are required, and the amine is readily isolated as the hydrochloride.

In view of the data available [1] the nitroso-naphtols should be readly converted by means of Baker's yeast to the corresponding amino-naphtols. However, the latter are only stable under inert conditions, unless isolated as hydrochlorides or acetyl-derivatives. The usual experimental procedures employed with Saccharomices cerevisiae are not compatible with isolation of such labile compounds as amino-naphtols. This inconvenient has been dealt with by us in different ways, in a quest for developing experimental procedures of general use as far as labile compounds and Baker's yeast are involved. Such procedures should involve work under inert atmosphere, use of organic (hopefully dry) solvents; immobilized cells may also prove useful.

RESULTS AND DISCUSSION

1-Nitroso-2-naphtol ***(I)***, 2-nitroso-1-naphtol ***(II)*** and 4-nitroso-1-naphtol ***(III)*** were used as substrates for the reductive action of Baker's yeast:

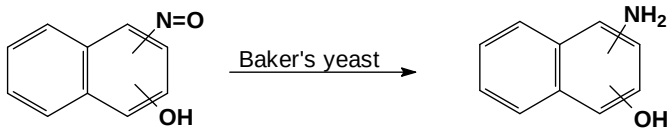

Fig. 1. *General equation for nitroso naphtol reductions*

A number of aminmo phenols have already been obtained by this procedure [1]. The expected amino-naphtols should be difficult to issolate, as they are known to be unstable in the presence of oxygen and water (both of which unavoidable in experimental procedures involving Baker's yeast). Thus, a mixture of water, yeast and nitroso-naphtol should provide, besides little amino naphtol (if any), at least one of its oxidation products. Indeed, the reaction mixtures showed an initial partial decolorization, but they then acquired different (intense) colours.

While the final product of amino naphtol oxidation is the corresponding quinone (which should therefore be present in our reaction mixtures), a number of other compounds resulted from partial oxidation have been described (formulae in Fig.2). 2-Amino-1,4-naphtoquinon-N^4-(1-hydroxy, 2-naphtil-imine) (1) was obtained by bubbling air in ammonia solution [2]; its colour is violet, though initially a green compound (not isolated) is formed. (1) is solid, soluble in alcohols, and has also been obtained by means of cytochrome c oxidase [3]. The amino naphtoquinone and a amino either bu enzymic or chemical means [4]. Coupling of a naphtoquinone and a amino naphtol has led to (4) [5]. 2-Amino-1-naphtol afforded the corresponding 1,2-napthoquinone by peroxidase action, although highly unstable intermediates of oxidation were shown to be formed and to bind to proteins [6]. Fungal tyrosinase also afforded quinones [7].

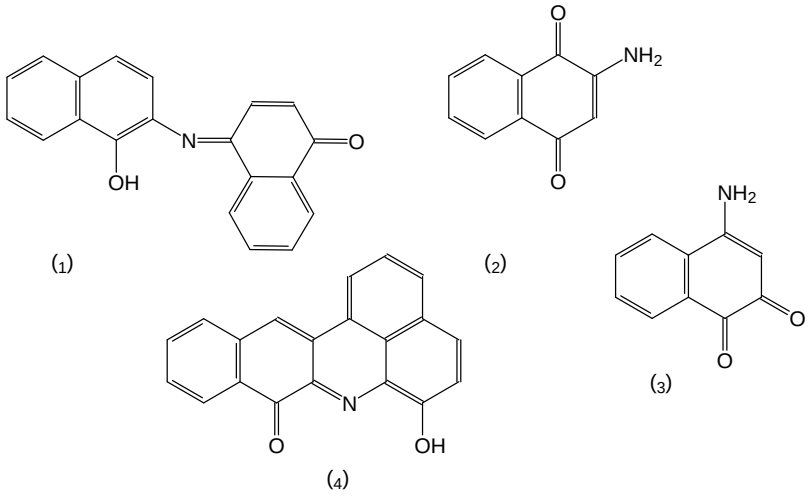

Fig. 2. *Partial reduction products of the amino naphtols*

Amino naphtols have been used as electron (and proton) carriers in peroxidasic systems [8], on the basis of their quinonimine-amino naphtol equilibria. Free radicals, expected and proven to be formed on aminonapthol oxidation, have been shown to bind to proteins and nucleic acids (accounting for the biological activity) [9].

A different explanation for the intense colors of the reaction mixtures may arise when we consider the features of the nitroso group, either of the following reaction pathways being possible:

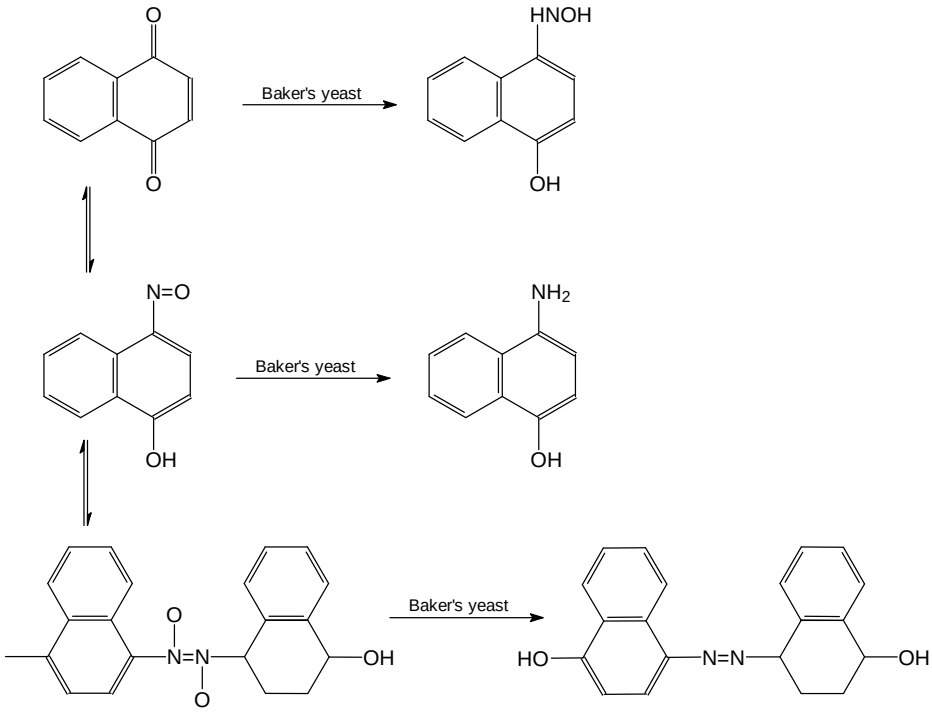

Fig. 3. *Nitroso group isomerism and its possible influence on the nature of yeast mediated reductions*

As quinones and nitroso phenols [1] yield respectively the correspondig hydroquinones and amino phenols, the oxime in Fig. 3 should eventually provide the amine; azo derivatives are not substrates for Baker's yeast, and may be responsible for the intense colours of the reaction mixtures.

Six different experimental procedures (***A-E***) were applied for the attempted nitroso naphtol reduction, in order to study the nature of the products and to minimize the degree of amine oxidation. Thus HCl, AcOH, and DMF media were employed, as well as inert atmosphere. Structures of the products identified are presented in Fig. 4.

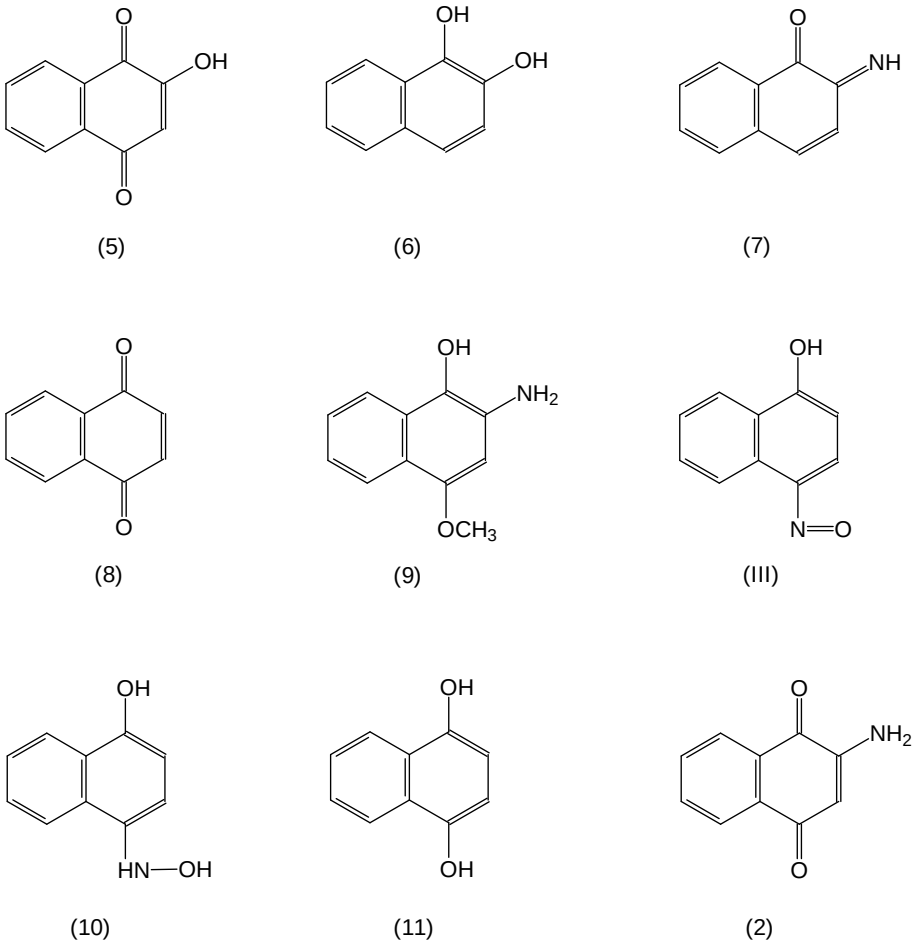

Fig. 4. *Compounds obtained upon nitroso naphtol reduction, as described below*

A. The classical proccedure involves mixing water and yeast and then adding a saturated solution of the substrate; the products are eventually extracted with organic solvents. In the case of the nitroso naphtols, extraction afforded intensely coloured solutions, which could not be extracted with HCl (no amino naphtol was present). TLC analysis proved them to be complex mixtures (at least 6 spots), which could not be totally resolved, as equillibria between the components occurred. GC-MS analysis of the sample resulted from 2-nitroso-1-naphtol proved the presence of 2-amino-1,4-naphtoquinone (2) and a methylated derivative (the samples were dissolved in methanol). The properties of the mixture suggested it to contain as the main component (1) [2,3]; however, (1) was not detected by GC-MS (and should not have been, in view of its molecular weight and polarity). A mixture,

identical to the one above described, was obtained from ***(II)*** with $NaBH_4$ in basic aqueous methanol, followed by ether extraction. Two main components were shown to be present by TLC (one violet, one green); these two appear to be involved in an equilibrium, as the violet component prevails in etheric solution and the green one prevails aqueous NaOH medium. The solution turns red in acidic medium. Sodium borohydride may react with the amino naphtol as well as its tautomer oxime; its mechanism of action is not radicalic, as opposed to the oxidation processes (peroxidasic or not) expected to take place in the yeast suspension. The mixture obtained from ***(I)*** after solvent evaporation and recristallization from concd. HCl affroded a red precipitate, which could not be analized (did not melt up tp 360^0C and provided no mass spectrum, was not soluble in the available deuterated solvents, had a poor IR spectrum and was obtained in very low yields).

B. A different approach implied addition of HCl (in various amounts) to the yeast suspension (before substrate addition). After filtering and boling with active C, the clear colourless solutions were mixed with DMF and the water removed, White precipitates were thus obtained; altough these were expected to be amino naphtol hydrochlorides, they did not redissolve in any solvent, did not release the amines in basic media, had poor IR spectra, did not melt up to 360^0C, tested positive with nihnydrin; they dissolved in HCl medium and reprecipitated when NaOH was added. It was concluded that these materials were of proteic nature.

C. HCl was added only before filtering the reaction mixture. Organic solvent extraction then afforded a mixture similar to that obtained in the ***A***. procedure. The aqueous phase was treated as in procedure ***B***., with similar results. The organic phases were analyzed by means of GC-MS. Identified in the mixture obtained from ***(I)*** was 2-hydroxy-1,4-naphtoquinone (5). The mixture obtained from ***(II)*** contained 1,2-naphtalenediol (6) and (in very low concentrations) 1,2 naphtoquinon-2-imine (7). The mixture obtained from ***(III)*** contained 1,4-naphtalenediol (11), 1,4-naphtoquinone (8), 4-nitroso, 1-naphtol ***(III)***, and 4-hydroxylamino 1-naphtol (10). As mentioned above, hydroquinone should ne expected to form: (10) may arise from either of the two tautometric states of ***(III)***; (8) should be present whenever the corresponding quinone is present, given that benzoquinone is known to be readily reduced in yeast medium to benzohydroquinone.

D. Ac_2O was added at times to the reaction mixture of ***(II)***, as amino naphtols have been acetylated under similar conditions [10]. Organic solvent extraction eventually afforded a mixture similar to that obtained by the procedures ***A*** and ***C***. A brown solid precipitated from the aqueous phase (m.p. $230\text{-}6^0$ C) and GC-MS analysis proved it to contain 2-hydroxy 1,4-naphtoquinone (5) and 2-amino,4-mehtoxy,1-naphtol (9); the latter may have been methylated in situ while performing the analysis, as methanol was the solvent. Non-methylated (9) is expected to form upon (2) reduction by the yeast.

E. The yeast was suspended in DMF and the mixture was placed under inert atmosphere. Should theoxidation processes have been due only to the oxygen/water system, they should have been greatly reduced. This was not the case; although the reaction mixtures did acquire intense colours, they were not identical to those obtained under aerobic conditions. Concd. HCl was eventually added, followed by the work-up of procedure ***C*** (the proteic material was also obtained).

No azo-derivatives were isolated; although the latter may well not be detectable by the Gc-MS system employed in analysis, we conclude that the processes taking place after nitroso group reduction are of oxidative or peroxidative nature, and at least part of them are not O_2-dependent (as proven by procedure ***E***). Some of the oxidation products were in turn reduced by the yeast.

Ab initio calculations were performed on the amino naphtols expected to form, and the results are presented in Table 1. These data provide insights as far as the oxidation processes of the amino naphtols in our experiments are concerned.

The stabilities of the three amino naphtols decrease in the order: 2-amino 1-naphtol>1-amino 2-naphtol>4-amino 1-naphtol; the energies are given in hartrees. The high energy values of their HOMO indicates the amino naphtols as very good electron donors, while the high values for LUMO suggests them to be poor electron acceptors. The HOMO-LUMO gaps are relatively large. Also given in Table 1 are the carbon atoms expected to be the most reactive on the basis of their relative charges.

Table 1. *Results of ab initio calculations for amino naphtols*

Compound	1-amino 2-naphtol	2-amino 1-naphtol	4-amino 1-naphtol
Energy	-510,385098	-510,386683	-510,377495
HOMO	-0,2861	-0,2773	-0,2504
LUMO	0,09484	0,1110	0,1192
HOMO-LUMO gap	0,3845	0,3883	0,3697
highest negative charge on carbon	C_3, C_6, C_8	C_4, C_7	C_2

EXPERIMENTAL

All reactives were Merck of Reactivul products. 2-nitroso-1-naphtol (II) and 4-nitroso-1-naphtol (III) were prepared according to the data available [11].

Procedure ***A***: 80 g yeast are suspended in water, and then 0,5 g nitroso naphtol is added (as satd. solution in methanol). The mixture is stirred 0,5-2 h, and then filtered; the filtrate is extracted with ethyl acetate/benzene, the solvent from the organic phase evaporated and the residue analyzed by GC-MS.

Procedure ***B***: 80 g yeast are suspended in water, 8 ml concd. HCl are added, followed by steps as in procedure ***A***. The aqueos phase is boiled with activated C, 10 ml DMF are added and the water evaporated; filtering and washing with benzene afforded 0,3-0,6 g of white precipitate. The amount of HCl may vary, without affecting the results.

Procedure ***C***: 80 g yeast are suspended in water, and then 0,5 g nitroso naphtol is added (as satd. solution in methanol). The mixture is stirred 0,5-2 h, and then 8 ml concd. HCl is added. Work-up follows for the organic phase as in procedure ***A*** and for the aqueous phase as in procedure ***B***. 0,1 g white precipitate were thus obtained.

Procedure ***D***: 80 g yeast are suspended in water, and then 0,5 nitroso naphtol is added (as satd solution in methanol). Every 20 minutes 5 ml Ac_2O are added, until the initial colour has faded. The mixture is filtered; the filtrate is extracted

with ethyl acetate/benzene, the solvent from the organic phase evaporated; the aqueos phase pH is made neutral, affording a brown precipitate, m.p. 230-236^0 C.

Procedure ***E***: 80 g yeast are suspended in dry DMF under nitrogen; nitrogen is bubbled through the suspension, and then 0,5 g nitroso naphtol is added (as satd. solution in methanol). The mixture is stirred 3,5 h, and then 15 ml concd. HCl are added, followed by steps as in procedure ***C***.

Sodium borohydride reduction: to a aqueos methanolic soln of nitroso-derivative (0,1 g in 15 ml, 10% NaOH) 0,1 g sodium borohydride are added. After 20 minutes the efervescence ceases and the reaction is complete. The mixture is extracted with ether and after solvent evaporation a violet powder is obtained.

IR spectra of the white precipitates: 3400, 1580, 1100 cm^{-1}, all broad and strong.

Organic phase extracts mass spectra:

(III): M/e: 173, m/e: M-30, M-17, M-30-28, M-16-26, 76,77.

(2): M/e: 173, m/e: 76, 105, 27, M-27, M-27-26, M-28

(5): M/e: 174, m/e: 75,76,77,105, M-28, M-28-28.

(6): M/e: 160, m/e: 131, 104, 75, 50, M-29-29, M-29.

(7): M/e: 157, m/e: M-16, M-28, M-27, M-29, M-16-27, 76,77,105,29.

(8): M/e: 158, m/e: M-28, M-28-28, M-30, M-28-26, 50, 75, 76,77,105.

(9): M/e: 189, m/e: M-15, M-17, M-30, M-30-16, M-30-28, M-30-16-25, M-30-16-29, M-30-16-28, 105,89,76.

(10): M/e: 175, m/e: M-17, M-17-28, M-17-28-26, M-29, M-29-17, M-29-31, M-29-44, 74,75,76,77,105.

(11): M/e: 160, m/e: M-29, M-29-27, 76, 50.

Calculation details: ab initio calculations were made in the Spartan package [12], using the 3-21G(*) basis.

ACNOWLEDGEMENTS

We are indebted to prof. dr. I. Oprean for the GC-MS analysis, and also to prof. dr. I. Silaghi-Dumitrescu, whose kindness allowed us to obtain the ab initio data.

REFERENCES

1. Fl.D. Irimie, Cs. Paisz, Fr. Joo, R. Silaghi-Dumitrescu, C. Majdik, M. Toşa, submitted for publication.
2. Beilsten's Handbuch der Organischen Chemie, Vierte Auflage, Bd. XXIV, Berlin, Julius Springer Verlag, 1936.
3. H.T. Nagasawa, H.R. Gutmann, *J. Biol. Chem.*, 1959, ***234***, 1593.

4. S. Belman, K. Ferber, W. Troll, *Proc. Soc. Exp. Biol. Med.*, 1967, ***125***(1), 239; S. Belman, W. Troll, *J. Biol. Chem.*, 1962, ***237***, 746; K. Shriever, *Arch. Pharm.*, 1956, ***289***, 343.
5. P. Beaudet, C. Beaudet, *Chim. Ter.*, 1973, ***8***(6), 669.
6. J. Boyd, T.E. Eling, *Cancer Res.*, 1987, ***47***(15), 4007.
7. N. Motoyama, *Pestic. Biohem. Phisiol.*, 1978, ***9***(3), 255.
8. H.G. Williams-Ashmann, M. Klavins-Johnson, *Enzymologia*, 1960, ***22***, 327.
9. R. Silaghi-Dumitrescu, *Studii asupra aminonaftolilor şi a obţinerii lor în cataliza celulară*, Disertation, 1998, "Babeş-Bolyai" University.
10. C. Przybylski, Barwniki-Srodki Pomocnicze, 1976, ***20***(1), 57.
11. H. Sanielevici, F. Urseanu, *Sinteze de intermediari aromatici*, Vol.I, Ed. Tehnică, Bucureşti, 1983.
12. SPARTAN VERSION 5.0, WAVEFUNCTION INC., 18401 Von Karman Avenue, Suite 370, IRVINE, CA92612 USA.

STUDIA UNIVERSITATIS BABEŞ-BOLYAI, CHEMIA, XLIII, 1-2, 1998

APPLICATIONS OF DIRECT VOLTAMMETRY IN THE STUDY OF HIGH TEMPERATURE SUPRACONDUCTOR / REDOX ELECTROLYTE INTERFACE

I.O. MARIAN*, E. PAPADOPOL, S. BORCA**, N. BONCIOCAT****

ABSTRACT. A new method based on direct voltammetry was used to study the variation of current density with temperature at the high temperature superconductor/ redox electrolyte interface (in the proximity of critical temperature).

For this purpose, we have solved the Volterra integral equation with known K(t,u) kernel and f(t) function, thus allowing the j(t) current density estimation.

From j(η) vs. η an explanation for the reversible solution form to a Butler-Volmer irreversible solution form trespassing in the case of critical temperature involvment, is suggested.

INTRODUCTION

In nonaqueous media direct voltammetry of Pb $|Bi_2\ Sr_2\ Ca\ Cu_2\ O_x$ (2212) phase is similar in appearence to that of noble metals [1].

Resonable results can be obtained, despite the distorsion induced by ohmic drop, in a nonstationary method.

A specific expresion of Volterra equation is considered for an inert electrodic material [2].

By solving this equation we found the current density j(t) in reversible and irreversible reactions cases (cathodic branch).

Until now there were not reported results about Tc estimation using nonstationary methods from classical point of view.

RESULTS AND DISSCUSIONS

In the Fredholm alternative [3] a Volterra integral equation is:

$$j_F(t) = \lambda \frac{j^0 N^*(t)}{\pi^{1/2}} \int_0^t \frac{j_F(u)}{(t-u)^{1/2}} du + f(t) \qquad (1)$$

where

* *Universitatea "Babeş-Bolyai", Facultatea de Chimie şi Inginerie Chimică, Cluj-Napoca.*
** *Institutul Național de Electrochimie şi Materie Condensată, Bucureşti*

$$N^*(t)=\frac{\exp(-\beta fvt)}{F\sqrt{D_O}c_O}+\frac{\exp[(1-\beta)fvt]}{F\sqrt{D_R}c_R};\quad f(t)=j^0\left\{\left[\exp(-\beta fvt)-\exp[(1-\beta)fvt]\right]\right\}$$

$$\lambda=-1 \tag{1'}$$

D - diffusion coefficient; c - concentration, f = F/RT; T - temperature; t - time; $|v|t$ is the overtension (η) and $v < 0$.

If $D_0 = D_R = D$ and $c_0 = c_R = c$, by neglecting capacitive current, $j_F(t)$ is the measured current density in closed circuit conditions.

In this case (1') is:

$$N^*(t)=\overline{N}\exp(\beta f|v|t)\left[1+\exp(-f|v|t)\right];\ f(t)=j^0\exp(\beta f|v|t)\left[1-\exp(-f|v|t)\right]$$
$$\overline{N}=\frac{1}{F\sqrt{Dc}};\ f=\frac{F}{RT} \tag{1''}$$

We can write integral eq. solution in serial form:

$$j(t)=j_0(t)+\lambda j_1(t)+\ ...\ +\lambda^k j_k(t)+\ ... \tag{2}$$

where:

$$j_0(t)=f(t)=j^0\exp(\beta f|v|t)[1-\exp(-f|v|t)] \tag{2'}$$

$$j_{k+1}(t)=\frac{j^0N^*(t)}{\pi^{1/2}}\int_0^t\frac{j_k(u)}{(t-u)^{1/2}}du \tag{2''}$$

and for $j_1(t)$ result:

$$j_1(t)=\frac{j^0N^*(t)}{\pi^{1/2}}\int_0^t j^0\exp(\beta f|v|u)\left[1-\exp(-f|v|u)\right](t-u)^{-1/2}du \tag{3}$$

In proximity of t, $(t-u)^{-1/2}\to\infty$ and: $\exp(\beta f|v|u[1-\exp(-f|v|u)]\ \to$
$\exp|\ \beta f|v|t\ [1-\exp\ (-f|v|t\ )]\ |$.

It was possible to be applied an average theorem for eq.(3), and we found:

$$\int_0^t j^0\exp(\beta f|v|u)\left[1-\exp(-f|v|u)\right](t-u)^{-1/2}du\cong j^0\exp(\beta f|v|t)\left[1-\exp(-f|v|t)\right]\cdot$$
$$\cdot\int_0^t(t-u)^{-1/2}du\cong j^0\exp(\beta f|v|t)\left[1-\exp(-f|v|t)\right]2\sqrt{t} \tag{4}$$

with

$$\int_0^t(u-0)^m(t-u)^n du=(t-0)^{m+n+1}\frac{\Gamma(m+1)\Gamma(n+1)}{\Gamma(m+n+2)} \tag{5}$$

(t>0; m>-1; n>-1)

where $\Gamma(\ )$ function is:

$$\Gamma(n)=\int_0^{\infty}u^{n-1}\exp(-u)du\ ;\ n\neq 0,-1,-2,-3,...$$
$$\Gamma(n+1)=n\Gamma(n)\ ;\ \Gamma(1)=1\ ;\ \Gamma(1/2)=\pi^{1/2} \tag{6}$$

Using (4) and (5):

$$j_1(t)=\left[j^0N^*(t)\right]j^0\exp(\beta f|v|t)\left[1-\exp(-f|v|t)\right]\frac{1}{\Gamma(1/2+1)}t^{1/2} \tag{7}$$

The little error occuring by averaging procedure from (4), failed, because odd therms in serial form (2) appear with (-) and even therms appear with (+).
Generally:

$$j_k(t)=\left[j^0N^*(t)\right]^k j^0\exp(\beta f|v|t)\left[1-\exp(-f|v|t)\right]\frac{t^{k/2}}{\Gamma(k/2+1)} \tag{8}$$

By using (2") in the same averaging conditions we obtained:

$$j_{k+1}(t)=\left[j^0N^*(t)\right]^{k+1}j^0\exp(\beta f|v|t)\left[1-\exp(-f|v|t)\right]\frac{t^{(k+1)/2}}{\Gamma\left[(k+1)/2+1\right]} \tag{8'}$$

and (8) is indeed a general expression.

Finaly the current density is:

$$j(t)=j^0\exp(\beta f|v|t)\left[1-\exp(-f|v|t)\right]\left\{1+\left\{\lambda j^0\overline{N}\exp(\beta f|v|t)\left[1+\exp(-f|v|t)\right]\right\}\cdot\right.$$
$$\left.\cdot\frac{t^{1/2}}{\Gamma(1/2+1)}+\ldots+\left\{\lambda j^0\overline{N}\exp(\beta f|v|t)\left[1+\exp(-f|v|t)\right]\right\}^k\frac{t^{k/2}}{\Gamma(k/2+1)}+\cdots\right\} \tag{9}$$

A (9) serie is convergente and deriving this expression, after few algebric operation finaly results [3]

$$\frac{1}{\left(\lambda j^0\overline{N}\right)^2}\left[\frac{dj(t)}{dt}-\frac{\beta+(1-\beta)\exp(-f|v|t)}{1-\exp(-f|v|t)}f|v|j(t)\right]=\left\{1+2\left[\beta-\frac{\exp(-f|v|t)}{1+\exp(-f|v|t)}\right]\cdot\right.$$
$$\left.\cdot f|v|t\right\}\exp(2\beta f|v|t)\left[1+\exp(-f|v|t)\right]^2 j(t)+\left\{1+2\left[\beta-\frac{\exp(-f|v|t)}{1+\exp(-f|v|t)}\right]f|v|t\right\}\cdot \tag{10}$$
$$\cdot\exp(2\beta f|v|t)\left[1-\exp(-2f|v|t)\right]\frac{1}{\lambda\overline{N}\pi^{1/2}t^{1/2}}$$

This is an ordinary diferential equation of first order for direct voltammetry.

a) current density for reversible redox reactions.

In this case $j^0 \rightarrow \infty$ and from (10) (with λ = -1) we have:

$$j(t) = \frac{1-\exp(-f|v|t)}{1+\exp(-f|v|t)} \frac{F\sqrt{D}\,c}{\pi^{1/2} t^{1/2}} \tag{11}$$

Equation (11) can be written

$$j(\eta) = \frac{F\sqrt{D\,c}\,v^{1/2}}{\pi^{1/2}} \cdot \text{th}\left(\frac{f\eta}{2}\right) \frac{1}{\eta^{1/2}} \tag{12}$$

(using overtension η)

b) current density for irreversible redox reactions.

With $j^0 \rightarrow 0$, from eq. (10)

$$\frac{dj(t)}{dt} = \left[\beta + \frac{\exp(-f|v|t)}{1-\exp(-f|v|t)}\right] f|v|\,j(t) \tag{13}$$

and by integration:

$$j(t) = j^0 \exp(\beta|v|t)[\,1-\exp(-f|v|t\,] \tag{14}$$

or $$j(\eta) = j^0 \exp(\beta\eta)[\,1-\exp(-f\eta\,)] \tag{14'}$$

By deriving the eq. (12) is obtained:

$$4f\eta\exp(-f\eta)-1+\exp(-2f\eta) = 0 \tag{15}$$

or: $$\text{sh}(f\eta) = 2f\eta \tag{15'}$$

and after numerical computation a maximum at:

$$\eta_p = 2{,}18 \cdot RT/F \tag{16}$$

dependent of the temperature.

Let's consider the diffusion coefficient at different temperatures of: 2 mM Cp_2* Fe in 0,2 M Bu_4NPF_6, 1/2 (PrCN/EtCl) solvent mixture [4].

Numerical computations was applied to eq.(12). This procedure generated nonlinear j vs. η plots for 50 mV/s scan rate (see fig.1) at low temperature conditions.

Initialy at 273 K j vs. η is a reversible shape, but finaly at about 100 K appears change. By decreasing the temperature both value j(η) and η_{peak} change. $\eta_{peak} \rightarrow \eta_{Tc}$ (for critical temperature), and the reversible current density j(η) should became a Butler -Volmer irreversible type.

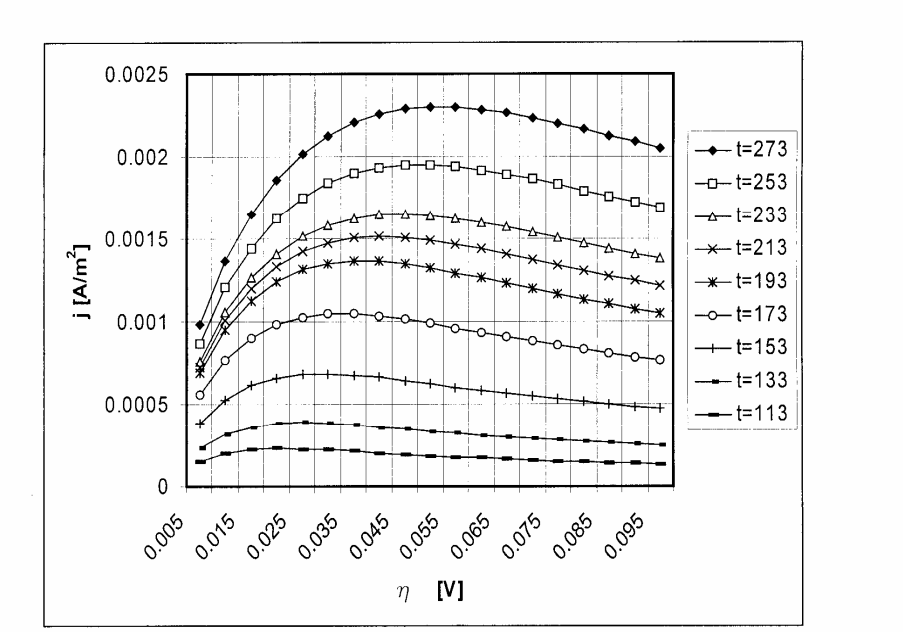

Fig.1. j vs. η plots (50 mV/s scan rate) in different temperature conditions between 113 K and 273 K

In critical conditions (T_c) the numerical estimation show that one can write:

$$FD^{1/2}c|v|^{1/2} \cdot \pi^{1/2} = j^0 \exp(\beta\eta_{Tc})[1+\exp(-f\eta_{Tc})] \cdot \eta_{Tc}^{1/2}$$

From this eq. it is possible to calculate the critical temperature in classical treatement.

REFERENCES

1. J.M. Rosamilia, B. Miller, L.F. Schneemeyer, J.V. Wazsczak, H.M. O'Bryan jr., *J.Electrochem.Soc*., 1987, ***134***, 1863.
2. N. Bonciocat, *Electrochimie şi aplicații*, Ed.Dacia Europa Nova, Timişoara, 1996, p. 268-282.
3. N. Bonciocat, *Alternativa Fredholm în electrochimie*, (in press).
4. S. Ching, J.T. McDevitt, S.R. Peck, R.W. Murray, *J.Electrochem.Soc*.,1991, ***138***, 2308.

STUDIA UNIVERSITATIS BABEŞ-BOLYAI, CHEMIA, XLIII, 1-2, 1998

SYNTHESIS OF PERHYDRO-1,3-OXAZINE DERIVATIVES

LUMINIȚA MUNTEAN, ION GROSU and SORIN MAGER*

ABSTRACT. The results of the exhaustive literature investigations on the methods used in the synthesis of the perhydro-1,3-oxazine derivatives bearing different substituents are chritically presented.

INTRODUCTION

Despite the interest for the perhydro-1,3-oxazines (used in the synthesis of carbapenems - a new class of antibiotics) there are few papers about their synthesis.

The routes for the perhydro-1,3-oxazine derivatives synthesis are illustrated by the following scheme:

1.Direct reaction between γ-aminoalcohols and carbonyl compounds
- 1.1.Condensation of aldehydes
  - 1.1.1.Aliphatic aldehydes
  - 1.1.2.Aromatic aldehydes
- 1.2.Condensation of ketones

2. Reaction between carbonyl compounds and 1,3,2-oxazaborinanes
3. Reduction of dihydro-1,3-oxazine derivatives
4. Synthesis from isoxazolidines and isoxazolidinium salts
5. Other methods

DISCUSSION

1. Direct reaction between γ-aminoalcohols and carbonyl compounds

A likely mechanism for the formation of perhydro-1,3-oxazine derivatives is shown in Scheme 1 [1].

The condensation reaction of aminopropanol and carbonyl compound leads to the intermediate α,β-carbindiolamine ***I***, which can undergo cyclodehydration to the perhydro-1,3-oxazine ***III***, via the Schiff base ***II***.

The conditions used for the reaction of the carbonyl compounds with γ-aminoalcohols are quite different and correlated with the reactivity of the starting compounds and the stability of the reaction product.

* "*Babeş-Bolyai" University, Organic Chemistry Department*, *11 Arany Janos str., RO-3400, Cluj-Napoca, Romania.*

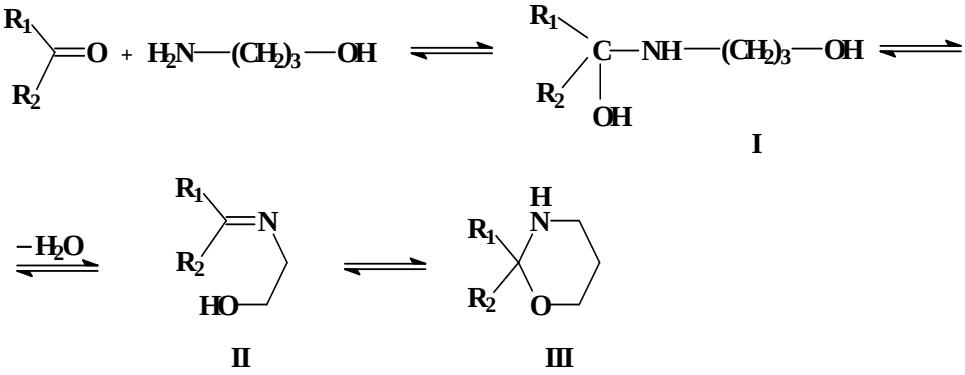

Scheme 1

1.1. Condensation of aldehydes

1.1.1. Aliphatic aldehydes

The condensation between CH_2O and γ-aminoalcohols was performed in different conditions depending on the structure of the used γ-aminoalcohol [Scheme 2;Tables 1 and 2]

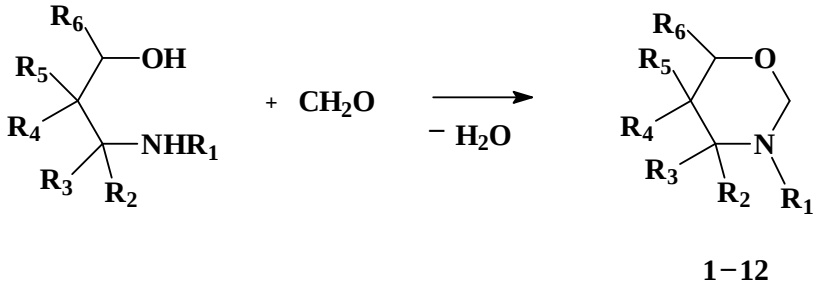

Scheme 2

Table 1

Perhydro-1,3-oxazine derivatives obtained starting from formaldehyde

Compound	R_1	R_2	R_3	R_4	R_5	R_6
1	Me	H	H	H	H	H
2	Et	H	H	H	H	H
3	i-Pr	H	H	H	H	H
4	t-Bu	H	H	H	H	H
5	Me	Me	H	H	H	H
6	Et	Me	H	H	H	H
7	i-Pr	Me	H	H	H	H
8	Benzyl	H	H	H	H	H

Compound	R_1	R_2	R_3	R_4	R_5	R_6
9	Benzyl	Ph	H	H	H	H
10	Me	Me	H	Me	H	H
11	Benzyl	Me	H	Me	H	H
12	Me	Me	Me	H	H	Me

Table 2

Conditions used in the synthesis of compounds 1-12

Compounds	Solvent	Temp. ^{0}C	Yield %	Ref.
1-7	benzene	78	65-79	2, 3, 4
8-11	THF	20	45-92	5
12	water	20	35	6

The best results are obtained at room temperature, using tetrahydrofurane as solvent and N-phenyl- and N-cyclohexylamino propanols as starting materials.

The nature of the γ-aminoalcohol determines the choice of conditions used in reactions. Thus the compounds with unsubstituted nitrogen atom [Scheme 3] are obtained at room temperature, in anhydrous methanol [7] or CH_2Cl_2 [8] as solvent (in the last case, the water formed in the reaction is removed with anhydrous K_2CO_3).

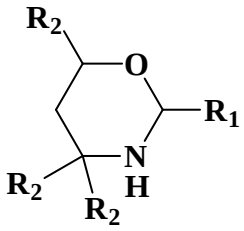

13

R_1 = CH_3 , CH_2CH_3 , CH_2Ph, CH_2OH

R_2 = H, CH_3

Scheme 3

The conditions used in the condensation reaction between N-substituted γ-aminoalcohols and aliphatic aldehydes are determinated by the volume of the N-alkyl substituent. The process for N-methyl substituted compounds [Scheme 4] can be performed without solvent, at room temperature (yields 36-59%) [2] or in water when higher yield (73% instead of 59%) [6] is obtained.

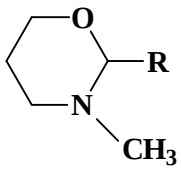

14

R = Me, Et, iPr, tBu

Scheme 4

The N-alkyl γ-aminoalcohols bearing ethyl or i-propyl groups react [Scheme 5] at room temperature, in diethyl ether under nitrogen atmosphere. The decreasing of the reactivity of carbonyl compound led to a decreasing of the yields.

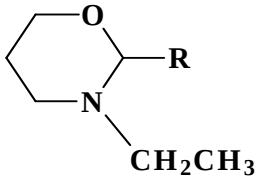

15

R = Me η = 89%
R = Et η = 46%
R = iPr η = 42%

Scheme 5

The steric effect of the alkylamino group determines the decreasing of the yield simultaneously with the increasing of the volume of the alkyl group [3].

The N-benzyl substituted compounds [Scheme 6] are obtained in toluene, at a temperature correlated with the reactivity of the carbonyl compound [9].

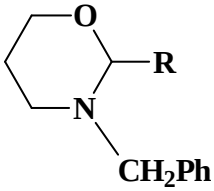

16

R = Me, Et, iPr, CH_2CH_2Ph, C_8H_{17}

Scheme 6

N-benzylaminopropanol and acetaldehyde (also propionaldehyde and butyraldehyde) react at room temperature. The water is remove using molecular sieves. The highest yield was obtained with the bulkyest aldehyde (the explanation being the better solvation in toluene). The carbonyl compounds with small reactivity react at the reflux of solvent in acidic conditions (para toluene sulphonic acid - PTSA; yields 91-94%).and the water resulted in the process is removed using a Dean-Stark trap.

1.1.2.Condensation of aromatic aldehydes

Aromatic aldehydes react with γ-aminoalcohols bearing a free amino group in anhydrous ethanol, at room temperature (yields 82-95%)[Scheme 7], [10-12].

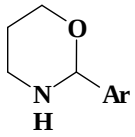

17

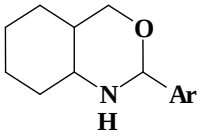

18

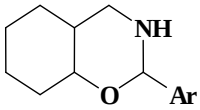

19

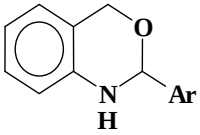

20

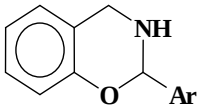

21

Ar = C_6H_4X or 2 , 3, 4 – pyridyl

X = o, m, p – NO_2 , p – Cl, p – CH_3

p– OCH_3 , p– NH_2 , p–$N(CH_3)_2$

Scheme 7

The reaction of nitrobenzaldehydes in anhydrous methanol revealed a decreasing of the yields in order o>m>p (93-86-60%) [7].

The N-alkyl aminopropanols (where the alkyl group can be methyl, ethyl, i-propyl) react with aromatic aldehydes in benzene or toluene, at the reflux of the solvent with the azeotropic removal of the water produced in the reaction. The yields (92-96%) are practically independent of the reactivity of the starting compounds [13].

For the series of N-benzyl derivatives **22** (obtained in toluene) yields of 91-98% are reported [9] [Scheme 8]

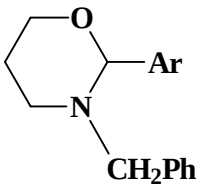

22

Ar = Ph, p–CH_3O–C_6H_4

Scheme 8

whereas the series of polysubstituted perhydro-3-benzyl-1,3-oxazines are obtained in benzene, in smaller yields (63%, chromatographic control) [14] [Scheme 9] using molecular sieves.

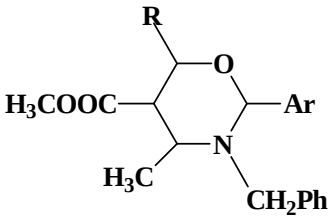

23

R = CH_3 , Ph

Ar = Ph, p– NO_2 – C_6H_4

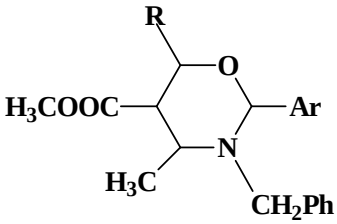

23

R = CH_3 , Ph

Ar = Ph, p– NO_2 – C_6H_4

Scheme 9

1.2.Condensation of ketones

Compound **24** derived from acetone was obtained at 65^{0}C, without solvent [15] [Scheme 10]

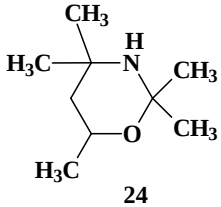

24

Scheme 10

The cyclic aliphatic ketones (cyclohexanone and derivatives) reacted with γ-aminoalcohols in benzene, at reflux [Scheme 11 and Table 3].

Table 3

Conditions used in the synthesis of spiro perhydro-1,3-oxazines

Compouns	Solvent	Temp ^{0}C	Yield %	Ref.
25, 26	-	65	-	15
27 - 34	Benzene	80		16
35 - 38	Benzene	80	-	15, 17, 18

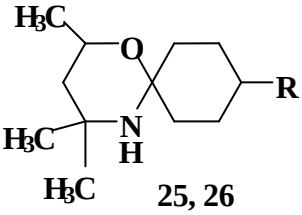

25, 26 R = H, tBu

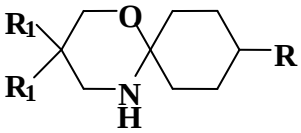

27–34 R = H, Me, tBu, Ph; R_1 = H, Me

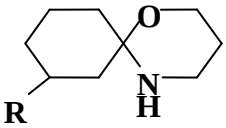

35, 36 R = H, Me

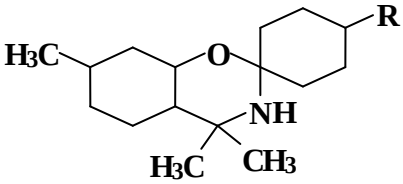

37, 38 R = H, tBu

Scheme 11

Acetophenone derivatives have been obtained in acidic conditions (PTSA), in toluene, at reflux [Scheme 12], [19, 20].

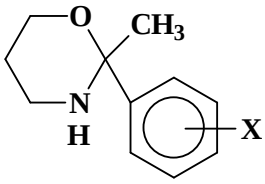

39

Scheme 12

2. Reaction between carbonyl compounds and 1,3,2-oxazaborinanes

The reaction of 1,3,2-oxazaborinanes with carbonyl compounds leads to perhydro-1,3-oxazine derivatives [Scheme 13], [21-23]

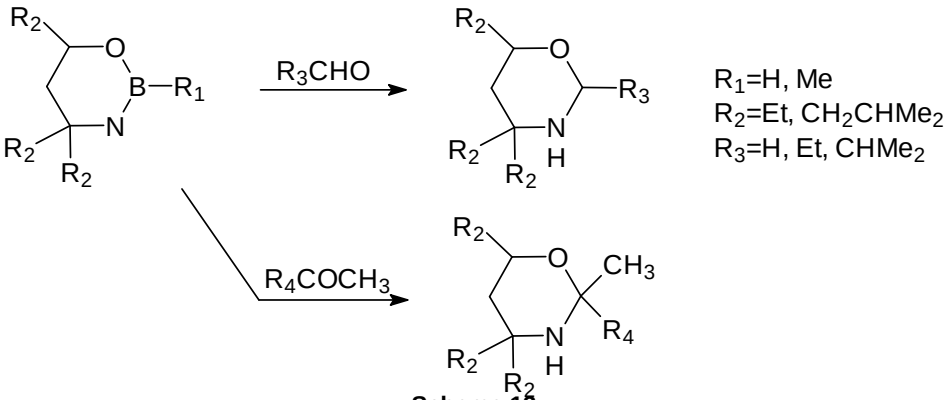

Scheme 13

The mechanism of the reaction involves transition structures obtained by the coordination of the carbonylic oxygen by boron or by the nucleophylic attack of the heterocyclic oxygen to the carbonylic carbon.

Different yield are reported for the reaction of ketones with 1,3,2-oxazaborinanes in different conditions: 83% in aqueous NaOH, 41% in the presence of $ZnCl_2$ and 30% without catalist.

1,3,2-Oxazaborinanes do not react with benzophenone and acetophenone.

3. Reduction of dihydro-1,3-oxazine derivatives

The reduction of dihydro-1,3-oxazine derivatives is performed in different conditions, depending on the position of the double bond.

5,6-Dihydro-2H-1,3-oxazine derivatives (obtained from 2-aza-1,3-dienes and aldehydes [24]) are reduced with Na/ i-PrOH, in tetrahydrofurane, at room temperature, in excelent yields (93-95%)[Scheme 14; 25]

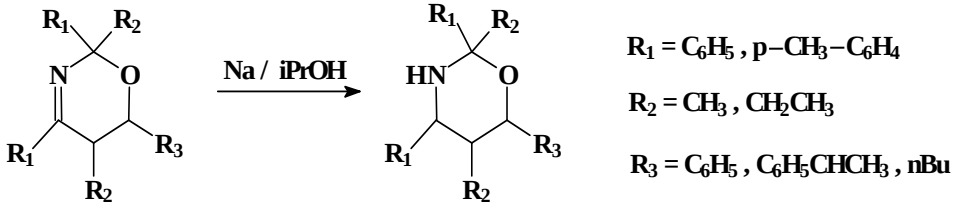

42

Scheme 14

The reduction with $LiAlH_4$ leads to γ-aminoalcohols by ring opening.

5,6-Dihydro-4H-1,3-oxazines (obtained from aldehydes and glycolonitril [26]) are reduced with $NaBH_4$ at low temperature (-45^0C)(yields 69-77%)[26-28; Scheme 15].

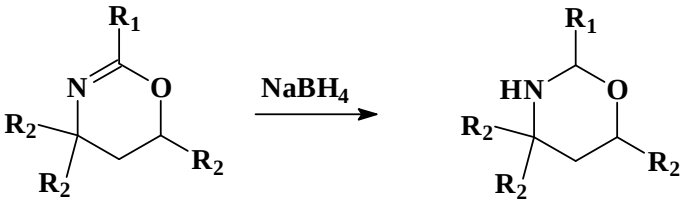

R_1 = H, Me , Ph

R_2 = H, Me

43

Scheme 15

4. Synthesis from isoxazolidines and isoxazolidinium salts

Isoxazolidines can react with CO, in catalitic conditions, to give perhydro-1,3-oxazines [Scheme 16; 29]

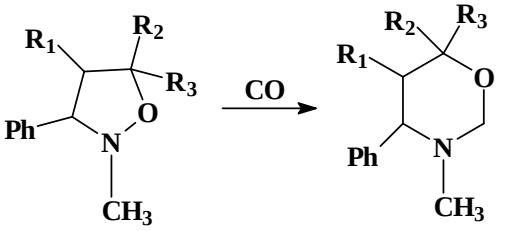

R_1 = $COOCH_3$, $COOC_2H_5$

R_2 , R_3 = alkyl, Ph

44

Scheme 16

The reaction is carried out in benzene, the catalists being Ir and Rh complexes.

The reaction of isoxazolidines (available from nitrones and alkenes [30]) with trimethylphosphate arises into perhydro-1,3-oxazinium salts (yields 93-98%). The reaction proceeds under nitrogen, at 100^0C and follows a four steps mechanism [Scheme 17]:

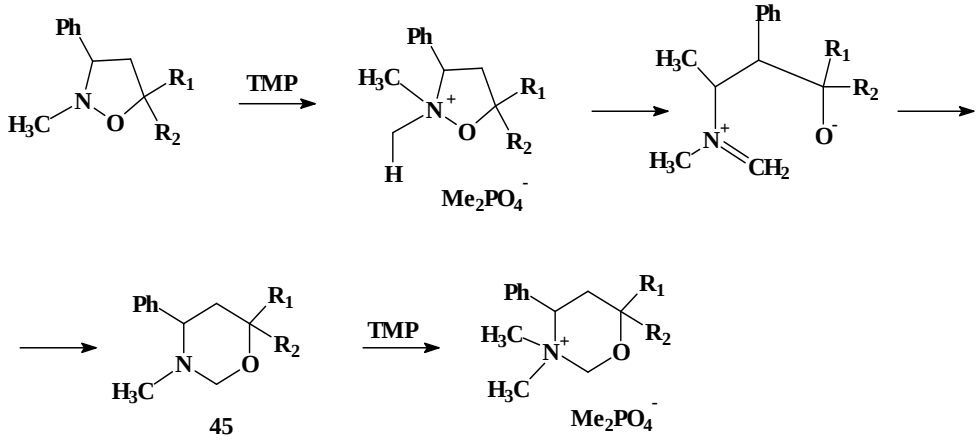

Scheme 17

Perhydro-1,3-oxazinium salts are reduced with NaH in acceptable yields (44-56%).

Isoxazolidinium salts leads to perhydro-1,3-oxazines by reduction with NaH, in dimethoxyethane (yields 51-85%)[Scheme 18; 31].

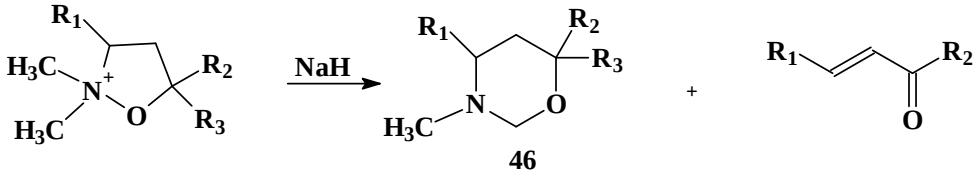

$R_1 = C_6H_5$, $p-CH_3O-C_6H_4$

$R_2 = C_6H_5$, $p-CH_3-C_6H_4$, $p-CH_3O-C_6H_4$, $p-Cl-C_6H_4$

$R_3 = H, C_6H_5$

Scheme 18

The reaction proceeds probably by the attack of the base at the methyl connected to the nitrogen atom; the intermediate β-hydroxyiminic derivative can undergo cyclisation with ring expansion.
α,β-Enone has been obtained as minor product (formed by the extraction of the C(5) hydrogen followed by a Hofmann like reaction).
The reduction can proceed also in 10% aqueous NaOH (yield 52%) [31].

5. 2-Acyl perhydro-1,3-oxazine derivatives can be obtained from aminoalcohols and phenylglioxal (yield 85-91%) [26] or from aminopropanol and ethylchlorocarbonate (yield 77%) [32] [Scheme 19].

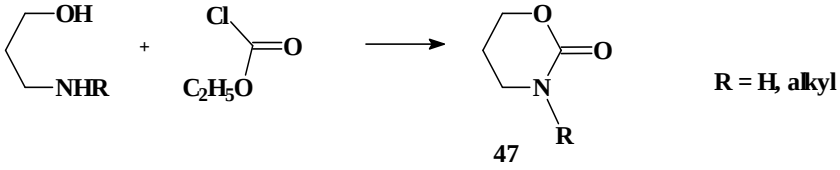

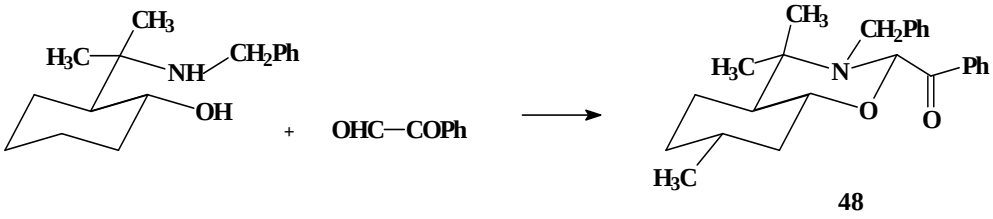

Scheme 19

REFERENCES

1. R.J. La France, H.W. Manning, K. Vaughan, *J.Org.Chem.*, 1985, **50**, 2229.
2. I.J. Ferguson, A.R. Katritzky, D.M. Read, *J.C.S.Perkin II*, 1977, 818.
3. A.R.Katritzky, V.J.Baker, F.M. Brito-Palma, *J.C.S.Perkin II*, 1980, 1739.
4. M.J. Cook, R.A.Y. Jones, A.R. Katritzky, M.M. Manas, A.C. Richards, A.J. Sparrow, D.L. Trepanier, *J.C.S.Perkin II*, 1973, 325.
5. C. Bartoli, C. Cimarelli, G. Palmieri, *J.Chem.Soc.Perkin Trans I*, 1994, 537.
6. H. Booth, R.U. Lemieux, *Canad.J.Chem.*, 1971, **49**, 777.
7. H. Singh, K. Singh, *Tetrahedron*, 1989, **45**, 3967.
8. R.F. Borch, R.R. Valente, *J.Med.Chem.*, 1991, **34**, 3052.
9. A. Alberola, M. Angeles Alvarez, C. Andres, A. Gonzales, R. Pedrosa, *Synthesis*, 1990, 153.
10. F. Fulop, K. Pihlaja, J. Mattinen, G. Bernath, *J.Org.Chem.*, 1987, **52**, 3821.
11. S. Jain, K. Sujatha, K.V. Rama Krishna, R. Roy, J. Singh, N. Anand, *Tetrahedron*, 1992, **48**, 4985.
12. F. Fulop, M. Dalqvist, K. Pihlaja, *Acta Chem.Scand.*, 1991, **45**, 273.
13. M.Le Lann, S. Saba, M. Shoja, *J.Heterocyclic Chem.*, 1991, **28**, 1789.
14. N. Asso, T. Uyehara, Y. Yamamoto, *Tetrahedron*, 1990, **46**, 4563.
15. A. Rassat, P. Rey, *Tetrahedron*, 1974, **30**, 3315.
16. L. Muntean, I. Grosu, G. Plé, S. Mager, *Chem.Comm.*, 1998, submitted.
17. T.C. Smale, *Tetrahedron Lett.*, 1984, **25**, 2913.
18. R.J. Ponsford, R. Southgate, *J.C.S.Chem.Comm.*, 1979, 846.
19. F. Fulop, K. Pihlaja, K. Neuvonen, G. Bernath, G. Argay, A. Kalman, *J.Org.Chem.*, 1993, **58**,1967.
20. P. Vainiotalo, F. Fulop, K. Pihlaja, *Org.Mass.Spectr.*, 1991, **26**, 438.
21. A.R. Kalyuskii, V.V. Kuznetsov, A.I. Gren, *Ukr.Khim.Zh.*, 1988, **54**, 998, CA **110**, 212729j.
22. A.R. Kalyuskii, V.V. Kuznetsov, A.I. Gren, *Zh.Obshch.Khim.*, 1989, **59**, 1438, CA **112**, 198260g.
23. V.N. Elokhina, A.S. Nakhmanovich, I.D. Kalikhman, R.V. Karnaukhov, *Zh.Org.Khim.*, SYNTHESIS OF PERHYDRO-1,3-OXAZINE DERIVATIVES 1989, **25**, 2202, CA **113**, 6252g.
24. J. Pitlik, I.Miskolczi, K.E. Kover, C.J. Jaszberenyi, F. Sztaricskai, *Tetrahedron Lett.*, 1989, **30**, 2005.
25. J. Barluenga, B. Olano, S. Fustero, *J.Org.Chem.*, 1985, **50**, 4052.
26. H. Singh, K. Singh, *Tetrahedron*, 1988, **44**, 5897.
27. P. Henley-Smith, D.A. Whiting, A.F. Wood, *J.C.S.Perkin I*, 1980, 614.
28. O. Arjona, R. Perez-Ossorio, A. Perez-Rubalcaba, M.L. Quiroga, *J.C.S.Perkin II*, 1981, 597.
29. K. Khumtaveeporn, H. Alper, *J.Org.Chem.*, 1995, **60**, 8142, CA **123**, 339951z.

30. U. Chiacchio, A. Liguori, G. Romeo, G. Sindona, N.Uccella, *Heterocycles*, 1993, **36**, 799.
31. A. Liguori, G. Romeo, G.Sindona, N. Uccella, *Gazzetta Chimica Italiana*, 1991, **121**, 393.
32. X.-C. He, E.L. Eliel, *Tetrahedron*, 1987, 43, 4979.

STUDIA UNIVERSITATIS BABEŞ-BOLYAI, CHEMIA, XLIII, 1-2, 1998

FURYL-BENZOTHIAZOLES. SYNTHESIS AND REACTIVITY

FL. D. IRIMIE, CS. PAIZS, C.CHENDER, FR. JOO, R. SILAGHI-DUMITRESCU[1], CORNELIA MAJDIK, MONICA TOŞA

ABSTRACT. Synthesis of some new furyl-benzothiazoles is presented. Formilation of these structures is possible when in position 6 of the benzothiazolic ring contained no vidrawing groups.

Reduction of these aldehydes with $NaBH_4$ is a convenient method for obtained corresponding hydroxymethyl derivatives.

INTRODUCTION

As a part of our research in the furan series the synthesis of some new 2-furyl-2-benzothyazoles its became necesarely for biological tests on bactericidal and bacteriostatic activity. It's well known that furyl-benzothiazolical structures have an antifungical activity [1] and its also known that the position of substituents at the benzenic ring have an influence on this biological activity [2].

In order to evaluate the biological behaviour of structures substituted in pozition 5 on the furan ring we formilated some of these structures and reduced them to the corresponding hydroxymethyl derivatives.

The 2-furyl-2-benzothiazoles were obtained from the corresponding tiofuranilides using the Jacobson method by oxidations with $K_3[Fe(CN)_6]$ in aqueous medium [3]. Tiofurananilides were obtained from furanilides using phosphorus pentasulphide (Scheme 1).

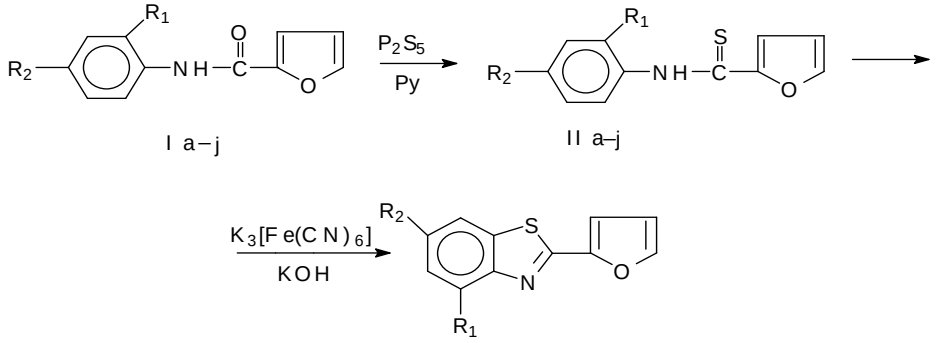

Scheme 1

a: R_1 =H, R_2 = H f: R_1 =H, R_2 = CH_3

[1] *"Babeş-Bolyai" University, Faculty of Chemistry and Chemical Engineering, 11 Arany Janos St., 3400 Cluj-Napoca, Romania.*

b: R_1 =H, R_2 = F
c: R_1 =H, R_2 = Cl
d: R_1 = H, R_2 =Br
e: R_1 =H, R_2 = I
g: R_1 =H, R_2 = OCH_3
h: R_1 =CH_3, R_2 = H
i: R_1 =Br , R_2 = H
j: R_1 =I , R_2 = H

The mechanism of cyclisation presented in Scheme 2 was proposed by Metzger and Plank [4]. The anion appeared in basic medium, was oxidized to sulphurous cation.

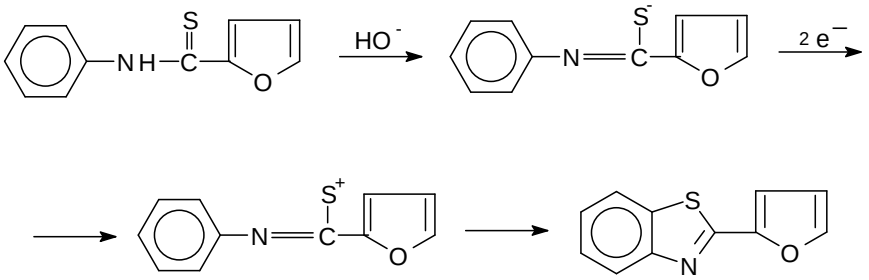

Scheme 2

The yield of cyclisation depends directly on the electron density in benzene ring (Tab.1):

Table 1

Structures	Yield %
I a	71
I b	22
I c	37
I d	61
I e	63
I f	74
I g	90
I h	72
I i	60
I j	63

The Vilsmeyer-Haack formilation of some of structures III is give in scheme 3:

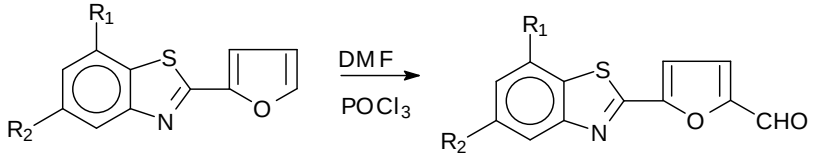

III IV

Scheme 3

a: R_1 = H, R_2 = H

d: R_1 = H, R_2 = Br
f: R_1 = H, R_2 = CH_3
g: R_1 = H, R_2 = OCH_3

The reducing of the formyl derivatives with $NaBH_4$ in 2- propanol is presented in scheme 4:

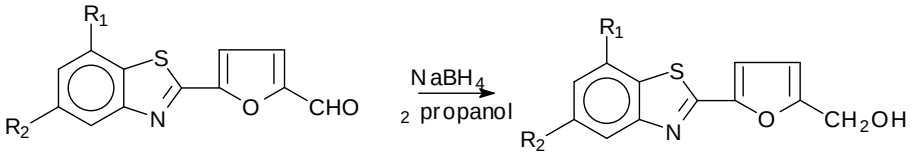

IV V

Scheme 4

a: R_1 = H, R_2 = H
d: R_1 = H, R_2 = Br
f: R_1 = H, R_2 = CH_3
g: R_1 = H, R_2 = OCH_3

EXPERIMENTAL

The elemental analysis for C, H, S, N and halogen were within +/- 0,4% of the theoretical values for III a-j, IV a, d, f, g, and V a, d, f, g. Melting points are given uncorrected. The reactions were monitored by TLC using benzene:ethylacetate 8:2 (v:v) as eluent, visualisation was made with an 260 nm wave light UV source.

The mass spectra were recorded on double focusing Varian Mat 311 spectrophotometer, with an electronic impact source at 70 eV and 300 μA. ^{1}H-NMR spectra were recorded using $CDCl_3$ as solvent with a Varian Gemini 300 MHz Spectrometer. For the recording of IR spectra, a FT-IR Nicolet 205 spectrophotometer, in KBr pellets was used.

Structures I a,d,f,i were prepared as in (5) and structures IV a,d,f as in [6].

General procedure for tionation: 0,003 mols of furanilide is dissolved in 50 ml boiling pyridine and its added 17,8 g (0,08 mols) fine pulvered small portions. Then the mass reaction is boiled 90 min. and after cooling its treated with 250 ml HCl (1:1). The precipitate is filtered, wash with cold water and treated with 250 ml 20% KOH solution and heated to 50 ^{0}C. The suspension is treated with active carbon, filtered, and after that solution is acidifiated with HCl (1:1) v:v. The precipitate is filtered, dryed and its recristalized from an ethanol: water mixture (3:1) v:v.

General procedure for cyclization: 0,005 mols of thioanilide is dizolved in 20 ml 40% KOH solution. To the solution is added 60 ml water and its warmed to 40-45^{0}C. To this solution is added 20 ml 20% $K_3[Fe(CN)_6]$ solution which is previously

warmed to 40-45^{0}C. After 12 hrs. the precipitate is filtered, dryed and recrystalized from methanol.

General procedure for formilation: To a mixture of 3 ml ice-cooled dimethylformamide and 1 ml phosphorous oxychloride a solution of 0,5 g of furanilide is dropwire add. The mixture is warmed at 100^{0}C for 2 hrs. and then poured on 50 g ice. The pH is adjusted at 6 with a solution of sodium acetate (10 g in 15 ml water) is add allowed to stand at room temperature for a few hours. The precipitate is filtered, wash with water and recristalized from glacial acetic acid.

General procedure for reduction: 0,1 g $NaBH_4$ is add to seven ml isopropanol. The mixture is stirred for 1,5 hours, while adding the formyl-derivative (0,2 g) in small amounts. The solution is alowed to stand over night, then diluate HCl is add until no more gas evolution is observe. The organic compounds are extract with $CHCl_3$ (five times), then the solvent is evaporate affording the hydroxyl-derivative which is wash with isopropanol.

RESULTS AND DISCUSSION

2-furyl-2-(6-fluoro-benzothiazole) (III b) m.p.=113^{0}C; IR(cm^{-1}): 1610, 1580, 1450 (for benzothiazole ring); ^{1}H-NMR spectrum (DMSO d_6): 6.8 (q, 1H), 7.23 (d, 1H), 7.60(d,1H), 7.93 (d, 1H), 8.13(d,1H), 8.43(s, 1H); MS (m/e): 219(100)M, 220(13)M+1, 221(12) M+2, 218(9) M-1, 191(46)M-CO, 164(30), 126(26)

2-furyl-2-(6-chloro-benzothiazole) (III c) m.p.=119^{0}C; IR(cm^{-1}): 1605, 1575, 1450 (for benzothiazole ring); ^{1}H-NMR spectrum (DMSO d_6): 6.8 (q, 1H), 7.21 (d, 1H), 7.57(d,1H), 7.98 (d, 1H), 8.02(d,1H), 8.3(s, 1H); MS (m/e) 235(100)M, 237(37)M, 207(60), 209(20) M-CO, 172(20), 145(12)

2-furyl-2-(6-iodo-benzothiazole) (III e) m.p.=124^{0}C; IR(cm^{-1}): 1600, 1575, 1430; ^{1}H-NMR spectrum (DMSO d_6): 6.75 (q, 1H), 7.3 (d, 1H), 7.5(d,1H), 7.6 (d, 1H), 7.93(d,1H), 8.01(s,1H); MS (m/e): 313(30)M, 283(13) M-CO, 220(3), 95(100)

2-furyl-2-(4-methyl-benzothiazole) (III f) m.p.= 107^{0}C, IR(cm^{-1}): 1590, 1560, 1430 (for benzothiazole ring); ^{1}H-NMR spectrum (DMSO d_6): 2.63 (s, 3H), 6.77 (q, 1H), 7.34-7.99(m,5H) ; MS (m/e) 215(100)M, 287(29)M-CO, 154(30), 121(41)

2-furyl-2-(chloro-benzothiazole) (III i) m.p.=129^{0}C; IR(cm^{-1}): 1605, 1580, 1450 (for benzothiazole ring); ^{1}H-NMR spectrum (DMSO d_6): 6.8 (q, 1H), 7.43(m, 2H), 7.62(d,1H), 8.02(d,2H); MS (m/e) 235(100)M, 237(37)M, 207(60), 209(20) M-CO, 172(20), 145(12)

2-furyl-2-(4-iodo-benzothiazole) (III j) m.p.=131^{0}C, IR(cm^{-1}): 1600, 1570, 1440; ^{1}H-NMR spectrum (DMSO d_6): 6.8 (q, 1H), 7.16 - 8.15(m,5H); MS (m/e): 323(30)M, 283(13) M-CO, 220(3), 95(100).

5-[2](6-methoxi-benzothiazolil)]-furyl-2-carboxaldehyde (IV g) m.p.=137^{0}C, IR(cm^{-1}): 1680 (CHO); ^{1}H-NMR spectrum (DMSO d_6): 3.57(s.3H), 7.19(d,1H), 7.5(d,1H), 7.75(d,1H), 7.80(s,1H), 7.99(d,1H); MS (m/e): 259(100)M, 244(80), 216(43)M-CH_3-CO, 159(29), 95(34)

2-hydroxymethyl-5-(2-benzothiazole)-furan (V a): yield = 73%, white crystals, m.p.=178^{0}C; IR spectrum (KBr)ν_{max}cm^{-1}: 1050, 3400 (OH). MS: m/e (rel.intensity, %): 231 (100 M^+, 232(11) M^++1, 233 (6) M^++2, 230 (8) M^+-1, 214 (56) M^+-17, 202 (53), 168 (32); ^{1}H-NMR spectrum ($CDCl_3$): 4.62 2H (s), 6.60 1H (d), 7.29 1H (d), 7.3-8.2 4Har (m)

2-hydroxymethyl-5-[6-methyl-(2-benzothiazole)]-furan (V b): yield = 78%, white crystals, m.p.=181^{0}C; IR spectrum (KBr) n_{max}: 1050, 3400 (OH). MS: m/e (rel.intensity, %): 245 (100)M^+, 246 (10) M^++1, 247 (8)M^++2, 244 (9)M^+-1, 228 (54)M^+-17, 216 (32), 200 (19); ^{1}H-NMR spectrum ($CDCl_3$): 2.49 3H (s), 4.73 2H (s), 6.60 1H (d), 7.15 1H (d), 7.2-8.1 3Har (m)

2-hydroxymethyl-5-[6-methoxy-(2-benzothiazole)]-furan (V c): yield = 75%, collorlenes crystals, m.p.=184^{0}C; IR spectrum (KBr) ν_{max} cm^{-1}: 1050, 3400 (OH); MS: m/e (rel.intensity, %): 261 (100) M^+, 262 (26) M^++1, 263 (11) M^++2, 260 (11) M^+-1, 246 (20), 245 (9), 244 (46) M^+-17, 232 (15); ^{1}H-NMR spectrum ($CDCl_3$): 3.90 3H (s), 4.73 2H (s), 6.67 1H (d), 7.18 1H (d), 7.2-7.9 3Har (m)

2-hydroxymethyl-5-[6-bromo-(2-benzothiazole)]-furan (V d): yield = 81%, white crystals m.p.=211^{0}C; IR spectrum (KBr) ν_{max} cm^{-1}: 1050, 3300 (OH). MS: m/e (rel.intensity, %): 311(100) M, 309(20)M, 313(4) M+2, 308(93)M-1, 294(23)M-17, 293(8)M-17, 292(30), 214(17), 212(16), 185(10), 184(2);^{1}H-NMR spectrum ($CDCl_3$): 4.75 2H (s), 6.65 1H (d), 7.23 1H (d), 7.4-8.3 3Har (m).

The yield of oxidative cyclisation of tiofuranilides with $K_3[Fe(CN)_6]$ depends of the behaviour of the substituent at the phenylic ring. In case of vidrawing groups the yield decrease because the electrophylic substitution is concured by hydrolyse of thioanilide to anilide.

Molecular peaks for ***IV a-h*** and ***V a-d*** are clear, the characteristic peaks for fragmentation of the benzilic type alcoholic group (M-17) were observed in case of ***V a-h*** and the characteristic peaks of aldehydes (M-28) in case of ***IV a-h*** are observed too.

For the structures ***V a-d*** the presence of the singlet at δ = 4,6 corresponding for two protons, indicated the existence of the methylenic group. At the same time the signals for the aldehydical protons at δ = 9,60 which are characteristic the compounds ***IV a-h*** are not observed in case of ***V a-d***.

CONCLUSIONS

Oxidative cyclisation with $K_3[Fe(CN)_6]$ in KOH aq. medium is a convenient method for furyl-benzothiazole synthesis.

Formilation of these structures is possible when in position 6 of the benzothiazolic ring contained no vidrawing groups. Reduction of these aldehydes with $NaBH_4$ is a convenient method for obtained corresponding hydroxymethyl derivatives.

The advantage of reduction with $NaBH_4$ is the mild conditions, good yields and the symplicity of the method.

REFERENCES

1. V. Fărcăşan, F. Paiu, *Studia Universitatis Babeş-Bolyai. Chemia*, 1966, ***11***, 107.
2. Gh. Miron, Gh. Ripeanu, *Comunicările Acad. RPR*, 1961, ***11***, 241.
3. P. Jacobson, *Ber. dtsch. chem. Ges.,* 1886, ***19***, 1067.
4. J. Metzger, H. Plank, *Chemie et Industrie*, 1956, **75**, 929
5. V. Fărcăşan, I. Meşter, *Studia Universitatis Babeş-Bolyai. Chemia*, 1967, ***2***, 69.
6. V. Fărcăşan, F. Paiu, *Studia Universitatis Babeş-Bolyai. Chemia*, 1971, ***16***, 111.

STUDIA UNIVERSITATIS BABEŞ-BOLYAI, CHEMIA, XLIII, 1-2, 1998

SYNTHESIS AND REDUCTION OF SOME NITRO-BENZOFURANS

CORNELIA MAJDIK, FL.D.IRIMIE, CS. PAIZS, R. SILAGHI-DUMITRESCU, FR. JOO and MONICA TOŞA[1]

ABSTRACT. During the acid catalysis the o- and p-(nitrophenyl)-acetophenoxymes ***1a-e*** undergo a transposition-cyclisation to 2-phenyl-5-nitrobenzofurans and 2 phenyl-7-methyl-benzofurans ***2a-e***. The reduction of ***2a-k*** was made using the Bechamp method. The synthetised structures were characterized with the ^{1}H-NMR, IR and MS-Spectrometry.

INTRODUCTION

In a previous work [1] was related the synthesis of some o-(nitrophenyl)-acetofenoxymes from the corresponding ketooxymes and o-, p-nitro-clorbenzene.

In literature is presented the transpozition of these o-arylketooxymes followed by cyclisation which gives the corresponding nitro-benzofurans [2-5] like in the Fischer's indol synthesis. The reactions undergoes in acid catalysis in boiling anhydrous ethanol as medium in presence of gasous HCl or in glacial acetic acid at 100^0 in presence of etherated BF_3 [2].

Morandi and Dupont [5-6], proposed a cyclisation mechanism for aryl-oxymes analogue with the Fischer transposition. This mechanism was confirmed by isolation of the ammonium salts of ***4*** as hydrochlorides [5] or hydrobromides [7] or the ketoform ***5*** obtained from hydrolysis of ***4*** in mild conditions [7].

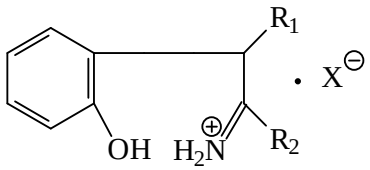

4 X= Cl, Br;

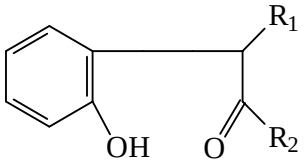

5

Scheme 1

In this paper we present the synthesis of 2-phenyl-7-nitrobenzofuran and 2-phenyl-3-methyl-5-nitrobenzofuran.

[1] *"Babeş-Bolyai" University, Faculty of Chemistry and Chemical Engineering, 11 Arany Janos St., 3400, Cluj-Napoca, Romania.*

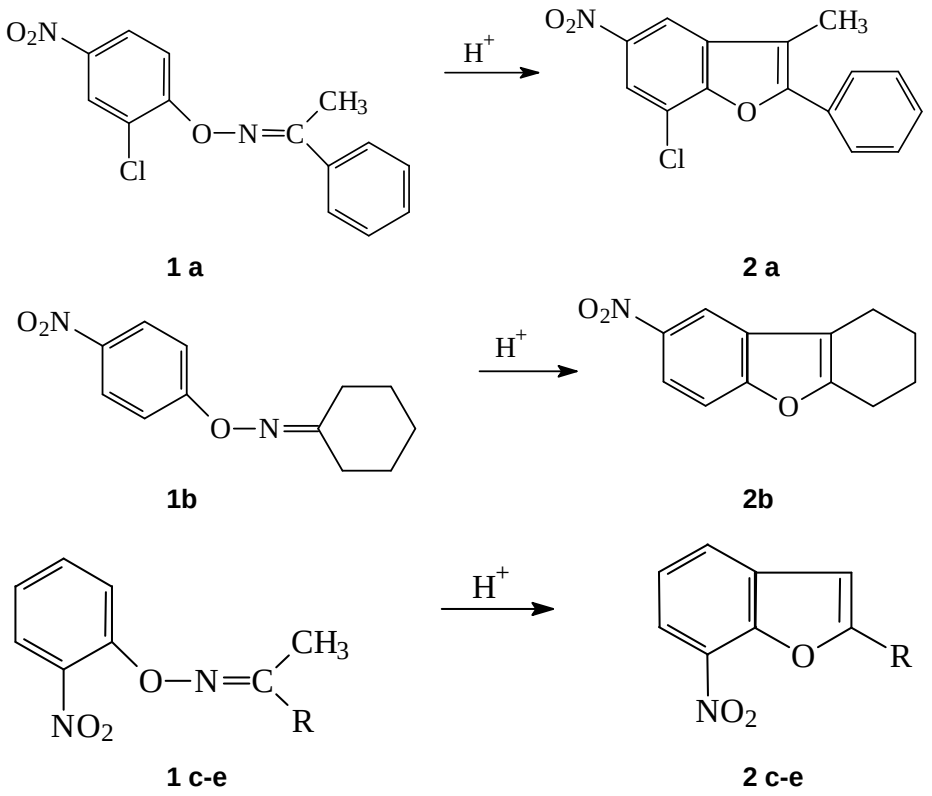

c) R = Ph ; d) R = 4-CH_3-O-Ph; e) R = 4-Cl-Ph

Scheme 2

EXPERIMENTAL

Reagents and solvents were standard grade comercial products and were used without further purification. The substances ***2f-k*** were prepared as in [8].

The elemental analysis for C, H,N and halogenes were within +/- 0,4% of the theoretical values for ***1 a-e*** and ***2 a-k***. Melting points are uncorrected and for ***2a-k*** are given for the chlorohydrates. The reactions were monitored by TLC using benzene:ethylacetate 8:2 (v:v) as eluent, visualisation was made with a 260 nm wave lenght UV source.

The mass spectra were recorded on double focusing Varian Mat 311 spectrometer, with an electronic impact source at 70 eV and 300 μA. ^{1}H-NMR spectra were recorded using $CDCl_3$ as solvent with a Varian Gemini 300 MHz Spectrometer. For the recording of IR spectra, a FT-IR Nicolet 205 spectrophotometer, in KBr pellets was used.

General method for synthesis of benzofurans from aryloxymes

0,1 Molls of ortho or para-nitro-aryloxyme was dissolved in 200 ml ethanol. The solution was refluxed and in this time dryed gasous HCl was barboted in the reaction mass. In case for a good solubilisation it was added 50-100 ml toluene. The heating was continued until the whole quantity of oxyme was transformed (the reaction was monitored by TLC). After that, the solvent was evaporated in vaquo, and the precipitate was washed with water and purified by recrystalization from glacial acetic acid.

General method for reduction

0,05 Molls nitro-benzofuran was suspended in 60 ml water and was added 15 g. $AlCl_3$ and 5 g NaCl. After that, to the suspension was added 50 ml toluene, 3 ml HCl 36% and 8 g powder iron. The mixture was stirred at 100^0C, 5 - 8 hours. The product was extracted with benzene, mass reaction was filtered, the organic layer was separated and concentrated in vaquo. The formed amino-benzofuran was recrystalised from ethanol.

For the reduction of nitrobenzofurans we used Bechamp method.

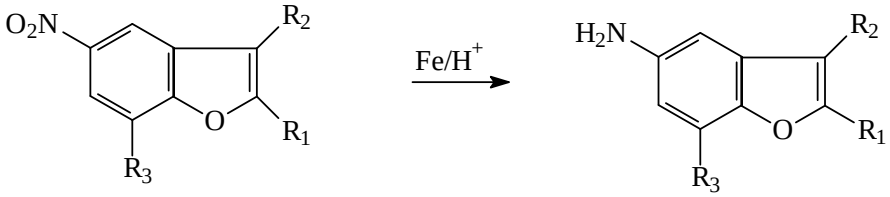

2 a-g **3 a-g**

a) $R_1 = CH_3$, $R_2 = H$, $R_3 = H$
f) $R_1 = CH_3$, $R_2 = CH_3$, $R_3 = H$
g) R_1 = 4-SO_2Et-Ph, $R_2 = H$, R_3 =H
h) R_1 = 4-Br-Ph, $R_2 = H$, R_3 =H
i) R_1 = 4-Cl-Ph, $R_2 = H$, R_3 =H
j) R_1 = Ph, R_2 =CH_3, R_3 =Cl
k) R_1 = 4-F-Ph, $R_2 = H$, R_3 =H

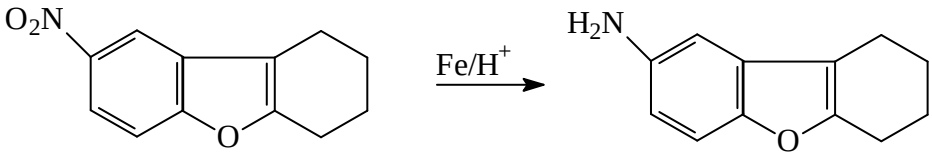

2 b **3 b**

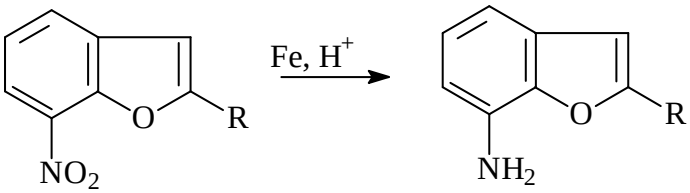

2 c-e **3 c-e**

c) R = Ph; d) R = 4-CH_3O-Ph; e) R = 4-Cl-Ph;

Scheme 3

RESULTS AND DISCUSSION

2-phenyl-3-methyl-7-chloro-5-nitro-benzofuran ***2a***: yield = 73% yellow crystals, m. p.= 173^{0}C. IR spectrum (KBr) ν_{max} cm^{-1}: 1570(C=C), 1380, 1490(NO_2), Mass spectrum: m/e (rel.intensity, %): 273(33) M, 275(10) M, 229(5), 227(16), 199(90), 163(100). ^{1}H-NMR spectrum ($CDCl_3$): 2.50(s, 3H), 7.52- 7.87(m, 5H), 8.33(s, 1H), 8.64(s, 1H).

8-nitro-1, 2, 3, 4- tetrahidro-dibenzofuran ***2b***: yield = 68% yellow crystals, m.p.= 157^{0}C. IR spectrum (KBr) ν_{max} cm^{-1}: 1600(c=c), 1370, 1480(NO_2), Mass spectrum: m/e (rel.intensity, %): 217(70) M, 202(5), 189(100), 171(15). ^{1}H-NMR spectrum ($CDCl_3$): 1.88-1.97(d.d.,4H), 2.73(d,4H), 7.45(d,1H), 8.14(d,1H), 8.33(s,1H).

2-phenyl-7-nitro-benzofuran ***2c***: yield = 65%, yellow crystals, m.p.= 133^{0}C, IR spectrum (KBr) ν_{max} cm^{-1}: 1580(C=C), 1380, 1470(NO_2); Mass spectrum: m/e (rel.intensity, %): 239(43) M, 223(2), 209(3), 193(18), 165(100); ^{1}H-NMR spectrum ($CDCl_3$): 7.13(s,1H), 7.33-7.98(m,7H), 8.12(d, 1H).

2-(4-methoxy-phenyl)-7-nitro-benzofuran ***2d***: yield = 69%, yellow crystals, m.p.= 113^{0}C, IR spectrum (KBr) ν_{max} cm^{-1}:1580(C=C), 1350, 1470(NO_2); Mass spectrum: m/e (rel.intensity, %): 269(38) M, 254(8), 223(35), 208(10),195(40), 152(100); ^{1}H-NMR spectrum (DMSO d_6): 3.82(s,3H), 7.12(d,2H), 7.46(s,1H), 7.49(m,1H), 7.92(d,2H), 8.06(d,1H), 8.12(s,1H).

2-(4-chloro-phenyl)-7-nitro-benzofuran ***2e***: yield = 57%, yellow crystals, m.p.= 133^{0}C, IR spectrum (KBr) ν_{max} cm^{-1}:1600(C=C), 1370, 1480(NO_2); Mass spectrum: m/e (rel.intensity, %): 273(33) M, 275(10)M, 216(3), 21490),180(100); ^{1}H-NMR spectrum ($CDCl_3$): 7.12(s,1H), 7.34-7.48(m,4H), 7.88(d,2H), 8.13(d,1H).

2-(4-chloro-phenyl)-5-amino-benzofuran ***3a***: yield = 56%, white crystals, m.p.= 183^{0}C; IR spectrum (KBr) ν_{max} cm^{-1}: 1650, 3240, 3420(NH_2); Mass spectrum: m/e (rel.intensity, %): 243(100)M, 245(33)M, 216(2), 214(6), 180(20); ^{1}H-NMR spectrum (DMSO d_6):4.73(NH_2), 6.61(d,1H), 6.72(s,1H), 7.25(s,1H), 7.29(d,1H), 7.85(d,1H)

8- *amino-1,2,3,4-tetrahydro-dibenzofuran* ***3b***: yield = 59%, white crystals, m.p.= 225^{0}C; IR spectrum (KBr) ν_{max} cm^{-1}: 1650, 3280, 3430(NH_2); Mass spectrum: m/e (rel.intensity, %): 180(100)M, 153(23), 125(50); ^{1}H-NMR spectrum (DMSO d_6): 188-197(d.d.,4H), 2.73(d,4H), 7.45(d,1H), 8.14(d,1H), 8.33(s,1H)

2-phenyl-7-amino-benzofuran ***3c***: yield = 60%, white crystals, m.p.= 182^{0}C; IR spectrum (KBr) ν_{max} cm^{-1}: 1640, 3190, 3300(NH_2); Mass spectrum: m/e (rel. intensity, %): 209(100)M, 182(7), 180(29), 152(8); ^{1}H-NMR spectrum (DMSO d_6): 5.40(NH_2), 6.57(d,1H), 6.80-7.98(m,9H)

2-(4-methoxy-phenyl)-7-amino-benzofuran ***3d***: yield = 55%, white crystals, m.p.= 263^{0}C; IR spectrum (KBr) ν_{max} cm^{-1}: 1650, 3380, 3450(NH_2); ^{1}H-NMR spectrum (DMSO d_6): 3.82(s,3H), 5.30(NH_2), 6.77-6.94(m,3H), 7.06(d,2H), 7.13(s,1H), 7.89(d,2H)

2-(4-chloro-phenyl)-7-amino-benzofuran ***3e***: yield = 55%, white crystals, m.p.= 193^{0}C; IR spectrum (KBr) ν_{max} cm^{-1}: 1630, 3360, 3430(NH_2); Mass spectrum: m/e (rel.intensity, %): 243(100)M, 245(33)M, 216(3), 214(9), 180(20); ^{1}H-NMR spectrum (DMSO d_6): 3.94(NH_2), 7.13-7.44(m,3H), 7.56(s,1H), 7.62(d,2H), 8.00(d,2H)

2,3-dimethyl-5-amino-benzofuran ***3f***: yield = 60%, white crystals, m.p.= 220^{0}C; IR spectrum (KBr) ν_{max} cm^{-1}: 1620, 3200, 3400(NH_2); ^{1}H-NMR spectrum (DMSO d_6): 2.38(s,3H), 2.52(s,3H), 3.98(NH_2), 7.18(d,1H), 7.41(s,1H), 7.53(d,1H)

2-(4-sulpho-ethyl-phenyl)-5-amino-benzofuran ***3g***: yield = 55%, white crystals, m.p.= 193^{0}C; IR spectrum (KBr) ν_{max} cm^{-1}: 1630, 3350, 3450(NH_2); Mass spectrum: m/e (rel.intensity, %): 239(100)M, 224(46), 212(8), 197(3), 196(13)

2-(4-bromo-phenyl)-5-amino-benzofuran ***3h***: yield = 58%, white crystals, m.p.= 192^{0}C; IR spectrum (KBr) ν_{max} cm^{-1}: 1640, 3350, 3420(NH_2); Mass spectrum: m/e (rel. intensity, %):285(100)M, 287(100)M, 260(8), 258(8), 209(11), 180(30); ^{1}H-NMR spectrum (DMSO d_6): 4.93(NH_2), 6.63(d,1H), 6.75(s,1H), 7.21(d,2H), 7.63(d, 1H), 7.84(d,2H)

2-methyl-5- amino-benzofuran ***3i***: yield = 52%, white crystals, m.p.= 220^{0}C, IR spectrum (KBr) ν_{max} cm^{-1}: 1620, 3400, 3550(NH_2); ^{1}H-NMR spectrum ($CDCl_3$): 2.48(s,3H), 4.21(NH_2), 6.73(s,1H), 7.19(d,1H), 7.40(s,1H), 7.53(d,1H)

2-phenyl-3-methyl-7-chloro-5-amino-benzofuran ***3j***: yield = 60%, white crystals, m.p.= 274^{0}C; IR spectrum (KBr) ν_{max} cm^{-1}: 1630, 3210, 3330, 3440(NH_2); ^{1}H-NMR spectrum (DMSO d_6): 2.50(s,3H), 5.14(NH_2), 6.66-7.77(m,7H)

2-(4-fluoro-phenyl)-5-amino-benzofuran ***3k***: yield = 51%, white crystals, m.p.= 243^{0}C; IR spectrum (KBr) ν_{max} cm^{-1}: 1650, 3300, 3460(NH_2); Mass spectrum: m/e (rel.intensity, %): 227(100)M, 210(2), 209(2), 200(15),170(8); ^{1}H-NMR spectrum (DMSO d_6): 4.89(NH_2), 6.59(d,1H), 6.72(s,1H), 7.17(s,1H), 7.26(d,1H), 7.32(d.1H), 7.87(d,2H), 7.89(d,2H).

The IR, MS and ^{1}H-NMR spectra and the elementhal analysis confirmed the structures of compounds ***2a-e*** and ***3a-k***.

The nitroderivatives ***2a-e*** have very strong bands at 1350 - 1380 and 1540-1560 cm^{-1}, characteristic for the nitro group which are not observed in the spectra of ***3a-k***; in that case at 1640-1680 and 3200-3400 cm^{-1} there appeared the tipical bands of amino-group. Molecular peaks for ***2a-e*** and ***3a-k*** are clear, the characteristic peaks for nitro (M-46) and amino-aromatic compounds (M-27) were observed. In case of ^{1}H-NMR spectra for ***3a-k*** which appeared in domenium δ= 6.4 - 7.8 ppm confirmed the presence of the amino-group at the phenylic ring and the disparition of the nitro group (in this case signals are appeared between δ=7-8.6).

REFERENCES

1. Majdik C., Kövendi A., Matei S. and Breazu D., *Rev. Chim*,1989, ***40***, 6, 490.
2. Sheradsky T., *J. Heterocycl. Chem*., 1967, 413.
3. Sheradsky T., *Tetrahedron Lett*.,1966, ***26***, 5225.
4. Ilvespaa I. and Marxer F., *Helv. Chim. Acta*, 1963, ***46***, 2009.
5. Mooradian A. and Dupont E., *Tetrahedron Lett*, 1967, ***3***, 2867.
6. Robinson C.M. and Robinson R., *J. Chem. Soc*., 1924, ***125***, 827.
7. Majdik C., Cotora E., Kövendi A. and Breazu D., *Rev. Chim*., 1985, ***36***, 1760.
8. Majdik C., Kövendi A., Matei S., Breazu D., *Rev. Chim*.,1989, ***40***, 8, 689.

STUDIA UNIVERSITATIS BABEŞ-BOLYAI, CHEMIA, XLIII, 1-2, 1998

KINETIC DETERMINATION OF EFFECTIVE DIFFUSION COEFFICIENT AND TORTUOSITY FACTOR OF A $LaMn_{0.8}Cu_{0.2}O_3$ - CATALYST IN HYDROGEN OXIDATION

FLORINA BUCIUMAN, FLORIN PĂTCAŞ[1]

ABSTRACT. The effective diffusion coefficient of hydrogen in porous pellets of $LaMn_{0.8}Cu_{0.2}O_3$ was indirectly determined using kinetic data on hydrogen oxidation taken in a gradientless recirculation reactor. Using the pore diffusion coefficient, evaluated by means of the usual procedures on the basis of textural characteristics of the catalyst, the tortuosity factor of the porous structure was also calculated.

INTRODUCTION

The mathematical modelling of catalytic processes, under conditions where the intrinsec chemical kinetics are coupled with internal mass and heat transfer phenomena, is often rendered difficult by the existing procedures for estimation of the effective diffusion coefficient for the porous catalyst pellet.

The common method used to get at least an approximate value of the effective diffusion coefficient involves the following steps [1-3]:

- calculation of the binary (molecular) diffusion coefficient (if no experimental values are available) [4];

$$D_{m,H} = \frac{\left(\frac{M_H + M_A}{M_H \cdot M_A}\right)^{1/2} \cdot T^{1.75}(K) \cdot 1.013 \cdot 10^{-3}}{P(bar) \cdot \left(v_H^{1/3} + v_A^{1/3}\right)^{1/2}} \qquad (1)$$

♦ calculation of the Knudsen diffusion coefficient. Taking into account that the real porous system consists of pores of different radii, an approximation regarding the average pore size is to be made:

$$D_{K,H} = 9.7 \cdot 10^3 \cdot \bar{r}_p \cdot \sqrt{\frac{T}{M_H}} \qquad (2)$$

♦ calculation of the combined molecular and Knudsen diffusion coefficient:

$$\frac{1}{D_p} = \frac{1}{D_{m,H}} + \frac{1}{D_{K,H}} \qquad (3)$$

♦ calculation of the effective diffusion coefficient of the catalyst pellet:

[1] *"Babeş-Bolyai" University of Cluj-Napoca, Department of Chemical Technology, M. Kogălniceanu Street 1, RO-3400 Cluj-Napoca, Romania.*

$$D_{eff} = \frac{D_P \cdot \Psi}{\tau} \qquad (4)$$

The tortuosity factor τ is meant to account for *(a)* the prolongation of the diffusion path because of the irregular form of the pores and their randomly orientation and *(b)* the resistance opposed to the transport by the strangled and closed pores. For some simplified models of pore systems it is possible to calculate the tortuosity factor using measurable structural parameters though for real systems they generally do not allow one to get satisfying values [2,5]. This is the reason why a number of methods for the experimental determination of the effective diffusion coefficient have been developed and are widely used. Most of them are based on the kinetics of some physical processes, as for example the permeation of gases through a catalyst pellet, the binary counter-current gas diffusion (the method of Wicke and Kallenbach [6]), the liquid phase diffusion, or the diffusion-controlled adsorption-desorption processes [5,7].

There is still considerable uncertainty whether the data obtained under conditions of the aforementioned experiments can be used for solving the problem of coupling diffusion and reaction within the porous structure. For this purpose, the most meaningful values of D_{eff} would be those obtained indirectly from data on chemical reaction rates [1].

The aim of the present contribution is to characterise the textural properties of an oxidation catalyst belonging to the family of perovskite oxides (formula: $LaMn_{0.8}Cu_{0.2}O_3$) and to evaluate its effective diffusion coefficient and tortuosity factor using kinetic data on hydrogen oxidation.

EXPERIMENTAL

Catalysts. Cylindrical pellets of $LaMn_{0.8}Cu_{0.2}O_3$ (diameter x height = 4 x 1 mm) were prepared by pressing the powder at 10 bar. For the kinetic runs, the pellets were crushed and a fraction of 0.3-0.5 mm was used.

BET - surface area. The surface area of the catalyst was measured by N_2 adsorption by means of the BET method using automatically operated equipment.

Hg - porosimetry. The porosity and the pore-size distribution of the catalyst were obtained by Hg-penetration in a Carlo-Erba porosimeter model 1540 with computer-assisted data acquisition and processing.

Kinetic tests for hydrogen oxidation. The catalytic experiments were carried out in a recirculation reactor equipped with a cold trap. The recycle ratio was close to 40, ensuring the gradientless behaviour of the system. The reactor was operated in a differential manner by keeping the grade of conversion under 10 %. Kinetics tests were performed using a mixture of 0.2-1.0 % (vol.) hydrogen in air at atmospheric pressure in the temperature range of 210 - 430 °C.

RESULTS AND DISCUSSION

Textural properties of porous pellets. The penetration curve and the pore-size-distribution are illustrated in Fig. 1.

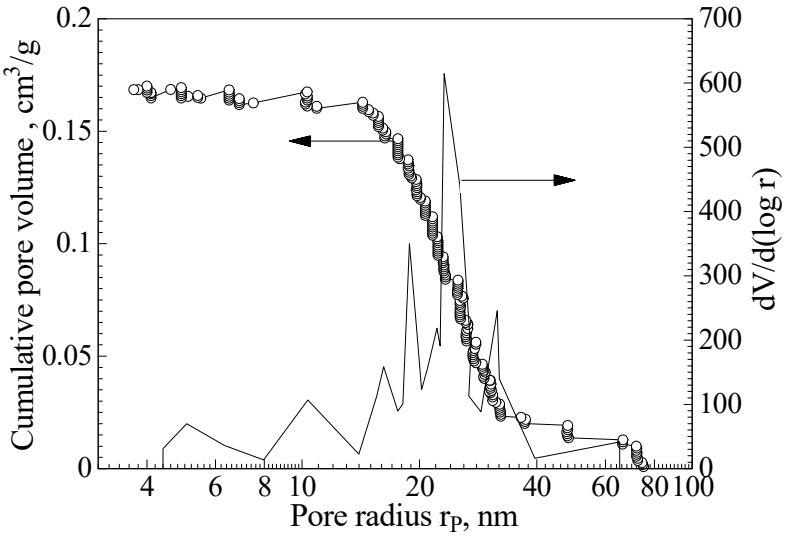

Fig. 1. Total pore volume and pore volume distribution curves of $LaMn_{0.8}Cu_{0.2}O_3$-pellets

It can be seen that the perovskite sample have a basically monodisperse pore structure with pore radii between 4 and 80 nm, the main fraction being that of ca. 15-40 nm. Other textural features of the catalyst are given in Table 1. The average pore radius can be estimated from the pore size distribution curve as about 24 nm. Using the Wheeler equation the average pore radius can also be evaluated on the basis of porosity, grain density and surface area [1]:

$$\bar{r}_P = \frac{2\Psi}{S_{BET} \cdot \rho_p} \qquad (5)$$

Table 1.

Textural characterisation of $LaMn_{0.8}Cu_{0.2}O_3$ porous pellets

[a)]Apparent (grain) density ρ_p, g/cm^3	[b)] True (skeletal) density ρ_r, g/cm^3	[c)]Porosity ψ, cm^3/cm^3	[d)]S_{BET} ($\pm$ 2 %) m^2/g	Average pore radius $\bar{r}_p$, nm	
2.90	5.56	0.4785	10.8	[e)]24	[f)]30.6

[a,b)] measured picnometrically with mercury, before and after penetration, respectively; [c)] $\psi=1-\rho_p/\rho_r$; [d)] determined after BET-method; [e)] from the pore size distribution curve; [f)] after Wheeler formula.

Kinetic features of H_2 - oxidation. The experimental data obtained in the gradientless recirculation reactor were processed according to the differential method, yielding concentration-rate plots. Due to the large excess of oxygen, its partial reaction order was considered as zero. As concerns hydrogen, kinetic data obeyed a first order rate equation:

$$r_m = k_m \cdot C_H \qquad (6)$$

The temperature dependence of the rate constants is represented in Fig. 2 according to the Arrhenius equation:

$$k_m = k_{m,0} \cdot \exp\left(-\frac{E_{a,ap}}{RT}\right) \quad (7)$$

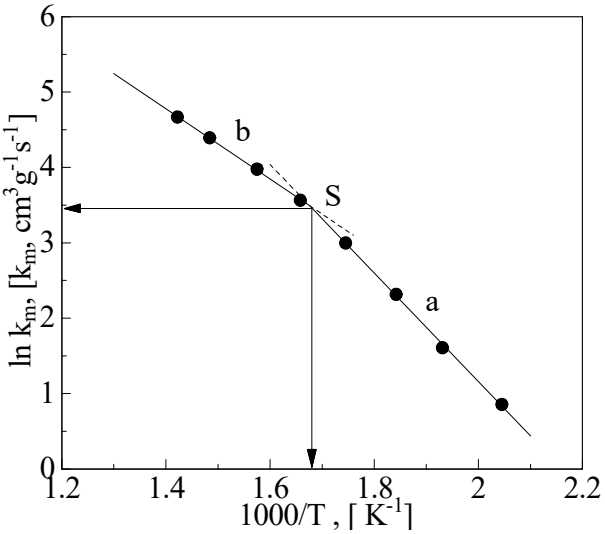

Fig. 2. The temperature dependence of the specific reaction rates for H_2-oxidation over $LaMn_{0.8}Cu_{0.2}O_3$.

The influence of internal diffusional limitations on the kinetical parameters. By examining Fig. 2 one can observe the existence of a turning point on the Arrhenius plot *ln k = f(1/T)* at 596.7 K, which marks the passing from the reaction-controlled to the reaction/internal diffusion-controlled regime.

By taking into account the definition of the effectiveness factor of a catalyst for a first order reaction in spherical pellets [1, 5]:

$$\eta = \frac{3}{\Phi_S} \cdot \left(\frac{1}{\tanh \Phi_S} - \frac{1}{\Phi_S}\right) \quad (8)$$

with

$$\Phi_S = R_p \cdot \sqrt{\frac{k_m \cdot \rho_p}{D_{eff}}} \quad (9)$$

depending on the relative values of k_m and D_{eff} there are two limit situations:

(a) $k_m << D_{eff}$; $\Phi_S << 1$ and $\eta \cong 1$

The intraparticle mass transport has no influence on the rate, which is controlled by the chemical reaction step. The corresponding kinetic equation has the form:

$$r_m = k_m \cdot C_H \tag{10}$$

(b) $k_m >> D_{eff}$, $\Phi_S >> 1$ and $\eta = 3/\Phi_S$

The intraparticle diffusion has a large influence on the rate which can be expressed by the equation:

$$r_m = \eta \cdot k_m \cdot C_H = \frac{3}{R_p} \cdot \sqrt{\frac{D_{eff} \cdot k_m}{\rho_p}} \cdot C_H \tag{11}$$

The cases *(a)* and *(b)* are illustrated by the lines *a* and *b* on the Arrhenius plot (Fig. 2). Hence, by taking into account the temperature dependence of the reaction rate constant for the reaction-controlled kinetic range:

$$k_m = k_{m,0} \cdot \exp\left(-\frac{E_a}{RT}\right) \tag{12}$$

the apparent activation energy for the intraparticle diffusion-controlled rate should be:

$$E_{a,ap} = \frac{E_a}{2} \tag{13}$$

which is the case for the kinetic constants which belong to the line *(b)* of the Arrhenius plot. Indeed, the equations that are describing the temperature dependence of the experimental determined rate constants are:

a) for T < 576.7 K

$$\ln k_m = 15.5596 - \frac{59.87\text{kJ/mol}}{RT} \tag{14}$$

b) for T > 576.7 K

$$\ln k_m = 11.3120 - \frac{46.66\text{kJ/mol}}{RT} \tag{15}$$

(the points were fitted numerically using a least squares procedure).

At the intersection point *S* of the lines *(a)* and *(b)* we have:

$$k_{m,S} = \frac{3}{R_p} \cdot \sqrt{\frac{D_{eff} \cdot k_{m,S}}{\rho_p}} \tag{16}$$

This means that the effective diffusion coefficient of the catalyst particle can be calculated on the base of the rate constant corresponding to the turning point *S* on the Arrhenius plot:

$$D_{eff} = \frac{k_{m,S} \cdot \rho_p \cdot R_p^2}{9} \tag{17}$$

The experimentally determined D_{eff} together with the calculated $D_{m,H}$, $D_{k,H}$, and D_P are listed in Table 2.

Table 2.

Calculated and experimentally determined diffusion coefficients of hydrogen in a 0.4 mm diameter $LaMn_{0.8}Cu_{0.2}O_3$ pellet[a)] at 596.7 K and 1 atm.

$D_{m,H}$, cm^2/s	$D_{K,H}$, cm^2/s	D_P, cm^2/s	D_{eff}, cm^2/s
2.52	0.402	0.347	0.0423

[a)] the textural characteristics are listed in Table 1

Using equation (4), a value of

$$\tau = 3.925$$

for the tortuosity factor can be achieved, which is in accordance with those given in the literature for porous oxides ($1 < \tau < 6$) [1].

CONCLUSIONS

Kinetic measurements allow the delimitation of reaction-controlled and intraparticle diffusion- controlled working regimes and the turning point temperature for a certain catalyst and reaction in specific conditions.

At the same time, kinetic studies yield an indirect value for the effective diffusion coefficient, which is perhaps the most meaningful taking into account that ordinary methods for determining it refer to conditions where no reaction can occur (usually, at room temperature). Using the experimentally determined effective diffusion coefficient and porosity and the calculated pore diffusion coefficient, the tortuosity factor can be also calculated. This value can then be used to evaluate the effective diffusion coefficient for pellets of the same catalyst having other sizes, but the same textural characteristics.

ACKNOWLEDGEMENTS. The authors express their gratitude to Mr. Priv. Doz. Dr.-Ing. T. Hahn (Technische Universität Karlsruhe) for helpful discussions and suggestions concerning this work.

LIST OF SYMBOLS

C_H	concentration of H_2 in the reaction mixture, $mol \cdot cm^{-3}$
$D_{m,H}$	diffusion coefficient for bulk ("molecular") diffusion of H_2 in a mixture of H_2 and air, $cm^2 \cdot s^{-1}$
$D_{K,H}$	Knudsen diffusion coefficient for a straight round pore, $cm^2 \cdot s^{-1}$
D_{eff}	effective diffusion coefficient for a porous pellet, $cm^2 \cdot s^{-1}$
D_P	pore diffusion coefficient (combined molecular and Knudsen diffusion), $cm^2 \cdot s^{-1}$
E_a	true activation energy, $kJ \cdot mol^{-1}$

$E_{a,ap}$	apparent activation energy, $kJ \cdot mol^{-1}$
k_m	intrinsic reaction-rate constant (specific rate) per unit mass of catalyst pellet, $cm^3 \cdot g^{-1} \cdot s^{-1}$
$k_{m,0}$	frequency factor in Arrhenius equation, $cm^3 \cdot g^{-1} \cdot s^{-1}$
M_A, M_H	molecular weights of air and hydrogen, respectively, $g \cdot mol^{-1}$
P	total pressure, atm
r_m	reaction rate per unit mass of catalyst pellet, $mol \cdot g^{-1} \cdot s^{-1}$
r_P	pore radius, cm
$\bar{r}_P$	average pore radius, cm
R_p	pellet radius, cm
R	gas constant, ($R = 8.314\ J \cdot mol^{-1} \cdot K^{-1}$)
S_{BET}	surface area of porous solid, $cm^2 \cdot g^{-1}$
T	absolute temperature, K
v_A, v_H	diffusion volumes of air and hydrogen, respectively
ψ	porosity (void fraction in the porous pellet), $cm^3 \cdot cm^{-3}$
η	effectiveness factor of the catalyst
ρ_p	apparent (grain) density of catalyst, $g \cdot cm^{-3}$
ρ_r	true (skeletal) density of catalyst, $g \cdot cm^{-3}$
τ	tortuosity factor
Φ_S	Thiele modulus for a spherical catalyst particle
ε, σ	Lnnard-Jones force constants
Ω_D	collision integral for diffusion

REFERENCES

1. C. N. Satterfield, T.K. Sherwood, *The Role of Diffusion in Catalysis*, Addison-Wesley Publishing 1963, Roading, Massachusetts-Palo Alto-London, p. 1-25.
2. J.M. Smith, *Chemical Engineering Kinetics*, 2nd Edition, Mc Graw-Hill, New York 1970, p. 400-419.
3. M. Baerns, H. Hofmann, A. Renken, *Chemische Reaktionstechnik*, Georg-Thieme-Verlag, 2. Auflage, Stuttgart 1987, p. 67-79.
4. VDI-Wärmeatlas, VDI-Verlag, 6. Auflage, Düsseldorf 1991, p. Da 23.
5. M. Kotter, P. Lovera, L. Riekert, *Ber. Bunsenges. Phys. Chem.,* ***80*** (1976) 61.
6. E. Wicke, R. Kallenbach, *Kolloid-Z.*, ***97*** (1941) 135.
7. P. Uchytil, P. Schneider, *Coll. Czech. Chem. Commun.*, ***53*** (1988) 1217.

STUDIA UNIVERSITATIS BABEŞ-BOLYAI, CHEMIA, XLIII, 1-2, 1998

PHYSICOCHEMICAL CHARACTERIZATION OF ALUMINA-SUPPORTED COBALT AND MOLYBDENUM MIXED OXIDES I. TEMPERATURE-PROGRAMMED REDUCTION (TPR) AND OXIDATION (TPO) STUDIES

FLORIN PĂTCAŞ, FLORINA BUCIUMAN[1]

ABSTRACT. Two series of Co-Mo-O/γ-Al_2O_3 catalysts having various metal loading and different Co:Mo atomic ratios were prepared by incipient wetness impregnation. The reducibility and reoxidability of reduced samples were investigated by means of TPR/TPO techniques. Three cobalt species were found: Co_3O_4, isolated Co^{3+} or Co^{2+} cations on the surface of alumina and $CoAl_2O_4$, while molybdenum forms a single species whose redox properties are influenced by the support at lower loading. The presence of molybdenum stabilises the isolated Co^{2+} and Co^{3+} species towards reduction.

INTRODUCTION

Alumina-supported cobalt and molybdenum oxides are widely used as catalysts in the hydrodesulphurisation (HDS) of crude oil [1-3], coal liquefaction [4], wastes incineration [5] or in various partial oxidation reactions of hydrocarbons [6]. In spite of their quite a long time application in industrial processes [7, 8] the nature of active sites in the Co-Mo-O/Al_2O_3 catalysts is still controversial. The literature offers very close performance data (activity, selectivity, and life length) for catalysts of very different compositions. The industrial catalysts contain generally about 5-15 % (mass) Mo and 1-5 % (mass) Co, the atomic ratio Co:Mo ranging between 0.2 and 1.0. Nahid et al. [7] found an optimum Co:Mo atomic ratio of 1.0 for their hydrotreating catalysts, while Engel et al. [8], Porter [9] and Sulimov et al. [10] found for the same test-reaction an optimum Co:Mo = 0.2. By studying the promoting effect of cobalt on the alumina-supported molybdenum oxide, Beuther et. al. [11] established an optimum ratio Co:Mo = 0.35.

In the working conditions of hydrodesulphurisation process, the Co-Mo-O/Al_2O_3 catalysts contain among other species, Al_2O_3, $CoAl_2O_4$, CoO, $CoMoO_4$ which are catalytically inactive [12]. The *in-situ* formed Co_9S_8 and MoS_2 have a weak to moderate activity. The highest activity seems to belong to MoO_3 promoted with an irreducible cobalt oxide species [12, 13]. The real nature of the active compound is yet unknown. Richardson [12] tried to elucidate it by measuring the alteration of the magnetic susceptibility before and after catalytic desulphurisation for a series of 10 % MoO_3/Al_2O_3 samples promoted with cobalt (Co:Mo were between 0.1 and 1.0). Other authors tried to correlate the catalytic properties of cobalt promoted molybdenum oxides with spectral features using FTIR [14], UV-VIS [15], Raman [13] or ESCA [16].

[1] *"Babeş-Bolyai" University of Cluj-Napoca, Department of Chemical Technology, M. Kogălniceanu Street 1, RO-3400 Cluj-Napoca, Romania.*

Poncelet et al. [6] present the sinergetic influence of Co and other metals on the catalytic activity of molybdates in the propene partial oxidation.

Dynamic techniques as temperature-programmed desorption (TPD), reduction (TPR) and oxidation (TPO) are widely used in the investigation of oxidic species in bulk and supported catalysts. Grimblot et al. [17] studied the oxidation behaviour of prereduced Co-Mo-O/γ-Al_2O_3-catalysts by means of gravimetric methods. Arnoldy et al. [18, 19] investigated the influence of calcination parameters on the reduction behaviour of Co-Mo-O/Al_2O_3 catalysts.

The redox properties of the oxidic species are of great importance with respect to their catalytic properties in oxido-reduction reactions. The mutual influence of different metal cations yielding sensible modifications of catalytic behaviour can be also highlighted by means of TPR/TPO-features.

The present paper describes preliminary results from a study of Co-Mo-O/γ-Al_2O_3 catalysts, which was undertaken in order to ascertain the oxidic species at the surface of alumina and their redox behaviour. The influence of the total (Co+Mo)-loading and of the Co:Mo atomic ratio, on the formation of and surface distribution of reducible species is studied.

EXPERIMENTAL

Catalysts preparation

A series of Co-Mo-O/γ-Al_2O_3 catalysts with various metal loading and Co:Mo atomic ratios were prepared by coimpregnation using aqueous solutions containing the appropriate quantities of $Co(NO_3)_3.6H_2O$ and $(NH_4)_6Mo_7O_{24}.4H_2O$ and γ-Al_2O_3 (Condea Hamburg, S_{BET} = 107 m^2/g) as powder having particle size under 200 μm. The solution was brought over the support and water was evaporated in a rotavapor at 40 Torr and room temperature. The samples were then dried at 120 °C and heated for 8 hours at 450 °C in air. The prepared catalysts together with their specific features (surface areas were measured using the BET-method by means of a Fisons-Instrument device type Sorptomatic 1900) are listed in the Table 1.

Table 1.

Characteristics of the Co-Mo-O/γ-Al_2O_3-catalysts

Catalyst	$CoO+MoO_3$ % (mass)	Co:Mo (atomic ratio)	S_{BET} ($\pm$ 2 %) m^2/g	*)n_{th} considering the oxides as ($CoO+MoO_3$)	*)n_{th} considering the oxides as $Co_3O_4+MoO_3$)
a.	5.0	0:100	105	0.20	0.20
b.	5.0	1:100	107	0.21	0.21
c.	5.0	10:100	106	0.22	0.22
d.	5.0	100:100	107	0.19	0.17
e.	5.0	100:10	104	0.22	0.14
f.	5.0	100:1	98	0.22	0.13
g.	5.0	100:0	96	0.22	0.12
h.	1.0	10:100	104	0.04	0.04
i.	3.0	10:100	105	0.13	0.13
j.	10.0	10:100	102	0.44	0.43

*)n_{th} theoretical coverage grade of the support

Temperature-programmed reduction/oxidation

TPR/TPO experiments were made in a conventional device having a quartz U-tube reactor, a cold trap to remove the water generated in the reaction and a

thermal conductivity detector (TCD) to measure the hydrogen or oxygen consumption. The temperature was measured using a NiCr-Ni thermoelement situated directly in the catalyst bed. For the TPR experiment a reducing gas containing 10 % (vol.) H_2 in N_2 at a flow rate of 30 ml/min (STP) was passed through the catalyst sample and the temperature was raised with a constant rate of 10 grd/min from 20 °C to 950 °C and then kept constant for 20 min. The reduced sample was cooled and then reoxidated with 40 ml/min (STP) oxidant gas containing 12.5 % (vol.) O_2 in He by heating with a rate of 10 grd/min from 20 °C to 600 °C then keeping it constant for 20 min. The signals of the TCD were calibrated by injecting known volumes of hydrogen or oxygen using a Valco sampling valve, while the reactor contained 100 mg inert quartz powder to avoid hydrodynamic effects.

RESULTS AND DISCUSSION

In order to understand the nature of the active component - support interaction and its role in determining the redox features of the former, low loaded (n_{th} = 4-44 %) metal oxide/alumina catalysts have been prepared. The theoretical coverage grade n_{th} was calculated by considering cobalt and molybdenum oxides as being dispersed in a monolayer on the surface of alumina with the atoms arranged in the <100> plane [20].

The mutual influence of the two metal oxides on the redox properties of the catalyst at Co:Mo ratios varying between 100:0 and 0:100 and constant (Co+Mo) loading are presented in Fig. 1 (A, B).

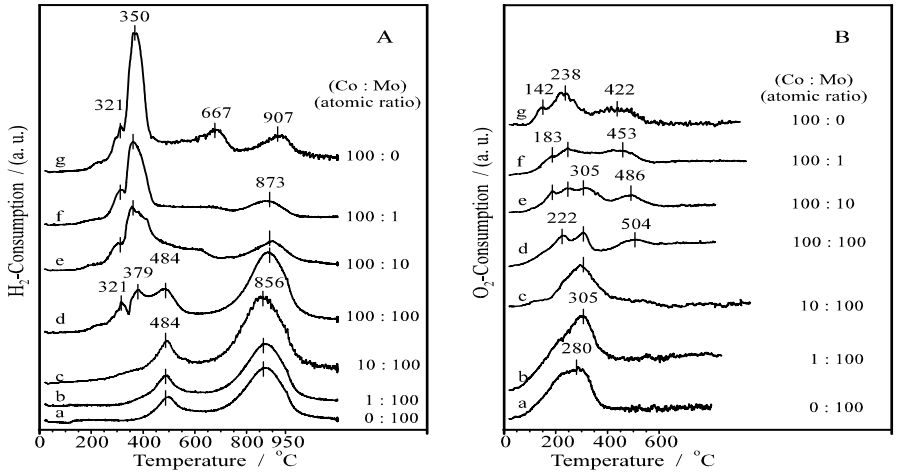

Fig. 1. The TPR (A) and TPO (B) profiles for the catalyst series containing 5 % cobalt and molybdenum oxides, with different Co:Mo atomic ratios

The reduction of alumina-supported molybdenum oxide (profile *a*, Fig. 1 A) takes place in two stages with peaks at 484 °C and 856 °C. The relative H_2 consumption of these peaks is about 1:2 which makes reasonable to assign them to a two-stage reduction of Mo^{6+} cations, first to Mo^{4+} then to Mo^0 in accordance with the reactions [18, 19]:

$$MoO_3 + H_2 \longrightarrow MoO_2 + H_2O \quad (1)$$

$$MoO_2 + 2\,H_2 \longrightarrow Mo + 2\,H_2O \qquad (2)$$

The position and relative intensity of the reduction peaks of molybdenum are not affected by addition of cobalt (Fig 1 A, curves *b* and *c*).

The reduction of alumina supported cobalt oxide (profile *g* in Fig. 1 A) shows four maximums at 290, 350, 667 and 907 °C. On the basis of previous literature data [18] these can be assigned as follows:

- to the reduction of Co_3O_4 spinel at ca. 290 °C;
- to the reduction of Co^{3+} associated with aluminium in compounds of type Co/AlO_6 or isolated Co^{3+} cations on the surface of alumina, at ca. 350 °C;
- to the reduction of surface Co^{2+} cations at ca. 667 °C;
- to the reduction of Co^{2+} incorporated as $CoAl_2O_4$ spinel, at ca. 907 °C.

The different preparation and TPR-experiments conditions [21] could explain the slight differences between the reduction profiles in this paper and those of Arnoldy et al. [18]. The lower calcination temperature employed in the preparation of present catalysts in comparison to those cited restricted the formation of Co_3O_4 and $CoAl_2O_4$ spinels.

The addition of small quantities of molybdenum did not influence the reduction of spinelic cobalt cations and isolated Co^{3+}, but it suppressed the further reduction of the later (isolated Co^{2+} cations), as shown by the disappearance of the reduction peak at 667 °C even at a very high Co:Mo ratio of 100:1 (curve *f* in Fig. 1 A). At higher molybdenum contents (curves *d*, *e* in Fig. 1 A) the first stage of reduction of isolated cobalt ions (Co^{3+} to Co^{2+}, peak at 350 °C) is also hindered.

The TPR/TPO profiles of the catalysts containing 1.0, 3.0, 5.0 and 10.0 % active component considered as $CoO+MoO_3$ (atomic ratio Co:Mo = 10:100) are presented in Fig. 2 A, B.

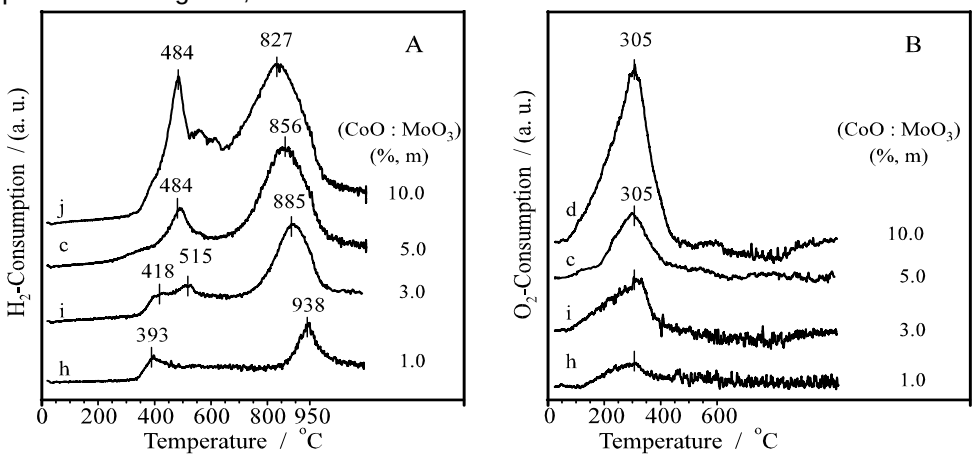

Fig. 2. The TPR (A) and TPO (B) profiles for the Co-Mo-O/γ-Al_2O_3 catalysts having different loading, at a constant Co:Mo atomic ratio of 10:100.

As the active components loading increased from 1 to 3 and 5 %, the first molybdenum reduction peak at 393 °C shifted to higher temperatures (418 and 484°C, respectively) while another increase to 10 % active component brought no other change of this peak. The second reduction maximum of molybdenum shifted

towards lower temperatures (from 938 to 827 °C) as the loading increased. The first effect can be assigned to a higher reactivity of oxygen anions bounded to isolated Mo^{6+} cations at lower loading [19] and the second, to the change of coordination number of Mo^{4+} cations from 4 to 8 which hinders their reduction [14]. The higher coordination number is promoted by the presence of OH groups of alumina support around the Mo^{4+} cation therefore it occurs most probably at lower loading where molybdenum is highly dispersed. At higher loading the influence of the support diminishes and the second reduction stage takes place at lower temperatures. The reduction of spinelic cobalt ions can be seen as a shoulder on the left side of the first molybdenum reduction peak (Co_3O_4 species) and another one on the right side of the second peak ($CoAl_2O_4$ species). The reduction of isolated cobalt ions does not appear, being hindered by the presence of molybdenum as shown before. An interesting reduction feature appears at the 10 % catalyst (considered as $CoO+MoO_3$) on the temperature range of about 550-650 °C. As it didn't show at any other catalysts with lower loading, or in the TPR-profiles of single cobalt or molybdenum oxides, we assign it to a binary Co-Mo-O oxide of type cobalt molybdate which can form only at sufficiently high cobalt and molybdenum loading. Such oxides are common active catalysts in the partial oxidation of alchenes [6, 22] and are supposed to be the active phases for the HDS activity [23].

The reoxidation profiles of samples containing mainly molybdenum is shown in Fig. 1 B (curves *a*, *b*, *c*) and consist of a single broad peak at 280 °C which shifts weakly towards higher temperature (305 °C) in the presence of cobalt. The reduced alumina-supported cobalt sample (profile *g* in Fig. 1 B) shows on the contrary several oxidation maxima at 142, 238 and 422 °C, most likely due to the presence of different cobalt species on the surface. The addition of even small quantities of molybdenum suppresses the first oxidation peak at 142 °C, which makes possible to assign it to the isolated cobalt ions, which were not reduced in the presence of molybdenum.

CONCLUSIONS

The investigation of reduction-oxidation features of the Co-Mo-O/γ-Al_2O_3 catalysts by means of the TPR/TPO technique leads to the following conclusions:

(1) Molybdenum oxide shows a very good dispersion on the surface of alumina. The interaction support-active component is strong at low loading and diminishes at higher molybdenum contents. The oxygen atoms bound on Mo^{6+} isolated cations are more active, yet these cations are more stable towards total reduction due to the influence of the support.
(2) The presence of cobalt does not influence the redox properties of molybdenum.
(3) Cobalt oxide deposited on the surface of alumina forms several species: Co_3O_4, dispersed Co^{3+} or Co^{2+} cations and $CoAl_2O_4$. Oxygen atoms bound on Co^{3+} in Co_3O_4 or isolated Co^{3+} are more reactive as those bound on Mo^{6+}.
(4) The presence of molybdenum stabilises isolated Co^{2+} ions and, in higher quantities, even isolated Co^{3+}, towards reduction.

ACKNOWLEDGEMENTS. The authors express their gratitude to Mr. Prof. D. Hönicke (Technische Universität Chemnitz) for supporting this research and Mr. Dipl. Chem. H. Eisenhuth for experimental contributions.

REFERENCES

1. R. Iwamoto, K. Inamura, T. Nozaki, A. Lino, *Appl. Catal. A-Gen.,* ***163(1-2)*** (1997) 217.
2. K. Hiroshima, T. Mochizuki, T. Honma, T. Shimizu, M. Yamada, *Appl. Surf. Sci.,* ***121*** (1997) 433.
3. P. Grange, X. Vanhaeren, *Catal. Today,* ***36(4)*** (1997) 375.
4. J. A. Legarreta, B. M. Caballero, I. Demarco, M. J. Chomon, P. M. Uria, *Fuel,* ***76(13)*** (1997) 1309.
5. M. J. Gordon, S. Gaur, S. Kelkar, R. M. Baldwin, *Catal. Today,* ***28(4)*** (1996), 305.
6. H. Poncelet, J.M.M. Millet, G. Coudurier and J.C. Védrine in: *ACS Symp. Ser*., vol. 523, New York 1993, p. 262.
7. P.G. Nahin and H.C. Huffman, US Patent 2,510,189 (June 06,1950).
8. W. F. Engel and H. Hoog, US Patent 2,697,683 (December 21, 1954).
9. F.W.B. Porter, *J. Inst. Petrol.*, ***41***, (1954) 18.
10. A.D. Sulimov, M.V. Lobeev, I.N. Kozhina, A.E. Al'tshnler, A.B. Gutman and V.M. Satyogov, *Khim. Sera-Org. Soedinenii Soderzhasheh. v. Naft. i Nefteprodukt., Akad. Nauk SSSR Bashkir. Filial., Materialy Vtoroi Sessii,* 1956, 135; CA ***53***, 1958, 10720a.
11. H. Beuther, R.A. Flinn and J.B. McKinley, *Ind. Eng. Chem.,* ***51***, (1959) 1349.
12. J.T. Richardson, *Ind. Eng. Chem. -Fundamentals,* ***3(2)***, (1964) 154.
13. P.L. Villa, F. Trifiró and I. Pasquon, *React. Kin. Catal. Lett.,* ***1(3)***, (1974) 341.
14. T. Fransen, O van der Meer and P. Mars, *J. Catal.,* ***42***, (1976) 79.
15. N.P. Martinez, P.C.H. Mitchell and P. Chiplunker, in *"Proc. of the Climax 2nd Int. Conf.on the Chemistry and Use of Molybdenum",* Climax Molybdenum Ltd., London 1977, p. 164.
16. T.A. Patterson, J.C. Carver, D.E. Leyden and D.M. Hercules, *Spectr. Lett.,* ***9(1)***, (1976) 65.
17. J. Grimblot, A. D'Huysser, J.P. Bonnelle and J.-P. Beaufils, *J. Electron Spectrosc. Relat. Phenom.,* ***6(1)***, (1975) 71.
18. P. Arnoldy, M.C. Franken, B. Scheffer and J.A. Mouliijn, *J. Catal.,* ***96***, (1985) 381.
19. P. Arnoldy and J.A. Mouliijn, *J. Catal.,* ***93***, (1985) 38.
20. H. Eisenhuth, *Seminararbeit*, Technische Universität Chemnitz, 1995.
21. D.E.M. Monti and A. Baiker, *J. Catal.*, ***83***, (1983) 323.
22. O. Lezla, E. Bordes, P. Courtine, G. Hecquet, *J. Catal.,* ***170(2)*** (1997) 346.
23. R. G. Leliveld, A. J. Vandillen, J. W. Geus, D. C. Koningsberger, *J. Catal.,* ***171(1)*** (1997) 115.

STUDIA UNIVERSITATIS BABEŞ-BOLYAI, CHEMIA, XLIII, 1-2, 1998

MODELING OF CATALYTIC STEAM REFORMING PROCESS USING NEURAL NETWORKS

ŞERBAN AGACHI, ANTON ALEXANDRU KISS, ZOLTAN NAGY, ALEXANDRU POP[1]

ABSTRACT. This paper discusses the analytical model of the catalytic steam hydrocarbon reforming process and also the possibility to model this process using Artificial Neural Network. Both models are used to calculate the conversions in different conditions of temperature, pressure and molar ratio. Very good results were achieved using Artificial Neural Networks.

INTRODUCTION

The catalytic steam-hydrocarbon reforming reaction is one of the most important processes of the chemical industry.

The following reaction can take place:

(1) $CH_4 + H_2O \longrightarrow CO + 3H_2O (\eta_1)$
(2) $CO + H_2O \longrightarrow CO_2 + H_2$ (η_2)
(3) $CH_4 + CO_2 \longrightarrow 2CO + 2H_2$
(4) $CH_4 + 2H_2O \longrightarrow CO_2 + 4H_2O$

From these reactions, only the first and the second are independent.

The reactions take place in adsorption layer formed on the solid catalyst surface. The scheme of the process is the following:

$$-T_{CH4} \longrightarrow -T_{CH4p} \longrightarrow \text{Ads. } CH_4 \longrightarrow$$
$$\longrightarrow \text{Ch. react.} \longrightarrow \text{Prod. desorb.}$$
$$-T_{H2O} \longrightarrow -T_{H2Op} \longrightarrow \text{Ads. } H_2O \longrightarrow$$

RESULTS AND DISCUSSION

Analytical model

The analytical model is based on mass balance, energy balance, thermo-dynamic and physico-chemical equations.

[1] *"Babeş-Bolyai" University of Cluj-Napoca, Faculty of Chemistry and Chemical Engineering, Arany Janos 11, 3400 Cluj-Napoca, Romania; Tel. 0040-64-193833 Fax. 0040-64-190818, E-mail: znagy@chem.ubbcluj.ro, ktony@chem.ubbcluj.ro.*

Physico-chemical properties:

Table 1.

Physico-chemical properties of the compounds

Compound	H^0_f (kcal/mol)	S^0_m (cal/mol·K)	G^0_f (kcal/mol)	C_p (cal/mol·K)			T_{cr} (°C)	P_{cr} (atm)
				a	$b \cdot 10^3$	$c \cdot 10^6$		
CH_4	-17.889	44.500	-12.140	3.42	17.84	-4.165	-82.5	45.8
CO	-26.416	47.301	-32.808	6.25	2.091	-0.475	-139	35
CO_2	-94.052	51.061	-94.260	6.85	8.533	-2.475	31.1	73
H_2	0	0	0	6.88	0.066	0.279	-239.9	12.8
H_2O	-57.798	45.106	-54.636	6.89	3.283	-0.343	374	217.72

The conductibility and viscosity of the reaction mixture can be calculated using properties of each component [1,2]:

$$\lambda\ \mathrm{am} = \frac{\lambda\ \mathrm{i} \cdot \mathrm{xi} \cdot (\mathrm{Mi})^{1/3}}{\mathrm{xi} \cdot (\mathrm{Mi})^{1/3}} \tag{1}$$

$$\mu\ \mathrm{am} = \frac{\mu\ \mathrm{i} \cdot \mathrm{xi} \cdot (\mathrm{Mi})^{1/2}}{\mathrm{xi} \cdot (\mathrm{Mi})^{1/2}} \tag{2}$$

The variation of conductibility and viscosity with temperature, for each component can be calculated using the following formulas [3,4]:

$$\mu\ \mathrm{i} = \mu\ \mathrm{i0} \cdot \frac{\mathrm{T0} + \mathrm{ci}}{\mathrm{T} + \mathrm{ci}} \cdot \left(\frac{\mathrm{T}}{\mathrm{T0}} \right)^{3/2} \tag{3}$$

$$\lambda\ \mathrm{i} = \lambda\ \mathrm{i0} \cdot \left(\frac{\mathrm{T}}{\mathrm{T0}} \right)^{\mathrm{n}} \tag{4}$$

The constants used in equations (3) and (4) are presented in Table 2.

Table 2.

Constants for computing the conductibility and viscosity of the compounds

Component	CH_4	CO	CO_2	H_2	H_2O
n	1.315	0.825	1.025	0.715	0.985
c_i	160	105	240	100	500

Variation of pressure in reactor is calculating using Ergun type formula:

$$\frac{\mathrm{dP}}{\mathrm{dz}} = 80 \cdot \frac{\rho\ \mathrm{am} \cdot \mathrm{w} \cdot \mathrm{dp}}{\eta\ \mathrm{am}(1-\varepsilon)} + 3.8 \cdot \frac{\rho\ \mathrm{am} \cdot \mathrm{w} \cdot \mathrm{dp}}{\eta\ \mathrm{am}(1-\varepsilon)^2} \cdot \frac{\eta\ \mathrm{am}^2 (1-\varepsilon)^3}{\varepsilon^3 \cdot \eta\ \mathrm{am} \cdot \mathrm{dp}^3} \tag{5}$$

Mass balance:

Table 3.

Mass balance of the process

Compound	Input (moles)	Output (moles)
CH_4	n^0CH_4	$n^0CH_4 \cdot (1-\alpha)$
CO_2	n^0CO_2	$n^0CO_2 + n^0CH_4 \cdot \beta$
CO	n^0CO	$n^0CO + n^0CH_4 \cdot (\alpha - \beta)$
H_2	n^0H_2	$n^0H_2 + 3 \cdot n^0CH_4 \cdot \alpha + n^0CH_4 \cdot \beta$
H_2O	n^0H_2O	$n^0H_2O - n^0CH_4 \cdot \alpha - n^0CH_4 \cdot \beta$
A	n^0A"	n^0A"
Total	N^0_t	$n_t = n^0_t + 2 \cdot n^0CH_4 \cdot (\alpha + \beta)$

Where $\alpha = \eta_1$ and $\beta = \eta_1 \cdot \eta_2$

Energy balance:

Input energy:

$$Qi = \sum_{i=1}^{n} n_i^0 \cdot \int_{273}^{Ti} Cpi \cdot dT + Qr2 \qquad (6)$$

where

$$Qr2 = n^0CH4 \cdot \beta \; (-\Delta\, ^{r2}H^0T) \qquad (7)$$

Output energy:

$$Qe = \sum_{i=1}^{n} n_i \cdot \int_{273}^{Te} Cpi \cdot dT + Qr1 \qquad (8)$$

where

$$Qr1 = n^0CH4 \cdot \alpha \; (-\Delta\, ^{r1}H^0T) \qquad (9)$$

Wasted energy:

$$Qp = b \cdot \sum_{j} Qj \qquad (10)$$

where b = 0.001 … 0.15 (0.1-15%)

Necessary energy: $Q_{nec} = Q_e + Q_p - Q_i$
Specific consume: $q = Q_{nec} / n^0CH_4 \cdot (\alpha + \beta)$

Process equilibrium:

The equilibrium of the process is reducing only to chemical equilibrium.

(1) $CH_4 + H_2O \longrightarrow CO + 3H_2O$ (K_{f1})
(2) $CO + H_2O \longrightarrow CO_2 + H_2$ (K_{f2})

$$Kf1 = \frac{fCO \cdot f_{H_2}^3}{fCO2 \cdot fH2O} = Kp1 \cdot K\gamma 1 \quad (11)$$

$$Kf2 = \frac{fCO2 \cdot fH2}{fCO \cdot fH2O} = Kp2 \cdot K\gamma 2 \quad (12)$$

$$\Delta^r G^0_T = -RT \cdot \ln K_p \quad (13)$$

$$\Delta^r G^0_T = \Delta^r H^0_T - T \cdot \Delta^r S^0_T \quad (14)$$

$$\frac{d\ln Kp}{dT} = \frac{\Delta^r H^0 T}{RT^2} \quad (15)$$

By integrating equation (15) we obtain [5,6]:

$$\ln Kp = -\frac{\Delta H^0}{RT} + \frac{\Delta a}{R} \cdot \ln T + \frac{\Delta b}{2R} \cdot T + \frac{\Delta c}{6R} \cdot T^2 + I \quad (16)$$

Using the data from Table 1 we can obtain K_{p1} and K_{p2} as functions of temperature:

$$\log K_{p1} = -9861.111/T - 11.87 - 2.0585 \cdot 10^{-3} \cdot T + 0.1779 \cdot 10^{-6} \cdot T^2 + 8.3432 \cdot \lg T \quad (17)$$

$$\log K_{p2} = 2217.180/T - 3.2746 + 0.3524 \cdot 10^{-3} \cdot T + 0.0507 \cdot 10^{-6} \cdot T^2 + 0.2969 \cdot \lg T \quad (18)$$

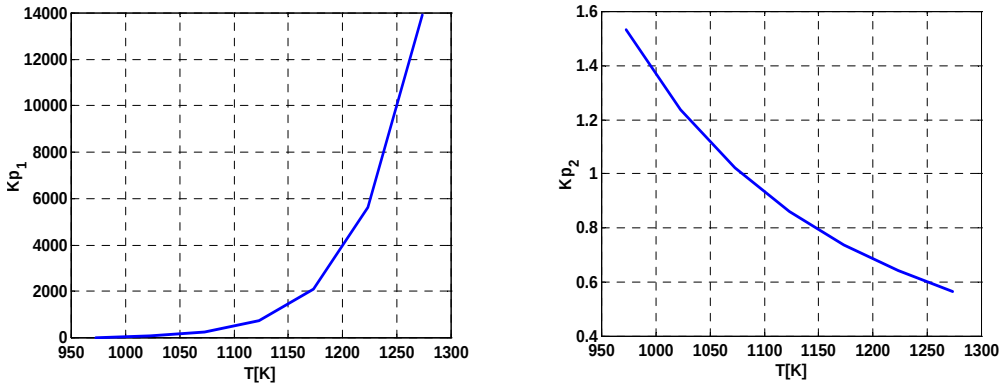

Figure 1. Variation of K_p with temperature for both reactions

The variation of the reaction enthalpies with temperature is shown in Table 4.

Table 4.

Variation of reaction entalpy for reaction 1 and 2

T [K]	773	873	923	973	1023	1073	1123	1173
$\Delta^r H_1 \cdot 10^{-4}$ ***[cal/mol]***	5.3581	5.4189	5.4461	5.4715	5.4951	5.5169	5.5373	5.5562
$\Delta^r H_2 \cdot 10^{-3}$ ***[cal/mol]***	-8.9374	-8.7065	-8.5877	-8.4673	-8.3455	-8.2227	-8.0993	-7.9755

The correction coefficients for the compounds are calculated with the following equation:

$$\ln\gamma_i = \frac{1}{128} \cdot \frac{T_{cr,i}}{P_{cr,i} \cdot T} \left(1 - \frac{6 \cdot T_{cr,i}^2}{T^2} \right) \cdot P \qquad (19)$$

Figure 2 shows that for all components of the reaction mixture γ is very close to 1, in different conditions of pressure and temperature.

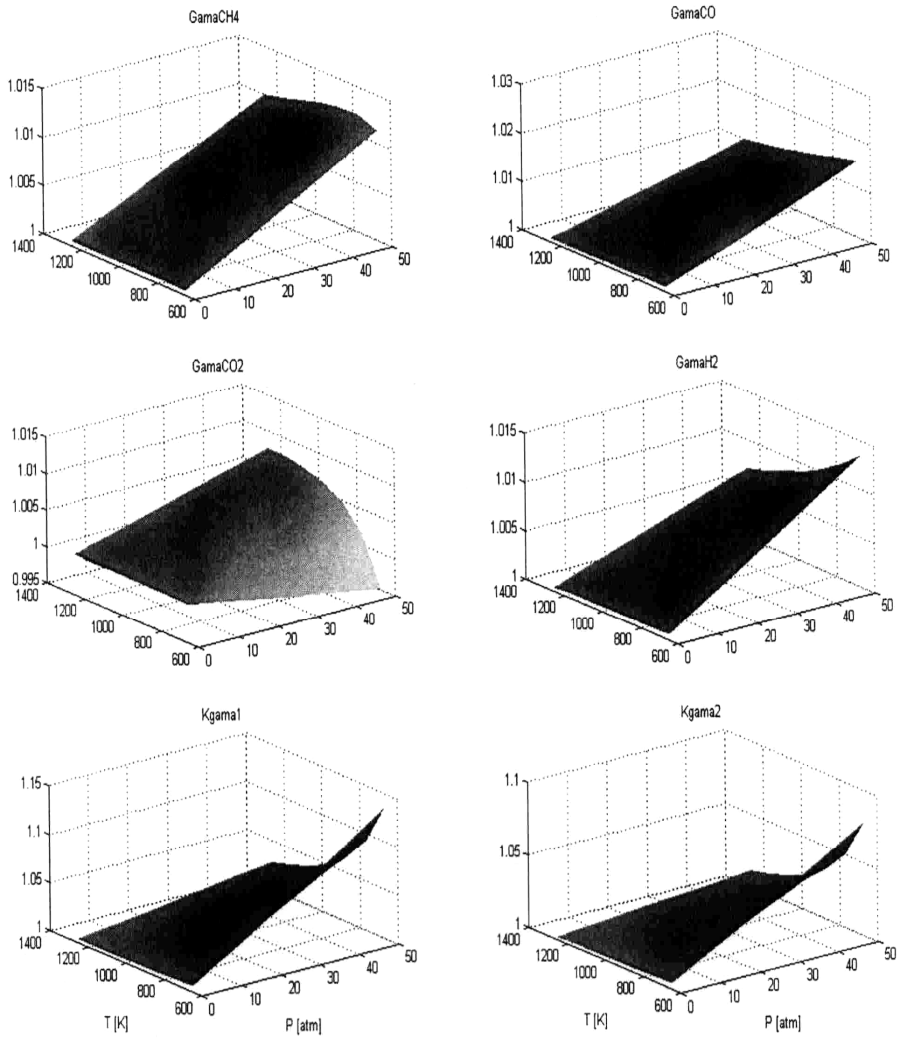

Figure 2. Variation of γ for the compounds as a function of temperature and pressure

The mathematical model described previously was used for the steady state simulation of the process. We studied the variation of the conversions as functions of molar ratio (H_2O/CH_4), temperature and pressure. The results obtained with the analytical model are briefly presented in figures 3 and 4.

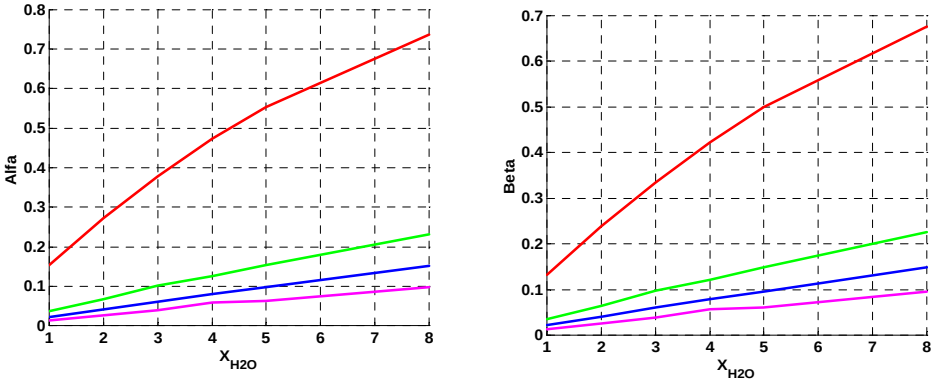

Figure 3. Variation of the conversion (Alfa - α, Beta - β) with molar ratio H_2O/CH_4 at different pressures (1,10,20,40 atm) and constant temperature T=773 K

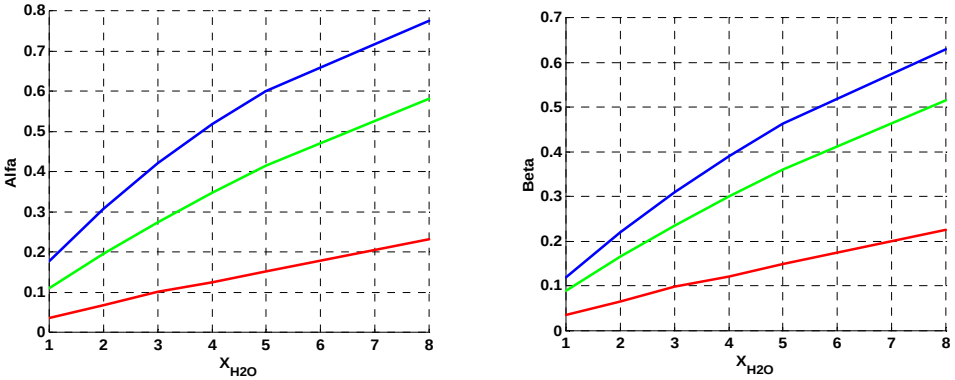

Figure 4. Variation of the conversion (Alfa - α, Beta - β) with molar ratio H_2O/CH_4 at different temperatures (773, 873, 923 K) and constant pressure P=10 atm.

Neural network based model

Inspired by research into the functioning of the human brain, artificial neural networks (ANN) are able to learn from experience. These powerful problem solvers are highly effective where traditional, formal analysis would be difficult or impossible. Their strength lies in their ability to make sense out of complex, noisy, or nonlinear data, which is the case of most of the chemical processes. ANNs can provide robust solutions to problems in a wide range of disciplines, particularly areas involving classification, prediction, filtering, optimization, pattern recognition, identification, modeling and control [7,8,9]. As the name suggests, a neural network is

a collection of connected artificial neurons. Each artificial neuron is based on a simplified model of the neurons found in the human brain. The complexity of the task dictates the size and structure of the network.

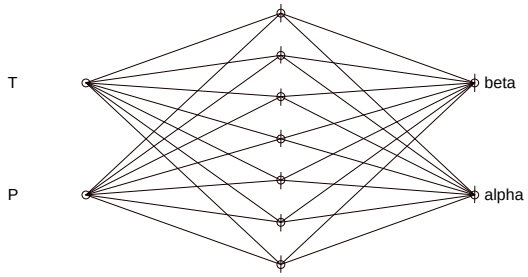

Figure 5. The feed-forward ANN used for simulation

For the catalytic steam reforming process model, we used a feed-forward neural network, trained to calculate conversion in almost any conditions of pressure and temperature. We used a set of over 250 data (conversion values in different conditions) to train different neural networks. One of the simplest neural networks (one hidden layer with 7 neurons) used is presented in the figure 5. The best results were obtained using a neural network with two hidden layers with 25 neurons. For training the network we used a Gauss-Newton based Levenberg-Marquardt algorithm, due to its rapid convergence properties and robustness.

The evolution of the sum-squared network error, during the training period of the neural network, is presented in figure 6. A good convergence of the algorithm can be seen. The error goal was achieved in only 164 epochs.

The difference between values calculated with analytical model and neural network based model is practically insignificant. Figures 7 and 8 shows the network error on the training and testing data, respectively.

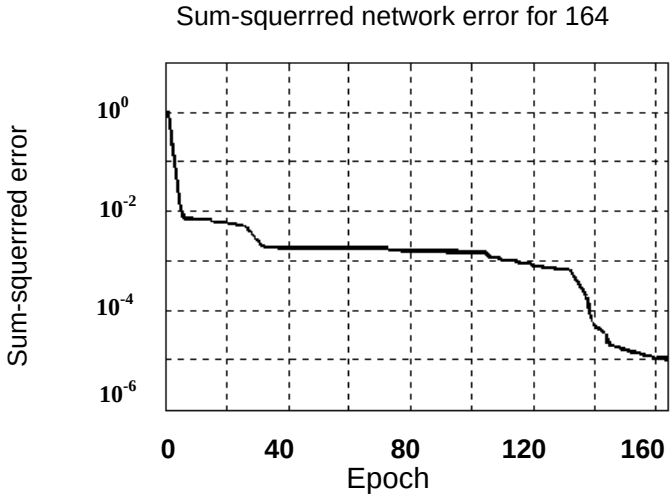

Figure 6. Sum-sequerred network error

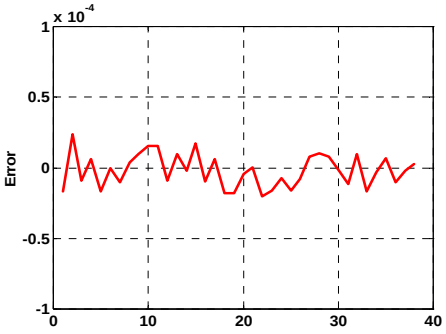

Figure 7. ANN model error on the training data

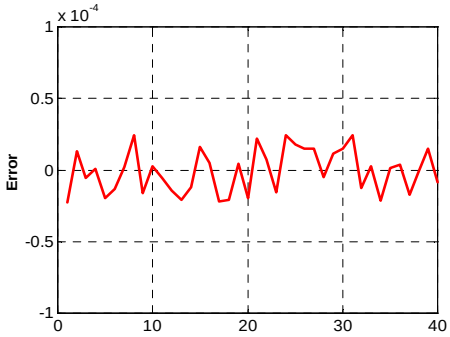

Figure 8. ANN model error on the testing data

Although the error for training was established less than 10^{-5}, the error obtained for the test data (a set of 50 data that wasn't in the training set) is sometimes double or higher but it is still under a convenient value. To illustrate how a network learned, we should represent the network predictions (y_{pred}) versus the measured (desired) data (y_D). In the ideal case $y_{pred} = y_D$. Taking into acount the learning error, the ideal case will never happen, instead of perfect equality the following linear dependence will be true:

$$y_{pred} = a \cdot y_D + b \qquad (20)$$

Where *a* and *b* are two parameters which can be used for the characterization of the network performance. The closer is *a* to 1 and *b* to 0, respectively, the better the network performance is. Figure 9 shows a very good neural network prediction on the testing data.

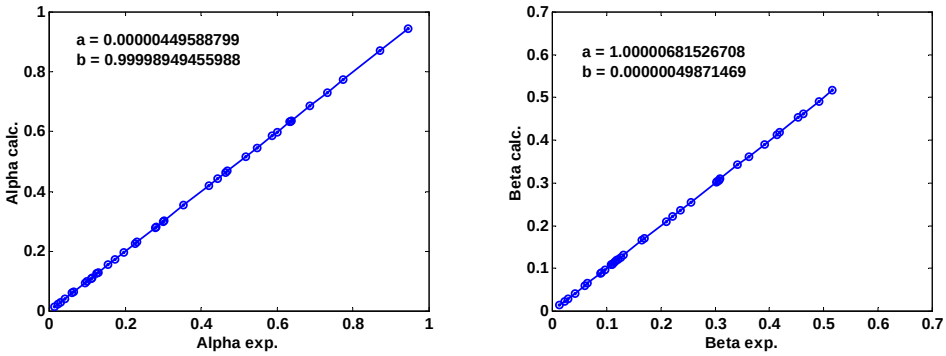

Figure 9. Network prediction on the testing data

The neural networks were also used successfully to calculate γ (correction coefficient) for all components.

CONCLUSIONS

The Neural Network based model can be used instead of the analytical model to calculate conversion of the catalytic steam reforming process, in different conditions of pressure, temperature and molar ratio, with a very good precision ($2.5 \cdot 10^{-5}$).

The main advantage of the Neural Network based model is the shorter computing time, which is over ten times lower than the analytical model computing time. (on a Pentium 200 MMX computer)

In perspective the Neural Network based model can be used together with a dynamic model of the industrial plant.

NOMENCLATURE

c_p - specific heat (J/kg·K)
d_p - particle diameter (m)
f – fugacity
F - flow (m^3/h)
c_i – Sutherland constant
m - mass (kg)
n^0 - initial number of moles
m_r - mass of reaction (kg)
P - pressure (atm)
Q - heat (KJ)
R - universal gas constant (J/kg·K)
T - temperature (K)
M - molecular mass (kg/kmol)
w - velocity of the gas in reactor (m/s)
z - reactor longitudinal dimension (m)
[] – concentration

SUPERSCRIPTS

^{0} - at standard temperature
r – reaction
T - at temperature T

SUBSCRIPTS

1,2 - reaction 1,2
am - mixture
i - compone nt I (CH_4 CO CO_2 H_2 H_2O)
r - reaction
nec - necessary
cr - critical value

GREEK SYMBOLS

ΔH_r - enthalpy of reaction (J/kg)
ΔS_r - enthropy of reaction (J/kgK)
α,β - conversions
γ - correction coefficient
μ - viscosity (Pa·s)
λ - thermal conductivity (W/m·K)
ξ - free space fraction
ρ - density (kg/m^3)
η_1,η_2 – conversion for reaction 1,2

REFERENCES

1. Gavrilă E., Bâldea I., Topan V., Agachi P., *Ingineria reacțiilor chimice, utilaje specifice, "Babeş-Bolyai" University*, Cluj-Napoca, vol.1.,2 (1988).
2. Muntean O., Woinaroschy A., *Aplicații la calculul reactoarelor chimice*, *Ed. Tehnică,* Bucureşti, (1984).
3. Niac G., Voiculescu V., Bâldea I., Preda M., *Formule, tabele, probleme de chimie- fizică, Ed. Dacia*, Cluj-Napoca (1984).
4. Othmer K., *Encyclopedia of chemical technology,* Intersciece Publishers, USA, vol. ***21*** (1970).
5. Agachi P. Ş., *Automatizarea proceselor chimice*, *Ed. Casa Cărții de ştiință*, Cluj-Napoca (1994).
6. Pavlov K.F., Romankov P.G., Noskov A.A., *Procese şi aparate în ingineria chimică*, *Ed. Tehnică,* Bucureşti (1981).
7. *** - Matlab Toolbox. Neural Network.
8. Aldrich, C. and J. van Deventer (1995), *Comparison of Different Artificial Neural Nets for the Detection and Location of Gross Errors in Process Systems, Ind. Eng. Chem. Res*., ***34*** (1), 216-224.
9. Bhat, N. V. and T. J. McAvoy (1990), *Use of Neural Nets for Dynamic Modeling and Control of Chemical Process Systems, Computers chem. Engng*, ***14*** (4/5), 573-585.

STUDIA UNIVERSITATIS BABEŞ-BOLYAI, CHEMIA, XLIII, 1-2, 1998

SYNTHESIS AND STEREOCHEMISTRY OF SOME 4-FURYLIDENE-1-PYRIMIDINYL-2-PIRAZOLIN-5-ONES

T. LOVASZ, CS. PAIZS, I. CRISTEA and FL.D. IRIMIE[1]

ABSTRACT. 1-(4-Hydroxy-6-methyl-2-pyrimidinyl)-3-methyl-pirazolin-5-one has been condensed with heterocyclic aldehydes, derivatives of 5-phenyl-furfural by Knoevenagel reaction, obtaining 4-(5-phenyl-furylidene) -1-(4-hydroxy-6-methyl-2-pyrimidinyl)-3-methyl 2-pyrazolin-5-ones (2a-h). The structures have been confirmed by elemental analysis and spectroscopic data.

INTRODUCTION

It is known that the 4-th position of 1 substituted 3-methyl-pyrazolin-5-ones is very reactive and undergoes a characteristic condensation of the active methylene group with aromatic aldehydes under acidic or basic catalysis, to give 4-arylidene pyrazolones [1,2,3].

The synthesis and chemistry of 4-arylidene pyrazolones have been of great interest because these compounds are very useful intermediates in synthesis of color dyes and substances with biological activity as for instance antibiotics and antipyretics [4,5].

Similary to the condensation reaction with aromatic aldehydes there are possible Knoevenagel condensations with heterocyclic aldehydes [6].

RESULTS AND DISCUSSION

1-(4-Hydroxi-6-methyl-2-pyrimidinyl)-3-methyl-pyrazolin-5-one 1, obtained by using aminoguanidine salts and ethylacetoacetate in basic catalysis with sodium hydroxide (NaOH), undergoes easily a Knoevenagel condensation with aromatic aldehydes to give 1-(4-hydroxy-6-methyl-2-pyrimidinyl)-3-methyl-2-pirazolin-5-ones [7].

We have extended this reaction on heterocyclic aldehydes using instead of aromatic aldehydes some derivatives of 5-phenyl-furfural obtaining 4-(5-phenyl-furylidene)-1-4-hydroxy-6-methyl-2-pyrimidinyl-3-methyl-2-pyrazolin-5-ones (2a-h).

We have studied this reaction using various 5-phenyl-furfurals with different susbtituents attached to the phenyl group.

---

[1] *"Babe¿-Bolyai" University, Faculty of Chemistry and Chemical Engineering, 11 Arany Janos St., 3400, Cluj-Napoca, Romania.*

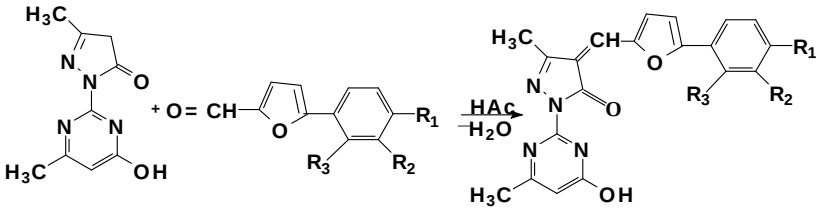

1 1a - h 2 a–h

Table 1

Compound	2a	2b	2c	2d	2e	2f	2g	2h
R_1	NO_2	H	H	COOEt	COOH	Br	Cl	CH_3
R_2	H	NO_2	H	H	H	H	H	H
R_3	H	H	NO_2	H	H	H	H	NO_2

The compounds 2a-h were prepared in various yields by heating under reflux of 1 with (5R-phenyl)-furylaldehydes using EtOH or MeOH as solvent, under acidic catalysis in presence of AcOH.

The reaction was studied also under basic catalysis but the obtained compounds couldn't be separated. The reaction was monitorized by TLC which indicated the presence of only one (stereoisomer) compound [10].

Some physico-chemical data of the obtained compounds are presented in the following table:

Table 2

Compound	Mp(^{0}C)	Yield %	Elementhal analysis Calculated / Found				Colour
			C%		N%		
2a	269	75	59,25	58,60	17,28	16,95	orange
2b	270	80	59,25	60,51	17,28	17,92	orange-red
2c	250	86	59,25	60,35	17,28	17,90	red
2d	218	67	63,88	62,70	12,96	12,36	red
2e	320	53	62,37	61,20	13,86	13,20	red
2f	205	91	54,67	55,70	12,75	12,70	orange-red
2g	190	44	60,83	60,06	14,19	14,23	red
2h	260	84	60,14	60,28	16,70	17,03	orange-red

In acidic catalysis pyrimidyl-pyrazolone (1) reacts in the enol form with heterocyclic aldehydes which are probably orientated with the heterocyclic system in anti to the methyl group, thus affording probably to the Z-isomer. The mechanism of the water elimination is probably E_2 [7].

The obtaining of Z-configuration stereoisomer can be explained by the higher energetic stability of this one, because with the heterocyclic ring in anti position to the methyl group from the third position of pyrazolinone ring the steric hindrance are minimized.

The structure of the synthesized compounds were studied using ^{1}H NMR and IR Spectroscopy. For clarify the stereochemical structure of the exocyclic double bond there were also performed NOE diff measurements and there was observed NOE diff activity for the vinylic proton.

In table 3 are presented the ^1H NMR spectroscopy data of the synthesized compounds.

Table 3

Compound	Pyrazolone-ring $CH_3(C_3)$	Pyrimidine-ring $CH_3(C_6)$	$H(C_3)$	Phenyl-ring H aromatic R	Furyl-ring H_1	H_2
2a	2,56	2,70	6,55	7,9 - 8,5 (m)	7,40(d)	7,62(d)
2b	2,50	2,65	6,55	7,8 - 8,5 (m)	7,45(d)	7,65(d)
2c	2,50	2,70	6,55	7,8 - 8,5 (m)	7,40(d)	7,65(d)
2d	2,55	2,75	6,60	7,9 - 8,4 (m)	7,50(d)	7,70(d)
2e	2,55	2,70	6,55	7,8 - 8,5 (m)	7,40(d)	7,65(d)
2f	2,55	2,65	6,55	7,7 - 8,1 (m)	7,35(d)	7,6)(d)
2g	2,55	2,65	6,50	7,6 - 8,1 (m)	7,35(d)	7,62(d)
2h	2,50	2,65	6,55	7,6 - 7,9 (m)	7,24(d)	7,55(d)

For the obtained compounds were also recorded the UV-VIS spectra in DMF (Table 4):

Table 4

Compound	λ_{max}(nm)	ε
2a	355; 420	7408
2b	310 ; 425	2382
2c	295; 408	11683
2d	325; 438	13926
2e	290; 410	6372
2f	285; 450	24080
2g	305; 435	4552
2h	296; 420	5199

EXPERIMENTAL

Melting points are given uncorrected. The purity of the compounds was checked by thin-layer chromatography on silicagel, using toluene: acetone 8:2 (v:v) as eluent. The elemental analysis for C, H, N, O, S was within $\pm$ 0,4% of the theoretical values for compounds ***2 a-h***.

IR spectra were recorded in KBr pellets on a FT-IR Nicolet 205 spectrophotometer. ^1H-RMN spectra were recorded usind CF_3COOD as solvent with a VARIAN GEMINI 300 MHz Spectrometer.

General procedure for synthesis of compounds 2a-h

1-pyrimidinil-3-methyl-pyrazolin-5-one (1) 0,01 mol and 0,01 mol arylfurfural were dissolved in EtOH and to the reaction mixture was added a small quantity of CH_3COOH. The mixture was refluxed for two hours and then allowed to stand at room temperature and the n cooled with ice. The precipitate was filtered, wash with EtOH (3 times, 3 ml) and dryed at 50^0C. The product was recrystallized from DMF.

REFERENCES

1. G.Cellerino, G.Desimoni, P.P.Righetti and G.Tacconi, *Gazz Chim. Ital*., 1973, ***103***, 1247.
2. J. de Ruiter, D.A.Carter, W.S. Artedge and J.J.Sulivan, *J.Heterocycl. Chem*., 1987, ***24***, 149.
3. A.Sammons, A. Abd-ElRanyf, M.Elkasaley and M.A.Hassan, *Egypt.J.Chem*., 1972, ***5***, 429.
4. Oriental Photo Ond.Co.Ltd.Jpn., Kokai Tokkyo Koho, 1980, 80155055, CA, 1981, 94, 176695k.
5. M.F.Abdel Magged, M.El Borai, M.Fahmy and El Saied A. Aly, *Rev.Roum.Chim*, 1987, ***32***, 515
6. I.Panea and I.Cristea, *Studia Univ.Babe¿-Bolyai, ser.Chemia*, 1996,***XL***, 9.
7. I.Cristea and I.Panea, *Studia Univ.Babe¿-Bolyai, ser.Chemia*, 1995, ***XL***, 171.
8. Hiroyshi Akashi and Royohei Oda, *Rept.Inst.Chem.Research, Kyoto* , no.19, CA,1981, 45, 7519
9. Hiroyshi Akashi and Rayohei Oda, *J.Chem.Soc.Jpn, Ind.Chem.Sect*.,1950, ***53***, 202, CA 1952, 49, 9312.
10. S.Gocan, L.Olenic and I.Cristea, *Rev.Roum.Chim*., 1989, ***34***, 1509.

STUDIA UNIVERSITATIS BABEŞ-BOLYAI, CHEMIA, XLIII, 1-2, 1998

THERMOGRAVIMETRIC STUDY OF THE SULPHUR DIOXIDE REACTION WITH LIME

S. DRAGAN[1], A. FRIEDL[2], M. HARASEK[2], MIHAELA DRAGAN[1], and I. SIMINICEANU[3]

ABSTRACT. Experimental thermogravimetric measurements, employing a CAHN TG- 121 system, have been performed on the reaction of sulphur dioxide and oxygen with calcined limestone. The conversions versus time of calcined limestone, ranging in particle size from 25 to 900μm, were measured over the temperature range 973- 1173 K and a gas rate of 0.0230 to 0.0277 m/s. On the basis of experimental data, using the unreacted core model, the kinetic parameters have been identified and the kinetic regimes evaluated. Although the external mass transfer had no influence, the internal diffusion resistance could not be avoided even with the particles as small as 25 μm in diameter.

INTRODUCTION

Sulphur dioxide is a major pollutant of the atmosphere, whose main effect is the *acid rain* [1]. It is produced whenever fuels, particularly coal and oil containing sulphur, burn in excess oxygen. One way of minimizing emissions of SO_2 is to absorb it on solid calcium oxide, produced by calcining limestone:

$$CaCO_3 = CaO + CO_2 \qquad (1)$$

The porous solid CaO can then react with SO_2 in the presence of oxygen to give calcium sulphate, via the reaction (2):

$$CaO + SO_2 + \tfrac{1}{2} O_2 = CaSO_4 \qquad (2)$$

This process, proposed by Borgwardt thirty years ago, is also known as the *dry injection process* [2].The limits and the potentials of the *dry injections process* were analyzed in detail by Bjerle et al. [1] by reviewing the published works. Their conclusion was rather optimistic: "the dry injection technique is really the dream process for the power plant operator because of low investment and operating cost, compared with other available choice". Maybe for this reason the process has

[1] *University "Babeş–Bolyai" of Cluj-Napoca, Faculty of Chemistry and Chemical Engineering, Str. Arany Janos 11, Cluj-Napoca, Romania, e-mail:sdragan@chem.ubbcluj.ro*
[2] *Technical University of Vienna, Austria.*
[3] *Technical University of Iaşi, Faculty of Industrial Chemistry, 71 Bd. Mangeron, 6600 Iaşi, Romania, Fax: 40-32-211667, e-mail: isiminic@ch.tuiasi.ro.*

been extensively studied both by scientists involved in the environmental protection [3-9] and by academics interested in solid-gas reactions [10–33]. The representative are Borgwardt for the first group, and professor Hartman from the Czech Academy, Prague, for the second. In spite of the large amount of theoretical and experimental work carried out on this process the dependence of its rate controlling mechanism upon the operating factors is still not clearly understood. The aim of the present paper is to present our thermogravimetric results and their interpretation in order to identify the rate determining step and the kinetic parameters.

EXPERIMENTAL

The primary kinetic data of any chemical process are the conversion versus time curves. Such data have been already obtained for the lime sulphation reaction by continuous measurement of gas phase SO_2 concentration at the outlet of the reactor [14,15]; discontinuous gravimetric or chemical analysis of reacted particles in a fixed bed reactor [3,12,16,17]; as well as by continuous thermogravimetric analysis [18-20]. The continuous weight measurement by a recording thermobalance seems to be the most suitable because of the accuracy and reproducibility of results. The reaction (2) is accompanied by an important solid weight increase, and the effects of side reactions are negligible. On the basis of materials balance equations (3):

$$\begin{aligned} m_{Cao} &= m^0{}_{CaO} - m^0{}_{CaO}.\eta_{CaO} \\ m_{CaSO_4} &= \frac{136}{56} m^0{}_{CaO}.\eta_{CaO} \\ m_{A''} &= m^0{}_{A''} \\ m_S &= m^0{}_S\left(1+\frac{80}{56}\bar{x}_{CaO}.\eta_{CaO}\right) \end{aligned} \qquad (3)$$

the relation between the solid mass increase (Δm_S) and the fractional conversion of lime (η_{CaO}) can be derived:

$$\eta_{CaO} = \frac{56}{80}\frac{\Delta m_S}{x^0{}_{CaO}.m^0{}_S} \qquad (4)$$

According to the equation (4), at an average conversion of 50 %, a sample of 100 mg pure lime increase in weight with 71.42 mg because of sulphation reaction (2).

The experimental equipment used in our kinetic measurements was a CAHN TG-121 system (Figure 1).

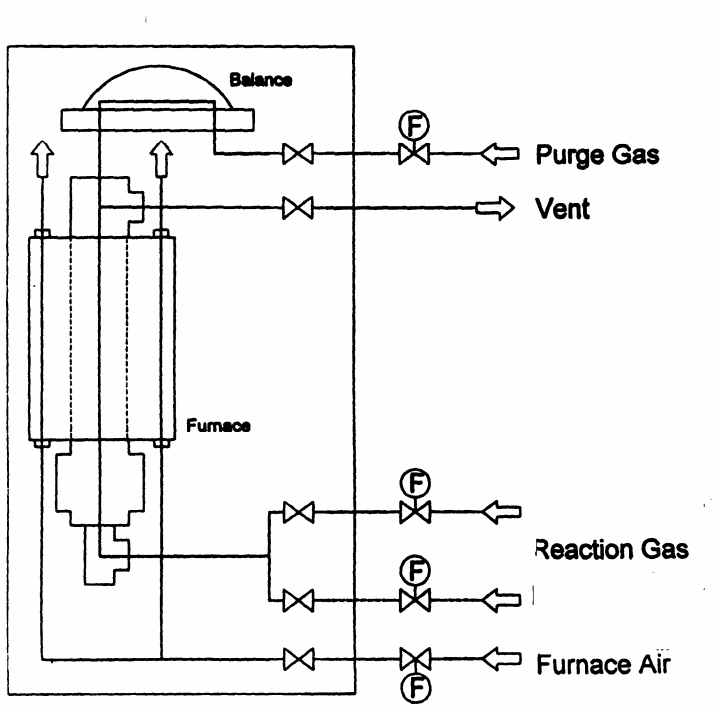

Figure 1. The gas circulation diagram in the main frame on the CHAN TG-121 experimental system**.**

It consisted of two main sections: the main frame and the Data Acquisition and Control Station (DACS) which controlled the system. The microbalance, the furnace, the cooling fan, the thermocouple, the gas and vacuum ports were the components of the main frame. The CAHN microbalance included in the TG-121 system is considered the finest apparatus available today for this application. Its sensitivity is of 0.1 μg and the maximum capacity of 1.5 g. This balance has a closed loop servo controlled transducer which automatically compensates for weight changes in the sample. The measured weight is displayed both on the DACS monitor and on the weight display in the front panel. The furnace assures an uniform heating zone with a temperature up to 1373 K. Typically, the ramping temperature in the thermogravimetric experiments varied from 5 ^{0} C /min. up to 25^{0}C/min. The reactor, located in the furnace, had a 125 cm^{3}volume (22 mm diameter and 329 mm hight) and was operated at a pressure of 0.3403 bar. Typical flow rates of reacting and purge gas were between 50 and 100 cm^3/min. The gas handling system provided a purge gas for the microbalance (argon), air flow for furnace cooling, and reactive pure gases from cylinders (sulfur dioxide, oxygen, and nitrogen).

Each sample of limestone has been primarily calcinated for 40 minutes at 973 K and 0.3403 bar. The thirty probes belonged to one of the following granulometric classes: 0- 50 μ m, 80 – 100 μ m, 160 –200 μ m, 400 –500 μ m, and 800 –1000 μ m.

After the complete calcination, each sample has been sulphated in a gas mixture containing 0.9 % (vol.) or 0.3 % (vol.) SO_2, 20 % (vol.) O_2, and nitrogen for the balance. The gas mixture was prepared from pure gases measured with rotameters.

The flow rate of the gas mixture was 50 cm^3/min.in 11 of the 12 runs. The temperature in the sulphation process was kept constant at 973 K, 1023 K, 1123 K, and 1173 K respectively. The solid weight has been continuously registered, and tabulated at five minutes intervals.

RESULTS AND DISCUSSION

The primary thermogravimetric measurements have been converted into kinetic curves with the equation (4). The conversion versus time curves for the extreme particles sizes are presented in Figures 2 and 3.

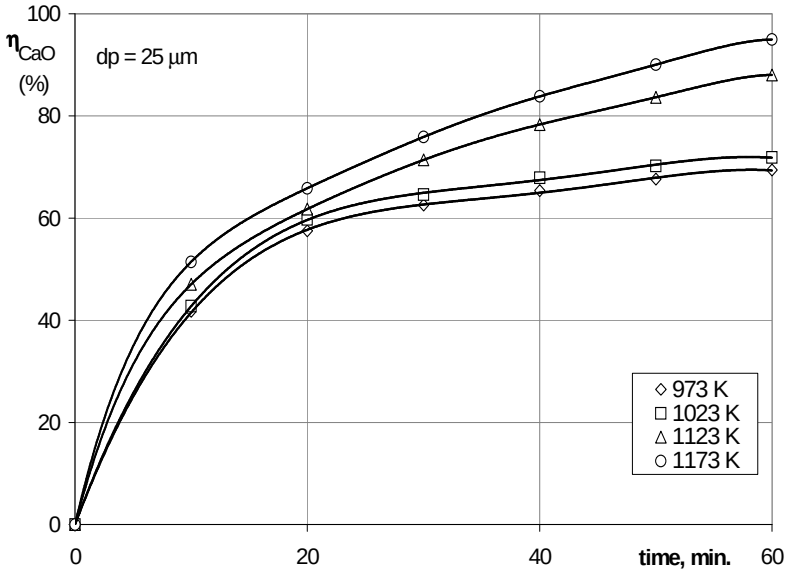

Figure 2. Isothermal kinetic curves, at: T_c = 973 K, τ_c = 40 min., P = 0.3403 bar, V_g = 50 cm^3/min, % vol SO_2 = 0.9, and R_0 = 12.5 μ m.

The experimental values of the fractional conversion of CaO illustrate the influence of two important parameters: temperature and particle size. With small particles (Figure 2) conversions above 50 % are possible in only 10 minutes, at 1173 K. The influence of temperature on the conversion of such particles, at a given time, is rather significant. This may suggest a transformation rate determining step, with a great activation energy. With large particles (Figure 3) the conversion of 50 % is not attainable even at the highest temperature and after a reaction times as long as 60 minutes. This could be due to a strong influence of the SO_2 diffusion through the solid product layer. The sensitivity to temperature of the conversion of

such large particles is less important, as one can see from the Figure 3. This lack of the sensitivity to temperature may be a qualitative confirmation for a mass transfer kinetic regime. Nevertheless, a more accurate and quantitatively supported interpretation of the experimental results is not possible without a postulated model describing the process.

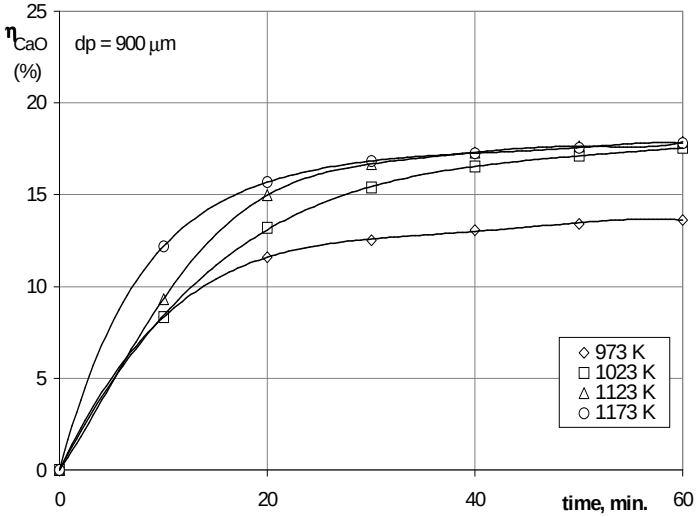

Figure 3. Isothermal kinetic curves at: T_c = 973 K, τ_c = 40 min, P = 0.3403 bar, V_g = 50 cm ^{3}/ min, % vol SO_2 = 0.9, and R_0 = 450 μm

Kinetic modeling

If the lime is considered to be made of spherical and homogeneous solid particles the *shrinking unreacted core model* may be applied for the kinetic modeling of this solid- gas process. Other improved models take into consideration the physical texture of the solid, and the intraparticular physical and chemical phenomena involved. The application of such grain or pore models needs complementary experimental data on the intraparticular surface area (BET measurements) molar volume / density of the solid product (X – ray difraction analysis) as well as pore size distribution in particles. In the absence of such complementary data the only model to be used is the unreacted core model. This model postulates that the overall chemical process is made of three steps in series: (I) mass transfer through the gas film to the outer surface of the particle with radius R_0; (II) the diffusion through the solid product layer; (III) the pseudo first order chemical reaction (2) at the surface of the unreacted core of radius R. The kinetic equations of the three steps are the following:

$$-\frac{dn_{SO_2}}{S_{ex}d\tau} = k_g (C_{SO2} - C^s_{SO2}) \qquad (5)$$

$$-\frac{dn_{SO_2}}{S_r d\tau} = D_s \frac{dC_{SO_2}}{dR} \tag{6}$$

$$-\frac{dn_{SO_2}}{S_r d\tau} = kC_{SO_2} \tag{7}$$

Using the pseudo- stationarity hypothesis, the integration of these equations gives the time required to move the reaction front from the external surface of the lime particle (a sphere of radius R_0) to the unreacted core of radius R:

$$\tau = \frac{R_0 C_{CaO}{}^0}{C_{SO_2}} \left[\frac{1}{3}\left(\frac{1}{k_g} + \frac{R_0}{D_S} \right)\left(1 - \frac{R^3}{R_0{}^3} \right) + \frac{R_0}{2D_S}\left(1 - \frac{R^2}{R_0{}^2} \right) + \frac{1}{k}\left(1 - \frac{R}{R_0} \right) \right] \tag{8}$$

By introducing the fractional conversion defined by (9) :

$$\eta_{CaO} = 1 - \left(\frac{R}{R_0} \right)^3 \tag{9}$$

the equation (8) becomes:

$$\tau = \frac{R_0 C_{CaO}{}^0}{C_{SO_2}} \left\{ \frac{1}{3k_g}\eta_{CaO} + \frac{R_0}{6D_S}\left[1 + 2(1-\eta_{CaO}) - 3(1-\eta_{CaO})^{2/3} \right] + \frac{1}{k_g}\left[1 - (1-\eta_{CaO})^{1/3} \right] \right\} \tag{10}$$

The time required for the complete conversion of the solid particle (τ^*) is found by setting $\eta_{CaO} = 1$ in the equation (10):

$$\tau^* = \frac{R_0 C_{CaO}{}^0}{C_{SO_2}} \left(\frac{1}{3k_g} + \frac{R_0}{6D_S} + \frac{1}{k} \right) \tag{11}$$

By combining equations (10) and (11) the kinetic model of the process can be derived in a dimensionless form:

$$\frac{\tau}{\tau^*} = \frac{\left[\frac{1}{3k_g}\eta_{CaO} \right] + \frac{R_0}{6D_S}\left[1 + 2(1-\eta_{CaO}) - 3(1-\eta_{CaO})^{2/3} \right] + \frac{1}{k}\left[1 - (1-\eta_{Cao})^{1/3} \right]}{\frac{1}{3k_g} + \frac{R_0}{6D_S} + \frac{1}{k}} \tag{12}$$

The equation (12) suggests that the three "resistances" involved are purely in series, the "overall" rate coefficient being of the form:

$$\frac{1}{K} = \frac{1}{3k_g} + \frac{R_0}{6D_S} + \frac{1}{k} \tag{13}$$

To prove its adequacy, the extreme cases also called "simple macrokinetic models", are derived from the general equation (10).

Case I. The external mass transfer is the rate determining step (RDS), the other two resistances being negligible. ($1/k = 0$; $R_0/ 6D_S = 0$):

$$\frac{\tau}{\tau^*} = F(\eta) = \eta_{CaO}\text{, where } \tau^* = \frac{R_0 C_{CaO}{}^0}{3k_g C_{SO_2}} \quad (14)$$

Case II. The diffusion through solid product layer ($CaSO_4$) is RDS (1/k = 0; $1/3k_g$ =0) and the equation (10) becomes:

$$\frac{\tau}{\tau^*} = 1 + 2(1-\eta_{CaO}) - 3(1-\eta_{CaO})^{\frac{2}{3}} = F(\eta), with\, \tau^* = \frac{R^2{}_0 C_{CaO}{}^0}{6D_S C_{SO_2}} \quad (15)$$

Case III. When the overall process is kinetically controlled by the chemical reaction at the core surface, the two mass transfer steps being very rapid ($1/3k_g$ = 0; $R_0/6D_S$ = 0) the equation (10) becomes:

$$\frac{\tau}{\tau^*} = F(\eta) = 1 - (1-\eta_{CaO})^{1/3}\text{, where } \tau^* = \frac{R_0 C_{cao}{}^0}{kC_{SO_2}} \quad (16)$$

In addition to these three extreme cases and the general one (IV) described by equation (10), other three cases, with two comparable step rates, are possible: (V) external transfer and diffusion, (VI) diffusion and reaction, (VII) external transfer and reaction. Which one of these seven kinetic regimes is the most advantageous for practice? By numerical solution of the equation (12), for five frequently encountered kinetic regimes, the simulated curves in Figure 4 have been generated.

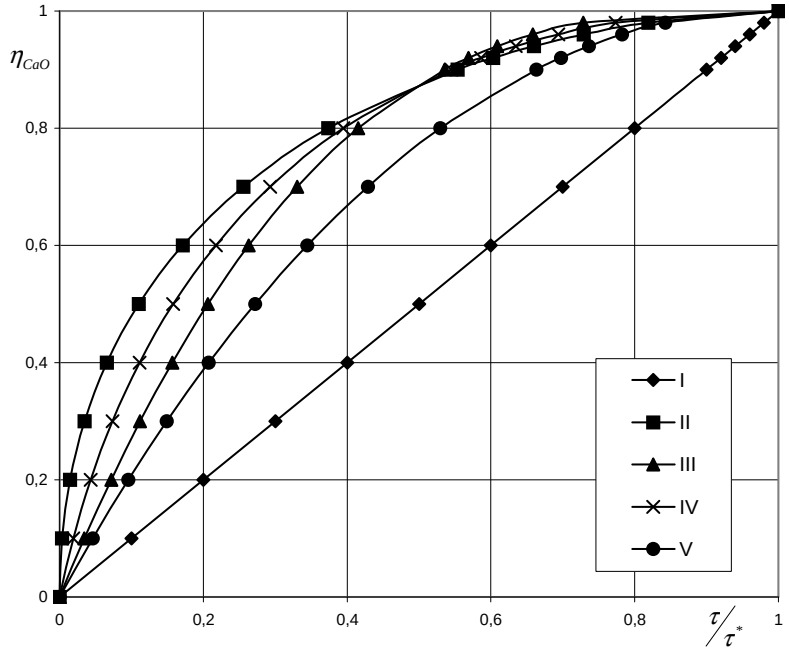

Figure 4. Conversion versus reduced time for different kinetic regimes (I, II, III, IV, V).

The most favorable kinetic regime is that providing the greatest conversion at a given time. It can be seen from Figure 4 that, to achieve conversions above 90%, the kinetic regime III, with no transfer limitation, is the most advantageous. Practically, the diffusion influence is not avoidable when a compact solid is formed.

Therefore, a regime of VI type may be frequently encountered in practice. This could be a rather effective regime when conversions under 90% would be accepted in practice.

The next paragraph is devoted to the estimation of the kinetic constants, on the basis of our own experimental data and the postulated unreacted core model, in order to evaluate the kinetic regime for a given set of operation factors: temperature, particle size, gas flow rate and composition.

Kinetic coefficients identification

The kinetic coefficients characterizing the three individual steps of the process have been defined by the kinetic equations (5), (6), and (7). They are k_g, D_S, and k respectively.

The mass transfer coefficient can be predicted quite accurately with the correlation proposed by Rantz and Marshall [21]:

$$Sh = 2.0 + 0.6\, Re^{1/2} Sc^{1/3} \qquad (17)$$

using experiments confined to the Reynolds number range 0 to 200. Froessling [22] had earlier presented an almost identical equation, and theoretically showed that the Sherwood number should take on a value of 2.0 in stagnant fluid. Froessling's experiments concerned the evaporation of nitrobenzene, aniline, water, and naphtalene into hot air stream. The Froessling – Rantz – Marshall equation (17) is still accepted as the most rigorous [23] in spite of the later extensive studies on the subject of mass transfer from solid spheres [24,25]. Therefore it has been used in previous papers on the lime – sulphur dioxide reaction [26-28].

The gas properties involved in the Sh, Re, and Sc numbers have been calculated for our experimental conditions. The molecular diffusivity of SO_2 has been evaluated with the equation proposed by Fuller et al. [29]. The results are presented in Table1:

Table 1.

Gas properties and flow rates for the experimental conditions:

P = 0.3403 bar, A = $3.8.10^{-4}$ m^2, V_g = 50 cm^3/min.

T, K	V_g, 10^6 m^3/s	v_g, m/s	ρ_g, kg / m^3	μ_g, 10^5 Pa.s	D_{SO2}, $10^4$$m^2$/s
973	8.7275	0.0230	0.123	4.086	2.930
1023	9.1760	0.0241	0.117	4.202	3.206
1123	10.0729	0.0265	0.106	4.434	3.775
1173	10.5213	0.0277	0.102	4.550	4.074

With the values from Table 1 introduced into the equation (17) the mass transfer coefficients in Table 2 have been obtained.

Table2.

Mass transfer coefficients (k_g, m/s) at the experimental conditions.

P = 0.3403 bar, V_g = 50 cm^3/min.

$d_p, \mu m$ T, K	25	90	180	450	900
973	23.7325	6.6653	3.3646	1.3711	0.6998
1023	25.9631	7.2905	3.6793	1.4912	0.7649
1123	30.5606	8.5789	4.3288	1.7627	0.8989
1173	32.9772	9.2563	4.6702	1.8298	0.9695

The value of k_g is more sensitive to the particle size variation than to the temperature change, as expected.

The reaction rate constant (k) can be derived from the thermogravimetric data obtained with the smallest particles (R_0 = 12. 5 μm) at low conversions (<10%) when the diffusion influence may be supposed as negligible. This is the extreme case III, described by the equation (10) reduced to the form:

$$F(\eta) = 1-(1-\eta_{CaO})^{1/3} = \frac{kC_{SO_2}}{R_0 C_{CaO}{}^0}\tau \qquad (18)$$

By representing $F(\eta)$ versus time, using the points from curves in Figure 2, the constant k can be calculated with the relation (19):

$$k = \frac{C_{CaO}{}^0 R_0}{C_{SO_2}}\left[\frac{dF(\eta)}{d\tau}\right]_{T=const.} \qquad (19)$$

Where: C^0_{CaO} =3370 x 0.95 / 56=57.17 kmol/m^3; C_{SO2} =0.009/22.4=4.01785.10^{-4} kmol/m^3, and R_0 = 12.5.10^{-6} m.

The values of k identified in such a manner are listed in Table 5 (with *superscript) together with those derived from Borgwardt ‘s data using the grain model [3,4] by Hartman and Trnka [13].

Table 3.

Kinetic constants of the reaction of lime with sulfur dioxide

T, K	k, 10^4 m/s	D_e, 10^5 m^2/s	D_s, 10^{12} m^2/s	r_g, 10^7 m
973	3.16*	-	-	-
1073	- 3.04	6.94	1.4	2.85
1123	3.75* 4.95	7.50	5.5	3.74
1173	4.15* 7.76	8.07	7.4	4.86

The values of k derived from our thermogravimetric data have the same order of magnitude with those calculated by Hartman and Trnka [13]. Nevertheless, there is a great difference regarding the activation energy: that from Borgwardt’s data is 79.6 kJ/ mol whereas our data lead to an activation energy smaller than 41. 8 kJ/mol. This means that our k is only an apparent rate constant, the process being in the kinetic regime VI (reaction controlled by diffusion).

Another way to check the kinetic regime is suggested by the equation (11), which may be translated into the following words: the time for complete conversion

of a particle is the sum of complete reaction times corresponding to extreme cases I to III:

$$\tau^* = \sum_{i=I}^{i=III} \tau_i^* \qquad (11')$$

Using the values of k_g, k, and D_S from Tables 4 and 5 it is possible to evaluate the relative complete reaction times at given values of parameters: temperature, particle size, gas flow rate. With T = 1.123 K, R_0 = 12.5 μm, and gas flow rate of 50 cm^3/min, the relative contributions of the three reaction steps are the following:

$$\left(\tau_I^* / \tau^*\right).100 = 0.02449\,;\ \left(\tau_{II}^* / \tau^*\right).100 = 84.8503\,;\ \left(\tau_{III}^* / \tau^*\right).100 = 15.1252$$

In other words, even with the smallest particles, the process investigated was kinetically controlled by diffusion in a proportion of 85 %. The chemical reaction share was only 15 %, whereas the external mass transfer had no influence. Consequently, the industrial process could be enhanced mainly through the factors accelerating the solid phase diffusion.

Conclusions and significance

The dry injection of limestone fine particles in the power plant furnaces is a promising process for flue gas desulphurization and acid rain mitigation. The limestone is quickly converted to lime which further reacts with sulphur dioxide. New kinetic studies have been carried out on the sulfation reaction using a CAHN TG –121 system for continuous thermogravimetric measurements. The kinetic curves are quantitatively analyzed on the basis of the unreacted core model integrated in the general form. This includes the three steps connected in series: external mass transfer, diffusion, and chemical reaction at the core surface. The corresponding kinetic coefficients are identified for the experimental operating conditions: temperature, particles size, gas composition and flow rate. The first practical conclusion is that, even with low gas rates used in the thermobalance (0.0230 to 0.0277 m/s) the external mass transfer has no influence on the overall rate of the process.

The second conclusion is that even with the smallest particles (d_p = 25 μm) and temperatures as low as 1123 K the internal diffusion "resistance" can not be avoided. Improved structured models and complementary experimental techniques are needed for a better understanding and quantitative description of the lime sulphation reaction in order to enhance the industrial process.

Notations

A – cross section area of the reactor, m^2;
A'' – inert substances in the solid, - ;
C – molar concentration, kmol / m^3;
d_p – particle diameter, m;
D_e – effective diffusion coefficient, m^2 /s;

D_S – diffusion coefficient in the product layer, m^2/s;
D_{SO2} – molecular diffusion coefficient of SO_2 in the gas mixture, m^2 /s;
H – hight of the reaction tube, m;
k – surface reaction rate constant, m/s;
k_g – mass transfer coefficient in the gas phase, m/s;
K – overall coefficient of the process, defined by equation (13), m/s;
m_i – mass of component, kg;
P – pressure, Pa;
r – radius of the grain unreacted core, m;
r_g – grain radius, m;
R – radius of the unreacted core of particle, m;
R_0 – initial radius of the particle, m;
S – surface area of particle, m^2;
T – temperature, K;
v_g – gas rate, m/s;
V_g – gas flow rate, m^3/s;
$\overline{x_{CaO}}^0$ – mass fraction of CaO in the lime, –;
Δm_s – thermogravimetric mass increase, kg;
η_{caO} – fractional conversion of CaO in the reaction (2), –;
μ_g – gas viscosity, Pa.s;
ρ_g – gas density, kg/m^3;
ρ_s – solid density, kg/m^3;
τ – reaction time, s;
τ^* – time for complete reaction, s;

Subscripts
c – related to calcination;
ex – external surface of the particle;
g – grain or gas phase;
L – lime;
LS – limestone;
r – reaction;
s – solid phase;

Superscripts
0 – initial state ($\tau = 0$);
s – surface of the particle.

REFERENCES

1. Bjerle, J., Ye, Z., Wang, W., *Limits and potentials of the dry injection process, 1993 SO_2 Control Symposium,* 1993 vol. 1, EPRI, Boston.
2. Dunderdale, J. (Editor), *Energy and the Environment,* Royal. Soc., 1990 Cambridge.
3. Borgwardt, R.H., *Environ. Sci. Technol*., (1970) 4, 59.
4. Borgwardt, R.H., Harvey, R.D., *Environ. Sci. Technol*., (1970) 6, 350.
5. Borgwardt, R.H., Roache, N.F., Bruce, K.R., *Environ. Prog*., (1984) 3, 129.
6. Borgwardt, R.H., *A.I. Ch. E. Journal*, (1985) 31, 1, 103.
7. Borgwardt, R.H., Roache, N.F., Bruce, K.R., *Ind. Eng. Chem. Fundam*., (1985) 25, 156.
8. Borgwardt, R.H., Bruce, K.R., Blake, J., *Ind. Eng. Chem. Res*., (1987) 26, 1993.
9. Borgwardt, R.H., *Chem. Eng. Sci*., (1989) 44, 1, 53.
10. Wen, C.Y., Ishida, M., *Environ. Sci. Technol*., (1973) 7, 703.
11. Pigford, R.L., Sliger, G., *Ind. Eng. Chem. Process Des. Dev*., (1973) 12, 85.
12. Hartman, M., Coughlin, W.R., *Ind. Eng. Chem.Process Des. Dev*., (1974) 13, 248.
13. Hartman, M., Trnka, O., *Chem. Eng. Sci*., (1980) 35, 1189.
14. Hartman, M., Svoboda, K., Trnka, O., *Sulfur dioxide removal in a batch fluidized bed reactor,* EFCE Publ. Series, (1984) No. 37, Pergamon Press, Oxford, 509.
15. Fields, R.B., Burdett, N.A., Davidson, J.F., *Trans. Instn. Chem. Engrs*., (1979) 57, 276.
16. Hartman, M., Colln. *Czech Chem. Commun*., (1975) 40, 1466.
17. Borgwardt, R.H*., 2nd Joint Symposium on Dry SO_2 and Simultaneous SO_2/NO_x Control Technologies*, San Diego, California, 1984.
18. Yang, R.T., Cunningham, P.T., Wilson, W.I., Johnson,S.A., *Adv. Chem. Ser.,* (1975) 134, 149.
19. O'Neil, E.P., Kearns, D.L., Kittle, W.F., *Thermochim. Acta*., (1976) 14, 209.
20. Bjerle, J., Xu, F., Ye, Z., *Chem. Eng. Technol*., (1992) 15, 151.
21. Rantz, W.E., Marshall, W.R., *Chem. Eng. Prog*., (1952) 48, 173.
22. Froessling, M., *Beitr, Geophys*., (1938) 52, 170.
23. Froment, G.F., Bischoff, K.B., *Chemical Reactor Analysis and Design,* 2nd Edition Wiley, New York, 1990.
24. Hughmark, G.A., *A.I.Ch.E. Journal*, (1967) 13, 1219.
25. Levender, W.J., Pei, D.C.T., *Int. J. Mass Trans*., (1967) 10, 529.
26. Alen, D., Hayhurst, A.N., *J.Chem.Soc. Faraday Trans*, (1996) 92, 7, 1227.
27. Dennis, J.S., Hayhurst, A.N., *Chem. Eng. Sci.,* (1990) 45, 5, 1175.
28. Tambe, S., Gauri, K.L., Li, S., Coburn, W.G., *Environ.Sci. Technol*., (1991) 25, 2071.
29. Fuller, E.N., Schettler, P.D., Giddings, J.C., *Ind.Eng. Chem*., (1966) 58, 5, 19.
30. Georgakis, C., Chang, C.W., Szekely, J., *Chem.Eng.Sci*., (1979) 34, 1072.
31. Sotirchos, S.V., Yu, H.C., *Chem.Eng.Sci*., (1985) 40, 2039.
32. Adanez, J., Gayan, P., Garcia-Labiano, F., *Ind.Eng.Chem.Res*., (1996) 35, 2190.
33. Fernandez, I., Garea, A., Irabien, A., *Chem.Eng.Sci*., (1998) 53, 1869.

STUDIA UNIVERSITATIS BABEŞ-BOLYAI, CHEMIA, XLIII, 1-2, 1998

A KINETIC STUDY UPON THE OXIDATION OF BENZALDEHYDE BY CERIUM(IV) IN SULPHURIC ACID MEDIA

CLAUDIA MUREŞANU, IOAN BÂLDEA and ANA-MARIA BUDUŞAN[1]

ABSTRACT. The kinetics of benzaldehyde oxidation to benzoic acid by ceric sulphate has been studied using spectrophotometrical means, in a H_2SO_4 – Na_2SO_4 – $NaClO_4$ mixture. The influence of organic substrate, hydrogen ion and sulphate ion concentration as well as the effect of ionic strength upon the rate was investigated over a wide range. The kinetic study revealed the existence of two stages, each of first-order with respect to Cerium(IV). The first step involves the formation of an intermediate complex between Ce(IV) and benzaldehyde. The second step consists of the electron transfer within this 1:1 Ce(IV):benzaldehyde complex. The rate laws for both processes were found and a mechanism was suggested in accordance with the experimental results. The activation parameters for both processes were obtained.

INTRODUCTION

Cerium (IV) is a good oxidizing agent for a large number of organic substrates, because of the relative high oxidation potential of Ce(IV)/Ce(III) system [1]. Many oxidations of various classes of organic molecules are reported in the literature. For example we mention the oxidation of aromatic hydrocarbons [2-4], aliphatic [5-8] and aromatic alcohols [9-12], aldehydes [13-16], organic acids [17-18], phenols [19] etc by Ce(IV) in various acidic media. The Ce(IV)/Ce(III) redox system was also successfully employed as a mediator in the indirect anodic oxidation of toluene [20] and p-xylene [21].

An extended kinetic study on benzaldehyde oxidation by Ce(IV) [16], which was performed in acetic acid medium established the formation of some intermediate complexes between Ce(IV) and benzaldehyde. The authors found the rate law for the oxidation process and developed a mechanism that included besides the complex formation the decay of the complex by internal electron transfer yielding the benzoyl radical.

It is the purpose of this study to complete the investigation on the oxidation of toluene and benzyl alcohol by Ce(IV), undertaken in our laboratory, using sulphuric medium.

[1] *Facultatea de Chimie şi Inginerie Chimică, Universitatea "Babeş-Bolyai", Catedra de Chimie Fizică, Str. Arany Janos 11, 3400 Cluj-Napoca, România.*

EXPERIMENTAL

All the chemicals employed were of reagent grade purity and came from "Reactivul Bucureşti", "Carlo Erba-Milano" and "Merck". Stock solutions were prepared in twice distilled water. Reaction kinetics was followed spectrophotometrically on a Spekol-Zeiss spectrophotometer provided with a temperature jacket surrounding the cells. The jacket was connected to a Wobser U-10 thermostat which kept the temperature constant within $\pm 0,1^0$C. The reaction mixtures were prepared directly in a quartz cell with 5 cm path length and the absorbance was measured at 350 nm. The kinetic runs were started by adding a measured amount of Ce(IV) stock solution to the mixture containing benzaldehyde, H_2SO_4, Na_2SO_4, $NaClO_4$ and twice distilled water.

RESULTS AND DISCUSSIONS

Preliminary investigations

The solubility check. Benzaldehyde solubility was determined by spectrophotometrical means in a H_2SO_4 – Na_2SO_4 – $NaClO_4$ aqueous mixture, at 20 and 40^0C. The hydrogen ion concentration of the nine solutions varied from 0,15 to 0,65 mol/dm^3 at constant sulphate ion concentration (0,6 mol/dm^3) and constant ionic strength (1,5 mol/dm^3). They were saturated in benzaldehyde.The solubility limits varied within this range of acidity from $1,88\cdot10^{-3}$ to $4,44\cdot10^{-3}$ at 20^0C and from $3,1\cdot10^{-3}$ to $7\cdot10^{-3}$ mol/dm^3 at 40^0C.

Complex formation and check on Lambert Beer law validity. The formation of an 1:1 complex between Ce(IV) and benzaldehyde with the apparent equilibrium constant K_{app} = 375±7 dm^3/mol ($[H^+]$ = 0,7; $[SO_4^{2-}]$ = 0,6 and ionic strength, μ = 1,5 mol/dm^3; t = 25^0C) was previously proved by recording the absorbance spectra of several benzaldehyde – Ce(IV) mixtures [22]. That approach did not make allowance of sulphate ion and hydrogen ion concentration. Taking into account the effect of these species on the complex formation a new value of 193±4 has been calculated from the equilibrium:

$$CeSO_4^{2+} + C_6H_5CH(OH)_2 \underset{k_{-1}}{\overset{k_1}{\rightleftharpoons}} CeSO_4 \bullet OCH(OH)C_6H_5 + H^+ \quad (1)$$

Because Ce(IV) forms many sulphatocomplexes in sulphuric acid solution [23-24] and because kinetic measurements were performed by spectrophotometrical means, the validity of Lambert-Beer law needed to be checked over the range of Ce(IV), SO_4^{2-} and H^+ concentrations used in our experiments. We obtained linear A = f([Ce(IV)] plots in the absence as well as in the presence of benzaldehyde, at two wavelengths.

Table 1.

Molar absorbance coefficients for ceric sulphate at 25^0C.

Mixture	λ nm	E $dm^3 \cdot mol^{-1} \cdot cm^{-1}$
$2 \cdot 10^{-5} \leq [Ce(IV)] \leq 5 \cdot 10^{-5}$ mol/dm^3 $[H^+] = 0.7$ mol/dm^3 $[SO_4^{2-}] = 0.6$ mol/dm^3 $\mu = 1.5$ mol/dm^3	350 360	5000±26 4000±8
$2 \cdot 10^{-5} \leq [Ce(IV)] \leq 5 \cdot 10^{-5}$ mol/dm^3 $[H^+] = 0.7$ mol/dm^3 $[SO_4^{2-}] = 0.6$ mol/dm^3 $[C_6H_5CHO] = 10^{-4}$ mol/dm^3 $\mu = 1.5$ mol/dm^3	350 360	4580±50 3800±15

As shown in table 1 the molar absorptivities are smaller the presence of benzaldehyde, a fact that may be also considered as an evidence for the formation of an complex between Ce(IV) and benzaldehyde.

Kinetics

All kinetic runs were performed in the presence of benzaldehyde excess. Under such set of experimental conditions, the absorbance readings were processed according to the integrated form of a first order rate law:

$$\ln(A - A_\infty) = \ln(A_0 - A_\infty) - k_{obsd} \cdot t \qquad (2)$$

where: - A_0, A_∞ and A stand for the absorbance at the beginning, at the end of the process and at different time intervals, t, from the start of reaction, respectively;

- k_{obsd} is the observed first-order rate constant.

The semilogarithmic plots $\ln(A - A_\infty) = f(t)$, that were obtained for several excess concentrations of benzaldehyde, exhibited an initial curved part at small degrees of reaction, followed by a linear part up to around 90% of completion (Fig. 1)

This biphasic plots can be attributed to a reaction sequence consisting of two processes:

$$Ce(IV) + C_6H_5CHO \underset{k_{-1}}{\overset{k_1}{\rightleftarrows}} Complex \xrightarrow{k_2} Ce(III) + Products \qquad (3)$$

Under the excess concentration of benzaldehyde it simplifies to:

$$A \xrightarrow{k_{obsd1}} B \xrightarrow{k_{obsd2}} C \qquad (4)$$

where A stands for Ce(IV), B for the Ce(IV)-benzaldehyde complex and C for the product.

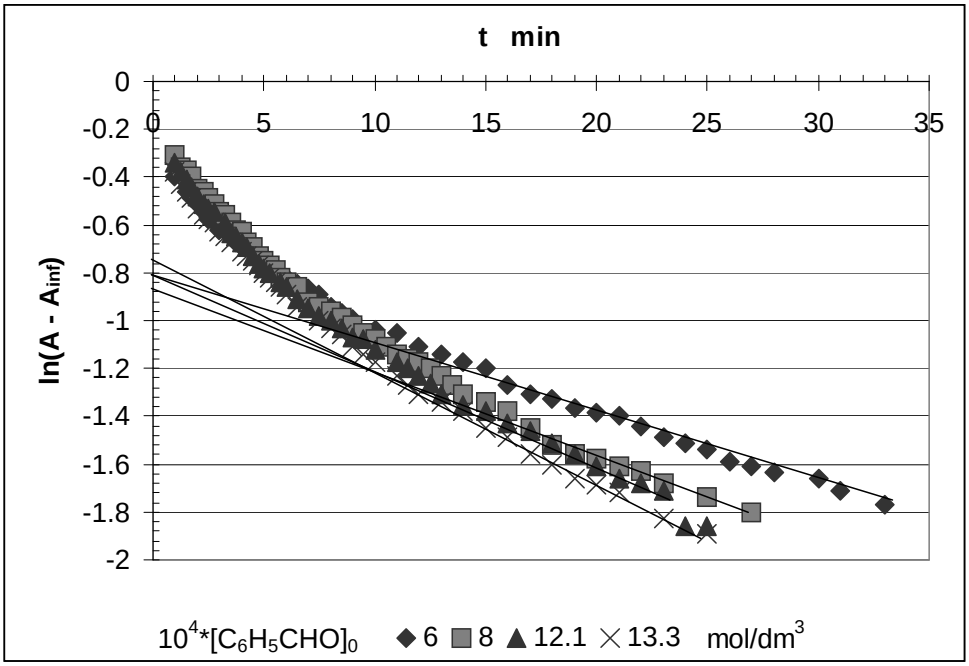

Figure.1. First-order plots for benzaldehyde oxidation with Ce(IV); [Ce(IV)]=5·10^{-5}; [H$^+$]=0.6; [SO_4^{2-}]=0.6 and (μ = 1.5 mol/dm^3; t=34^{0}C

The first order rate constant for the complex formation process is $k_{obsd1} = k_1 \cdot [C_6H_5CHO] + k_{-1}$ and the first order rate constant for the oxidation process is k_{obsd2}. In order to determine the rate constants for these two processes we employed a method that is further described.

The absorbance of the reaction mixture, at any moment, results from the contributions of all coloured species at 350 nm. In this case they are: the ceric sulphate, the complex and, with a rather very small contribution, the product.

$$A = \varepsilon_A \cdot d \cdot C_A + \varepsilon_B \cdot d \cdot C_B + \varepsilon_C \cdot d \cdot C_C \qquad (5)$$

where A stands for the absorbance of the mixture, ε is the molar absorbance coefficient, C is the concentration and d stands for the cells path length. If C_A, C_B and C_C from relation (5) are replaced with the well known, time dependent equations of reactant, intermediate and product concentration for a first-order consecutive reaction, we obtain:

$$A - A_\infty = C_{A0} d \left[\varepsilon_A + \frac{k_{obsd2}\varepsilon_C - k_{obsd1}\varepsilon_B}{k_{obsd1} - k_{obsd2}} \right] \exp(-k_{obsd1} t) + C_{A0} d \frac{k_{obsd1}(\varepsilon_D - \varepsilon_C)}{k_{obsd1} - k_{obsd2}} \cdot \exp(-k_{obsd2} t) \qquad (6)$$

where $A_\infty = \varepsilon_C \cdot C_{A0}$

Including all constant values into a preexponential factor, the equation (6) becomes:

$$A - A_\infty = \gamma_1 \exp(-k_{obsd1} t) + \gamma_2 \exp(-k_{obsd2} t) \qquad (7)$$

The semilogarithmic plot of $\ln(A - A_\infty)$ vs t would be a curve that becomes a straight line at higher degrees of transformation. For long reaction times, provided that $k_{obsd1} > k_{obsd2}$, which is valid to our system, the term $\exp(k_{obsd1} \cdot t)$ has a negligible contribution to the sum and:

$$\ln(A - A_\infty) = \ln\gamma_2 - k_{obsd2} \cdot t \qquad (8)$$

It allows to determine the constant γ_2 and the first-order rate constant k_{obsd2} from the intercept and slope of the line respectively.
At short reaction times, when the oxidation process is unimportant, the time dependent parameter Δ may be defined:

$$\Delta = A - A_\infty - \gamma_2 \exp(-k_{obsd2} \cdot t) = \gamma_1 \exp(-k_{obsd1} \cdot t) \qquad (9)$$

The slope of the line described by equation (8) and the linear form of (9) were obtained using a least square method. Two to four individual experiments were used for each set of conditions. First order dependence on [Ce(IV)] for complex formation and for its oxidation is proved by linear $\ln\Delta = f(t)$ and $\ln(A - A_\infty) = f(t)$ plots we obtained for all kinetic runs.

First-order rate constants calculated for both processes at several excess concentration of benzaldehyde are presented in table 2.

Table 2.

The dependence of first-order rate constants for complex formation and complex oxidation on the initial benzaldehyde concentration; $[Ce(IV)]=5 \cdot 10^{-5}$; $[H^+]=0.6$; $[SO_4^{2-}]=0.6$ and $\mu = 1.5$ mol/dm^3; t=34^{0}C.

$10^4 \cdot [C_6H_5CHO]_0$ mol/dm^3	$10^3 \cdot \overline{k_{obsd1}}$ s^{-1}	$10^4 \cdot \overline{k_{obsd2}}$ s^{-1}
6	3.9	5.8
8	4.8	6.6
10	5.6	7.1
12.1	6.3	7.4
13.3	6.7	7.7

The values of the first-order rate constants, for both processes increased with increasing benzaldehyde concentration according to:

$$k_{obsdi} = \frac{a_i \cdot [C_6H_5CHO]_0}{b_i + c_i \cdot [C_6H_5CHO]_0} \quad i = 1;2 \qquad (10)$$

with a trend to level off. A similar behaviour has been found in the case of glycolic acid oxidation. These findings indicate that the reaction order lies between zero and unity and that intermediate complex formation occurs [25].

Equation (10) may be transposed into the linear form:

$$\frac{1}{k_{obsdi}} = \frac{c_i}{a_i} + \frac{b_i}{a_i} \cdot \frac{1}{[C_6H_5CHO]_0} \qquad i = 1;2 \qquad (11)$$

with: $c_1/a_1 = (59.2 \pm 0.1)$ s $\qquad c_2/a_2 = (918 \pm 62)$ s

$b_1/a_1 = (0.12 \pm 0.01)$ s·mol·dm^{-3} $\qquad b_2/a_2 = (0.48 \pm 0.06)$ s·mol·dm^{-3}

From the intercept/slope ratio of the complex formation (eq.(11)) we obtained the apparent equilibrium constant $K_{app} = (493 \pm 3)$ dm^3/mol. Considering the effect of H^+ and SO_4^{2-} ions upon the reaction constant a value of 296 ± 8 has been calculated. There is a relative good agreement between this value of the apparent equilibrium constant (K_{app} = 493 dm^3/mol at 50^{0}C) and the equilibrium constant calculated from the absorbance spectra (K_{app} = 375 dm^3/mol at 25^{0}C) taking into account that these values were obtained at different values of temperatures,

To determine $[H^+]$ terms in the rate law we simply determined the first-order rate constant by varying the hydrogen ion concentration between 0.1 and 0.6 mol·dm^{-3} at constant concentration of benzaldehyde and sulphate. Table 3 assembles the rate data for four temperatures. Both the rate coefficients were affected by the hydrogen ion, suggesting the involvement of some acid-base equilibria.

As seen, the first stage first-order rate constant depends upon the hydrogen ion concentration by a linear equation:

$$k_{obsd1} = k_{01} + k_H \cdot [H^+] \qquad (12)$$

On the basis of these findings we can conclude that a $[H^+]$ ion dependent and a linear dependent path contribute to the formation of the intermediate benzaldehyde-Ce(IV) complex.

Table 3.

The dependence of first-order rate constants for both stages on $[H^+]$; $[Ce(IV)] = 5 \cdot 10^{-5}$; $[C_6H_5CHO]_0 = 10^{-3}$; $[SO_4^{2-}] = 0.6$ and μ = 1.5 mol/dm^3

	$[H^+]$ mol·dm^{-3}						T
	0.1	0.2	0.3	0.4	0.5	0.6	K
$10^3 \cdot \overline{k_{obsd1}}$ s^{-1}	1.65	1.97	2.33	2.68	3.11	3.41	
$10^5 \cdot \overline{k_{obsd2}}$ s^{-1}	3.72	10.2	13.9	18.6	21.5	25.7	297
$10^3 \cdot \overline{k_{obsd1}}$ s^{-1}	3.15	3.51	4.24	4.39	5.11	5.58	
$10^5 \cdot \overline{k_{obsd2}}$ s^{-1}	12.1	22.6	32.9	42.1	56.7	71.1	307
$10^3 \cdot \overline{k_{obsd1}}$ s^{-1}	3.65	4.15	4.82	5.20	5.72	6.36	
$10^5 \cdot \overline{k_{obsd2}}$ s^{-1}	21.3	40.9	62.9	78.3	99.6	113	312
$10^3 \cdot \overline{k_{obsd1}}$ s^{-1}	4.49	4.87	5.66	6.33	7.00	7.84	
$10^5 \cdot \overline{k_{obsd2}}$ s^{-1}	63.4	105	169	218	284	337	321

On the other hand the second stage first-order rate constant shows only a linear dependence on $[H^+]$, with a zero intercept, suggesting a catalytical process of the electron-transfer stage:

$$k_{obsd2} = k_2 \cdot [H^+] \qquad (13)$$

From the parameters of equation (12) and (13) we calculated the rate constant zero-order and first-order on the hydrogen ion concentration respectively. Data are summarized in table 4, along with the activation parameters calculated from them.

Table 5.

First-order and zero-order rate constants in $[H^+]$, for both stages and the corresponding activation parameters; $[Ce(IV)]=5\cdot10^{-5}$; $[C_6H_5CHO]_0 = 10^{-3}$; $[SO_4^{2-}]=0.6$ and μ = 1.5 mol/dm^3

T K	Complex formation		Complex oxidation
	$10^3\cdot k_0$ s^{-1}	k_H $dm^3\cdot mol^{-1}\cdot s^{-1}$	$10^4\cdot k_2$ $dm^3\cdot mol^{-1}\cdot s^{-1}$
297	1.27	3.59	4.24
307	2.62	4.89	11.6
312	3.12	5.33	18.5
321	3.65	6.80	55.8
E_a $kJ\cdot mol^{-1}$	35.2±5.0	20.9±2.0	84.6±4.0
ΔH^* $kJ\cdot mol^{-1}$	32.4±5.0	18.3±2.0	82.1±4.0
ΔS^* $J\cdot mol^{-1}\cdot K^{-1}$	-190±14	-230± 10	-33.6±3.0

The activation parameters include the thermal and entropical effects of several preequilibria involved in the reaction mechanism.

On the contrary, sulphate ion exhibited an inhibitory effect on the rate, as shown in figure 2. An explanation for this behaviour consists on the expulsion of some sulphate ions from the first coordination sphere of Ce(IV) prior to the linkage of the benzaldehyde. The curves in figure 2 could be described by the equation:

$$k_{obsdi} = \frac{a_i}{b_i + c_i \cdot [SO_4^{2-}]^2} \qquad i = 1;2 \qquad (14)$$

which may be transposed into the linear form:

$$\frac{1}{k_{obsdi}} = \frac{b_i}{a_i} + \frac{c_i}{a_i} \cdot [SO_4^{2-}]^2 \qquad i = 1;2 \qquad (15)$$

with the parameters:

c_1/a_1 = (113 ± 10) $dm^3\cdot mol^{-1}\, s^{-1}$ $\quad$ c_2/a_2 = (2550 ± 200) $dm^3\cdot mol^{-1}\, s^{-1}$

b_1/a_1 = (88 ± 4) s $\quad$ b_2/a_2 = (9.7 ± 1.3) s

found by using Slide Write 2.0 Plus computer program.

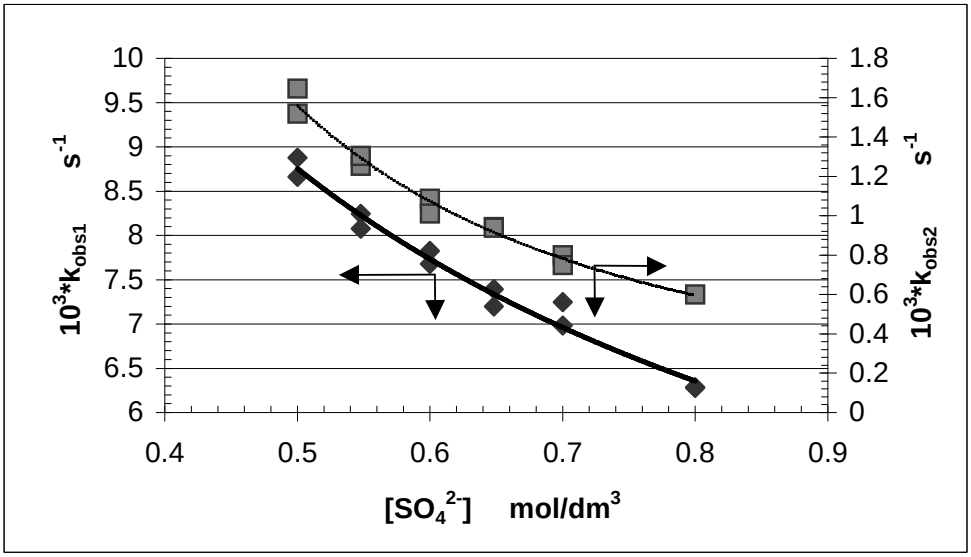

Figure 2. The influence of sulphate ion on the rate constants of complex formation, k_{obsd1}, and complex oxidation, k_{obsd2}; $[Ce(IV)]=5\cdot10^{-5}$; $[C_6H_5CHO]_0 = 10^{-3}$; $[H^+]=0,2$; μ=1,5 mol/dm^3; t = 48^{0}C.

An increase of the ionic strength in the range of 0.73 to 1.76 mol/dm^3 at 48^{0}C, caused an increase of first order rate constants for both processes(table 4). The effect of ionic strength should be due to both primary and secondary salt effects. We found a linear dependence of same type for complex formation and for complex oxidation:

$$\ln k_{obsdi} = a_i + \frac{b_i \cdot \sqrt{\mu}}{1 + c_i \cdot \sqrt{\mu}} - d_i \cdot \mu \quad I = 1;2 \qquad (16)$$

Table 4.

The dependence of rate constants of complex formation and complex oxidation on the ionic strength; $[CE(IV)]=5\cdot10^{-5}$; $[C_6H_5CHO]_0 = 10^{-3}$; $[SO_4^{2-}]=0.6$ and $[H^+]$ = 0.2 mol/dm^3; t = 48^{0}C

μ mol/dm^3	$10^3 \cdot \overline{k_{obsd1}}$ s^{-1}	$10^4 \cdot \overline{k_{obsd2}}$ s^{-1}
0.73	3.99	1.64
0.97	4.71	3.13
1.50	7.75	10.5
1.63	8.66	18.7
1.76	10.0	22.6

Considering the influence of the above mentioned factors like: cerium sulphate, benzaldehyde, hydrogen ion and sulphate ion concentration upon the reaction rate, we found the following experimental rate laws:

- for the process of complex formation:

$$r_1 = \frac{(\alpha_1 + \beta_1 \cdot [H^+]) \cdot [C_6H_5CHO]_0}{\gamma_1 \cdot [SO_4^{2-}]^2 + \delta_1 \cdot [C_6H_5CHO]_0} \cdot [Ce(IV)]_t \qquad (17)$$

- for the process of complex oxidation:

$$r_2 = \frac{\beta_2 \cdot [H^+] \cdot [C_6H_5CHO]_0}{\gamma_2 \cdot [SO_4^{2-}]^2 + \delta_2 \cdot [C_6H_5CHO]_0} \cdot [Ce(IV)]_t \qquad (18)$$

Mechanism

A reaction mechanism, considering the factors that exert an influence upon the reaction rates of the two processes as well as the negative values of their activation entropies, has been suggested.

As it was mentioned before cerium (IV) forms several sulphatocomplexes in sulphuric acid medium: $Ce(SO)_4^{2+}$, $Ce(SO_4)_2$, $Ce(SO_4)_3^{2-}$, $HCe(SO_4)_3^-$ etc. [23-24]. The species $Ce(SO_4)_3^{2-}$ prevails in the range of $[H^+]$ and $[SO_4^{2-}]$ in which we performed our measurements. But the inhibitory effect of sulphate ion indicates that the kinetic active species must be a ceric sulphatocomplex coordinated with less sulphate ions, like $CeSO_4^{2+}$. For its formation we considered the equilibrium:

$$Ce(SO_4)_3^{2-} + H^+ \rightleftarrows CeSO_4^{2+} + HSO_4^- + SO_4^{2-} \qquad K \quad (19)$$

The kinetic active species will react with the benzaldehyde in its hydrated form [26-30]:

$$C_6H_5CHO + H_2O \rightleftarrows C_6H_5CH(OH)_2 \qquad K_h \quad (20)$$

to yield the complex:

$$CeSO_4^{2+} + C_6H_5CH(OH)_2 \rightleftarrows CeSO_4 \cdot OCH(OH)C_6H_5 + H^+ \qquad K_f = k_1/k_{-1} \quad (21)$$

The complex undergoes an internal electron transfer:

$$CeSO_4 \cdot OCH(OH)C_6H_5 \longrightarrow C_6H_5CH(OH)O\bullet + Ce(III) \qquad k_2 \qquad (22)$$

The radical formed in this stage will be further oxidized by Ce(IV) to benzoic acid:

$$CeSO_4 \cdot OCH(OH)C_6H_5 \longrightarrow C_6H_5CH(OH)O\bullet + Ce(III) \qquad k_2 \qquad (23)$$

Besides these steps we considered also the dissociation of HSO_4^-:

$$HSO_4^- \rightleftarrows SO_4^{2-} + H^+ \qquad K_a \qquad (24)$$

The concentration of $CeSO_4^{2+}$ from (19) is:

$$[CeSO_4^{2+}] = \frac{K \cdot [Ce(SO_4)_3^{2-}] \cdot [H^+]^2}{K_a \cdot [SO_4^{2-}]_t^2} \qquad (25)$$

where the total sulphate concentration is:

$$[SO_4^{2-}]_t = [SO_4^{2-}] + [HSO_4^{-}] = [SO_4^{2-}] \cdot \left\{1 + \frac{[H^+]}{K_a}\right\} \quad (26)$$

Considering $K_a << [H^+]$, the sulphate concentration may be approximated by:

$$[SO_4^{2-}] \approx \frac{[SO_4^{2-}]_t \cdot K_a}{[H^+]} \quad (27)$$

If only the contributions of $Ce(SO_4)_3^{2-}$ and the complex are considered, the mass balance for Ce(IV) is given by:

$$[Ce(IV)]_t = [Ce(SO_4)_3^{2-}] + [CeSO_4 \cdot OCH(OH)C_6H_5] \quad (28)$$

Employing the expression of complex concentration from its formation equilibrium (eq. 21) into the mass balance for Ce(IV), the concentration of the kinetic active species may be expressed as a function of total cerium sulphate concentration, $[Ce(IV)]_t$:

$$[CeSO_4^{2+}] = \frac{K \cdot [H^+]^2 \cdot [Ce(IV)]_t}{K_a \cdot [SO_4^{2-}]_t^2 + K_f \cdot K \cdot K_h [H^+][C_6H_5CHO]_0} \quad (29)$$

The rate law deduced for the formation of the Ce(IV)-benzaldehyde complex is:

$$r_1 = k_1 \cdot K_h [CeSO_4^{2+}] \cdot [C_6H_5CHO] - k_{-1} \cdot [CeSO_4 \cdot OCH(OH)C_6H_5] \cdot [H^+] \quad (30)$$

or:

$$r_1 = \left(k_1 \cdot [H^+]^2 - k_{-1} \cdot K_f \cdot [H^+]\right) \frac{K_h \cdot K \cdot [C_6H_5CHO]_0 \cdot [Ce(IV)]_t}{K_a \cdot [SO_4^{2-}]_t^2 + K_f \cdot K \cdot K_h [H^+][C_6H_5CHO]_0} \quad (31)$$

The rate law found for the oxidation process is:

$$r_2 = \frac{k_2 \cdot K_f \cdot K_h \cdot [CeSO_4^{2+}] \cdot [C_6H_5CHO]_0}{[H^+]} \quad (32)$$

or:

$$r_2 = \frac{k_2 \cdot K_f \cdot K \cdot K_h \cdot [CeSO_4^{2+}] \cdot [H^+] \cdot [C_6H_5CHO]_0}{K_a \cdot [SO_4^{2-}]_t^2 + K_f \cdot K \cdot K_h [H^+][C_6H_5CHO]_0} \cdot [Ce(IV)]_t \quad (33)$$

Both rate laws deduced from the suggested mechanism resemble to the experimental rate laws we found for the formation of the intermediate complex and its futher oxidation (eq. 17 and 18) and justifies the inhibition by sulphate. It gives support for this reaction scheme. Research are in progress in our laboratory and new data will illuminate these oxidations with cerium(IV).

REFERENCES

1. G. Gopal Rao and B. Madhava Rao, *Anal. Chim. Acta*, ***1972***, *59(3)*, 461-465.
2. W.S. Trahanovsky and L.B. Young, *J. Org. Chem*., ***1966***, *31(6)*, 2033-2035.
3. L. Syper, *Tetrahedron Letters*, ***1966***, *37*, 4493-4498.
4. E. Baciocchi, C. Rol and G.V. Sebastiani, *J. Chem. Research(Synopsis)*, ***1983***, *9*, 232-233.
5. M. Ignaczak, J. Dziegiec and M. Markiewicz, *Pol. J. Chem*., ***1980***, *54*, 1121-1128.
6. M. Ardon, *J.Chem. Soc*., ***1957***, 1811-1816.
7. B. Sethuram and S.S. Muhammad, *Acta Chim. Acad. Sci. Hung*., ***1965***, *46*, 115-124.
8. B. Sethuram and S.S. Muhammad, *Acta Chim. Acad. Sci. Hung*., ***1965***, *46*, 125-136.
9. W.S. Trahanovsky, L.B. Young and G.L. Brown, *J. Org. Chem*., ***1967***, *32*, 3865-3868.
10. M.P. Doyle, *J. Chem. Educ.*, ***1974***, *51*, 131-132.
11. D. Paquette and M. Zador, *Can. J. Chem*., ***1968***, *46*, 3507-3510.
12. H. Kwart and T.J. George, *J. Org. Chem*., ***1979***, *44*, 162-165.
13. M. Melicherik and L. Treindl, *Chem. Zvesti*, ***1981***, *35*, 153-163.
14. J. Shorter, *J.Chem. Soc*., ***1950***, 3425-3429.
15. P. Singh Sankhla and R. Narain Mehrotra, *J. Inorg. Nucl. Chem*., ***1972***, *34*, 1050-1052.
16. K.B. Wiberg and P.C. Ford, *J. Amer. Chem. Soc*., ***1969***, *91*, 124-132.
17. S.B. Hanna and S.A. Saruc, *J. Org. Chem*., ***1977***, *42*, 2063-2068.
18. V.K. Grover and Y.K. Gupta, *J. Inorg. Nucl. Chem*., ***1969***, *31*, 1403-1416.
19. M. Ignaczak and M. Deka, *Pol. J. Chem*., ***1980***, *54*, 259-266.
20. K. Kramer, P.M. Robertson and N. Ibl, *J. Appl. Electrochem*., ***1980***, *10*, 29-36.
21. R. Ramaswamy, M.S. Venkatachalapathy and H.V.K. Udupa, *Bull. Chem. Soc. Jpn*., ***1962***, *35*, 214-218.
22. C. Mureşanu, I. Baldea, *Analele Univ. Craiova, Chim.*, ***1996***, *23*, 107-115.
23. T.J. Hardwick and E. Robertson, *Can. J. Chem*., ***1951***, *29*, 828-833.
24. T.N. Bondareva, V.F. Barkovskii and T.V. Velikanova, *Zh. Neorgan. Khim*., ***1965***, *10(1)*, 127-131.
25. G. Calvaruso, F.P. Cavasino, C. Sbriziolo and R. Triolo, *Int. J. Chem. Kinetics*, ***1983***, *15(5)*, 418-32.

26. A.C. Chatterji and S.K. Mukherjee, *Z. Physik. Chem.*, ***1965***, *159*, 228-232.
27. A.C. Chatterji and S.K. Mukherjee, *J.Amer. Chem.Soc.*, ***1958***, *80*, 3600-3605.
28. L.E.T. Graham and F.H. Westheimer, *J.Amer. Chem.Soc.*, ***1958***, *80*, 3030-39.
29. K.B. Wiberg and T. Mill, *J.Amer. Chem.Soc.*, ***1949***, *71*, 25-32.
30. M. Avram, *Chimie Organică*, *vol. 2*, 161, Ed. Zecasin, Bucureşti, ***1995***.

STUDIA UNIVERSITATIS BABEŞ-BOLYAI, CHEMIA, XLIII, 1-2, 1998

MASS SPECTROMETRY OF SOME NEW 2-HYDROXYMETHYL-5-PHENYL-FURANS OBTAINED THROUGH CELL CATALYSIS

FL.D. IRIMIE*, CS.PAIZS*, R. SILAGHI-DUMITRESCU*, G. DAMIAN, CORNELIA MAJDIK, MONICA TOŞA**

ABSTRACT. Eight 2-hydroxymethyl-5-phenyl-furans were obteined from the corresponding aldehydes through reaction with *Saccharomyces cerevisiae*. The fragmentation scheme showed the M^+ - 17 peaks for every system studied and characteristic features for the heterocyclic moiety of the alcohols. Some details are discussed within the fragmentation scheme for each compounds.

INTRODUCTION

As a part of our researches in the furan series we have prepared eight new from the corresponding aldehydes using Sacharomices cerevisiae as reducting agent [6].

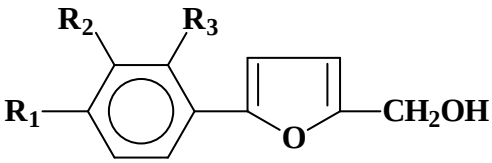

a: R_1 = F; R_2 = H; R_3 = H
b: R_1 = Cl; R_2 = H; R_3 = H
c: R_1 = Br; R_2 = H; R_3 = H
d: R_1 = I; R_2 = H; R_3 = H
e: R_1 = H; R_2 = Br; R_3 = H
f: R_1 = H; R_2 = H; R_3 = Cl
g: R_1 = H; R_2 = H; R_3 = Br
h: R_1 = H; R_2 = H; R_3 = I

Scheme 1

This paper deals with the mass spectra of these compounds. We considered it of interest to find out to what extent the characteristic fragmentation modes of furans[1-5], are also presents in the case of a-h and what is the influence of the hydroximethyl group in position 2 on the furan ring upon the fragmentation process.
Mass spectral data m/e (I%):

* *Department of Chemistry and Chemical Engineering.*
** *Department of Physics, "Babeş-Bolyai" University, 3400 Cluj-Napoca, Romania.*

a: 51(10,6), 57(8,6), 75(15,5), 83(9,6), 91(10,5), 95(19,5), 107(10,8), 109(10,8), 118(11,3),120(6,4), 123(34,8), 133(48,3), 134(11,2), 135(10,1), 145(12,7), 146(23,7), 147(19,6), 163(9,1), 164(8,7), 175(99), 176(13), 187(3), 188(7,3), 192(100), 191(13)
b: 29(13,4), 39(12), 46(21,3), 63(31,4), 75(41,3), 87(26,3), 91(11), 111(33), 112(6), 113(16,7), 114(19,8), 115(41,6), 116(22,2), 117(11,6), 127(33,8), 128(41,6), 139(39,7), 140(9,1), 141(9,3), 142(3), 149(43,6), 150(6,3), 151(22,8), 161(2), 162(8,3), 163(7,1), 164(5), 165(4), 178(6), 179(8), 180(10,1), 181(6,3), 182(4,1), 191(74,5), 192(13,6), 193(26,3), 194(5,1), 205(10,1), 206(23,1), 208(100), 209(25,3), 210(33,5), 211(6,1)
c: 29(10), 50(11), 63(18,2), 78(13), 88(16), 91(13), 109(33), 110(43,6), 111(43,6), 112(43,6),113(53), 114(41,6), 115(21,6), 127(30), 128(57,2), 129(59,6), 144(27), 145(13),155(14),157(14), 183(32),185(32),193(12),195(12),224(13), 226(13),235(62), 236(20), 236(62), 237(20), 250(8), 251(13,6), 252(100), 253(31,3), 254(100), 255(10)
d: 63(3), 74(2), 88(4), 91(11,2), 115(13), 135(6,3), 149(2), 171(2,6), 203(6,3), 241(21), 270(6), 283(81), 298(60), 299(30), 300(100), 301(10)
e: 29(10), 50(11), 63(18,2), 78(13), 88(16), 91(13), 109(33), 110(43,6), 111(43,6), 112(43,6),113(53), 114(41,6), 115(21,6), 127(30), 128(57,2), 129(59,6), 144(27), 145(13), 155(14),157(14), 183(32), 185(32), 193(12), 195(12), 224(13), 226(13), 235(62),236(20), 236(62),237(20), 250(8), 251(13,6), 252(100), 253(31,3), 254(100), 255(10)
f: 29(13,4), 39(12), 46(21,3), 63(31,4), 75(41,3), 87(26,3), 91(11), 111(33), 112(6), 113(16,7), 114(19,8), 115(41,6), 116(22,2), 117(11,6), 127(33,8), 128(41,6), 139(39,7), 140(9,1), 141(9,3), 142(3), 149(43,6), 150(6,3), 151(22,8), 161(2), 162(8,3), 163(7,1), 164(5), 165(4), 178(6), 179(8), 180(10,1), 181(6,3), 182(4,1), 191(74,5), 192(13,6), 193(26,3), 194(5,1), 205(10,1), 206(23,1), 208(100), 209(25,3), 210(33,5), 211(6,1)
g: 29(10), 50(11), 63(18,2), 78(13), 88(16), 91(13), 109(33), 110(43,6), 111(43,6), 112(43,6),113(53), 114(41,6), 115(21,6), 127(30), 128(57,2), 129(59,6), 144(27), 145(13), 155(14),157(14), 183(32), 185(32), 193(12), 195(12), 224(13), 226(13), 235(62), 236(20), 236(62),237(20), 250(8), 251(13,6), 252(100), 253(31,3), 254(100), 255(10)
h: 63(3), 74(2), 88(4), 91(11,2), 115(13), 135(6,3), 149(2), 171(2,6), 203(6,3), 241(21), 270(6), 283(81), 298(60), 299(30), 300(100), 301(10)

RESULTS AND DISCUSSION

In order to simplify the interpretation of the mass spectra of our compounds we recorded also the spectrum of 5-phenyl-furyl-2-carboxaldehydes substituted with halogenes at the phenylic ring as model.

In case of bioproducts we observed a fragmentation characteristic for benzylic alcohols. The molecular ion is the base peak M - 1, M - 2, M - 3 are observed too. Slow intensity M+1 peak is appeared.

For exemplification we presented the fragmentation mode of chloroderivatives.

The fragments presents in Scheme 3 are also appeared in the mass spectras of the corresponding aldehydes too.

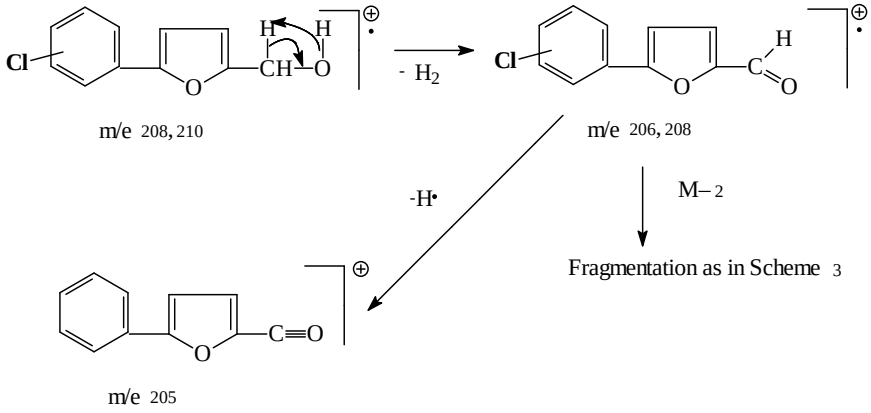

Scheme 2

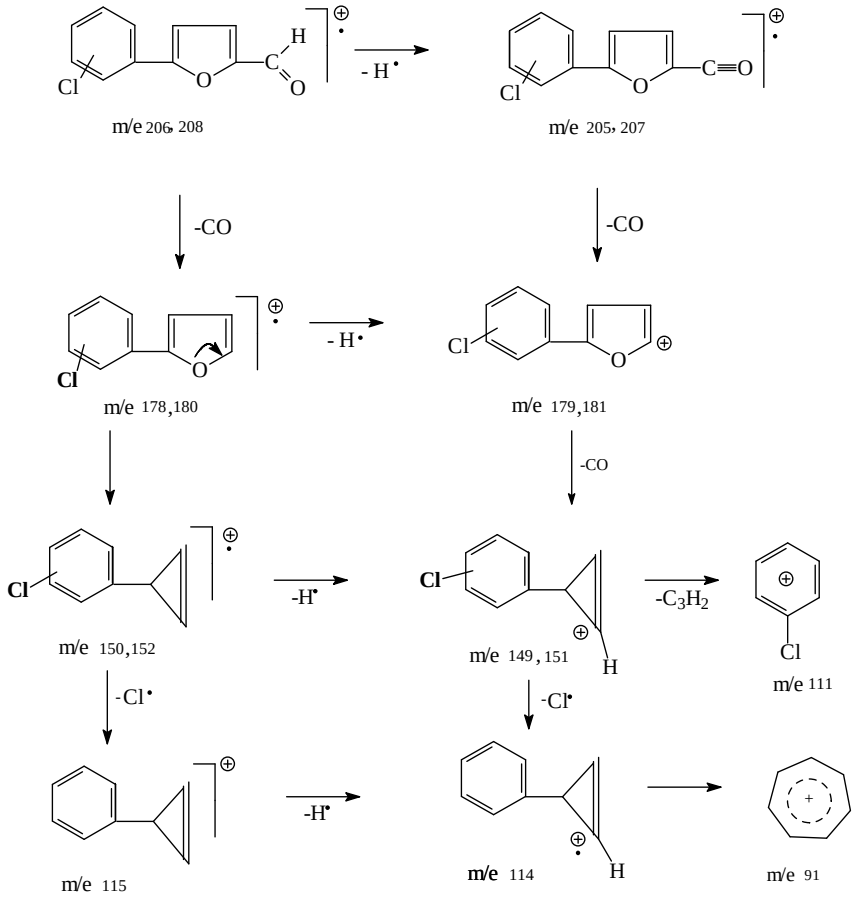

Scheme 3

An other way for the cleavage presented in Scheme 4 is with elimination of an -OH radical. We supposed that the M - 17 sufered a ring rearrangement which cleaves with elimination of -CO and gives a cyclobutadienylic ring as in case of hydroxymethyl-furyl benzothiazoles [7].

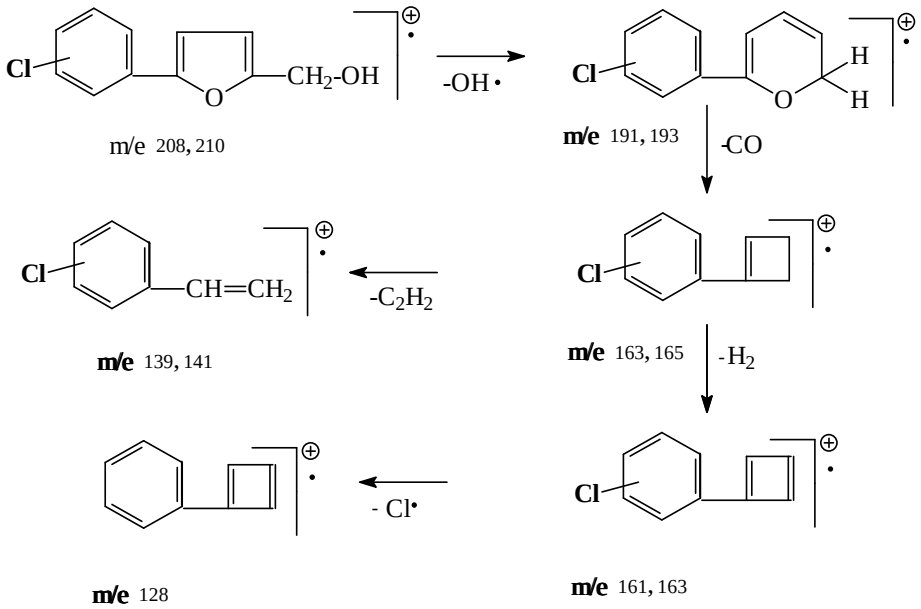

Scheme 4

Each substances presents the same pattern of the fragmentation. In case of c, e, g its observed the presence of two bromine isotope (79,81).

The substance presents two molecular peaks (M= 252, 254) with the same abundance and two characteristic fragments for the benzylic alcohols, M-17 (225, 227). For substances b and f the two chloro isotope (35, 37) are present, two molecular peaks (208, 210) and two characteristic fragments, M-17 (191, 193) are appeared.

Molecular peaks for (a-h) are clear with an relative abundance of 100%.

EXPERIMENTAL

The purity of the substances was checked by TLC on silica gel. The mass spectra were recorded using a Double focusing VARIAN MATT 311 Spectrometer with an electronic impact at 70 eV and 300 mA. The source temperature was 150-200^{0}C.

REFERENCES

1. R.I. Reed, W.K. Reid, *J.Chem.Soc*., 1963, 5933.
2. H. Budzikiewicz, C. Djerassi, D.H. Williams, *Mass Spectrometry of Organic Compounds*, Holden-Day Inc., 1968, 615.
3. R. Grigg, M.W. Sargent, D.H. Williams, J.A. Knight, *Tetrahedron,* 1965, ***21***, 3441.
4. K. Heyns, R. Stute, M. Scharmann, *Tetrahedron*, 1966, ***22***, 2223.
5. C. Mercier, *Bull.Soc.Chim.France*, 1969, 145.
6. F.D. Irimie, Cs. Paizs, R. Silaghi-Dumitrescu, C. Majdik, Fr. Joo, M. Toşa, *Synth.Commun*., 1999, (in press).
7. F.D. Irimie, Cs. Paizs, V. Miclăuş, C. Afloroaei, M. Toşa, G. Damian, *Balkan Phys. Lett*, 1997, ***5***, 227.

STUDIA UNIVERSITATIS BABEŞ-BOLYAI, CHEMIA, XLIII, 1-2, 1998

SYNTHESIS AND RING-RING TAUTOMERISM OF SOME SPIRO-OXAZOLIDINES BASED ON *l-p*-NITROPHENYLSERINOL SKELETON

MIRCEA DĂRĂBANȚU[1], GERARD PLÉ[2], LUIZA GĂINĂ[1], CARMEN MĂIEREAN[1] and ION SILAGHI-DUMITRESCU[1]

ABSTRACT. The synthesis of three spirooxazolidines starting from the title compound is discussed from the regioselectivity and diastereoselectivity point of view and their unexpected isomerization in solution is examined by means of high resolution NMR spectra.

INTRODUCTION

We have recently described the ring-chain tautomerism of some Schiff-Bases of *l*-2-amino-1-(4-nitrophenyl)-propane-1,3-diol, better known by its trivial name issued from pharmaceutical chemistry as "*l-p*-nitrophenylserinol "[1]. Starting from our previously reported results, we have considered of interest to enlarge the study in the field by examining certain spirooxazolidines derived from the title compound. As the Schiff-Bases, this class of compounds exhibited some applicative importance in the period of '50's, in connection with *chloromycetineĂ* synthesis [2]. To the best of our knowledge, any oxazolidine ring-system built form the title aminodiol has been treated so far as a single and stable structure.

Then, our most recent data [3] has revealed that spirooxazolidines possessing free hydroxymethyl-groups (*e.g*. starting from more simple aminopolyalcohols skeleton) can isomerize in certain conditions and these equilibria are suitable to NMR monitoring.

RESULTS AND DISCUSSION

1. Synthesis

As depicted in ***Scheme 1*** three spirooxazolidines ***2a, b, 3*** have been prepared following the classical method of Bergmann [4] (see ***EXPERIMENTAL***) (hereafter ***p-NPh***- is the abreviation for ***p-nitrophenyl*** group). Surprisingly, even from the beginning of our research, the versatile reactivity of ***1*** has allowed synthesis of ***2a, b*** (yields 40-60%) but starting from racemic ***1*** (in ***Scheme 1*** only the 1*S*,2*S* enantiomer of ***1*** is shown). Anyhow, pure enantiomeric ***2a, b*** have been also isolated by us but as oils, very unstable on storage, in complete contradiction with Bergmann's earlier data [4] (*e.g*. ***2a***, claimed as crystalline solid, m.p.= 107-8^{o}C).

[1] *"Babeş-Bolyai" University Cluj-Napoca, Department of Organic Chemistry, 11 Arany Janos str., RO-3400 Cluj-Napoca*
[2] *Université de Rouen, Faculté des Sciences et des Techniques IRCOF-UPRES A 6014 CNRS 76821 Mont Saint Aignan, Cedex, France*

The same has been valid for the synthesis of the new compound ***2b***. Extention of the procedure to C-5 and C-7 monocyclanones has failed (no reaction occurred,

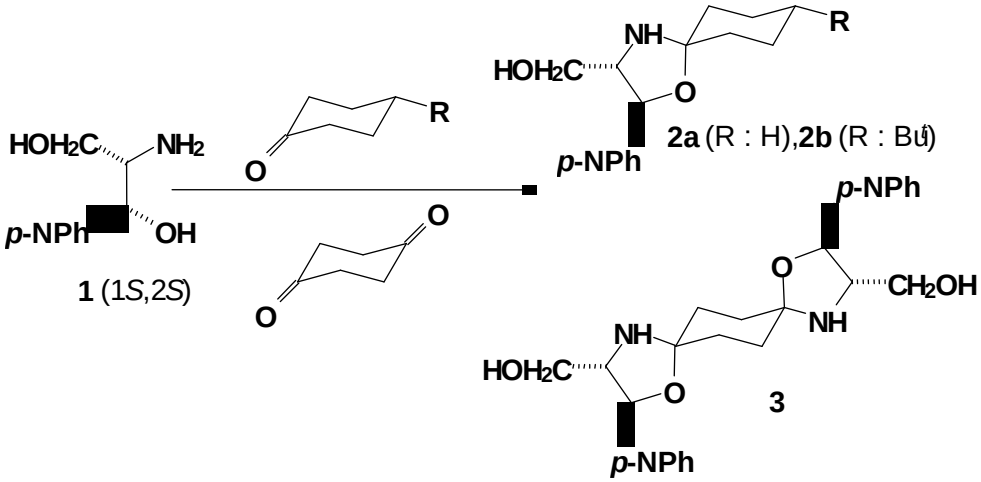

Scheme 1

TLC monitoring). We should believe the negative influence of *I-strain*, in both cases [5] but the reactivity of TRIS (α,α,α-trimethylolaminomethane) and its methyl (or ethyl) analogs have afforded, in identical conditions, promising results [3].

The dispirane ***3***, has raised none of the mentioned problems and has been isolated as pure *trans*-2*S*,3*S*,10*S*,11*S* enantiomer.

All syntheses have occurred with no epimerization of ***1*** and complete diastereoselectivity. In fact, the remarkable configurational stability of the starting aminodiol ***1*** is not surprising but already a well-established and fully argued behaviour [6]. Illustration in ***Scheme 1***, depictes that diastereomers possessing –NH- group in eq. position *vs*. alkoxy one in ax. position but tied together in a five member ring will be hereafter considered. This stereochemistry is supported only by RHF/3-21G* molecular orbital calculations (with full geometry optimization). Thus, A-values in this class range between 0.84 – 1.06kcal/mol. All NMR spectra (solvent DMSO-d_6) have been consistent with the presence of a single diastereomer in any of the syntheses [3].

2. The rin-ring tautomerism

The ^{1}H-NMR spectrum of compound ***2a*** in DMSO-d_6 (***Figure 1***, heterocyclic zone) will be first considered as a typical example.

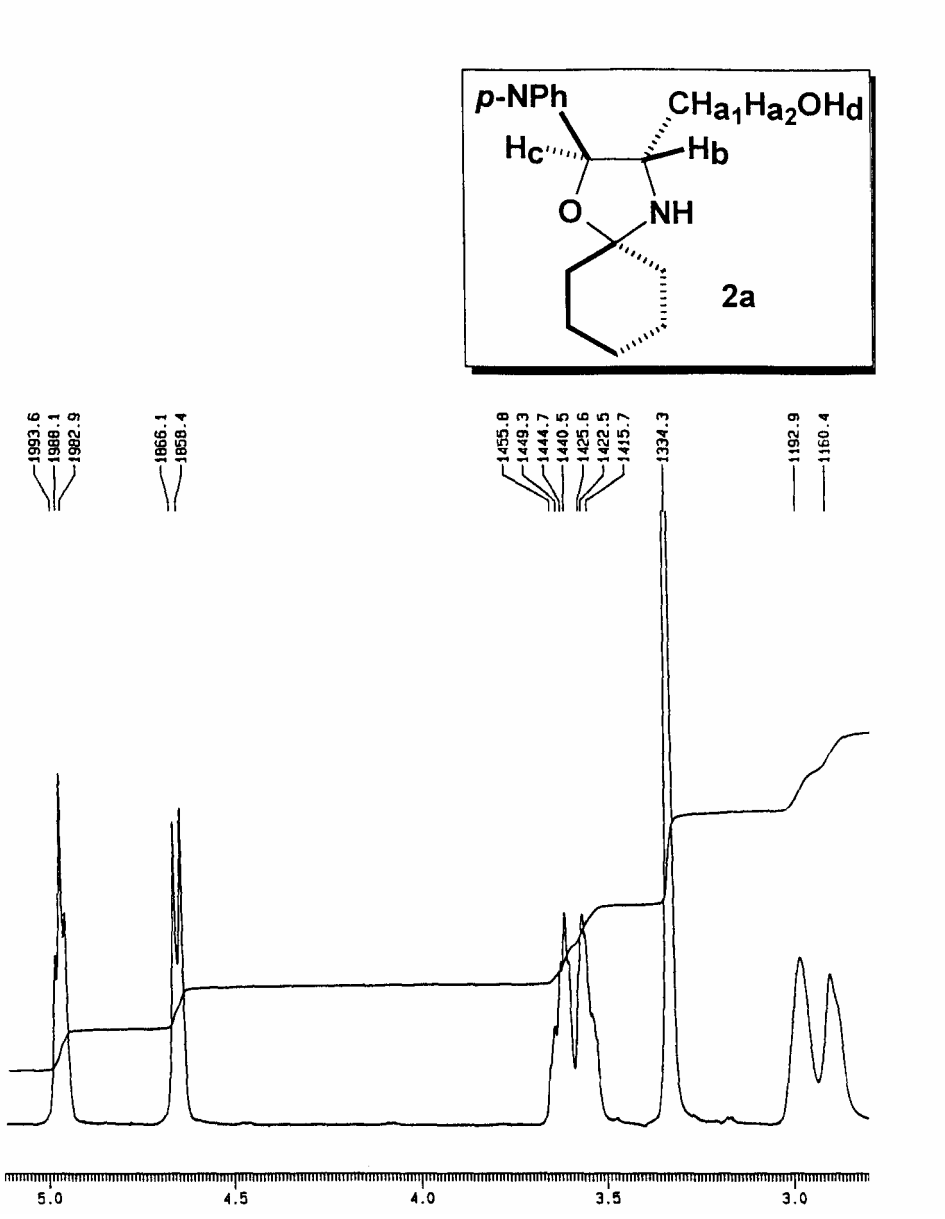

Figure 1. ^{1}H-NMR spectrum of compound **2a**; solvent DMSO-d_6

Regioselectivity of the ring-closure is easily to observe since primary hydroxylic proton -OH_d is clearly exhibited as a triplet (in fact a doublet of doublets partially overlapped) at 4.97ppm. We note here the same regioselectivity, previously reported by Bergmann and Resnick [4], based only on IR spectra (characteristic bands for 1,3-oxazolidine ring in the region 1080 – 1200 cm^{-1} and primary hydroxyl group in the region 1030 – 1060 cm^{-1}). Then, IR spectra were claimed as measured in suspension of paraffin to suggest the role of crystalline interactions (not discussed, *op.cit.*). Proton H_c (4.66ppm) is *trans*-splitted by H_b (J = 7.7Hz); upfield, one can located the diastereotopic methylene –C$H_{a1}H_{a2}$OH_d as a doublet of quartets (3.62 and 3.56ppm resp., J_{gem} = 9.3Hz). It had been normally expected that proton H_b is the most splitted one but, unfortunately, just an unresolvable broad singlet is revealed at 2.98ppm. COSY-experiment (not depicted) has indicated with any doubt its coupling with H_c. Finally, the aminic proton is found at 2.90ppm. ^{13}C-NMR has been fully consistent with a single proposed strucutre. The same spectrum performed in $CDCl_3$ (compound ***2a***, ***Figure 2***, heterocyclic zone) put in evidence both possible regioisomers: ***2a(I)*** (major) and ***2a(II)*** (minor). Before discussing this spectrum, some essential notes should be outlined:

a) the poor solubility of all compounds in $CDCl_3$ that made difficult to perform relevant QC-NMR spectra for both ***2a(I)*** and ***2a(II)*** regioisomers; similar situation was encountered in C_6D_6.

b) the ratio between ***2a(I)*** and ***2a(II)*** has remained unchanged if spectra have been repeated after several days.

c) one may suppose that ***2a(I)*** and ***2a(II)*** are not regioisomers but the two terms of a slow conformational equilibrium of ***2a***; this hypothesis was ruled out because spirane ***2b*** (possessing the Bu^t as an anancomerizing group at C-8) has exhibited an identical behaviour as ***2a*** (see farther).

d) best discrimination and assignment between regioisomers ***2a(I)*** and ***2a(II)*** have been basically made on the magnitude of geminal coupling patterns J H_{a1a2} (typical values about 11Hz in type ***I*** and about 8.5Hz in type ***II***) as we have already reported [7] and COSY experiment.

The spectrum in ***Figure 2*** indicates the following relevant peaks:

- H_c in ***2a(I)*** (4.76ppm, doublet, J_{trans} = 8.0Hz) and H_c in ***2a(II)*** (4.45ppm, doublet, J = 7.4Hz). The ratio between ***2a(I)***: ***2a(II)*** is about 3.4: 1.
- the diastereotopic methylene $H_{a1}H_{a2}$ in ***2a(I)*** (each proton as doublet of doublets, at 3.84 and 3.65ppm, resp., J_{gem} = 11.2Hz) and in ***2a(II)*** (each proton asdoublet of doublets, partially overlapped, at 3.76 and 3.70ppm, resp., J_{gem} = 8.8Hz). It must be observed that in none of the regioisomers have been detected couplings with hydroxylic protons H_e or H_d.
- proton H_b in ***2a(II)*** (3.42ppm as an overlapped multiplet) and H_b in ***2a(I)*** (3.16ppm, as an overlapped but resolvable ddd).

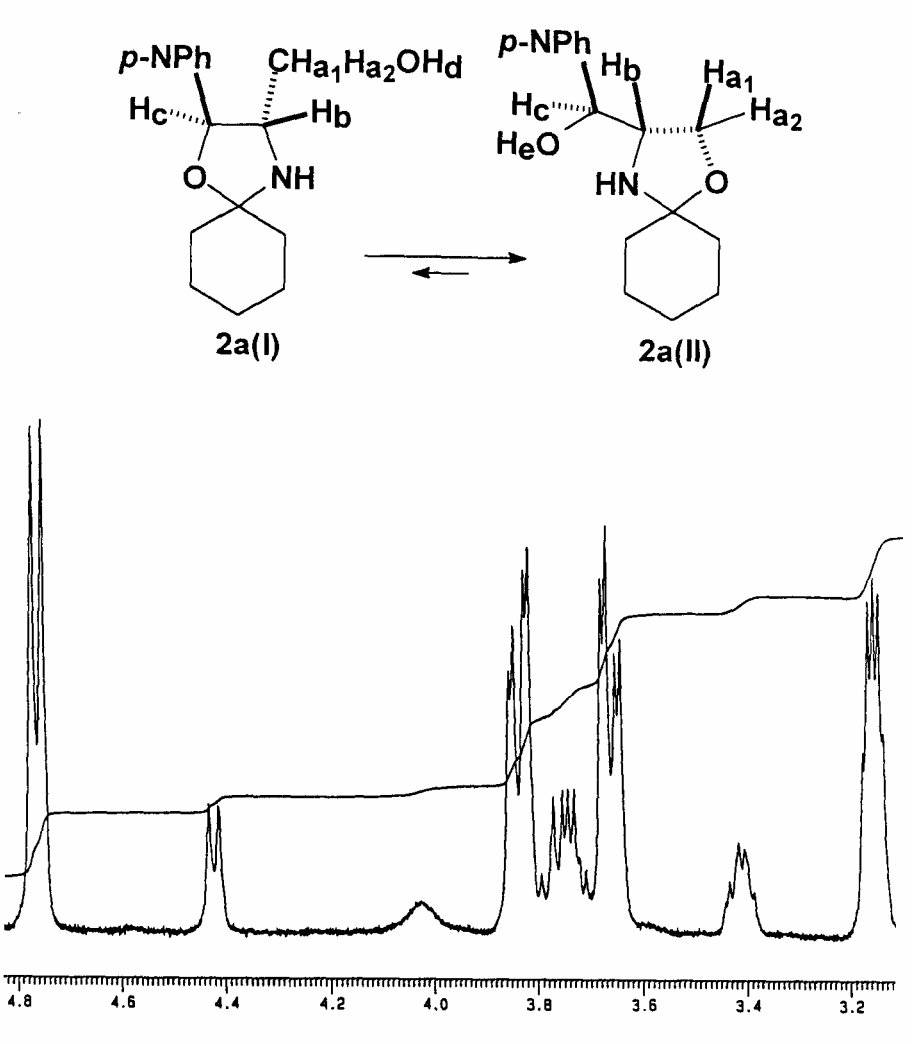

Figure 2. ^{1}H-NMR spectrum of the mixture of regioisomers **2a(I)** and **2a(II)** in $CDCl_3$

The spectrum discussed above has not allowed the precise location of aminic or hydroxylic protons. This fact has been connected with their intramolecular mobility as soon as the solvent used was unable to developpe hydrogen bonds (or rapid change) with them.

Therefore, this isomerization, favoured by a generic name as *intramolecular interactions*, involving mobile protons, we will call hereafter as case of ***ring-ring tautomerism***. Since the phenomenon has been observed only if (non)polar solvents (or unable to interact with hydroxylic or aminic protons) have been used,

the role of these protons to promote this tautomerism should be crucial. Moreover, one can imagine nonionic transition state (or intermediates) that make possible this evolution (***Scheme 2***). Equilibria of the monospiranes ***2a, b*** let to identify only two tautomers and it is pertinent to assume that they are diastereoselctive, regarding the cyclohexane fragment (-NH- group, in both tautomers is still placed in eq. position).

In ***Table 1*** the quantitative results, as ratios between the tautomers, are summarized, depending on the NMR-solvent used.

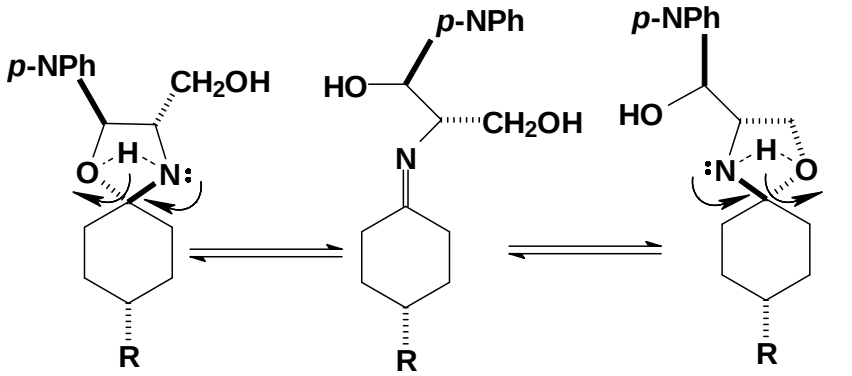

2a(I) (R : H) **2a(II)** (R : H)
2b(I) (R : Bu*t*) **2b(II)** (R : Bu*t*)

Scheme 2

Table 1

Regioselective ring closure for the monospirane ***2a, b***

Solvent	***Regioselective ratio I*** *vs.* ***II****	
	2a	***2b***
DMSO-d_6	Single **2a(I)** found	Single **2b(I)** found
C_6D_6	3.7 : 1	4.0 : 1
$CDCl_3$	3.4 : 1	4.0 : 1
Acetone-d_6	5.6 : 1	6.6 : 1

*As issued form ^{1}H-NMR spectra performed with successive increased sensitivity (300 and 400MHz, see ***EXPERIMENTAL***); reference protons chosen for calculations: H_c (see ***Figure 2***).

Data listed in ***Table 1*** illustrate, on the other hand, the similar behaviour of spirooxazolidines ***2a, b*** with their analogs C-2-substituted(hetero)aryl: the most acidic hydroxyl–group (secondary) is more involved in the ring closure although it is the most sterically hindered. We have already reported that about $\Delta\delta$=1ppm is the difference between ^{1}H-NMR chemical shifts protons of secondary and primary hydroxyl-group in a large series of acyclic derivatives of ***1***, (itself included) [1].

It had been expected that dispirane ***3*** should support these considerations. In fact, NMR-spectra put in evidence more than expected constitutional changes, depending on the solvent (***Scheme 3***). The ^{1}H-NMR spectrum performed in DMSO-d_6

has exhibited a single structure and chemical shifts are not different than the same δ-values encountered for the monospirane ***2a*** (***Figure 1***). Therefore, as a trivial case, this spectrum will be not analyzed.

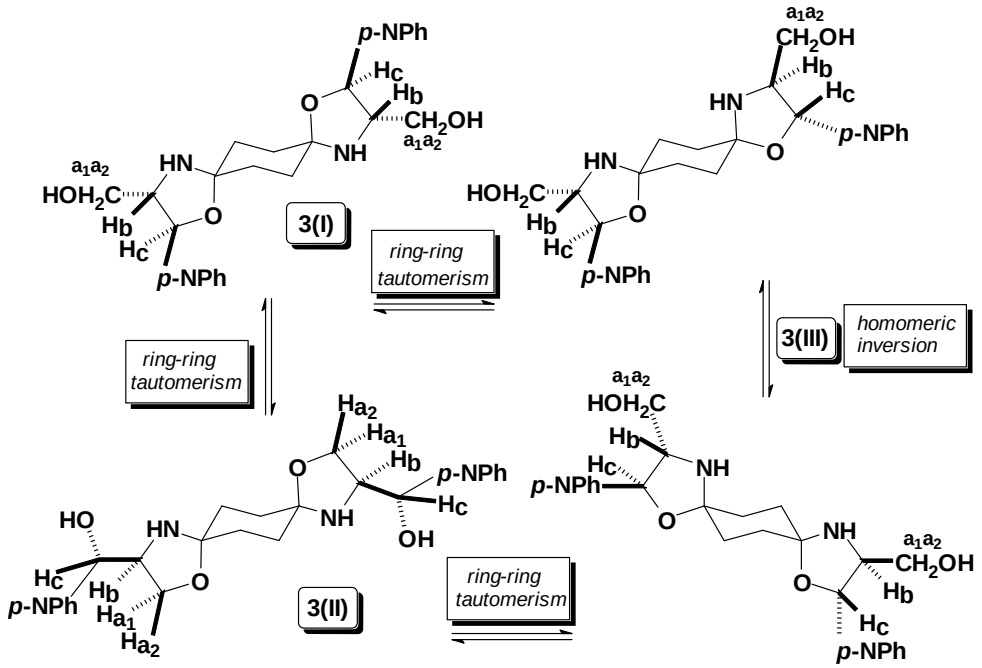

Scheme 3

The spectrum performed in $CDCl_3$ (***Figure 3a***) shows, in the region of benzylic protons, three types of environment of the reference benzylic proton H_c:

- the doublet at 4.93ppm is a H_c type assigned to ***3(III)*** environment as the doublet at 4.83 (the last one is partially overlapped).

- the most intense doublet (4.86ppm) is assigned to H_c in ***3(I)***

- the most shielded doublet at 4.51ppm should be assigned to another environment of H_c, tautomer ***3(II)*** (see similar value for H_c in ***Figure 2***, tautomer ***2a(II)***. The COSY experiment (not depicted) is consistent with this assumption since it is twice *gauche* coupled with H_{a1a2} in the region 3.80-3.90ppm.

As issued from ***Scheme 3***, it had been also expected that ***3(III)*** should be a flipping structure but all our evidence prove that if really does occur, the homomeric inversion is slow enough for both H_c environments be observed. This region also allows to estimate the ratio betwwen ***3(I)***: ***3(III)***: ***3(II)*** as 2.75: 1: 1.25. Then, in ^{13}C-NMR spectrum (not depicted) there are four signals for C-5, C-8 carbons, consistent with three structures.

In ***Figure 3b*** one can discriminate 3 AMX systems: three types of methylenic protons H_{a1a2} splitted by H_b as three doublets of quartets: ***3 (I)*** (***o***), ***3 (III)*** (×) and ***3 (II)*** (*******,); typical J_{gem} values: 11.2-11.3Hz in free –CH_{a1a2}-OH moiety and 8.1Hz in oxazolidinic –CH_{a1a2}-).

The same spectrum performed in acetone-d_6 (***Figure 4***, detail in the heterocyclic zone) has depicted another unpredictable behaviour.

Thus, if acetone-d_6 is seen somehow similar to DMSO-d_6 a single tautomer is expected to detect and regioselectivity of the ring closure should involved the secondary hydroxyl-group. In ***Figure 4*** one can discriminate between two type of mobile protons as broad singlets (4.18 and 2.91ppm, resp). A rapid change with the solvent may be considered.

Then, from downfield to upfield, the following signals are revealed:

- benzylic protons H_c as two doublets (4.87 and 4.88ppm, resp., typical J_{trans} value 8.0Hz); their intensity is the same and, based on the magnitude *J*-value, the *trans*-coupling with H_b demostrates that no epimerization has occurred at the benzylic carbon (if did, H_b-H_c are *cis*-coupled). The very small difference between δ-values suggests minor difference between environments so the single ***3(III)***-epimer is a valid structure in these conditions.

- the hydroxymethylenes protons –CH_{a1Ha2}-OH as two partially overlapped doublets of doublets are located at 3.84, 3.83 and 3.79ppm, resp.(J_{gem} = 11.6Hz).

- protons H_b are identified as a single multiplet at 3.18ppm but carefully analysis of this signal indicates two δ-values 3.19 and 3.17ppm (two splittings 8.0Hz and 3.8Hz; the third, about 3.8Hz is not exhibited; that is, each H_b as doublet of doublets instead of quartets of doublets).

To conclude, in acetone-d_6, tautomer ***3(III)*** is the unique structure; if flipping, the conformational equilibrium is very slow and interactions with the solvent are the reason of this behaviour.

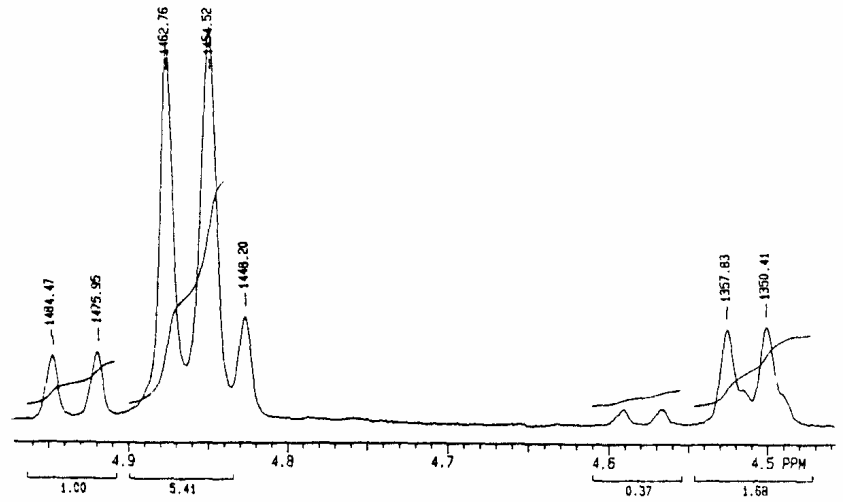

Figure 3a. 1H-NMR spectrum of tautomers **3(I)**,**3(II)** and **3(III)** (detail) from downfield to upfield : H_C **3(III)** 4.93ppm, H_C **3(I)** 4.86ppm, H_C **3(III)** 4.83ppm, H_C **3(II)** 4.51ppm

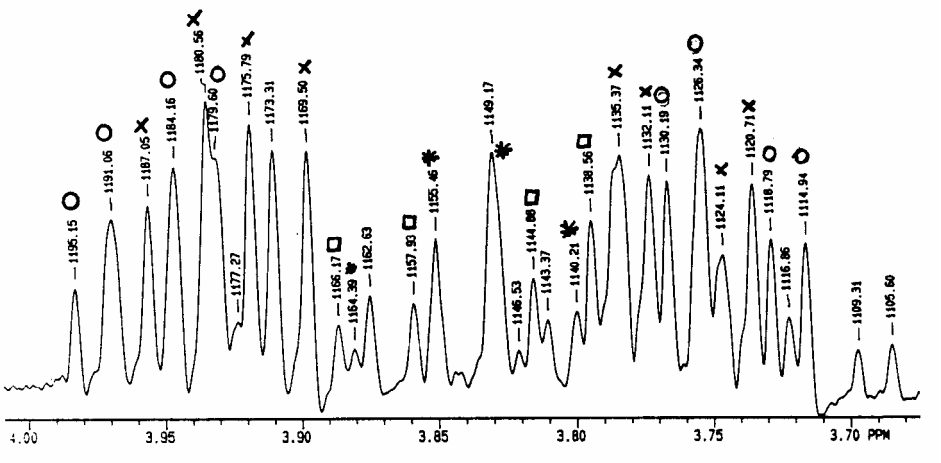

Figure 3b . 1H-NMR spectrum of tautomers **3(I)**, **3(II)** and **3(III)** (detail) from downfield to upfield : H a1 **3(I+III)**, Ha1Ha2 **3(II)**, Ha2 **3(I+III)**

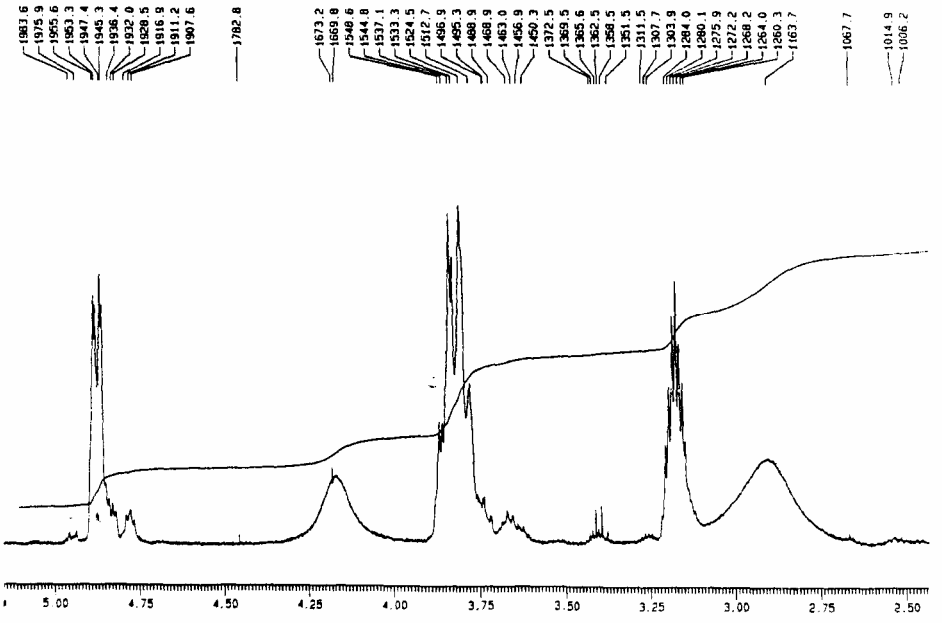

Figure 4 . 1H-NMR spectrum of compound **3** as tautomer **3(III)**; solvent acetone-d6

CONCLUSIONS

Reaction of *l*-p-nitrophenylserinol with simple C-6 mono- and dicyclanones has afforded spirooxazolidines; they easily isomerize as soon as intramolecular interactions due to mobility of –O*H* and –N*H*- protons are effective (intramolecular hydrogen bonds included). Regioselectivity of ring closure depends on the solvent but the reactivity of the most acidic hydroxyl-group (secondary) is always dominant against steric requirements.

EXPERIMENTAL

Melting points (Boetius) are not corrected.

All reactives were purchased from Aldrich.

^{1}H-NMR and ^{13}C-NMR were performed on VARIAN-Gemini 300 and Brucker AM 400 spectrometers. QC-NMR spectra were performed on VARIAN-Gemini 300 operating at 75MHz for ^{13}C by using 80-100mg/sample in standard tubes and a delay time D1=10. No $SiMe_4$ was added; chemical shifts were measured against the solvent peak. Samples were prepared by using commercially available DMSO-d_6 and measured after complete dissolution in standard tubes (about 30mg for ^{1}H- and 60-70mg for ^{13}C-NMR spectra). For spectra recorded in $CDCl_3$ 5-10mg/sample in standard tubes were used. Hyperfine structure of ^{1}H-NMR was obtained on diluted samples only by using RESOLV macro (special attention was paid to neglect negative peaks) on VARIAN-Gemini 300, after 128 transients. Hereafter protons and carbons are labelled as shown in the ***Figures 1-3***.

All reactions were monitored by TLC on MERCK silica gel, by using Benzene: Acetone 3:1 or ligroine : acetone 3 : 1 v/v as eluent (visualisation on I_2 bath).

RHF/3-21G* molecular orbital calculations were performed by using Spartan 5.0 package of programs; Spartan version 5.0, Wavefuntion, Inc., 18401 Von Karman Avenue, Suite 370, Irvine, CA 92612 U.S.A.

Specific rotations $[\alpha]_D^{20}$ were determined on POLAMAT K. Z. JENA instrument.

Typical procedure to prepare spirooxazolidines 2-3

Synthesis: l-p-Nitrophenylserinol 2.12g (10mmol) (for dispirooxazolidine 3 pure enantiomeric 1S,2S staring material is used) was suspended in benzene (50mL) in a Dean-Stark trapp. Monocyclanone was added as 300% molar excess (for ***3***, stoechiometric molar ratio was used). The r.m. was refluxed on a steam-bath with continuous removal of water until TLC monitoring indicated constant ratio between the desired compound and unreacted starting material (the last one detected in small traces only). ***Isolation***: compound ***2***: the r.m. was filtered at r.t. to remove the unreacted starting material, neutralized with anh. Na_2CO_3 and, after evaporation in vacuo, the oily residue was twice crystallized form 2: 1 MeOH: H_2O. For the compound ***3***, the same procedure afforded an oily residue that was crystallized from ligroine, then from min. MeOH, at r.t. For dispirane ***3***, benzene was decanted and the gummy solid was stirred with ether until a fine powder was obtained. After filtering, the solid was dissolved in min. MeOH, then poured in water, to remove the unrected starting material. After filtering and drying at r.t., the crude product was crystallized from THF: Ether.

l-4-Aza-3-hydroxymethyl-2-(4-nitrophenyl)-4-aza-1-oxaspiro[4.5]decane 2a(I) and ***l-4-Aza-3-(4-nitrohydroxybenzyl)-1-oxaspiro[4.5]decane 2a(II)***

Yield 62%. M.p. = 83-5°C (MeOH : H_2O = 2 : 1) yellowish crystalline powder (Found : C, 61.90; H, 7.00; N, 9.53; $C_{15}H_{20}N_2O_4$ requires C, 61.62; H, 6.89; N, 9.58%);

Tautomer 2a(I):

δ_H(400 MHz; DMSO-d_6) 8.21 (2 H, d, *J* 8.6, H-3, -5 arom), 7.61 (2 H, d, *J* 8.6, H-2, -6 arom.), 4.97 (1 H, t, *J* 5.4, -O*H*$_d$), 4.66 (1 H, d, *J* 7.7, H_c), 3.62 (1 H, dd, *J* 9.3 and 6.4, H_{a1}) 3.56 (1 H, dd, *J* 9.3 and 4.2, H_{a2}), 2.98 (1 H, br s, -N*H*-), 2.90 (1 H, unresolved large singlet, H_b according to COSY exp.), 1.69 – 1.29 (10 H, cyclohexyl)

δ_H(400 MHz; C_6D_6) 7.89 (2 H, d, *J* 8.6, H-3, -5 arom), 7.07 (2 H, d, *J* 8.6, H-2, -6 arom.), 4.54 (1 H, d, *J* 8.0, H_c), 3.40 (1 H, dd, *J* 11.1 and 3.9, H_{a1}) 3.19 (1 H, dd, *J* 11.1 and 3.7, H_{a2}), 2.75 (1 H, ddd, *J* 8.0 3.9 and 3.7, H_b), 1.68 – 1.14 (12 H, cyclohexyl, -O*H*, –N*H*-)

δ_H(400 MHz; $CDCl_3$) 8.17 (2 H, d, *J* 8.7, H-3, -5 arom), 7.50 (2 H, d, *J* 8.7, H-2, -6 arom.), 4.76 (1 H, d, *J* 8.0, H_c), 4.02 (1 H, br s, -O*H*), 3.84 (1 H, dd, *J* 11.2 and 3.6, H_{a1}) 3.65 (1 H, dd, *J* 11.2 and 4.1, H_{a2}), 3.16 (1 H, ddd, *J* 8.0, 3.8 and 3.5, H_b), 2.06 (1 H, br s, -N*H*-), 1.81 – 1.44 (10 H, cyclohexyl)

δ_H(400 MHz; CD_3COCD_3) 8.25 (2 H, d, *J* 8.8, H-3, 5 arom.) 7.72 (2 H, d, *J* 8.8, H-2, -6 arom.) 4.84 (1 H, d, *J* 8.2, H_c) 3.84 (1 H, dd, *J* 11.6 and 3.6, H_{a1}) 3.77 (1 H, dd, *J* 11.6 and 2.9, H_{a2}) 2.09 (1 H, m, H_b) 1.83 – 1.49 (12 H, m, cyclohexyl, -O*H*, -N*H*-)

δ_C(100 MHz; DMSO-d_6) 150.1 (1 C, *C*-NO_2), 146.6 (1 C, C-1 arom.), 127.1 (2 C, C-2, -6 arom.), 123.4 (2 C, C-3, -5 arom.), 96.7 (1 C, C-5), 78.6 (1 C, C-2), 67.5 (1 C, C-3), 58.9 (1 C, -*C*H_2OH), 37.3 and 37.0 (2 C, C-6, -10), 25.1 (1 C, C-8), 23.7 and 23.6 (2 C, C-7, -9)

Tautomer 2a(II) (only distinct peaks or clearly correlated by COSY exp. are depicted)

δ_H(400 MHz; C_6D_6) 6.98 (2 H, *J* 8.6, H-2, -6 arom.), 4.10 (1 H, d, *J* 7.5, H_c), 3.48 (1 H, dd, *J* 4.7 and 8.6, H_{a1}), 3.40 (1 H, dd, H_{a2}), 2.75 (1 H, m, H_b)

δ_H(400 MHz; $CDCl_3$) 4.45 (1 H, d, *J* 7.4, H_c), 3.76 (1 H, d, *J* 8.8, H_{a1}), 3.70 (1 H, dd, *J* 4.1 and 8.8, H_{a2}), 3.42 (1 H, m, H_b)

δ_H(300 MHz; CD_3COCD_3) 4.77 (1 H, d, *J* 5.5, H_c), 3.63 (1 H, d, *J* 7.0, H_{a1}), 3.58 (1 H, *J* 7.0, H_{a2}), 2.30 (1 H, m, H_b)

l-4-Aza-8-t-tertbutyl-3-hydroxymethyl-2-(4-nitrophenyl)--1-r-oxaspiro[4.5]decane 2b(I) and

l-4-Aza-8-t-tertbutyl-3-(4-nitrohydroxybenzyl)-1-r-oxaspiro[4.5]decane 2b(II)

Yield 40%. M.p. = 155-7°C (MeOH) white crystalline powder (Found : C, 65.59; H, 7.90; N, 8.20; $C_{19}H_{28}N_2O_4$ requires C, 65.43; H, 8.10; N, 8.04%)

Tautomer 2b(I)

δ_H(400 MHz; DMSO-d_6) 8.20 (2 H, d, *J* 8.6, H-3, -5 arom), 7.61 (2 H, d, *J* 8.6, H-2, -6 arom.), 4.95 (1 H, t, *J* 5.7, H_d), 4.64 (1 H, d, *J* 7.9, H_c), 3.63 (1 H, ddd, *J* 11.7, 5.4 and 4.7, H_{a1}), 3.55 (1 H, ddd, *J* 11.7, 5.4 and 3.6, H_{a2}), 2.95 (1 H, br s, -N*H*-), 2.82 (1 H, unresolved large singlet, H_b according to COSY exp.), 1.86 – 1.22 (9 H, m), 0.85 (9 H, s, 3 × -C*H*$_3$)

δ_H(400 MHz; C_6D_6) 7.92 (2 H, d, *J* 8.8, H-3, -5 arom), 7.10 (2 H, d, *J* 8.8, H-2, -6 arom.), 4.59 (1 H, d, *J* 8.0, H_c), 3.40 (1 H, dd, *J* 11.0 and 3.6, H_{a1}) 3.18 (1 H, dd, *J*

11.0 and 3.6, H_{a2}), 2.76 (1 H, ddd, *J* 8.0, 4.0 and 4.0, H_b), 1.82 – 0.98 (11 H, cyclohexyl, -O*H*, –N*H*-), 0.90 (9 H, s, 3 × -C*H*$_3$)
δ_H*(400 MHz; CDCl*$_3$*)* 8.18 (2 H, d, *J* 8.8, H-3, -5 arom), 7.52 (2 H, d, *J* 8.8, H-2, -6 arom.), 4.79 (1 H, d, *J* 8.1, H_c), 3.88 (1 H, dd, *J* 11.3 and 3.7, H_{a1}), 3.67 (1 H, dd, *J* 11.3 and 4.0, H_{a2}), 3.16 (1 H, ddd, *J* 8.0, 4.0 and 3.7, H_b), 1.87 – 1.07 (11 H, cyclohexyl, -O*H* and –N*H*-), 0.86 (9 H, s, 3 × -C*H*$_3$);
δ_H*(400 MHz; CD*$_3$*COCD*$_3$*)* 8.21 (2 H, d, *J* 8.8, H-3, -5 arom.), 7.69 (2 H, d, *J* 8.8, H-2, -6 arom.), 4.81 (1 H, d, *J* 7.5, H_c), 4.15 (1 H, t, *J* 5.2, H_d), 3.83 (1 H, ddd, *J* 11.6, 5.4 and 5.2 H_{a1}), 3.77 (1 H, ddd, *J* 11.6, 5.0 and 3.8, H_{a2}), 3.09 (1 H, *J* 7.5, 5.2 and 3.8, H_b), 2.75 1 H, br s, -N*H*-), 1.83 – 1.49 (10 H, m, cyclohexyl, -O*H*), 0.89 (9 H, s, 3 × -C*H*$_3$)
δ_C*(100 MHz; DMSO-d*$_6$*)* 150.0 (1 C, *C*-NO_2), 146.6 (1 C, C-1 arom.), 127.1 (2 C, C-2, -6 arom.), 123.4 (2 C, C-3, -5 arom.), 97.5 (1 C, C-5), 78.2 (1 C, C-2), 67.7 (1 C, C-3), 58.6 (1 C, -*C*H_2OH), 46.8 (1 C, C-8), 38.7 and 38.0 (2 C, C-6, -10), 32.0 [1 C, -*C*$(CH_3)_3$], 27.5 (3 C, -*C*H_3), 25.1 and 24.8 (2 C, C-7 -9)
δ_C*(75 MHz; CDCl*$_3$*)* 148.8 (1 C, *C*-NO_2), 147.5 (1 C, C-1 arom.), 126.8 (2 C, C-2, -6 arom.), 123.8 (2 C, C-3, -5 arom.), 98.0 (1 C, C-5), 78.4 (1 C, C-2), 67.5 (1 C, C-3), 60.0 (1 C, -*C*H_2OH), 47.5 (1 C, C-8), 38.7 and 37.7 (2 C, C-6, -10), 32.4 [1 C, -*C*$(CH_3)_3$], 27.7 (3 C, -*C*H_3), 25.6 and 25.2 (2 C, C-7, -9)
Tautomer 2b(II) (only distinct peaks or clearly correlated by COSY exp. are depicted)
δ_H*(400 MHz; C*$_6$*D*$_6$*)* 7.89 (2 H, d, *J* 8.8, H-3, -5 arom.), 7.00 (2 H, *J* 8.8, H-2, -6 arom.), 4.13 (1 H, d, *J* 7.3, H_c), 3.50 (1 H, dd, *J* 8.8 and 4.6, H_{a1}), 3.40 (1 H, dd, *J* H_{a2}), 2.76 (1 H, ddd, H_b)
δ_H*(400 MHz; CDCl*$_3$*)* 8.20 (2 H, d, *J* 7.6, H-3, -5 arom.), 4.44 (1 H, d, *J* 7.5, H_c), 3.77 (1 H, dd, *J* 9.0 and 6.6, H_{a1}), 3.73 (1 H, dd, *J* 9.0 and 4.6, H_{a2}), 3.43 (1 H, ddd, *J* 7.2, 6.6 and 4.6, H_b)
δ_H*(400 MHz; CD*$_3$*COCD*$_3$*)* 4.77 (1 H, d, *J* 5.5, H_c), 3.63 (1 H, d, *J* 7.0, H_{a1}), 3.58 (1 H, *J* 7.0, H_{a2}), 2.30 (1 H, m, H_b)
δ_C*(75 MHz; CDCl*$_3$*)* 148.8 (1 C, *C*-NO_2), 147.5 (1 C, C-1 arom.), 127.4 (2 C, C-2, -6 arom.), 123.8 (2 C, C-3, -5 arom.), 96.2 (1 C, C-5), 79.0 (1 C, C-2), 66.8 (1 C, C-3), 60.3 (1 C, -*C*H_2OH), 47.4 (1 C, C-8), 38.2 and 37.5 (2 C, C-6, -10), 32.4 [1 C, -*C*$(CH_3)_3$], 27.7 (3 C, -*C*H_3), 24.4 and 23.9 (2 C, C-7, -9)

Trans-(2S,3S,10S,11S)-4,12-diaza-3,11-bishydroxymethyl-2,10-di(4-nitrophenyl)-1,9-dioxadispiro[4.2.4.2]tetradecane 3(I), Trans-(3S,11S)-4,12-diaza-3,11-bis(S-4-nitrohydroxybenzyl)-1,9-dioxadispiro[4.2.4.2]tetradecane 3(II) and ***Cis-(2S, 3S,10S,11S)-4,12-Diaza-3,11-bishydroxymethyl-2,10-di(4-nitrophenyl)-1,9-dioxa-dispiro[4.2.4.2]tetradecane 3(III)***,
Yield 75%. M.p. = 110-1°C (THF – Et_2O) yellowish crystalline powder (Found: C. 57.50; H, 5.75; N, 11.00; $C_{24}H_{28}N_4O_8$ requires C, 57.59; H, 5.64; N, 11.19%); $[\alpha]_D^{20}$ = + 48.9 (0.8%, MeOH)

Tautomer 3(I)

δ_H *(400 MHz; DMSO-d_6)* 8.20 (4 H, d, *J* 8.5, 2 × H-3, -5 arom.), 7.62 (4 H, d, *J* 8.5, 2 × H-2, -6 arom.), 5.07 (2 H, br s, 2 × H_d), 4.71 (2 H, d, *J* 7.1Hz, 2 × H_c), 3.67 (2 H, d, *J* 9.0, 2 × H_{a1}), 3.64 (2 H, d, *J* 9.0, 2 × H_{a2}), 3.05(2 H, m, 2 × H_b), 2.50 (2 H, br s, 2 × -N*H*-), 1.92 and 1.85 (8 H, *J* 9.8 and 12.9, cyclohexyl)

δ_H *(400 MHz; $CDCl_3$)* 8.22 (4 H, d, *J* 8.3, 2 × H-3, -5 arom.), 7.56 (4 H, d, *J* 8.3, 2 × H-2, -6 arom.), 4.86 (2 H, d, *J* 8.2, 2 × H_c), 3.95 (2 H, dd, *J* 11.3 and 5.5, 2 × H_{a1}), 3.74 (2 H, d, *J* 11.3 and 3.7, 2 × H_{a2}), 3.25 (2 H, ddd, *J* 8.2, 5.5 and 3.7, 2 × H_b), 2.70 – 0.70 (12 H, m, -N*H*-, -O*H*, cyclohexyl)

δ_C*(75 MHz; DMSO-d_6)* 150.0 (2 C, 2 × C-4 arom.), 146.6 (2 C, 2 × C-1 arom.), 127.0 (4 C, 2 × C-2, -6 arom.); 123.4 (4 C, 2 × C-3, -5 arom.), 96.2 (2 C, C-5, -8), 78.6 (2 C, C-2, -10), 67.5 (2 C, C-3, -11), 58.8 (2 C, 2 × -*C*H_2OH), 34.4 and 34.1 (4 C, C-6, -7, -13 and -14)

δ_C*(75 MHz; $CDCl_3$)* 149.0 (2 C, 2 × C-4 arom.), 146.7 (2 C, 2 × C-1 arom.), 127.4 (4 C, 2 × C-2, -6 arom.); 123.9 (4 C, 2 × C-3, -5 arom.), 95.9 (2 C, C-5, -8), 76.6 (2 C, C-2, -10), 67.1 (2 C, C-3, -11), 60.0 (2 C, 2 × -*C*H_2OH), 34.9 and 34.7 (4 C, C-6, -7, -13 and -14)

Tautomer 3(II) (only distinct peaks or clearly correlated by COSY exp. are depicted)

δ_H *(300 MHz; $CDCl_3$)* 4.51 (2 H, d, *J* 8.1, 2 × H_c), 3.87 (2 H, dd, *J* 8.1 and 2.1, 2 × H_{a1}), 3.81 (2 H, dd, *J* 8.1 and 3.0, 2 × H_{a2}), 3.50 (2 H, ddd, *J* 8.1, 3.0 and 2.1, 2 × H_b)

δ_C*(75 MHz; $CDCl_3$)* 96.2 (2 C, C-5, -8), 73.5 (2 C, C-2, -10), 66.9 (2 C, C-3, -11), 59.6 (2 C, 2 × -*C*H_2OH), 34.8 and 34.5 (4 C, C-6, -7, -13 and -14)

Tautomer 3(III) (only distinct peaks or clearly correlated by COSY exp. are depicted)

δ_H *(300 MHz; $CDCl_3$)* 4.93 (1 H, d, *J* 8.1, H_c), 4.83 (1 H, d, *J* 6.3, H_c), 3.92 (2 H, dd, *J* 11.2 and 5.3, 2 × H_{a1}), 3.76 (2 H, dd, *J* 11.3 and 3.7, 2 × H_{a2}), 3.19 (2 H, ddd, *J* 8.1, 5.3 and 3.7, 2 × H_b)

δ_C*(75 MHz; $CDCl_3$)* 95.5 and 95.1 (2 C, C-5, -8), 78.58 and 78.7 (2 C, C-2, -10), 66.8 and 66.7 (2 C, C-3, -11), 64.1 and 63.9 (2 C, 2 × -*C*H_2OH), 38.2, 38.1, 36.5 and 36.4 (4 C, C-6, -7, -13 and -14)

δ_H *(400 MHz; acetone-d_6)* 4.88 (1 H, d, *J* 8.0, H_c), 4.87 (1 H, d, *J* 8.1, H_c), 4.18 (2 H, br s, -O*H*), 3.85 (1 H, dd, *J* 11.6 and 3.8, H_{a1}), 3.84 (1 H, dd, *J* 11.6 and 3.8, H_{a1}), 3.79 (2 H, dd, *J* 11.6 and 3.8, 2 × H_{a2}), 3.19 (1 H, dd, *J* 8.1 and 3.8, H_b), 3.17 (1 H, dd, *J* 8.1 and 3.8, H_b), 2.91 (2 H, br s, -N*H*-), 2.09 – 1.79 (8 H, m, cyclohexyl)

REFERENCES

1. M. Dărăbanțu, G. Plé, S. Mager, E. Cotora, L. Gaina, L. Costas and A. Mateş, *Tetrahedron,* 1997, ***53***(5), 1873.
2. E. Bergmann, *Chem. Rev.*, *1953*, ***53***, 309.
3. M. Dărăbanțu, G. Plé, I. Silaghi-Dumitrescu, L. Gaina, C. Maierean and I. Turos, *Unpublished data*.
4. E. Bergmann and H. Resnik, *J. Chem. Soc*., 1956, 1662.

5. E. L. Eliel and S. H. Wilen, *Stereochemistry of Organic Compounds*, John Wiley & Sons, Inc., 1994, p.769-771.
6. M. Dărăbanțu, S. Mager, G. Plé and C. Puşcaş, *Heterocycles*, 1995, ***41***(10), 2327.
7. M. Dărăbanțu, G. Plé, S. Mager, L. Gaina, E. Cotora, A. Mates and L. Costas.
8. *Tetrahedron,* 1997, ***53***(5), 1891-1908.

STUDIA UNIVERSITATIS BABEŞ-BOLYAI, CHEMIA, XLIII, 1-2, 1998

L'ÉLECTROOXYDATION DU PHÉNOL. VOLTAMMÉTRIE CYCLIQUE

LIVIU ONICIU*, CARMEN GONCEA

ABSTRACT. The electrochemical oxidation of phenol at a platinum anode using linear sweep cyclic voltammetry was studied. The oxidation potential of phenol in 0,1M H_2SO_4 medium and in 1M NaOH solution, together with the mediated oxidation potential of phenol with $K_3Fe(CN)_6$, in alkaline medium were determined.

INTRODUCTION

L'électrooxydation du phénol présente un intérêt écologique pour la purification des eaux industrielles résiduelles [1-4] et pour la préparation de certains produits d'oxydation comme l'hydroquinone ou la benzoquinone [5].

Les anodes utilisées pour l'oxydation anodique du phénol ont été: Pt, grapgyte, Au et PbO_2 [6].

La méthode utilisée a été la voltammétrie cyclique.

Études antérieures [7] ont montré que l'électrooxydation du phénol à un potentiel de 0,5 V/EHN.

Employant la même méthode d'investigation, nous avons étudié l'électro-oxydation du phénol sur anode de platine, en milieu acide (H_2SO_4 0,1M) et basique (NaOH 1M), ainsi que l'électrooxydation médiée du phénol avec $K_3Fe(CN)_6$ en milieu basique.

Expérimental

Les substances employées ont été de pureté analytique et ont été dissoutes dans l'eau doublement distilée.

Les mesures voltammétriques ont été effectuées utilisant une cellule à trois électrodes: électrode de travail, électrode de référence (l'électrode de calomel saturé) et la contreélecrode en platine.

L'électrode de travail a été un disque en platine ayant le diamètre de 1mm; après chaque expérimentation il y a avait polissage mécanique avec du papier émeri et rinçage à l'eau distilée.

Les potentiels sont exprimés par rapport à l'électrode de calomel saturé. La vitesse de balayage (v), la sensibilité (S) et les limites du potentiel explorées sont spécifiées sur les voltamogrammes obtenues.

* *Université Babeş-Bolyai, Facultéde Chimie et Génie Chimique, 11, Arany Janos, 3400, Cluj-Napoca, Roumanie.*

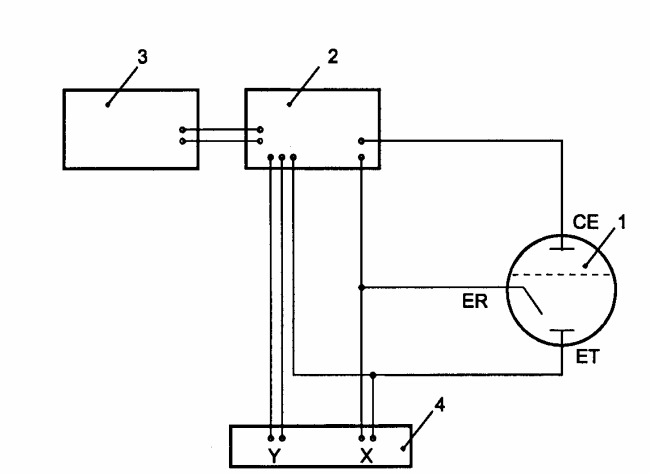

Fig. 1. Le montaje expérimental employé dans les mesures de voltammétrie cyclique
1 - la cellule expérimentale:
ET = l'électrode de travail (Pt)
ER = l'électrode de référence (calomel saturé, ECS)
CE = le contreélectrode (Pt)
2 - le potentiostat
3 - le générateur de signal du type PS_3
4 - l'enregistreur X-Y du type Recorder, Moseley 135 AM

RÉSULTATS ET DISCUSSION

L'électrooxydation du phénol en milieu acide

L'électrooxydation du phénol en milieu de H_2SO_4 0,1M sur Pt a lieu à un potentiel de 0,2 V/ECS ou 0,447 V/EHN (figure 2).

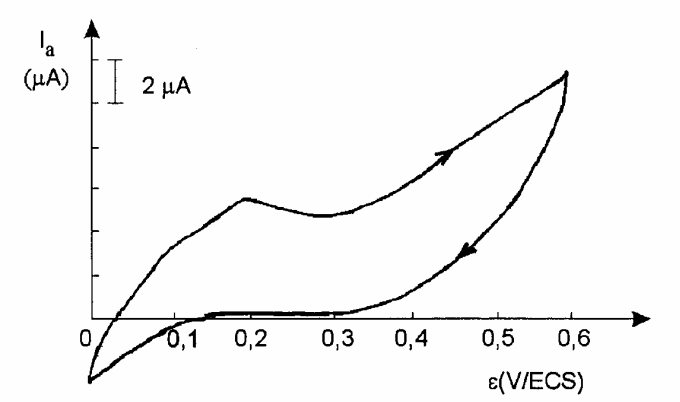

Fig. 2. Voltamogramme du phénol 10^{-2} M en solution de H_2SO_4 0,1 M à v=60mV/s et S=0,1 mA/V.

L'électrooxydation du phénol en milieu basique

En milieu de NaOH 1M, le phénol est oxidé sur l'électrode de Pt à un potentiel de 0,27 V/ECS ou 0,5 V/EHN (figure 3).

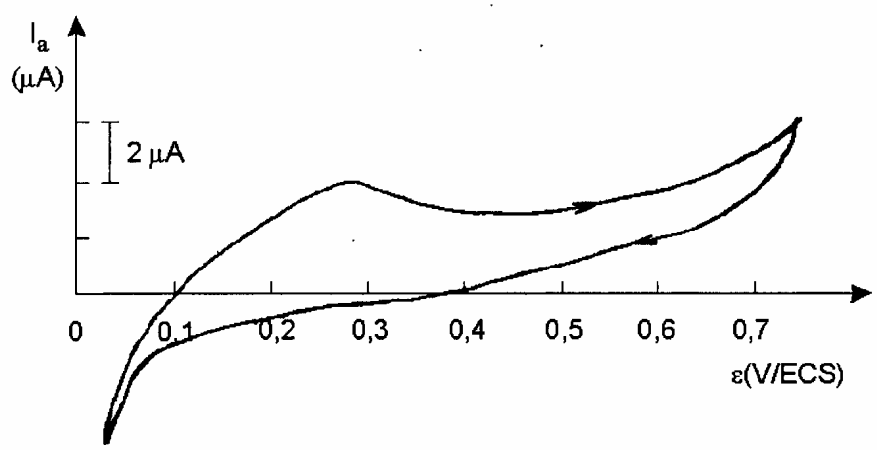

Fig. 3. Voltamogramme du phénol 10^{-2} M en solution de NaOH 1M à v=60mV/s et S=0,1 mA/V.

Sur l'électrode disque tournant de Pt, en milieu de NaOH 1M, le phénol présente un maximum d'oxydation don't la hauteur diminue avec le nombre de cycles (figure 4). Ce fait peut être une preuve de la formation d'une pellicule de polymère, le transfert de charge ayant lieu à travers de celle-ci [8-10].

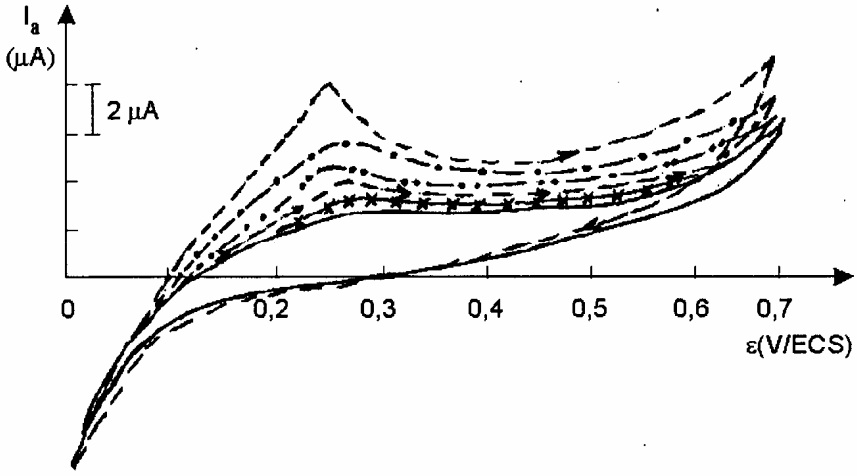

Fig. 4. Voltamogramme du phénol 10^{-2} M en solution de NaOH 1M sur disque tournant de Pt à v=60mV/s et S=0,1 mA/V.

De même, on observe dans la figure 4, qu'une augmentation de la vitesse de rotation du disque de 1600 à 1800 rotations/minute n'influence pas la valeur du courant limite d'oxydation du phénol. Celle-ci est une preuve pour une cinétique d'ordre zéro et s'expliquerait par la formation de la pellicule de polymère sur l'anode [8-10].

Si on compare les voltamogrammes des figures 2 et 3, on constate que le courant limite d'oxydation en milieu basique est plus petit que celui du milieu acide. On considère [11] que cette diminution de courant limite serait due à d'adsorption d'oxygène plus forte en milieu basique et qui concourt l'électrosorption du phénol à l'anode. D'autres [8, 12] afirment que la diminution du courant limite est due à certains produits solubles, fixés par adsorption sur l'électrode.

L'électrooxydation médiée du phénol avec $K_3Fe(CN)_6$

La voltamogramme du système $K_3Fe(CN)_6 10^{-3}$M - $K_4Fe(CN)_6 10^{-3}$ M en solution de NaOH 1M sur Pt est illustrée dans la figure 5; le maximum d'oxydation du $Fe(CN)_6^{4-}$ est à 0,26 V/ECS et le maximum de réduction du $Fe(CN)_6^{3-}$ à 0,24 V/ECS.

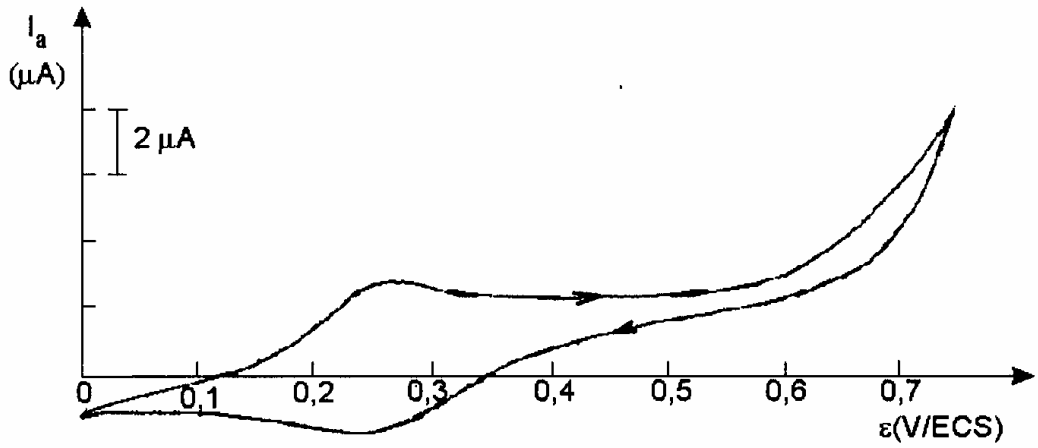

Fig. 5. Voltamogramme du système $K_3Fe(CN)_6$ 10^{-3} M - $K_4Fe(CN)_6$ 10^{-3} M en solution NaOH 1M à v=60mV/s et S=0,1 mA/V.

L'électrooxydation médiée du phénol avec $K_3Fe(CN)_6$ en milieu basique (NaOH 1M) est illustrée dans la figure 6.

On constate des déplacements petits vers des valeurs plus grandes autant du maximum d'oxydation du $Fe(CN)_6^{4-}$, de 0,26 V/ECS à 0,3 V/ECS que du maximum de réduction du $Fe(CN)_6^{3-}$, de 0,24 V/ECS à 0,31 V/ECS.

Le maximum d'oxydation du phénol se superpose sur celui d'oxydation du $Fe(CN)_6^{4-}$, parce que les potentiels sont très proches. De même, la diminution du courant limite d'oxydation du phénol purrait être due à la formation d'un complexe entre $C_6H_5O^-$ et $Fe(CN)_6^{3-}$.

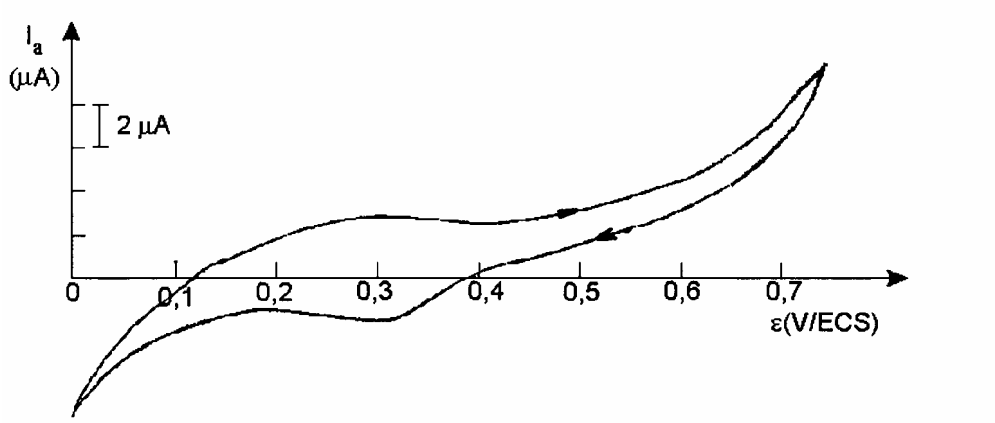

Fig. 6. Voltamogramme du système phénol 10^{-2} M- $K_3Fe(CN)_6$ 10^{-3} M - $K_4Fe(CN)_6$ 10^{-3} M en solution NaOH 1M à v=60mV/s et S=0,1 mA/V.

Les résultats concernant l'électrooxydation du phénol à l'anode de platine dans des conditions expérimentales différentes conduisent aux conclusions suivantes:

- Le potentiel obtenu correspondant à l'oxydation anodique du phénol sur Pt, en milieu acide et basique, concorde très bien avec ceux obtenus par d'autres auteurs, à savoir 0,5 V/EHN.
- L'électrooxydation du phénol en milieu basique a lieu avec la formation d'une pellicule de polymère, ce fait étant constaté aussi par d'autres auteurs.
- L'oxydation électrochimique du phénol médiée par $K_3Fe(CN)_6$ en milieu basique n'est pas facile à relever parce que le potentiel d'oxydation du $Fe(CN)_6^{4-}$ en milieu basique est proche du potentiel d'oxydation du phénol.

REFERENCES

1. H. Scharifian, D.W. Kirk, *J. Electrochem. Soc.*, 1986, **133**, 921.
2. Ch. Comninellis, E. Plattner, *Chimia*, 1988, **42**, 250.
3. Ch. Comninellis, C. Pulgarin, *J. Appl. Electrochem.*, 1993, **23**, 108.
4. Ch. Comninellis, A. Nerini, *J. Appl. Electrochem.*, 1995, **25**, 23.
5. C. Oloman, *A.I. Ch. E. Symposium Series*, 1981, **77**, 264.
6. T.A. Kharlamova, G.A. Tederadze, *Uspehii. Khim.*, 1987, **56** (1), 29.
7. A. Avrutskaya, M.Y. Fioshin, *Zh. Prikl. Khim.*, 1967, **42**, 2294.
8. I. Izumi, M. Oue, A. Kunugi, *Memories of the Faculty of Engineering Osaka*, 1980, **21** (21), 131.
9. T. Fichter, *Trans. Amer. Electrochem. Soc.*, 1924, **45**, 107.

10. B. Fleszar, J. Ploszynska, *Zeszyty naukove politeh. slaskiej*, 1979, **91**, (631), 327.
11. G.D. Levina, G.M. Kolosova, Ju.B. Vasilev, *Electrokhimija*, 1977, **13**, 1056.
12. T. Shimizu, A. Kunugi, Sh. Nagaura, *Denki Kagaku*, 1975, **43** (5), 269.

STUDIA UNIVERSITATIS BABEŞ-BOLYAI, CHEMIA, XLIII, 1-2, 1998

THE RELATIONSHIP BETWEEN INDEX OF HYDROGEN DEFICIENCY AND MOLECULAR MASS FOR HYDROCARBONS. APPLICATION IN SOLVING OF SOME ORGANIC CHEMISTRY PROBLEMS

CHEREJI-MACH I.Z., MĂRGINEANU D., NAUMESCU A.

ABSTRACT. In this paper we examine the possibilities to determine with mathematical methods, implying the *limits* and the *Index of Hydrogen Deficiency (IHD)* [1], the molecular formulas for hydrocarbons, having minimum available primary data, that is the carbon percentage % C. In this way we establish the class of hydrocarbons including the studied substance.

The proposed method proves to be a rapid solution to solve this type of Organic Chemistry problems.

I: Preliminary Considerations; Calculation Methods

At present, a prominent tendency towards approaching chemistry from mathematical perspectives has become increasingly manifest. The present paper gives prominence to this spirit aiming at the transposition in mathematical language of some chemical notions, with reference to the composition and structure of the molecules of organic substances.

Examining the possibilities to determine *the molecular formulas for hydrocarbons, having the carbon percentage*, the paper aims at the systematization and delimitations of the values range within which the new calculation methods can be applied.

We start from the premise that minimum information is provided, namely, the carbon percentage (% C) of the hydrocarbon whose identity must be determined.

The following mathematical considerations are established, in order to appeal only to carbon percentage with no other auxiliary data in the process of solving the problems:

By using the *Index of Hydrogen Deficiency* (*IHD*) and the mathematical notion of *limit*, we tried to determine a variation law of the carbon percentage within the homologous series for different classes of hydrocarbons.

First of all, we will try to establish certain regularities in the variation of carbon percentage for different classes of hydrocarbons, calculating the following types of limits:

$$\lim_{n \to \infty} \frac{\% \ C}{100}$$

Taking into account that:

$$\%C = \frac{mC}{M} \bullet 100 \quad - \quad \frac{\%C}{100} = \frac{mC}{M}$$

where M = the molecular mass of the hydrocarbon,
m_C = the carbon atoms mass.

The limit becomes: $\lim_{n \to \infty} \frac{\%\ C}{100} = \lim_{n \to \infty} \frac{mC}{M}$

For *IHD* = 0 , ALKANES (C_nH_{2n+2}), $n \in [\,1\,,\infty\,)$:

$$\frac{12\,n}{14\,n\ +\ 2}\Big|_{n\ =\ 1} = 0{,}75\ ,\quad \lim_{n \to \infty} \frac{12\,n}{14\,n\ +\ 2} = \frac{6}{7} \quad 0{,}857143.$$

For *IHD* = 1 , ALKENES, CYCLOALKANES, (C_nH_{2n}), $n \in [\,2\,,\infty\,)$:

$$\frac{12\,n}{14\,n}\Big|_{n\ =\ 2} = \frac{6}{7} \quad 0{,}857143\ ,\quad \lim_{n \to \infty} \frac{12\,n}{14\,n} = \frac{6}{7} \quad 0{,}857143.$$

Constant sequence ; the value <u>does not depend on "n"</u>.

For *IHD* = 2 , ALKYNES (C_nH_{2n-2}), $n \in [\,2\,,\infty\,)$:

$$\frac{12\,n}{14\,n-2}\Big|_{n\ =\ 2} = \frac{12}{13} \quad 0{,}923\ ,\quad \lim_{n \to \infty} \frac{12\,n}{14\,n-2} = \frac{6}{7} \quad 0{,}857143;$$

DIENES, CYCLOALKENES (C_nH_{2n-2}), $n \in [\,3\,,\infty\,)$:

$$\frac{12\,n}{14\,n-2}\Big|_{n\ =\ 3} = 0{,}9\ ,\quad \lim_{n \to \infty} \frac{12\,n}{14\,n-2} = \frac{6}{7}$$

For *IHD* = 3 , compounds with formula C_nH_{2n-4}, $n \in [\,4\,,\infty\,)$:

$$\frac{12\,n}{14\,n-4}\Big|_{n\ =\ 4} = \frac{12}{13} \quad 0{,}923\ ,\quad \lim_{n \to \infty} \frac{12\,n}{14\,n-4} = \frac{6}{7} \quad 0{,}857143.$$

For *IHD* = 4 , DIYNES (C_nH_{2n-6}), $n \in [\,4\,,\infty\,)$:

$$\frac{12\,n}{14\,n-6}\Big|_{n\ =\ 4} = \frac{24}{25} = 0{,}96\ ,\quad \lim_{n \to \infty} \frac{12\,n}{14\,n-6} = \frac{6}{7} \quad 0{,}857143;$$

MONONUCLEAR ARENES (C_nH_{2n-6}), $n \in [\,6\,,\infty\,)$:

$$\frac{12\,n}{14\,n-6}\Big|_{n\ =\ 6} = \frac{12}{13} \quad 0{,}923\ ,\quad \lim_{n \to \infty} \frac{12\,n}{14\,n-6} = \frac{6}{7} \quad 0{,}857143.$$

For *IHD* = 5 , compounds with formula C_nH_{2n-8}, $n \in [\,6\,,\infty\,)$:

$$\frac{12\,n}{14\,n-8}\Big|_{n\ =\ 6} = \frac{18}{19} \quad 0{,}9473\ ,\quad \lim_{n \to \infty} \frac{12\,n}{14\,n-8} = \frac{6}{7} \quad 0{,}857143$$

and so on.

From the above data it results:

- In the case of alkanes, the carbon percentage ranges from 75% to ≈ 85,7143 % ; the carbon minimum percentage corresponds to methane and the carbon percentage tends towards the limit value of 85,7143 % , asymptotically along with the increase of the carbon atoms number in the molecule.

- In the case of the other hydrocarbon classes with the Index of Hydrogen Deficiency of *IHD*>1, the carbon percentage decreases simultaneously with the increase of the carbon atoms number in the molecule, manifesting an asymptotic tendency towards the limit value of 85,7143 % .

In order to find a more accurate correlation among the number of carbon atoms, the Index of Hydrogen Deficiency and the carbon percentage, we will resort to the following argumentation:

Let us take a random hydrocarbon, whose molecular formula can be put down in two ways:

(1) $C_n H_{2n+2-2\bullet IHD}$

(2) $(C H_a)_n$

where n = the number of carbon atoms in the molecule;
IHD = the Index of Hidrogen Deficiency (sites of unsaturation);
a = the average number of hydrogen atoms belonging to a carbon atom of the substance under question.

The following mathematical restrictions are, obviously, required:

$$n \in \{1, 2, \ldots\ldots \infty\}; \; IHD \in \{0, 1, 2, \ldots\}; \; a \in \{0, 1, 2, 3, 4\}$$

Identifying the number of hydrogen atoms in formula (1) with the number of hydrogen atoms in formula (2), the following can be obtained:

$$2n + 2 - 2 \bullet IHD = a \bullet n$$

where *IHD* is expressed:

(3) $$IHD = \frac{n \bullet (2 - a)}{2} + 1$$

On the other hand, taking into account the definition of a (= the average number of hydrogen atoms belonging to a carbon atom for the substance under question) and denoting by p the carbon percentage expressed as decimal fraction

0, the following relation can be written down:

(4) $$a = \frac{12 \bullet (1 - p)}{p}$$

Replacing the relation (4) by (3) the following expression can be obtained at the end:

(5) $$IHD = \frac{(7p - 6) \bullet n}{p} + 1$$

which can be simplified to:

(6) $$IHD = A \bullet n + 1$$

where $A = \frac{(\ 7\ p - 6\ )}{p}$

In order to check out and discuss the solutions of the expression (5), the following table has been drawn up, in which the second column represents the carbon percentage (*p*) calculated for hydrocarbons with known molecular formulas; further on, the results of the calculations with relation (6) noted in the last column, should be compared with the first column content (the molecular formulas of the hydrocarbons under question) to put into evidence the efficiency and possible limits of the calculation method proposed hereby.

The molecular formula of the hydrocarbon	*p*	*A*	Conclusions calculated *n* values	*IHD* values
CH_4	0,7500	- 1,00	only for $n = 1$ $\Rightarrow$	$IHD = 0$
C_2H_6	0,8000	- 0,5000	only for $n = 2$ $\Rightarrow$	$IHD = 0$
C_3H_8	0,8181	- 0,3340	only for $n = 3$ $\Rightarrow$	$IHD = 0$
C_4H_{10}	0,8275	- 0,2507	only for $n = 4$ $\Rightarrow$	$IHD = 0$
C_5H_{12}	0,8333	- 0,2002	only for $n = 5$ $\Rightarrow$	$IHD = 0$
C_6H_{14}	0,8372	- 0,1667	only for $n = 6$ $\Rightarrow$	$IHD = 0$
C_7H_{16}	0,8400	- 0,1428	only for $n = 7$ $\Rightarrow$	$IHD = 0$
C_8H_{18}	0,8421	- 0,1250	only for $n = 8$ $\Rightarrow$	$IHD = 0$
C_9H_{20}	0,8437	- 0,1115	only for $n = 9$ $\Rightarrow$	$IHD = 0$
$C_{10}H_{22}$	0,8450	- 0,1006	only for $n = 10$ $\Rightarrow$	$IHD = 0$
$C_{25}H_{52}$	0,8522	- 0,0406	only for $n = 25$ $\Rightarrow$	$IHD = 0$
$C_{50}H_{102}$	0,8547	- 0,0200	only for $n = 50$ $\Rightarrow$	$IHD = 0$
$C_{75}H_{152}$	0,8555	- 0,0134	only for $n = 75$ $\Rightarrow$	$IHD = 0$
$C_{100}H_{202}$	0,8559	- 0,0101	only for $n = 100$ $\Rightarrow$	$IHD = 0$
C_nH_{2n}	0,8571	0	for any n $\Rightarrow$	$IHD = 1$
C_2H_2	0,923	0,499	for $n = 2$ $\Rightarrow$	$IHD = 2$
			for $n = 4$ $\Rightarrow$	$IHD = 3$
			for $n = 6$ $\Rightarrow$	$IHD = 4$
			for $n = 8$ $\Rightarrow$	$IHD = 5$
C_3H_4	0,900	0,333	for $n = 3$ $\Rightarrow$	$IHD = 2$
			for $n = 6$ $\Rightarrow$	$IHD = 3$
			for $n = 9$ $\Rightarrow$	$IHD = 4$
			for $n = 12$ $\Rightarrow$	$IHD = 5$
C_4H_6	0,888	0,243	for $n = 4$ $\Rightarrow$	$IHD = 2$
			for $n = 8$ $\Rightarrow$	$IHD = 3$
			for $n = 12$ $\Rightarrow$	$IHD = 4$
			for $n = 16$ $\Rightarrow$	$IHD = 5$
C_5H_8	0,882	0,199	for $n = 5$ $\Rightarrow$	$IHD = 2$
			for $n = 10$ $\Rightarrow$	$IHD = 3$
			for $n = 15$ $\Rightarrow$	$IHD = 4$

The molecular formula of the hydrocarbon	*p*	*A*	Conclusions calculated *n* values *IHD* values
C_6H_{10}	0,878	0,166	for *n* = 6 ⇒ *IHD* = 2 for *n* = 12 ⇒ *IHD* = 3 for *n* = 18 ⇒ *IHD* = 4

II: Discussion and Conclusions:

II.1. Analyzing the previously reported data, a series of conclusions on the method efficiency and also on the manner of approaching the problem can be drawn.

Thus, it can be found that simply indicating, determining or calculating the carbon percentage, important information about the hydrocarbons class including the studied substance can be obtained, namely:

$p < \frac{6}{7}$ $0,857143$, the hydrocarbon is certain to be an alkane;

$p = \frac{6}{7}$ $0,857143$, the hydrocarbon is certain to be an alkene or a cycloalkane;

$p > \frac{6}{7}$ $0,857143$, the hydrocarbon has *IHD*>1.

The table shows that we can determine the molecular formula of alkanes directly from % C (*p*) with no supplementary information, as relation (5) admits unique solution in the case of alkanes. This finding seems extremely important.

Mention should be made that the *p* values for the two consecutive homologues show a tendency to become ever closer along with the increase of *n* values. Nevertheless, the calculations have revealed that, at the accuracy of *p* values given in textbooks and reference materials of two decimals, the molecular formulas for alkanes up to C_{75} - C_{80} can be determined univocally. The unique solution of relation (5) for alkanes lies in the fact that the term *A* is negative and as a result, there is only one *n* value satisfying all the supplementary requirements simultaneously $(n \in N^*, N E \in N)$.

In the case $p = \frac{6}{7}$ $0,857143$ it is determined that *A* = 0 and consequently, relation (5) can give no information at all about *n* ; irrespective of *n* value, relation (5) has the solution *IHD* = 1. there must be other ways to find the molecular formula of the hydrocarbon on the basis of further data provided by the problem. Relation (5) verifies both the gross and molecular formulas of alkenes and cycloalkanes.

If $p > \frac{6}{7}$ $0,857143$, the term *A* becomes positive and consequently, relation (5) admits of an infinity of solutions for *IHD*, these representing multiples of the solution with minimum *n*. A distinct value *IHD* corresponds to each *n*, so we can conclude that the hydrocarbons are part of classes of different substances. However, only the gross formula of the compound has been determined; further data from the text are required to determine the molecular formula of the hydrocarbon. As the

correlation between *n* and *IHD* is already known, relation (1), it seems much easier to write down the structural formulas, especially if the general expression of the hydrocarbon formula proposed by P. Budrugeac [2] is taken into account:

$$C_n H_{2n+2-2d-4t-2c}$$

where: *d* , *t* , *c* represent the number of *d*ouble bonds, *t*riple bonds, and *c*ycles (rings) present in the molecule of the studied organic compound respectively.

II.2. The method under proposal facilitates the solving of this type of Organic Chemistry problems included in text books for the X^{th} and XII^{th} grades [3], [4].

It must be taken into account that a number of mathematical operations - particularly the division operations - is considerably reduced, contributing in this way to a greater accuracy of the results. It has been noticed that the majority of errors in the solving of numerical problems are caused by *division* because, almost every time, a certain number of decimals is ignored, which ultimately leads to erroneous results.

The Index of Hydrogen Deficiency (*IHD*) notion [1] is remarkably efficient not only in problems solving but also in the systematization of the theoretical material, particularly when it comes to structure or isomery; that is the reason why special attention has been paid to this notion in the process of searching the most various correlations with other parameters characteriszing the organic molecule.

At first sight, the newly proposed method of calculation is adequate only for *alkanes* and less efficient for *alkenes, cycloalkanes* and hydrocarbons with *IHD* > 1.

Nevertheless, taking into account the supplementary information provided by the proposed method even in the cases named before, we are convinced that *the implementation of the proposed method in solving the problems referring to structure determination of hydrocarbons is entirely justified.*

REFERENCES

1. Stanley H. Pine, *Organic Chemistry*, fifth edition, Mc.GRAW-HILL BOOK COMPANY, New York, U.S.A., 1990, pp. 19-21.
2. Budrugeac P., *CHEMISTRY problems*, Ed. Academy, Bucharest, Romania, 1986, pp. 122.
3. Albu C.D., Petrescu O., Cosma I., *CHEMISTRY, textbook for X^{th} grade*, E.D.P., R.A., Bucharest, Romania, 1994, pp. 12, 13, 19, 30.
4. Albu C.D., Ionescu I., Ilie Şt., *CHEMISTRY, textbook for XII^{th} grade*, E.D.P., R.A., Bucharest, Romania, 1994, pp. 28, 29, 83.

STUDIA UNIVERSITATIS BABEŞ-BOLYAI, CHEMIA, XLII, 1-2, 1998

NUMERICAL SIMULATION OF A PRESSURE SWING ADSORPTION UNIT

THOMAS KLEINHEMPEL, MARIETA ATANASIU, FLORIN ATANASIU*

ABSTRACT. The paper presents a numerical model that simulates the bulk separation of a two component gas mixture, on 5 A molecular sieve. Experimental results are compared with theoretical ones, to reveal the influence of some operating parameters on the product purity and recovery. Experiments have been carried out for air separation on 5 A zeolite molecular sieve on a two column laboratory PSA unit. The theoretical model provides a good representation of the performances of an experimental unit over the range of operating conditions.

INTRODUCTION

SKARSTROM [1] presents in 1960 "a new method for air drying" for the first time, based on selective adsorption process that is called ***"heatless adsorption"*** or ***"pressure swing adsorption"*** at the present time. The process consists in a cyclic operation of two adsorption columns between two limiting pressures: a low one (p_L) and a high one (p_H). The standard operational cycle consists in four steps: pressurization with feed from the pressure p_L up to p_H, constant pressure production (adsorption) step at p_H, followed by blowdown from p_H down to p_L and constant pressure purge at p_L with a fraction of the purified product, withdrawn during the production step. The bulk separation of the feed mixture is processed during pressurization and production steps. The bed regeneration is accomplished by reducing the partial pressure of the more strongly adsorbed component during blowdown step, when the total pressure decreases and then by purging the adsorption bed with purified gas, when the molar fraction of the stronger adsorbed components is reduced on the adsorbent surface.

Beginning with 1970, the process was widely used for various gas separations [2], on laboratory units, as well as on industrial plants, by experimenting other operating cycles, other adsorbents like zeolites and – during the last decade - carbon molecular sieves. Thus the PSA technology has been extended from drying of the gases to air separation, in order to obtain pure oxygen and/or nitrogen, air purification, hydrogen and helium separation, by retaining impurities such as CO_2, H_2O, H_2S, NO_2, SO_2, NH_3 and CH_4.

* *S.C. "GAS" S.R.L. Societate Comercială pentru Gaze şi Aparatură, Cluj-Napoca.*

Together with technology development, the numerical modeling of the process gained greater attention, for plant design as well as for simulation, in order to find the best sets of values for the operating conditions.

This paper presents a local equilibrium model for the simulation of a two-bed PSA unit operation, based on the standard four-step cycle presented above. The model consists in integral molar balance equations, considered between the initial and final moments of each step. The computed results exhibit a good agreement with the experimental ones. A parametric study was also accomplished, in order to reveal the influence of the purge velocity and the product velocity on the purity and the recovery fraction of the product.

THEORETICAL MODEL

A two-bed process operated on a standard cycle is considered, as shown in fig.1. The pressure changes in the adsorption bed during a whole cycle are presented in figure 2.The following four steps comprise the cycle:

1) Pressurization,
2) Adsorption,
3) Countercurrent blowdown,
4) Countercurrent purge.

In step 1, bed 1 is pressurized to the high operating pressure with feed and bed 2 is blown down to the atmospheric pressure in the reverse flow direction. In step 2, the high pressure feed flow trough bed 1. During this step the more strongly adsorbed component is retained in the bed and the interstitial gas stream is enriched in the lighter component, that leaves as effluent. A fraction of the effluent stream is

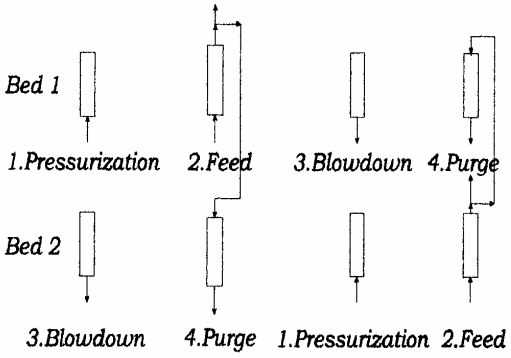

Fig.1. Schematic diagram of the P.S.A. cycle

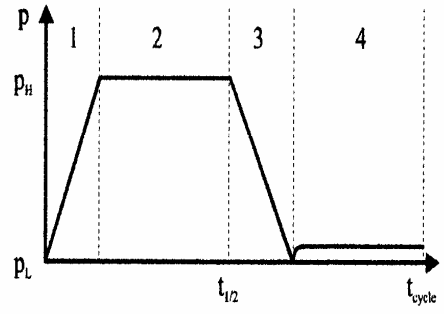

Fig. 2. Pressure changes in the bed during a whole cycle

withdrawn as product and the rest is used for countercurrent purge of bed 2 at reduced pressure. The operations are switched between beds in steps 3 and 4.

In order to develop the mathematical model for this system, the following assumptions are introduced:

1) Air is considered as a binary mixture of ideal gases 78% nitrogen (1) and 22% oxygen together with argon (2). Because argon exhibits almost the same adsorption affinity for 5A zeolite molecular sieve (ZMS-5A) as oxygen in the range of ambient temperatures, these two components are considered unseparated. They are enriched in the raffinate product.

2) Local equilibrium is assumed. The mass transfer between gas and solid phase is considered to be instantaneous.

3) The system is assumed to be isothermal. When small diameter columns are used, with high thermal conductivity, as in the present study, the pressure flow direction is changed frequently and the heat evolved during adsorption does not exceed 5 kcal/mol, thermal effects can be neglected.

4) Equilibrium relationships for both components are represented by binary LANGMUIR isotherms.

5) Pressure drop along the column is neglected.

6) Repressurization is carried out only with feed mixture.

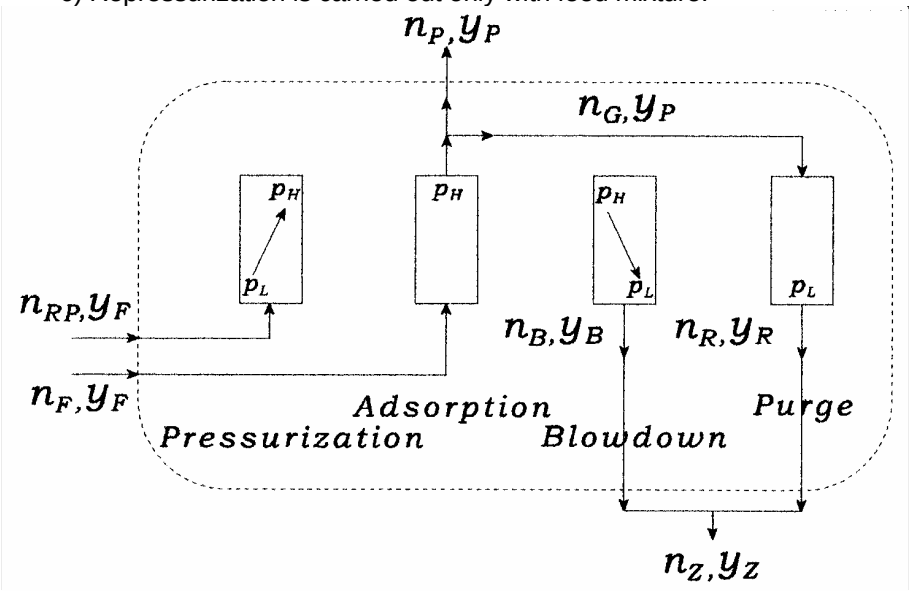

Fig.3. Schematic diagram of the molar balance

The molar balance equations are written for the entire stream and for the most strongly adsorbed component, in this case – nitrogen, between the initial and the final moment of each PSA step. Figure 3 shows the schematic diagram used to complete the balance and the meaning of the symbols.

Starting from an initial equilibrium state of the bed with feed mixture (air) at the pressure p_L and the average concentration y^o_4 of the nitrogen in the interstitial gas phase, the adsorbent is put in contact with the feed during the pressurization step. The pressure raises to p_H and the average concentration of the interstitial gas phase changes to y_1 due to the incipient adsorption. The average mole number of

gas fed in the column during pressurization is n_{RP}. Then, the column is feed with n_F moles of air in the adsorption step, the pressure remain unchanged at p_H and the composition become y_2 at the end of the step.

Table 1.

The state of the bed at the beginning and end of each PSA step.

P.S.A. step	PRESSURIZATION	ADSORPTION	BLOWDOWN	PURGE
Initial state of the bed	p_L, y_4	p_H, y_1	p_H, y_2	p_L, y_3
Final state of the bed	p_H, y_1	p_H, y_2	p_L, y_3	p_L, y_4

From the column (n_P+n_G) moles of oxygen enriched gas are extracted, the average gas phase composition being y_P. One fraction represents the useful product (n_P) and the other one is used to regenerate the neighbor column during the purge step. In the blowdown step the pressure decreases to p_L, n_B moles of gas are vented with the average composition y_B and the column remain in equilibrium with an interstitial gas phase with y_3 average nitrogen concentration. During the final step of the cycle, the pressure remain unchanged at p_L, n_G moles of oxygen enriched gas are fed at the outlet end of the column and n_R moles of gas with the average concentration y_R are vented at the inlet end of the column. At the end of the step, the bed remains in equilibrium with an interstitial gas having y_4 nitrogen concentration. Starting from the remaining y_4 equilibrium composition, this computation algorithm is continuing until the product composition reaches a constant value. At this moment the PSA unit has reached its steady state functioning.

The time duration of adsorption and purge steps is t_1 and of pressurization and blowdown is t_2. By combining the two vented gas fractions from blowdown and purge, a resulting "residue" can be obtained, having n_Z number of moles and y_Z average nitrogen mole fraction.

Subject to these considerations, the system of governing equations describing the cyclic operation is presented below.

Pressurization step (1):

Overall molar balance:

$$n_{RP} + [m_s.W^*_{1+2}(p_L,y_4) + N_{g,L}] = [m_s.W^*_{1+2}(p_H,y_1) + N_{g,H}] \quad (1)$$

Partial molar balance, made on the component 1 (nitrogen):

$$n_{RP}.y_F + [m_s.W^*_1(p_L,y_4) + y_4.N_{g,L}] = [m_s.W^*_1(p_H,y_1) + y_1.N_{g,H}] \quad (2)$$

Isobaric production step (2):

Overall molar balance:

$$n_F + [m_s.W^*_{1+2}(p_H,y_1) + N_{g,H}] = (n_P+n_G) + [m_s.W^*_{1+2}(p_H,y_2)+N_{g,H}] \quad (3)$$

Partial molar balance, made on the component 1 (nitrogen):

$$n_F.y_F + [m_s.W^*_1(p_H,y_1) + y_1.N_{g,H}] = (n_P+n_G).y_P + [m_s.W^*_1(p_H,y_2)+y_2.N_{g,H}] \quad (4)$$

Blowdown step (3):

Overall molar balance:

$$[m_s.W^*_{1+2}(p_H,y_2) + N_{g,H}] = n_B + [m_s.W^*_{1+2}(p_L,y_3) + N_{g,L}] \quad (5)$$

Partial molar balance, made on the component 1 (nitrogen):

$$[m_1.W^*_1(p_H,y_2) + y_2.N_{g,H}] = y_B.n_B + [m_s.W^*_1(p_L,y_3) + y_3.N_{g,L}] \quad (6)$$

Isobaric purge step (4):

Overall molar balance:

$$n_G + [m_s.W^*_{1+2}(p_L,y_3) + N_{g,L}] = n_R + [m_s.W^*_{1+2}(p_L,y_4) + N_{g,L}] \quad (7)$$

Partial molar balance, made on the component 1 (nitrogen):

$$n_G.y_P + [m_s.W^*_1(p_L,y_3) + y_3.N_{g,L}] = n_R.y_R + [m_s.W^*_1(p_L,y_4) + y_4.N_{g,L}] \quad (8)$$

where: $N_{g,H} = p_H.\varepsilon.A.H/(R.T)$ and $N_{g,L} = p_L.\ \varepsilon.A.H/(R.T)$

The volumetric purge-to-feed ratio (the reflux ratio) represents the ratio between the volume of purge gas V_G and feed gas V_F. The purge gas is extracted from the high purity product and recirculated in the bed at p_L during the purge step, countercurrently with the feed. The feed gas volume is considered at high pressure. The value of γ is equal to the molar ratio multiplied with the pressure ratio, as shown in equation (9).

$$\gamma = \frac{V_G(p_L)}{V_F(p_H)} = \frac{n_G}{n_F} \cdot \frac{p_H}{p_L} \quad (9)$$

The equilibrium isotherms, together with a van't HOFF type of temperature dependence, can be either linear or LANGMUIR type (i=1,2).

- linear: $W_i^* = K_i.p.y_i = W_i^*(p,y_i,T)$ (10)

$K_i = K_{oi}.\exp[q_i/(R'.T)]$ (11)

- binary LANGMUIR type:

$$W_i^* = \frac{m_i \cdot b_i(T) \cdot p \cdot y_i}{1 + b_1(T) \cdot p \cdot y_1 + b_2(T) \cdot p \cdot y_2} = W_i^*(p, y_i, T) \quad (12)$$

$b_i = c_i.\exp[q_i/(R'.T)] = b_i(T)$ (13)

The linear equations describe correctly the adsorption equilibrium of nitrogen and oxygen on 5A - ZMS only in the range of small partial pressures (up to 1 atm). Because the operation of the unit is carried out under super-atmospheric pressures, the binary LANGMUIR equation is preferred. It correlates correctly the experimental gas-solid equilibrium data on the entire range of partial pressures.

As initial conditions, the bed is considered to be in equilibrium with air, at the low pressure of the system. There is no flow trough the column.

$$y_{(t=0)} = y^o_4 = y_F; \qquad q_{(t=0)} = 0; \quad (14)$$

The average mole numbers is converted to average flow rates by using the equation of state of the ideal gases and the duration of each step of the cycle. For the isobaric steps we have:

$$G^o_{V,F} = n_F.R.T^o/(t_1.p^o), \quad G^o_{V,G} = n_G.R.T^o/(t_1.p^o), \quad G^o_{V,P} = n_P.R.T^o/(t_1.p^o) \quad (15)$$

and for the non-isobaric steps:

$$G^o_{V,RP} = n_{RP}.R.T^o/(t_2.p^o), \quad G^o_{V,B} = n_B.R.T^o/(t_2.p^o) \quad (16)$$

The model was numerically solved by NEWTON's method, applied to the systems of non-linear equation [3]. As known parameters are considered: the flow rate and the composition of the feed, the diameter and the height of the adsorption bed. There are also considered the volumetric purge-to-feed ratio (γ), the ambient temperature (T), the limiting pressures (p_H and p_L), the steps' duration t_1 and t_2, the porosity and bulk density of the adsorbent bed, equilibrium parameters. As unknown parameters, the model calculates the average flow rates and compositions of production, blowdown, purge inlet and purge outlet streams and the average composition of the interstitial gas at the end of each step. In order to obtain a unique solution for the governing system we used the following assumption: the column is operated up to very close to the breakthrough moment. That means, in the view of the local equilibrium theory that the whole adsorbent is in equilibrium with the feed gas at the end of the production step. The mathematical reflection of this assumption is equation (17):

$$y_2 = y_F \tag{17}$$

By assuming local equilibrium, the length of the mass transfer zone is neglected. So, at the breakthrough moment of the most strongly adsorbed component in the purified product, the entire bed is in equilibrium with the feed mixture. In reality, the length of the mass transfer zone cannot be neglected. The length of the mass transfer zone is significant in bulk separation, when there are more then one adsorbed component in the feed, with significantly high concentration. This is the case of oxygen/nitrogen separation on 5A –ZMS. At the breakthrough moment it's presence determines the existence of a quantity of adsorbent material that can separate new quantities of feed, amount that will not be used. From this point of view the use of a so-called "dynamic adsorption capacity", instead of the equilibrium adsorption capacity, will approach the simulated results to the experimental ones.

From the experimental breakthrough curves of the authors [12], with the help of the algorithm presented by TARAN [5], it has been estimated that the experimentally used adsorbent exhibits only 65-75% of its equilibrium adsorption capacity, in dynamic conditions. This value depends on the operating conditions, but an average value of 71% can be considered for our purpose. So, the simulations have been carried out with a correction factor of 0.71 to multiply the adsorption capacity computed from LANGMUIR type equations.

The residual wasted gas extracted from the PSA unit and collected both during blowdown and purge steps, is enriched in nitrogen and it's concentration is somewhat greater than in the feed air. The mean value of this can be computed by using the equation (18).

$$y_Z = \frac{n_B \cdot y_B + n_R \cdot y_R}{n_B + n_R} \tag{18}$$

Based on the above equations, the authors developed a computation program by using the Pascal language.

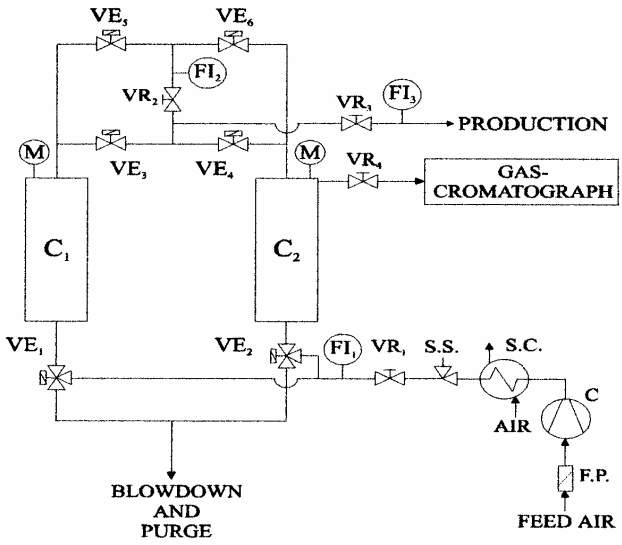

Fig. 4. The experimental PSA unit

EXPERIMENTAL

The experimental PSA unit used is shown in figure 4. It consists in two adsorption columns C_1 and C_2, six solenoid valves to lead the gas streams in order to accomplish the four steps of the cycle. There are also three flow indicators FI_1-FI_3, with the appending regulating valves, in order to measure and regulate the flow rates of feed, purge and production. Two pressure gauges M indicates the pressure at the top of the columns and the regulating valve VR_4 extract samples to the gas chromatograph coupled with a thermal conductivity detector. The compressor C feeds Air is passed trough the dust filter FP, compressed in the compressor C and cooled to atmospheric temperature in the SC cooler. The safety valve SS leads to the atmosphere the exceeding compressed air.

The dimensions and other details of the unit together with the equilibrium parameters are summarized in table 2.

Table 2.

The main parameters of the experimental PSA unit.

Adsorbent:		5A-ZMS
Adsorption bed length:	H [m]	0,51
Internal diameter of the column:	D_i [m]	0,074
Diameter of adsorbent particle:	d_p [mm]	1-2
Adsorbent porosity:	ε [/]	0,4
Bulk density of the adsorption bed:	ρ_s [kg/m^3]	772
Ambient temperature:	T [^{0}C]	20

Low pressure:	p_L [atm]	1
High pressure:	p_H [atm]	3,2
Feed flow rate:	F [Nl/min]	14-45
Production flow rate:	P [Nl/min]	0,5-3
Feed composition:		22% (oxygen + argon), 78% nitrogen
LANGMUIR parameters:		
Saturation adsorption capacity:	m_1 (N_2) [kmol/kg]	2,217.10-3
Saturation adsorption capacity:	m_2 (O_2) [kmol/kg]	3,120.10-3
Saturation adsorption capacity:	m_3 (Ar) [kmol/kg]	3,966.10-3
Pre-exponential factor:	c_1 (N_2) [atm^{-1}]	4,459.10-5
Pre-exponential factor:	c_2 (O_2) [atm^{-1}]	13,53.10-5
Pre-exponential factor:	c_3 (Ar) [atm^{-1}]	11,078.10-5
Isosteric heat of adsorption:	q_1 (N_2) [kcal/kmol]	4880
Isosteric heat of adsorption:	q_2 (O_2) [kcal/kmol]	3325
Isosteric heat of adsorption:	q_3 (Ar) [kcal/kmol]	3248

The adsorption isotherms for oxygen, nitrogen and argon on commercial 5A ZMS have been obtained at 20^{o}C, by using a volumetric method. It was fount out that the experimental values were very close to those reported by VERELST and BARON [6], so there were used the LANGMUIR parameters reported in [6].

RESULTS AND DISCUSSION

The program have been tested by using, first a set of experimental data published by FAROOQ and RUTHVEN [7] and then with a few sets of experimental data obtained on the PSA unit presented schematically in fig.4. The experimental and simulated data are presented in Table 3. In both situations the relative errors of computed oxygen purity, recovery and flow rate lied between 0.4-5%, as the experiment can be more or less approximated by the model.

In computation, we have used the dynamic adsorption capacity, instead of the equilibrium values, as we have been explained above. This takes somehow account for the finite mass transfer velocity and axial dispersion of the gas and allows a good prediction for the experimental values.

Starting from the equilibrium state of the adsorbent with air, to achieve the maximum purity of oxygen (96% O_2) the equipment needs 20-30 experimental cycles, while simulation needs only 2-6 full cycles, depending on the purge ratio. This difference has both experimental and modeling causes. The retention of humidity (2-3% v/v) and carbon dioxide (300-600 ppm) from the ambient air, both with high adsorption affinity for 5A-ZMS, follows the same cycle as the useful nitrogen-oxygen separation. So the oxygen-enriched stream is completely dry and CO_2 free (max 2 ppm humidity and max 1 ppm CO_2). A part of the bed works to accomplish that during pressurization and production steps, but this part needs also to be regenerated with the purge stream. This behavior delays a little the experimental unit to reach the steady state conditions. The mathematical model does not account for the presence of humidity and CO_2. Furthermore, to obtain compatibility for the equations' system we considered the bed operated close to the breakthrough point. These assumptions may reduce the simulated transient period time.

An important parameter that evaluates the performances of any separation equipment is the ***recovery*** fraction of the useful product from the feed. For our case it is defined [4,7,8] to be the ratio of the moles of oxygen from the main product and the moles of oxygen from the feed.

$$R_C = \frac{P \cdot y_P}{F \cdot y_F} \tag{19}$$

Table 3 presents the main experimental results compared to the simulated ones. The table covers a large range of the production composition, between 40-95% oxygen purity. We have obtained a good correlation between experimental and simulated results, especially for oxygen purity above 90%.

Table 3.

Experimental and simulated results for oxygen/nitrogen separation.

Run	F [l/kg/cycle]	PG [l/kg/cycle]	PR [l/kg/cycle]		O_2 Purity [%]		O_2 Recovery [%]	
			Exp.	Calc.	Exp.	Calc.	Exp.	Calc.
1	0,6872	0,4270	0,0809	0,0828	86,35	86,26	48,41	49,21
2	0,6536	0,4371	0,0453	0,0448	92,63	92,84	30,60	30,15
3	0,7459	0,4491	0,096	0,0974	77,45	86,32	47,77	53,34
4	0,7794	0,4251	0,1223	0,1230	71,52	86,60	53,42	64,73
5	0,7375	0,4152	0,0096	0,0101	94,61	96,00	5,86	6,23
6	0,8530	0,0253	0,0083	0,0108	70,08	68,20	53,95	68,5
7	0,6360	0,4251	0,0646	0,0498	89,34	88,42	43,18	32,75
8	1,1150	0,4626	0,0453	0,0446	88,48	94,20	17,20	17,83
9	0,5765	0,3260	0,0453	0,0457	91,89	93,20	34,38	35,14
10	0,4286	0,2741	0,0483	0,0550	67,08	67,60	35,12	41,17
11	0,3576	0,1720	0,0483	0,0512	44,35	46,47	28,55	31,69

The studied PSA configuration does not exhibit high recoveries, its' values do not exceeding 30% for oxygen purity over 90%. Even if the feed air is cheep, the major operating cost is supported by the compression energy. So the rather low recovery decreases the efficiency of the compression energy's expense. A raise of the recovery can be accomplished only with a significant decrease of the purity, for this PSA configuration. In order to obtain higher recoveries together with high purity of the enriched product, other configurations have been imagined [2], which use vacuum or intermediate pressurization steps, for oxygen separation, or even combination with other separation procedures, like in the case of helium separation [8,9].

The influence of the purge flow rate on the purity and the recovery of oxygen have been studied. The results are presented in figure 6 and 7. We have also studied the influence of the purge-to-feed ratio on the transient behavior of the PSA unit. The results are shown in figure 5.

From equation (9) we can find that a value of $\gamma = 0$ represents the zero reflux situation, when the purity of the product is minimum and the recovery is maximum. This situation is similar to the distillation. In this case the PSA separation occurs only

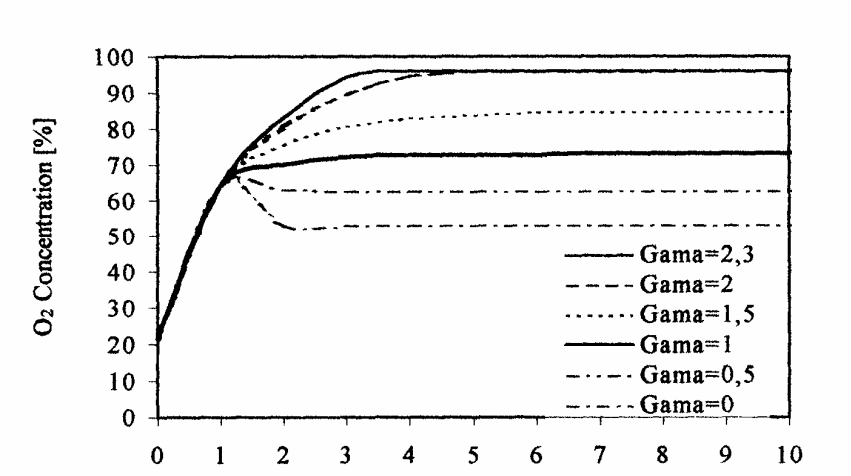

Fig. 5. The influence of the purge-to-feed ratio on the transient behavior

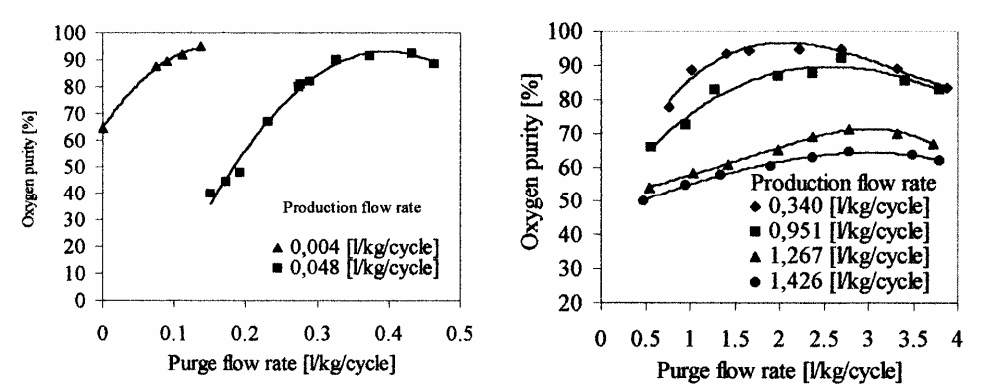

Fig. 6. The influence of the purge flow rate on the oxygen purity

during the pressurization step, when the maximum oxygen purity does not exceed 50-60%. That depends on the pressurization velocity, high and low pressure ratio, production flow rate, equilibrium and kinetic particularization. Figure 5 also shows the existence of a minimum value of the purge ratio $\gamma = 1$ that allows the achievement of a high purity product. In practice $\gamma > 1$ is required. For higher values of γ, the higher is the necessary feed rate – for a given product rate, the higher is the separation effort of the bed and the start-up transient state is longer. This, because the gain of the oxygen purity between two cycles is lower.

Figure 6 shows the influence of the reflux on the oxygen purity, at different values of the production flow rate and figure 7 on the recovery ratio, at different values of the purge flow rate. The solid lines represent simulated results and the dotted lines, the experimental ones. Figure 5 and 6 shows that increasing the purge ratio the purity of the high-pressure product can be increased and figure 7 shows that in these circumstances the recovery of the desired product lowers. The

general trend of the process indicates that for a given production flow rate, the high pressure product purity raises up to a maximum value by raising the purge flow rate and then the purity decreases slowly. The purity gain is achieved by regenerating the bed with a supplementary quantity of purge gas, with higher purity, which is obtained by raising the feed. From a certain value, the separation capacity of the column will be exceeded and the purity of the product will decrease. For each value of the production flow rate will be an optimum value of the purge rate that allows the maximum possible purity.

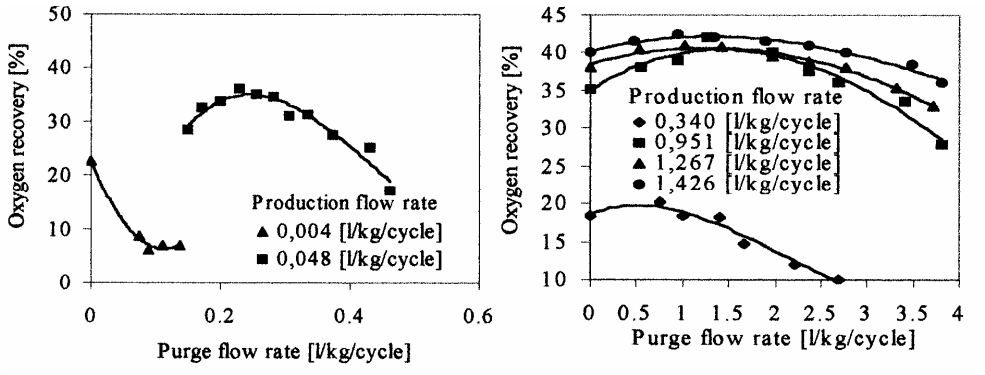

Fig. 7. The influence of the purge flow rate on the oxygen recovery.

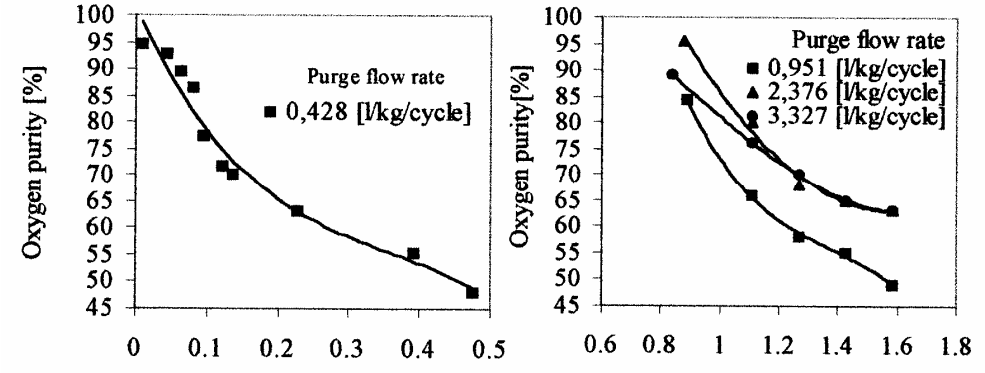

Fig. 8. The influence of the production flow rate on the oxygen purity

The trend of the oxygen recovery generally follows the trend of the purity, as can be seen in figure 7. But if at low production flow rates the recovery raise is due to the raise of the product purity, at higher production flow rates the recovery raise is due to the raise of the production flow rate. We can understand from these figures that, for a given production flow rate, the PSA unit can be operated either at high purity, with the afferent loss of purity, or at high purity, with the resulting recovery fraction, depending on the specific application.

We have also studied the influence of the production flow rate on the purity and recovery of oxygen, for a given purge flow rate. Figure 8 shows that increasing

the production flow rate the purity decreases quite rapidly. The high purity can be regained by further increase of the purge, until the separation capability of the bed starts to be exceeded. For a given value of the purge flow rate, only the raise of the feed can do the raise of the production. This determines some breakthrough of the nitrogen in the high-pressure product that lowers its purity. In any case figures 6 and 8 shows that this PSA configuration can exhibit a production spare of production capacity between 8-50%, with the afferent loss of purity. These are useful in some applications of low concentration oxygen, like water oxygenation, natural gas burning enhancement and other oxidation processes.

Figure 9 presents the influence of the production flow rate on the recovery fraction of the high-pressure product for a given purge flow rate. As the production raises, the recovery raises, despite the decreasing of the oxygen purity. From the figures we can observe that for low purge rates the raise of the recovery is greater then at higher purge rates. As the later one still raise, a new raise of the production determines a smaller raise of the recovery.

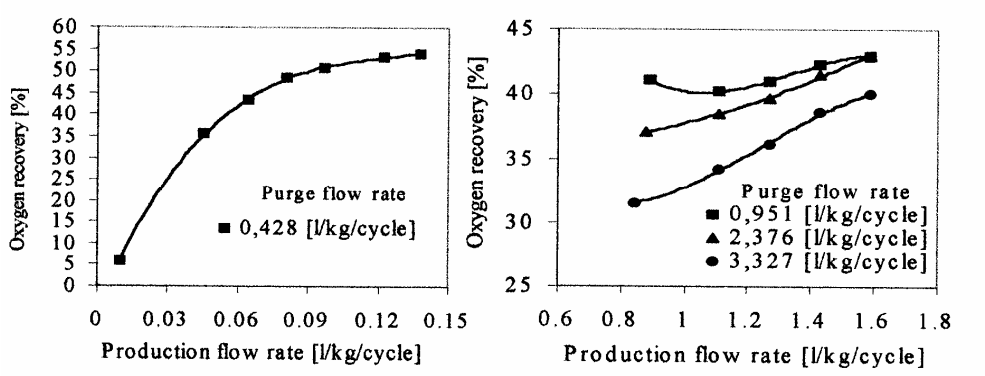

Fig. 9. The influence of the production flow rate on the oxygen purity.

For the studied PSA configuration and for oxygen purity over 90%, we cannot expect recoveries greater then 30-35%, because this purity can be obtained only with a high value of the purge-to-feed ratio, laying between 1.5-2. There have been imagined other configurations [2], by using vacuum steps instead of low pressure purge, different pressurization policies, that involves one or more pressure equalization step and higher number of columns (3 to 5) for a continuous production flow rate. Even with these improvements, the recovery fraction does not exceed about 50-55%, for oxygen concentrations above 90%.

CONCLUSIONS

An equilibrium mathematical model have been developed for the simulation a PSA unit operated with 4 steps/cycle, that separates a binary bulk feed mixture with the adsorption of both components. Based on this model, a numerical program has been carried out.

A laboratory scale PSA unit has been built, with two columns, operated with the above mentioned cycle, that separates air on 5 A zeolite molecular sieve and delivers an oxygen enriched high pressure product. We have been obtained

oxygen purity up to 94%. The experimental values obtained have been compared with the simulated ones and a good agreement has been found between these.

Some parametric studies have been accomplished by using both the experimental unit and the simulation program, in order to stand out the influence of the production and purge flow rates on the high-pressure product purity and recovery fraction. The complexity of the interdependence of the operating parameters has been emphasized. From the above shown figures, we can find the optimum values of the purge flow rate for a given yield.

NOTATION

A = cross section of the bed, m^2
$b_{1,2}$ = gas-solid interaction parameter in Langmuir equation, atm^{-1}
$c_{1,2}$ = pre-exponential parameter in Langmuir equation, atm^{-1}
D_i = internal diameter of the bed, m
F = feed flow rate
G^o_V = volumetric flow rate of the gas flow rate, Nm^3/s
H = height of the bed, m
$m_{1,2}$ = saturation adsorption capacity, kmol/kg
m_s = adsorbent quantity, kg
n = moles of gas
N_{GH} = moles of interstitial gas, at pressure p_H
N_{GL} = moles of interstitial gas, at pressure p_L
p = total pressure, atm
p_H = high pressure of the system, atm
p_L = low pressure of the system, atm
$q_{1,2}$ = isosteric heat of adsorption, in Langmuir equation, kcal/kmol
R = 0,082 m^3.atm/kmol/K, R' = 1,9872 kcal/kmol/K, gas constant
Rc = recovery fraction, %
t_1 =duration of isobaric phases, s
t_2 = duration of non-isobaric phases, s
T = temperature, K
V_F = volume of feed gas, at pressure p_H, m^3
V_G = volume of purge gas, at pressure p_L, m^3
w^o_f = gas velocity in the empty column, Nm/s
$W^*_{1,2}$ = adsorbed quantity, kmol/kg
y = molar fraction of the stronger adsorbed component
γ = volumetric purge-to-feed ratio
ε = porosity of the bed
ρ_s = bulk density of the bed, kg/m^3

REFERENCES

1. Skarstrom, C.W., U.S. Patent, 2 944 627, 1960.
2. Tondeur, D., Wankat, P.C., Sep.Purif.Methods, **14**, 1985, 2, p.157-212.
3. Démidovitch, B., Maron, I., Éléments de calcul numérique, Ed. MIR-Moscova, 1973 p.454.
4. Flores-Fernandez, G., Kenney, C.N., Chem.Eng.Sci., **38**, 1983, 6, p. 827.
5. Taran, C., în *Ingineria prelucrării hidrocarburilor*, vol. 3, cap. 7, Editura Tehnică, Bucureşti, 1987.
6. Verelst, H., Baron, J., *J.Chem.Eng.Data*, **30**, 1985, p. 66-70.
7. Farooq, S., Ruthven, D.M., Boniface, H.A., *Chem.Eng.Sci.*, **44**, 1989, 12, p. 2809.
8. Hasselden, G.G., *Gas.Sep.Purif.*, **4**, 1989, p. 209.
9. Asahara, W., Teneda, K., Tsukenda, M., *Gas Sep.Purif.*, **4**, 1988, p. 204.
10. Kleinhempel, M.T., Atanasiu, F., Literat, L., *Revista de chimie*, **46**, 1995, 8.
11. Kleinhempel, M.T., Atanasiu, M., Atanasiu, F., *Oxygen Enrichment by Pressure Swing Adsorption*, Conferința Națională de Chimie şi Inginerie Chimică, Bucureşti, octombrie 1998.
12. Kleinhempel, M.T., Mihăilescu, G., Atanasiu, M., Atanasiu, F., *Modelarea matematică a curbelor de străpungere pentru separarea oxigenului de azot*, Simpozion Național de Inginerie Chimică, Bucureşti, 1998.
13. Barrer, R.M., Sutherland, J.W., *Proc.Roy.Soc.*, **A 237**, 1956, 439.
14. Barrer, R.M., Bultitude, F.W., Sutherland, J.W., *Trans. Faraday Soc.*, **53**, 1957, 1111.
15. Ruthven, D.M., Nature, *Phy.Sci.*, **70**, 1971, p. 232.

STUDIA UNIVERSITATIS BABEŞ-BOLYAI, CHEMIA, 1-2, XLIII, 1998

REAGENTS WITH CHELATANT ACTION FOR Pb (II) AND THE POSSIBILLITY OF USING THEM IN FLOTATION

GABRIELA OPREA and CRISTINA MIHALI*

ABSTRACT. In this paper we followed up the data corelation of analitical chemistry of complexation for Pb (II) with chelatants in aqueous solution and the collector power of these reagents in the flotation of the minerals cerusite and galena that contain this ion.

INTRODUCTION

Reagents with chelatant action are used in analytical chemistry due to their selectivity to certain metal ions in solution [1]. In the formation and stability of the chelated cycles the following factors have an important role: the pH of the solution, the basicity of the ligants, the size and number of the chelated cycles, the resonance effect and the steric effects.

The following reagents with chelatant action that form chelat compounds with the ion Pb (II) in solution have been studied: 8-hydroxyquinoline (oxyne), eriochrome black T, acetylacetone, 2 hydroxyphenyl azonaphtol 2 ,2 hydroxytrimethylene-diaminotetraacetic acid.

The stability of the complex obtained between the cations and the ligants depends on the pH, the modifications resulting from the variation of the pH being characterised by the apparent constant of formation, K'.

We have taken into consideration the curves of variation log K' depending on the pH for the chelatant systems Pb (II) and Ca (II).

The role of the chelatic compound in the separation of minerals by flotation is increasing [2 - 5]. In the choice of flotation reagents it is considered that their fixation on the surface of the minerals takes place, in many cases, through chemical links between the superficial center of adsorbtion and the reagent, obtaining the chelat compounds. Because of this we can expect the reagent which has proved specific with a metallic ion in solution, to keep its selectivity in certain conditions, in the case of adsorbtion over the surface of the minerals that contain this metallic ion.

We followed the collecting action over both galene (PbS) and on ceruzite ($PbCO_{3)}$ to check how both the mineralogical form and the nature of the anion, influence the action of the collectors. The calcite that usually accompany the minerals in ores, should float very little with these reagents. To check this, the reagents with chelatant action were tested in parallel with calcite.

* *Universitatea de Nord Baia Mare, Romania.*

To study the collecting action of the reagents with chelatant action we used the flotation which has been done in the Hallimond cell. The experiments were orientated towards the determination of the optimum conditions necessary for a good recovery, the concentration of the reagent and the pH domain.

I.R. spectroscopic detemination have also been used for surveying the formation of certain species at the surface of minerals during adsorbtion of various reagents and there are many reports on this subject [6-12].

The nature of the compounds formed with the action of 8-hydroxyquinoline on ceruzite had been also studied using the I.R. spectroscopy.

EXPERIMENTAL

The Hallimond cell used is an instrument of pneumatic microflotation showed in figure1.

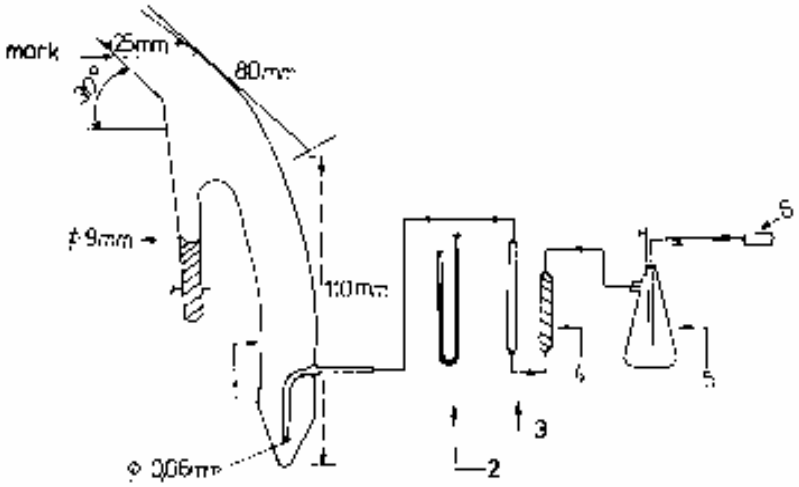

Figure 1. Instalation of microflotation: 1. Hallimond cell; 2. pressure gauge; 3. rotametre; 4 and 5 washing devices; 6. steam roller.

The minerals used, galene, ceruzite and calcite, had the grading ranging between 100-250 μ.

"A" grams of mineral are introduced in the cell. Then the cell is filled up to the mark with the solution of the pH collector, the concentration and the temperature are constant. At a small debit of air the samples are conditioned, then the debit of air increases and the particles covered by the collector are stimulated to the separation surface solution/air. Here the ballons break and the mineral particles are collected into the lateral vertical tube. Throughout this procedure, conditioning time (180 seconds), flotation time (30 seconds) and debit of air 10l/hour that was regulated from a steam roller, following the values on a pressure gauge and on a rotametre were constant. The flotated product is filtrated, dried in the drying stove at 80^{o}C and weighed with the mass "C". The unflotated product is reccovered just the same

having the mass "m". It has been observed that the difference between A and C+m is under 5%. That is why in determinations only C has been weighted.

The procent of recuperation, %R (the extraction in weight or the extraction in concentrate) has been obtained by the raport between the mass of the flotant mineral "C" and the mass of the alimented mineral "A".

$$\%R = (C/C+m) \cdot 100 = (C/A) \cdot 100$$

We have used 1 gram mineral. This means that A = 1 gram.

The preparation of the reagent solutions has been done in 1l marked ballone such as

- 0,23 g eriochrome black T are dissolved in water, it is brought to the mark and a solution $5 \cdot 10^{-4}$ M is obtained.
- 14,5 g oxyne are dissolved in acetone and are brought to the mark; a solution 10^{-1} M is obtained which is diluated to obtain the tested solution.
- 1 g acetylacetone is dissolved in water, it is brought to the mark and a solution 10^{-2} M is obtained which is diluated to obtain the tested solutions.
- 0,023 g 2 hydroxyphenyl azonaphtol 2 are dissolved in 6 cm^3 solution 0,25 N NaOH and 10 cm^3 acetone, 300 cm^3 of water is added and it is stirred after which it is brought to the mark with water.
- for a solution 10^{-2} M 2 hydroxytrimethilenediaminotetraacetic acid 3,223 g reagent in 40 cm^3 solution NaOH 10% is dissolved and then it is brought to the mark. The tested solution is 10^{-4} M and it is obtained by dilution.

The I.R. spectra have been realised using the technique of the potasium bromure tablets for ceruzite, Pb (II) oxynate and ceruzite after being treated with solution of oxyne in acetone.

- the natural pure ceruzite has been ground in the agate mortar till 2-10 μ; part of the sample obtained is used to draw the spectrum I.R.; some part of the sample is treated with solution of oxine in acetone for pH = 9, followed by filtration, drying in air and the drawing of the I.R. spectra.
- the Pb (II) oxynate was prepared by using 150 cm^3 aqueous solution of $Pb(CH_3COO)_2 \cdot 3H_2O$ 0,1 M which is treated with 100 cm^3 oxyne 0,3 M solution in acetic acid 10%, it is warmed up and 25 cm^3 oxyne are added; on cooling the pH is established at 10 by NH_4OH, it is filtrated, washed and dried in a drying stove, for one hour at 110^o C.

RESULTS AND DISCUSSIONS

Eriochrome black T

This reagent presents the structure Ia and forms the chelat compound with structure Ib for Pb (II).

The curves from figure 2 indicates the variation of the apparent constant ($\log K^{'}$) with the pH for the complexes formed between Pb (II) and Ca (II) with eriochrome black T. A stabillity is noticed, not too big, for Pb(II) in the domain of pH between 7 and 10. Between 6 and 8 allows the separation from the Ca (II).

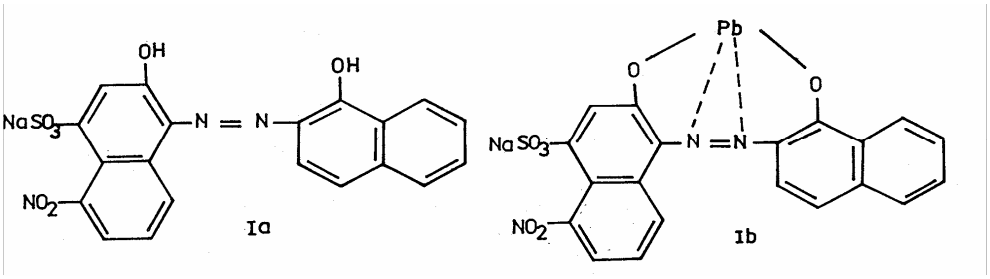

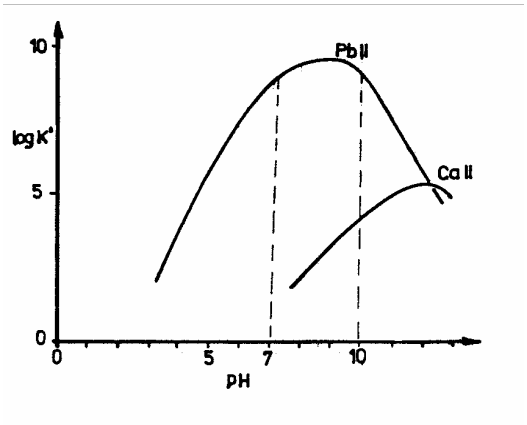

Figure 2. The variation of log K ' with the pH for the complexes of eriochrome black T with Pb (II) and Ca (II).

For flotation we used solution 5 $\cdot 10^{-4}$ mol/l in the presence of 0,1 g/l isooctane (for a suitable foam). Figure 3 shows the variation of the recuperation percent, %R depending on the pH for galena, ceruzite and calcite.

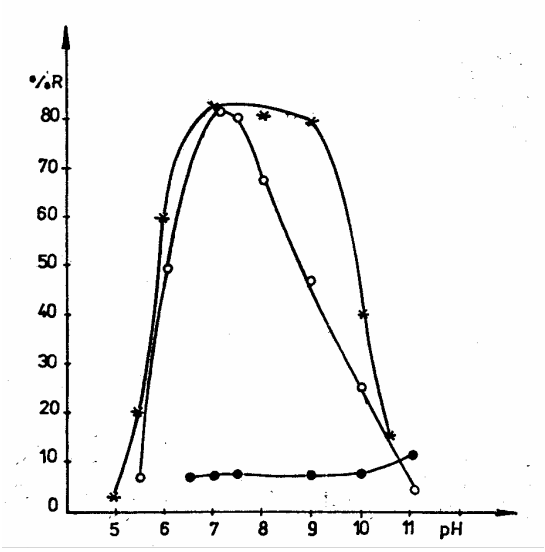

Figure 3. The variation of the recovery procent (%R) depending on the pH for 0,23 g/l eriochrome black T and 0,1 g/l izooctane for:
✱ galene
o ceruzite
● calcite.

It is noticed that eriochrome black T floats with good results for galene and ceruzite, achieving maximum recuperations of 82% for pH = 7. The calcite floats very little. The results are in concordance with the foresights deducted from the data in analitical chemistry.For ceruzite at pH = 7 had determinations been made using reagent solutions of different concentrations in the presence and in the absence of isooctane. The results are presented in Table 1.

Table 1.

Ceruzite variation %R with the concentration of eriochrome black T solution.

concentration eriochrome black T, mol/l $\cdot 10^{-4}$		0,25	2,5	5	10	15	20
%R ceruzite	with 0,1 g/l izooctane	78	80	82	80	76	74
	without izooctane	12	24	30	28	30	28

The recuperations are high, 78% even if concentration in the reagent is small, 0,25 $\cdot 10^{-4}$ mol/l in the presence of isooctane.

8 - hydroxyquinoline

This reagent presents the structure IIa and forms with Pb (II) a chelat compound with structure IIb.

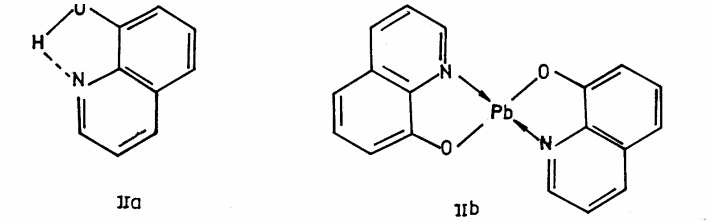

If the precipitation takes place in solution, the Pb (II) oxynate presents the maximum stability for the pH between 8 and 11, as indicated in figure 4.

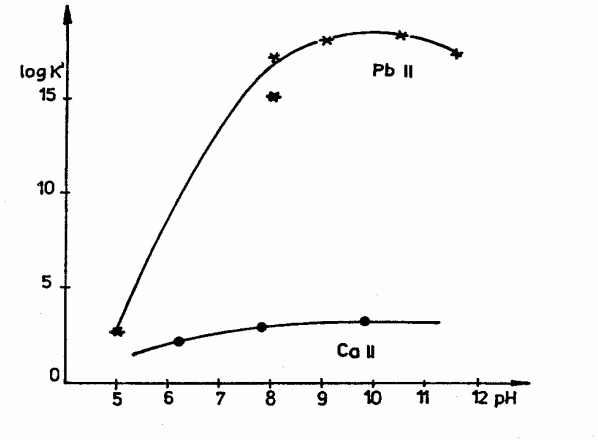

Figure 4. The variation of log K' with the pH for the Pb (II) oxynate and Ca (II) oxynate.

During the determinations in the Halimond cell we have maintained constant the concentration of the oxine, 10^{-3} mol/l, in the presence of 0,1 g/l diesel oil and we have changed the pH from 5 to 12.

Figure 5 shows the variation of the recovery percent depending on the pH for galene, ceruzite and calcite. The maximum recovery of 98% or 100% was obtained for galene with the pH between 8 and 11 and for ceruzite with the pH between 9 and 10. Calcite is to a certain extent floatable with oxyne. Galene and ceruzite float well for the same domaine of pH where the stability of the chelats formed in solution is maximum.

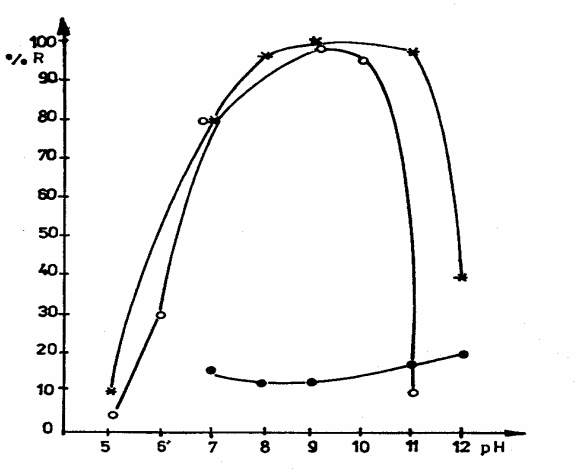

Figure 5. The variation of the recovery percent (%R) depending on the pH with 0,145 g/l oxine and 0,1 g/l diesel oil for:
✸ galene
o ceruzite
● calcite.

For ceruzite with pH = 9 we have followed the variation %R depending on the concentration of the oxyne solution in the presence and in the absence of diesel oil, table 2.The maximum recovery (100%) is obtained only in the presence of diesel oil and at the minimum concentration of 10^{-3} mol/l oxyne.

Table 2.

The variation %R of ceruzite with the concentration of oxyne.

concentration oxyne mol/l $\cdot 10^{-3}$		0,2	0,5	1	2	3	6	8	10
%R ceruzite	with 0,1 g/l diesel oil	10	70	100	98	100	98	30	20
	without diesel oil	2	-	2	-	3	-	-	-

The oxyne has a superior critical concentration of 6 $\cdot 10^{-3}$ mol/l because ceruzite is a mineral with a big mass and which, if under concentrations of oxyne forms heavy compounds that reach the surface with great difficulty.

The experiments without diesel oil show that there does not exist a possibbility of ceruzite flotation only with oxyne.

Acetylacetone

It presents the structure IIIa,b and forms the chelate compound with the structure IIIc for Pb (II).

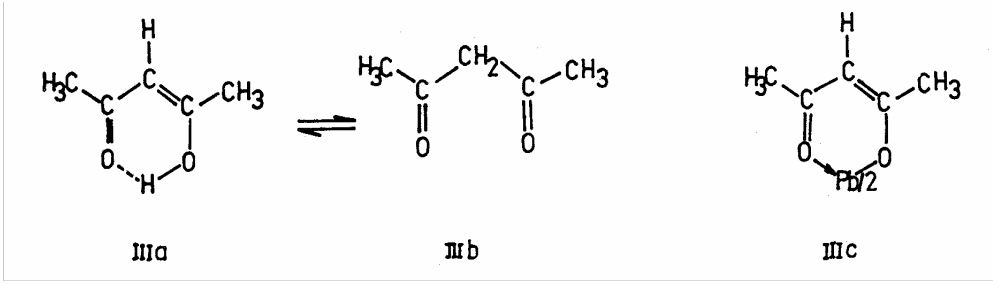

From figure 6 it can be seen that acetylacetonate of Pb (II) has small stability, respectively log $K' < 6$.

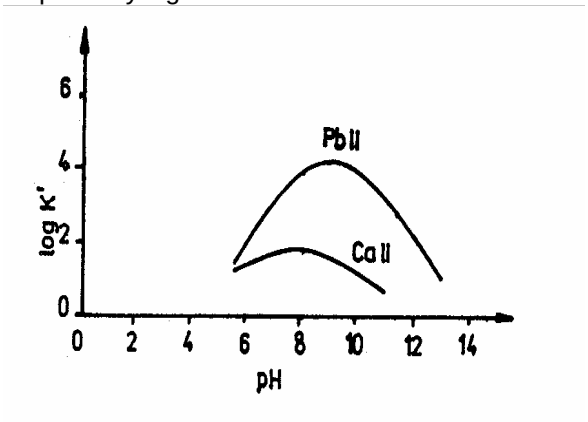

Figure 6. The variation of log K' with the pH for Pb (II) and Ca (II) acetylacetonate.

The tested solution includes 0,5 g/l acetone, that means $5 \cdot 10^{-3}$ mol/l and 0,1 g/l isooctane.We have worked with a pH between 5,5 and 10,5 for galene, ceruzite and calcite. The experimental results are presented in figure 7.

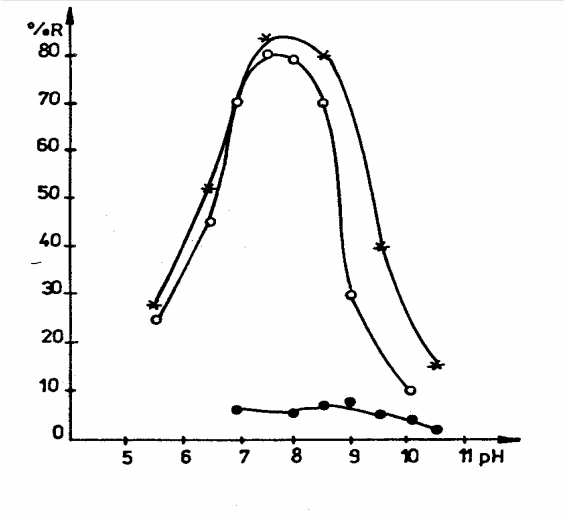

Figure 7. The variation of %R depending on the pH with 0,5 g/l acetylacetone and 0,1 g/l isooctane for:
✷ galene
o ceruzite
● calcite.

It can be noticed that galene and ceruzite float well maximum recuperations of 84% for galene and 80% for ceruzite at pH = 7,5 being realised. The result obtained is in contradiction with the small stability of the chelates Pb (II) with acetylacetone in solution.

2 hydroxyphenyl azonaphtol 2

This reagent presents the structure IVa and forms with Pb (II) a chelat compound with the structure IVb.

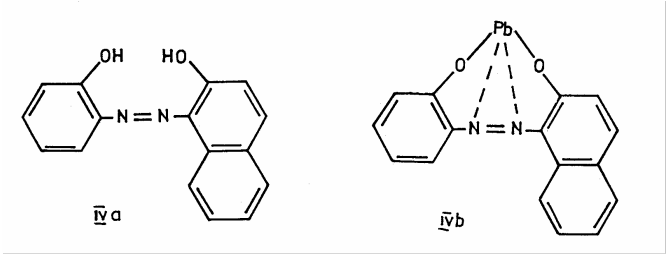

The chelat compound formed in solution has a maximum stability for the pH between 7 and 10, as shown in figure 8.

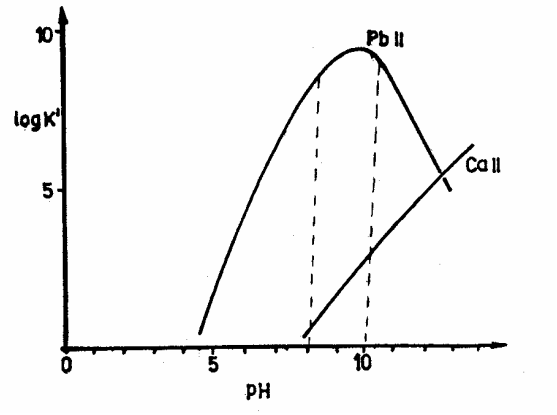

Figure 8. The variation log K" with the pH for the compounds formed by 2 hydroxy-phenyl azonaphtol with Pb (II) and Ca (II).

The solution tested for flotation gives sufficient foam without isooctane. The pH used was between 6 and 9,5.The results presented in figure 9 show that the maximum recoveries are 68% for galene and 64% for ceruzite both for pH = 7,5. Calcite floats little, only 14%, for pH = 9,5.

The results obtained are in concordance with the foresights deducted from the data of analitical chemistry.

2 hydroxytrimethylenediaminotetraacetic acid

The reagent presents the structure Va and forms stable compounds with Pb (II) in solution with the structure Vb,for pH between 7 and 10, as shown in figure 10.

This solution does not float ceruzite and galene in contradiction with the pretty high stability of the Pb (II) chelat compounds in solution.

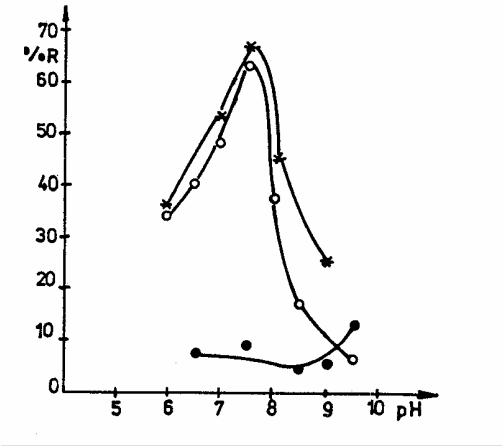

Figure 9. The variation of %R depending on the pH with 0,023 g/l 2 hydroxyphenyl azonaphtol 2 for:
✸ galene
o ceruzite
● calcite.

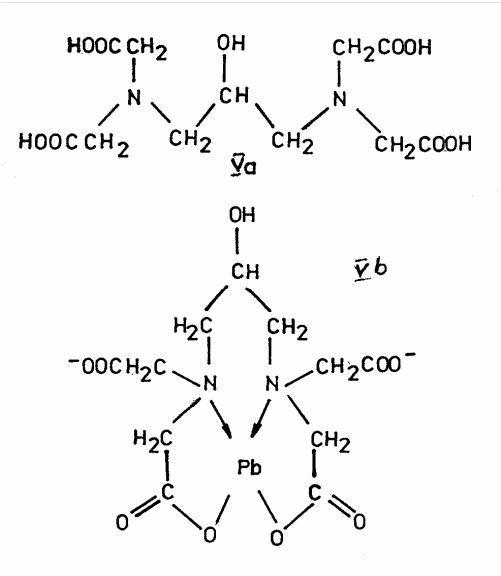

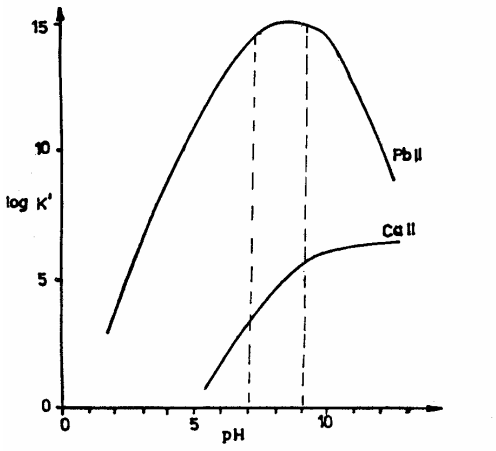

Figure 10. The variation log K' with the pH for the compounds formed by 2 hydroxy trimethyl-enediamino-tetraacetic acid with Pb (II) and Ca (II).

The spectra I.R. for the system 8 - hydroxyquinoline - ceruzite

In figure 11 are reunited the spectra I.R. for pure ceruzite, curve (a), Pb (II) oxinate, curve (b) and ceruzite after the treatement with oxyne solution in acetone with pH = 9, curve (c), respectively. By comparing the spectres we can notice the presence of bands characteristic to the Pb (II) oxynate from 1320, 1280, 1110, 865, 728 cm^{-1} in the spectre of ceruzite treated with 8 - hydroxyquinoline. Therefore on the surface of ceruzite treated with the solution of reagent with chelatant action is formed the Pb (II) oxynate.

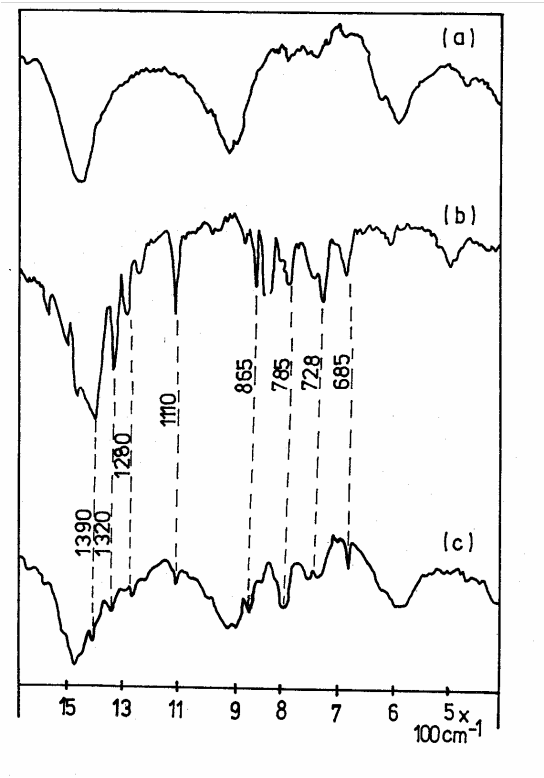

Figure 11. The I.R. spectra indicating the adsorbtion of oxyne onto ceruzite a) ceruzite in KBr b) Pb (II) oxynate c) ceruzite after treatment with acetone solution of oxyne.

CONCLUSIONS

8- hydroxyquinoline floats well galene and ceruzite and the maximum recoveries takes place in a pH domain where the stability of the chelat complexes formed is also maximum, the collector system must contain both oxyne and diesel oil, because oxyne forms along with the cation Pb (II) on the surface of the mineral insoluble metallic chelats to which diesel oil adheres by physical adsorbtion, ensuring the hydrophobization of the mineral.

Eriochrome black T in the presence of isooctane and ***2 hydroxyphenyl azonaphtol 2*** in the absence of isooctane float well galene and ceruzite, the results being in concordance with the foresights deducted from the data of analitical chemistry referring to the apparent constant of complexation and the pH domain for chelats formed with Pb (II) in solution.

Acetylacetone floats well galene and ceruzite in the presence of isooctane, in contradiction with the small stability of the Pb (II) chelats with this reagent in solution.

2 hydroxytrimethilenediaminotetraacetic acid forms stabile compounds with Pb (II) in solution but it does not float the analysed minerales.

Calcite floats very little with the mentioned reagents.

For the reagents 8 - hydroxyquinoline, eriochrome black T, 2 hydroxyphenyl azonaphtol 2 and acetylacetone, the achieved recoveries for ceruzite (Pb (II) oxidized mineral) are comparable to those achived for galena (sulphure). Thus, by using a reagent with chelatant action we can remove the barrier between the sulphuric non-ferrous minerals and the oxidical ones which do not behave identically under the action of the same conventional collector.

The I.R. spectra analysed in the present work give evidence of the formation of Pb(II) oxinate on the surface of ceruzite during the flotation process in which 8-hydroxyquinoline is used as a collector. This evidence is supported by the numerous bands belonging to Pb (II) oxynate in the I.R. spectrum of ceruzite treated with the reagent with chelatant action.

REFERENCES

1. A. Rigbom, Les complexes en chimie analitique, Dunod, Paris (1967).
2. G. Rinelli, A. M. Marabini, International Minerala Processing Congress, London (1978).
3. S. Mukai, I. Wakamatsu, 11th International Minerala Processing Congress, Cagliari (1975).
4. J.L. Cecille, M. J. Cruz, G. Barbery, J. J. Fripiat, Journal of Colloid and Interface Science (1980).
5. G. Oprea, Scientific Symposium with International Participation: Technologies for processing of refractory raw materials and for environment protection in areas with extractive industry, vol. I, p. 127-135, Baia Mare, 17-19 May (1995).
6. V. M. Lovel, L. A. Goold, N. P. Finkelstein, Internat. J. Mineral Process. ;vol. 1, p. 183 (1974).
7. R. G. Grendler, J. Phis. Chem.; vol. 66, p. 879 (1962).
8. J. Mielczarski, P. Novak, J. W. Strojek, A. Pomianowski, 13th Internat. Miner. Process. Congress. Varszawa, p. 61 (1979).
9. G. Rinelli, A. M. Marabini, V. Aless, Symposium A. M. Gaudin Flotation, vol. 1, p. 549-560, AIME, New York (1976).
10. S. Raghavan, D. W. Fuerstenau, J. Colloid Interface Sci. ; vol. 50, p. 319-330 (1975).
11. G. Oprea, International Beijing Conference and Exhibition on the Instrumental Analisis,BCEIA 1997, 14-17 Octombre, China (1997), in press.
12. G. Oprea, The Conference of Chemistry and Chemical Engineering, vol. III, part I, p. 115-121, Bucuresti, 20-21 Octombre (1995).

STUDIA UNIVERSITATIS BABEŞ-BOLYAI. CHEMIA, XLIII, 1-2, 1998

SOLVENT EXTRACTION-SPECTROPHOTOMETRIC DETERMINATION OF ANIONIC SURFACTANTS IN WASTE WATER WITH CATIONIC DYES

GABRIELA OPREA and CRISTINA MIHALI*

ABSTRACT. Anionic surfactants have large applications in household cleaning and in many industrial fields but they are also environmental pollutants. We used the solvent extraction-spectrophotometric method to determinate the anionic surfactants in aqueous solutions and waste water samples using cationic dyes. We determined the effects of experimental variables as pH, dye concentration, shaking and standing time and we discovered the best procedure. We followed the pollution level of Săsar River during the first six month in 1996-1998. We tested the concordance between the extractive-spectrophotometric method with ethyl violet and the standard methylene blue method.

INTRODUCTION

Surfactants are playing an increasingly important role in industrial applications and household cleaning. Typical anionic surfactants contain anionic and hydrophobic part and both contribute to the surfactant physicochemical properties. The most important classes of anionic surfactants are the long chain alkanesulfonates (RSO_3^-), alkylsulfates ($ROSO_3^-$) and linear alkylbenzensulfonates (LAS). All these anionic surfactants are water-soluble and are widely used in commercial products and processes in which detergent action is required. Anionic surfactants are also environmental pollutants. Although some parts of the anionic surfactants used for washing are discharged into the aquatic environment by sewer systems and waste water treatment plants, considerable parts of them are drained off directly in the aquatic environment. Anionic surfactants have a negative impact on waters because, even in small amount can cause a lowering of the water surface tension. Anionic surfactants emulsify greases and oils, disperse the colloids making difficult their sedimentation. Surfactants produce thin films at the air-water interface and perturb the air-water transport of oxygen with negative effects on the aquatic life.

Due to their large solubility, the surfactants are able to modify the soil permeability and, in certain conditions, to penetrate into and to impurify the underground water.The determination of anionic surfactants at concentration of traces amount is often necessary in waste water control. Among the analytical methods described in the literature, those based on spectrophotometric measurement constitute an important part [1-6].

*Universitatea de Nord Baia Mare, Catedra de Chimie, Romania.

Almost all of the methods used for the spectrophotometric determination of anionic surfactants depend on the formation of a salt, an ion associate between the bulky anion of anionic surfactant such as RSO_3^- or RSO_4^- and a cation. The cationic substance can be a basic dye, among them the most known is methylene blue. That's why anionic surfactants are also called methylene blue active substances. The anion of anionic surfactant and the cationic dye makes up a colored and hydrophobic complex, which can be extracted using a suitable organic solvent. The absorbance of this complex, which depends on the surfactant concentration, can be examined with a spectrophotometer.

Other cationic dyes used for anionic surfactants determinations by extractive-spectrophotometric method are methyl green and crystal violet.

We try to use another cationic dye, which forms a hydrophobic ion associate with the surfactant anion according the following reaction:

$$A^- Na^+ + C^+ X^- \rightarrow A^- C^+ + Na^+ X^-$$

where A^- is the surfactant anion and $C^+ X^-$ is the cationic dye.

To be suitable in the extractive spectrophotometric determination of anionic surfactants, the ionic associate $A^- C^+$ must have a large extractibility into a certain organic solvent and also the organic extract has to present a good molar absorptivity.

Among the cationic dyes we used ethyl violet as reagent in the extractive spectrophotometric method. We used as extracting solvent benzene and toluene. In the paper we followed to establish the best condition for the use of ethyl violet in the anionic surfactants determination in wastewaters, using the solvent-extraction method.

EXPERIMENTAL

During the first six months of 1996 – 1998 we followed the anionic surfactants pollution level for the water of Săsar River that passes through the center of Baia Mare.

We determined the anionic surfactants concentration using the standard method based on methyl blue. For the absorbance measurement we used a spectrophotometer Jenway with glass cells of 10-mm path length and for pH measurements was used a Cast pH meter equipped with a combined electrode. As etalon surfactant for preparing the surfactant solutions with known concentration we used sodium lauryl sulfate from Merck, with the purity of 99%.

We evaluated ethyl violet as a reagent for extractive spetrophotometric determination of the anionic surfactants using sodium lauryl sulfate 3×10^{-7} M and 4×10^{-7} M. It was used a 10^{-3} M solution of ethyl violet. To extract the ionic associate complex between sodium lauryl sulphate and ethyl violet were used benzene and toluene. To mentain the pH sample solution in a certain range we used acetate and phosphate buffer solutions.

After a series of experiments we established the following method: 100 ml from the sample that contains anionic surfactants are introduced into the funnel. Then 5 ml acetate and phosphate buffer, 2 ml ethyl violet solution 10^{-3} M and 5 ml extraction solvent are added. After shaking the funnel for 5 minutes the organic phase is separated from the aqueous phase. The organic phase absorbance is measured at maximum absorbance wavelength (615 nm).

In the case of waste water determination the phases' separation is more difficult. 5 ml sodium sulfate 1 M are added for a faster phases' separation and 90 ml aqueous phase was discarded. This way the phases' separation time was reduced from 20-60 minutes to 1 minute. We tested the concordance between the standard method and ethyl violet method for the anionic surfactant determination. For the measurement were used samples of Săsar River at its emergence from Baia Mare.

RESULTS AND DISCUSSIONS

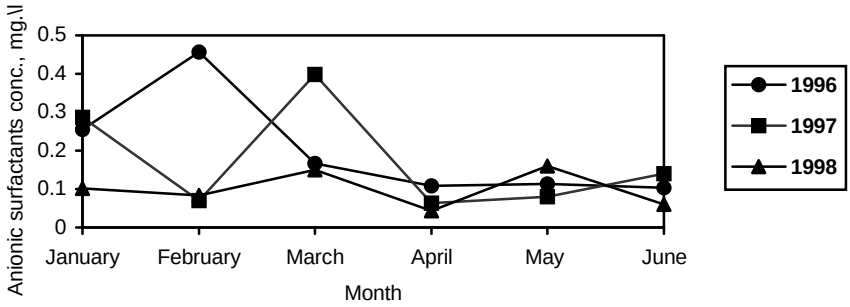

Fig. 1. Levels of anionic surfactant concentrations monitored the first six month, 1996-1998

The anionic surfactant pollution development of Săsar river water during the first 6 months of 1996 - 1998 is represented in figure 1 and 2.
The samples had a concentration of anionic surfactants that varied between 0,1-0,5 mg/l that correspond to a slight anionic surfactant pollution.

A decrease in the level of anionic surfactant pollution of Săsar River was observed.

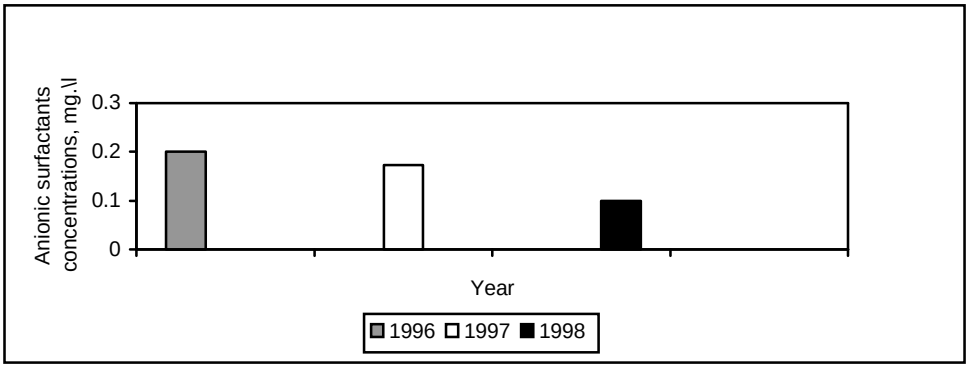

Fig. 2. The average values of the anionic surfactants concentrations at Săsar River, monitored the first 6 month, 1996-1998

This decrease is shown in figure 2 where are presented the average anionic surfactant concentrations for the first 6 months of 1996 - 1998.

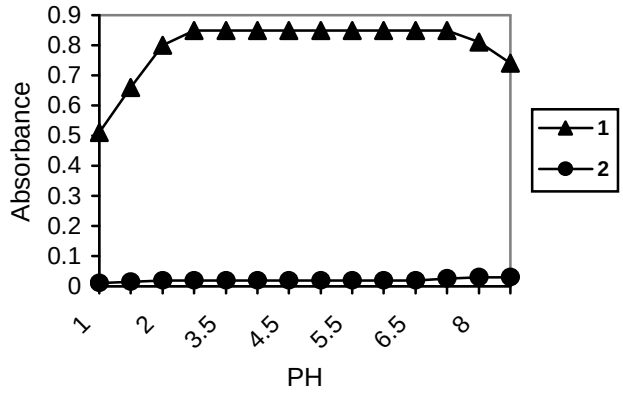

Fig. 3. Effect of pH on the extraction with benzene (anionic surfactant, sodium lauryl sulfate SLS)
Curve 1:benzene extract, $[SLS]_{initially}$ $4x10^{-7}$ M, reference, reagent blank)
Curve 2: reagent blank (reference, solvent)

To establish the best working conditions for the measurement of anionic surfactant with ethyl violet we made a series of determinations following the sample pH influence upon the absorbance values. We mentained the ethyl violet volume at 5 ml and the shaking time at 5 minutes. The results are presented in figure 3 and 4.

As it is shown in figure 3 the absorbance of the complex benzene extract was maximum for a pH between 3.5 and 6.5. In this pH range the absorbance is constant. It increases for a pH between 1 and 3.5 and it decreases for pH above 6.5.

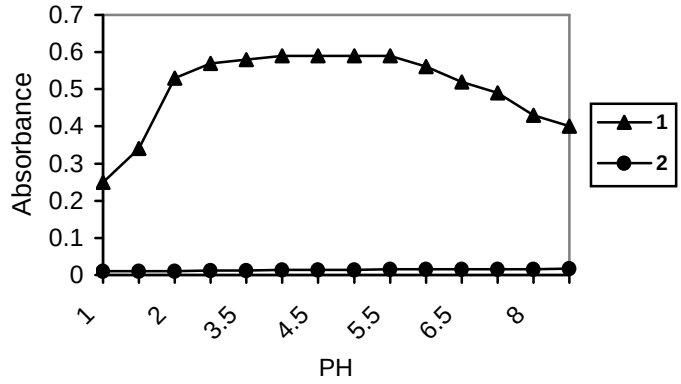

Fig. 4. Effect of pH on the extraction with toluene (anionic surfactant, sodium lauryl sulfate SLS)
Curve 1: toluene extract, $[SLS]_{initially}$ $3x10^{-7}$ M, reference, reagent blank;
Curve 2: reagent blank; reference, solvent

In the case of complex toluene extract the absorbance was maximum for a pH between 3.5 and 6,5. Depending on the results obtained we chose pH=5 from the maximum absorbance range.

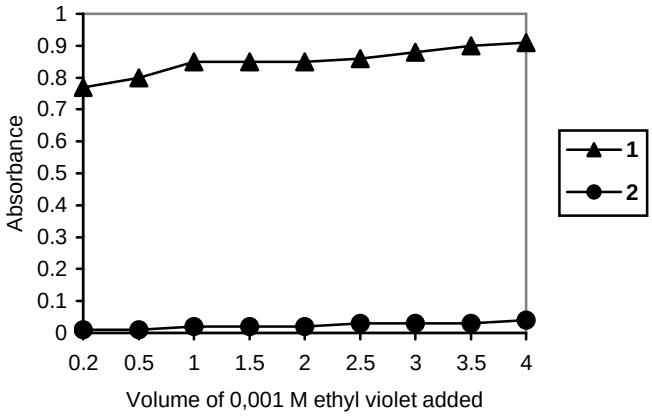

Fig. 5. Effect of 0,001 M ethyl violet volume on the extraction with benzene (anionic surfactant SLS)
Curve 1: benzene extract, $[SLS]_{initially}=4x10^{-7}M$; reference, reagent blank)
Curve 2: reagent blank; reference, solvent

In another series of determinations we maintained pH=5 and we varied the ethyl violet solution volume from 0.2 to 4 ml. As it is shown in figure 5 the absorbance was maximum and constant for 1 to 2.5 ml ethyl violet solution for benzene.

In the case of toluene extract maximum and constant absorbances were obtained at the amounts from 1 to 3 ml 10^{-3}Methyl violet. The results are shown in figure 6.

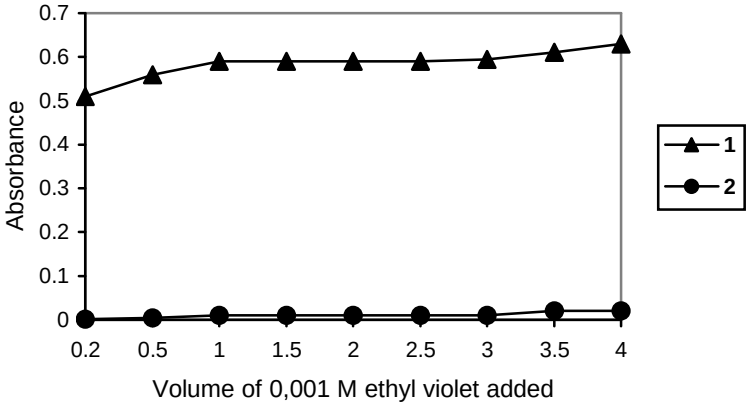

Fig. 6. Effect of 0,001 M ethyl violet volume on the extraction with toluene (anionic surfactant SLS)
Curve 1: toluene extract, $[SLS]_{initially}=3x10^{-7}M$; reference, reagent blank)
Curve 2: reagent blank; reference, solvent

Based on the determinations made, we considered pH=5 and 2ml ethyl violet as the best conditions.

It was also examinated the shaking time on the absorbance value. It was found that the value of absorbance is constant for a shaking time above 3 minutes. The experimental determinations were made using a shaking time of 5 minutes.

The wastewater samples contain colloids and suspensions and during the shaking time an emulsion that provides the increase of the time necessar to the separation phases is obtained. But, by adding a 1 M sodium sulfate solution as salting-out agent this time can be reduced from 20 minutes to 1 minute.

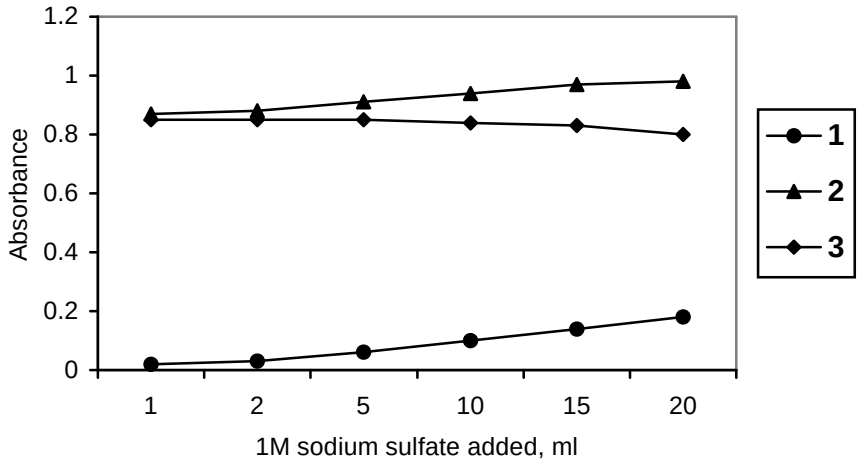

Fig. 7. Effect of salting-out agent (Na_2SO_4 1M) on the extraction with benzene (anionic surfactant SLS)
Curve 1: reagent blank; reference, solvent;
Curve 2: benzene extract, $[SLS]_{initially}=4x10^{-7}$M; reference, reagent blank;
Curve 3: benzene extract, $[SLS]_{initially}=4x10^{-7}$M; reference, reagent blank (net).

It was tested the effect of the salting-out agent volume added to the extraction system. In the case of benzene extraction the reagent blank absorbance increased proportionally with the salting-out agent volume added. The results are shown in figure 7.

The salting-out agent causes the increase of the sample's absorbance and also the reagent blank' absorbance and in conclusion the net absorbance value is not influenced.

In the case of the toluene extraction was observed that the salting-out agent does not influence the absorbance.

The method determined for ethyl violet used for the measurements of the anionic surfactants was tested on 6 samples. Every result is the average of three measurements. The samples from 1 to 3 are from Săsar River and 4 to 6 from the entering into the wastewater treatment plant.

The results obtained are shown in Table 1.They are compared with those from the methylene blue standard method. A good concordance was observed.

Table 1.

Determination of anionic surfactants on wastewater samples

Sample		Concentrates found, mg.\ l	
		Methylene blue method	Ethyl violet method
1.	Săsar River water 1	0,121	0,117
2.	Săsar River water 2	0,044	o,o42
3.	Săsar River water 3	0,016	0,015
4.	Wastewater treatment plant sample 1	0,336	0,319
5.	Wastewater treatment plant sample 2	0,114	0,1o9
6.	Wastewater treatment plant sample 3	0,568	0,557

CONCLUSIONS

The cationic dye ethyl violet was tested as a reagent for the anionic surfactants determination from water. The best procedure was established for pH=5 and 2 ml ethyl violet.

In the case of waste waters to decrease the phases separation time from 20 minutes to 1 minute, 5 ml sodium sulfate solution 1 M was added.

It was found that toluene is more useful than benzene because the reagent blank absorbance is smaller than that of benzene and toluene is less toxic than benzene.

The results of the determinations made with ethyl violet are in good concordance with those obtained with standard method, but ethyl violet method is simpler and faster because a single extraction is necessary.

REFERENCES

1. K. Higuchi, Y. Shimoishi, H. Miyata, K. T∗el, T. Hayami, Analyst, 1980, **105**, 768-
2. D. C. Abbott, Analyst, 1963, **88**, 240-241
3. S. Motomizu, S. Fujiwara, A. Fujiwara, K. T∗el, Anal. Chem., 1982, **54**, 392-397
4. H. Kubota, M. Idei, S. Motomizu, Analyst, 1990, **115**, 1109-1115
5. Y. Shimoishi, N. Saito, H. Miyato, M. Zenki, Analytical Sciences, 1997, **13**, 365-368
6. K. Fytianos, D. Vasilikakis, N. Raikos, J. Environ. Sci. Health, 1997, **A32**, 953-962

STUDIA UNIVERSITATIS BABEŞ-BOLYAI, CHEMIA, XLIII, 1-2, 1998

OXIDATION OF R-(+)- LIMONENE WITH HYDROGEN PEROXIDE CATALYZED BY POLYOXOMETALATE COMPLEXES

IOAN CRISTEA*, ERIKA KOZMA

ABSTRACT. The oxidation of R-(+)-limonene (***1***) by d-electron-transition-metal-substituted polyoxometalate complexes (TMSP) with hydrogen peroxide as oxidant in acetone at 50^0C has been studied. In all cases, 1-methyl-4-(1-methylethenyl)-1,2-cyclohexanediol (***2a***, only one diastereoisomer) was the major oxidation product (around 30% yield).

INTRODUCTION

The development of new catalytic systems for selective oxidation of olefins by simple and stable peroxides (t-butyl hydroperoxide, hydrogen peroxide), continues to be the focus of many researches to develop new technologies for future industrial applications.

The oxidation of organic substrates with aqueous hydrogen peroxide is very atractive from the viewpoint of industrial technology anf synthetic organic chemistry since aqueous hydrogen peroxide is cheap and easy to handle. For instance, extensive attention has been devoted for a long time to the direct epoxidation of olefins by aqueous hydrogen peroxide. The transition metals are widely useful in many organic reactions, especially in oxidation of organic substrates. For the activation of hydrogen peroxide, catalytically active intermediates may be classified by the mechanism of their reaction. Thus, heterolytic cleavage is common for electron-poor d^0 complexes of Ti, V, Mo, W and Re. In the intermediate peroxo complex, the O-O bond is polarized, leading to transfer of an electrophilic oxigen to a nucleophilic substrate as in epoxidation of alkenes.

In recent years, it has been reported that olefins can be epoxidized by molybdenum and tungsten derivatives as catalysts with dilute hydrogen peroxide under phase-transfer conditions [1,2]. Heteropoly acids (HPA) such as 12-molybdophosphoric acid ($H_3PMo_{12}O_{40}$) or 12-tungstophosphoric acid ($H_3PW_{12}O_{40}$) are often used not only for the acid-catalyzed reactions, but also for many oxidation of organic substrates [3].

Other transition metal oxygen anion clusters (polyoxometalates) are widely useful in many organic reactions, especially in oxidation of organic substrates [4-9].

R-(+)-limonene one of the most inexpensive natural product was the purpose of many researches concerned the oxidation of it to carvone. With low reggae and

* *Universitatea "Babeş-Bolyai", Facultatea de Chimie şi Inginerie Chimică, Catedra de Chimie Organică, Str. Arany Janos, nr. 11, 3400, Cluj-Napoca, Romania, Fax: 40-64-190818, e-mail: cristea@chem.ubbcluj.ro*

stereoselectivity, oxidation of limonene leads to a mixture of many products, both epoxides (1,2-epoxide, 8,9-epoxide and dioxide), diols and allylic oxidation products (cis and trans carveol, carvone, cis and trans dihydrocarvone, isopiperitenone etc).

In most cases, chromium (VI) reagents (t-butyl chromate [10], chromium trioxide in pyridine [11] have the best results in allylic oxidation of limonene to carvone (20-30% yield), but a large molar excess of complex to substrate 15:1 is required.

More recently, the TMSP complexes [11] and metalloporphirin catalysts [13] were used in epoxidation of limonene. Thus, epoxidation of (+)-limonene with the Mn(III) Wells-Dawson TMSP gave a 53% yield of 1,2-epoxide and a 22% yield of 8,9-epoxide [12]. Zeolites have also been successfully employed in allylic oxidation of limonene to carvone [14,15].

RESULTS AND DISCUSSION

In this paper we report on the use of transition metal substituted Keggin type polyoxometalates (TMSP) with the general formula, $Me^{n+}[PMo_xV_yO_{40}]$, as catalysts, in the oxidation of (+)-limonene. The reaction was performed in liquid homogeneous phase, by dissolving the catalyst in a small amount of hydrogen peroxide (35%), then added to the acetone solution of substrate. The aqueous hydrogen peroxide (35%), was then dropwise added, and the reaction mixture stirred for an extended period of time (10h) at 50^0C. The reaction was monitored by GC-MS analysis using a 20m methylsilicone capillary column. In all cases, the limonene was predominantly epoxidized to the endocyclic double bond to give 1,2-epoxide, which further transforms into *trans*-glycol (***2a***, see Scheme 1). This compound is obtained by cleavage reaction involving ring opening of epoxide in acid-catalysis.

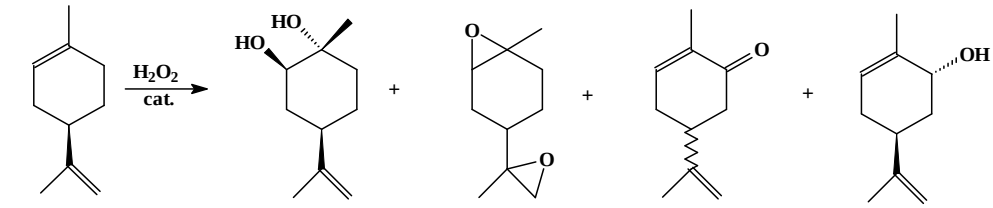

1 R-(+)-limonene | 2a | 2b limonene-dioxide (mixture of stereoisomers) | 2c carvone | 2d trans-carveol

Scheme 1

Thus 1-methyl-4-(1-methylethenyl)-1,2-cyclohexanediol (***2a***, only one diastereo-isomer, [10,11] was obtained as a major oxidation product (yield around 30%) and the corresponding limonene dioxide (***2b***) in about 12% yield. The allylic oxidation products trans carveol and carvone were obtained as minor products (yield around 10% for ***2c***, and 5% for ***2d***). The other oxidation products: limonene 1,2-epoxide,

limonene 8,9-epoxide, isopiperitenone, piperitenone, trans-dihydrocarvone, were identified and quantified by GC-MS in very small amounts (around 15% combined yield).

The best results were obtained with $(NH_4)_5H_4[PMo_6V_6O_{40}]$ which led to a mixture consisting of glycol ***2a*** (37.2), limonen-dioxide (12%) and carvone (11,5%) as major products. (see Table 1). Probably, the NH_4 salt of heteropoly acid increases the stability and solubility of the catalyst in acidic solution. Decreasing the catalytic amount of polyoxo-metalate decreased the percentage of all oxidation products (run 5). Increasing two times the proportion of oxidizing agents increased slowly, only the yield af allylic oxidation products (carvone from 10% to 12% and trans-carveol from 5% to 8%, run 6).

The main oxidation products ***2a***, ***2b***, ***2c*** and ***2d*** were optically inactive. Most probably the abstraction of hydrogen from C-4 in allylic oxidation takes place with racemization. This study of (+)-limonene oxidation indicates attack primarly at the 1,2 double bond rather than allylic oxidation at C-6 to form these oxidation products (carveol and carvone).

Table 1.

Oxidation of (+)-limonene with H_2O_2 35% catalyzed by polyoxometalates

Run	Catalyst	GLC peak area %				Conversion
		2a	**2b**	**2c**	**2d**	
1	$Pd_{4,5}[PMo_6V_6O_{40}]$	28.8	11.5	7.6	3.2	71[a]
2	$Mn_{4,5}[PMo_6V_6O_{40}]$	32.6	13.4	9.9	4.3	72[a]
3	$Cu_{4,5}[PMo_6V_6O_{40}]$	24.7	10.5	7.6	3.2	69[a]
4	$(NH_4)_5H_4[PMo_6V_6O_{40}]$	37.2	12	11.5	4.7	80[a]
5	$(NH_4)_5H_4[PMo_6V_6O_{40}]$	21.3	7.4	4.3	2.1	67[b]
6	$(NH_4)_5H_4[PMo_6V_6O_{40}]$	38.4	12.7	12	8.1	80.5[c]

Reaction conditions: [a]0.10 mol substrate, 0.15 mmol catalyst, 0.20 mol H_2O_2
[b]0.10 mol substrate, 0.10 mmol catalyst, 0.2 mol H_2O_2
[c]0.30 mmol catalyst, 0.20 mol H_2O_2

EXPERIMENTAL

Gas chromatography-mass spectroscopy (GC-MS) coupling analyses were performed on a Hewlett-Packard 5890 (GCL)-5972 (MSD) using a HP-5MS 20m x 0.25 x 0.25μm capillary.

Polyoxometalates catalyst were prepared according to the literature procedure [16,17]. (+)-Limonene, (+)-carvone and trans-carveol were purchased from Aldrich.

Typical oxidation procedure. To the stirred solution of limonene (13.6 g, 0.1 mol) in 80 ml acetone, polyoxometalate catalyst 0.15 mmol (run 4) dissolved in 1 ml of 35% H_2O_2 was then added. After 10 min. 20 ml (0.2 mol) H_2O_2 35% was dropwise added for 2 h, and the solution was stirred at 50^0C for 10 hours. The solution was treated with a solution of 10% sodium hydrogen sulfite to decompose unreacted H_2O_2, them the solvent removed by distillation. The residual liquid was extracted wirh chloroform, dried on $MgSO_4$, filtered and final reaction product was analyzed by GC-MS (see Table 1). The material, after removal of unreacted

limonene by distillation, was subjected to separation by column chromatography (basic alumina grade III, eluent hexane-ether) which gave pure ***2a*** (2g, 15% yield, m.p. 68^0C [11], 67^0C).

The compounds ***2a***, ***2b***, ***2c*** and ***2d*** were analyzed by means of MS database. MS (m/e, rel. intensity); for ***2a***: 170(5,M^+), 152(34), 137(21), 71(85), 43(100); for ***2b***: 168(2,M^+), 107(26), 67(30), 43(100); for ***2c***: 150(12,M^+), 108(31), 82(100), 54(63), 39(53); for ***2d***: 152(M^+), 137(23), 109(100), 84(78), 55(64), 43(51).

REFERENCES

1. A.H. Hains, *Methods for the Oxidation of Organic Compounds*, Academic, London, 1985.
2. O. Bortolini, F.D. Furia, G. Modena, R. Seraglia, *J.Org. Chem.*, 1985, **50**, 2688.
3. I. Yasutaka, Y. Kazumasa, O. Masaya, *J. Org.Chem.*, 1988, **53**, 3587.
4. C.L. Hill, C.M. Prosser-McCartha, *Coordination Chemistry Reviews*, 1995, **143**, 407.
5. G. Strukul, *Catalytic Oxidations with Hydrogen Peroxide as Oxidant*, Kluwe, Dordrecht, The Netherlands, 1992.
6. R. Neumann, A.M. Khenkin, *Inorg.Chem.*, 1995, **34**, 5735.
7. D.C. Duncan, R.C. Chambers, E. Hecht, C.L. Hill, *J.Am.Che.Soc.*, 1995, **117**, 681.
8. R. Neumann, M. Dahan, *J.Chem.Soc., Chem. Commun.*, 1995, **171**.
9. R. Neumann, M. Gara, *J.Am.Chem.Soc.*, 1995, **117**, 5066.
10. K. Fujita, *Nippon Nagaku Zasshi*, 1960, **81**, 1676.
11. W.G. Dauben, M. Lorber, D.S. Fullerton, *J.Org.Chem.*, 1969, **34**(11), 3587.
12. D. Mansuy, J.F. Bartoli, P. Battioni, D. Lyon, G. Finke, *J.Am.Chem.Soc.*, 1991, **113**, 7222.
13. P. Battioni, J.P. Renaud, F.J. Bartoli, M. Reina-Artiles, D. Mansuy, *J.Am.Chem.Soc.*, 1988, **110**, 8462.
14. Y. Fujyiwara, M. Nomura, K. Igawa, *Jpn.Kokai Tokio Koho* JP 03, 11,031; C.A. 1991, **114**, 164562h.
15. M. Nomura, T. Tada, T. Ionue, Y. Fujyihara, *Chemistry Expres*, 1993 **8**(9), 689.
16. R.G. Finke, M.W. Droege, P.J. Domaille, *Inorg. Chem.*, 1987, **26**, 3886.
17. A.F. Wells, *Structural Inorganic Chemistry*, 3rd ed., p. 451, The Clarendon Press, 1962.

STUDIA UNIVERSITATIS BABEŞ-BOLYAI, CHEMIA, XLIII, 1-2, 1998

ELECTRONIC SPECTRA OF SOME bis-DIOXIMINO-COMPLEXES OF Co(III) WITH ALICYCLIC α-DIOXIMES

JÁNOS ZSAKÓ[*], CSABA VÁRHELYI jr.[**], GHEORGHE MARCU[*]

ABSTRACT. Electronic spectra of 22 $[Co(Diox.H)_2X_2]$ and of 26 $[Co(Diox.H)_2XY]$ type complexes (Diox.H - deprotonated alicyclic α-dioxime: 1,2-cyclopentane-, -cyclohexane-, -cycloheptane- and cyclooctane-dione dioxime) are compared and discussed. Mean values of the wave numbers are calculated for complexes containing a given ligand. An attempt is made to assign the absorption bands to crystal field transitions and electronic transitions in the co-ordinated ligand.

INTRODUCTION

Visible and UV spectra of $[Co(Diox.H)_2XY]$ type complexes (where $Diox.H_2$ stands for dimetylglyoxime) were studied first by Ablov and Filippov [1]. These authors have found an absorption band at about 40 kK, assigned by them to the common moiety of all bis-dioximino-cobalt(III) complexes, viz. to

The charge transfer (CT) bands of some bis-dioximino-complexes of Co(III) have been studied by Matsumoto and al. [2 - 4].

In the last 20 years we found no spectral data of bis-dioximato-Co(III) complexes in the literature.

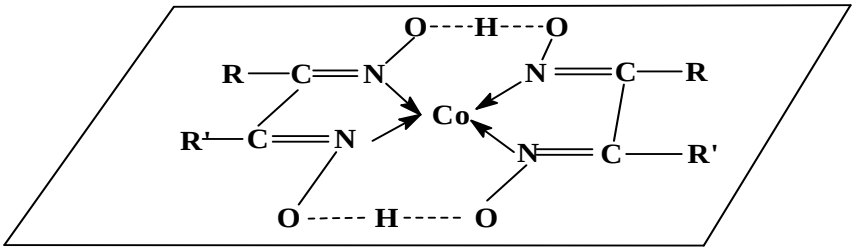

In our earlier papers [5] an attempt was made to study the ligand field transition bands of several dimetylglyoximato- and diphenylglyoximato-Co(III) derivatives and to derive Racah parameters, tetragonal perturbation parameters and nephelauxetic ratio from the position of these bands.

[*] *Faculty of Chemistry, Babeş - Bolyai University, Cluj - Napoca, Romania.*
** *Part of the PhD thesis.*

In the case of alicyclic dioximes as 1,2-cyclopentane-dione-dioxime (Cpdox.H_2), 1,2-cyclohexane-dione-dioxime (Niox.H_2), 1,2-cycloheptane-dione-dioxime (Heptox.H_2) and 1,2-cyclooctane-dione-dioxime (Octox.H_2) electronic spectra have been recorded for many [Co(Diox.H)$_2X_2$] and [Co(Diox.H)$_2$XY] type complexes [6 - 12]. In the present paper these results are discussed.

EXPERIMENTAL

The spectra were recorded in aqueous or diluated alcoholic solutions (1:3) with SPECORD Spectrophotometer. Conc. of samples: 1 - 3•10^{-3} M/l in visible and 1 - 2•10^{-4} - 10^{-5} M/l in UV region.

DISCUSSIONS

Electronic spectral data of some compounds and those reported in [6 - 12] are presented in Tables 1 and 2. viz. in Table 1 for 22 complexes of [Co(Diox.H)$_2X_2$] type, corresponding to a D_{4h} local symmetry and in Table 2 for 26 complexes of [Co(Diox.H)$_2$XY] type, of C_{4h} symmetry.

As seen the number of absorption bands found varies between 2 and 5, and they are situated in 8 spectral regions, denoted as A, B, C, D, E, F, G and H. Bands A and B appear in the visible region and have relatively small molar absorption coefficients. Therefore, these bands may be considered to correspond to crystal field transitions, i.e. to Laporte forbidden d - d transitions. Since band A is reported only for 3 complexes, and B for 14 ones, their interpretation is rather difficult. Nevertheless, one may observe that generally the wave number of B is higher with X ligands situated in the second part of the spectrochemical series, i.e. creating a strong crystal field. This observation is in agreement with the above presumption that B is a ligand field transition band.

Table 1.

Absorption bands of the [Co(Diox.H)$_2L_2$]$^+$ and [Co(Diox.H)$_2X_2$]$^-$ type complexes (Wave numbers - $\bar{\nu}$, in kK).

Diox.H	L or X	$\bar{\nu}_A$	$\bar{\nu}_B$	$\bar{\nu}_X$	$\bar{\nu}_\Delta$	$\bar{\nu}_E$	$\bar{\nu}_\Phi$	$\bar{\nu}_\Gamma$	$\bar{\nu}_H$	Ref.
	α-naphtylamine	-	20.0	24.4	-	32.3	39.2	-	-	4
	β-naphtylamine	-	19.2	25.0	-	31.2	42.6	-	-	4
Niox.H	aniline	-	20.0	23.8	-	31.2	40.3	-	-	7
	o-ethylaniline	-	19.2	24.4	-	31.7	40.0	-	-	7
	p-ethylaniline	-	18.9	25.0	-	32.3	40.5	-	-	7
	4-amino-m-xylene	-	20.6	26.3	28.2	32.3	40.5	-	-	7
	o-toluidine	-	20.8	23.5	26.7	33.3	40.0	-	-	8
Cpdox.H	p-toluidine	-	20.8	23.5	26.7	32.8	40.0	-	-	8
	aniline	-	20.0	23.8	-	31.3	40.3	-	-	
	NH_3	-	-	23.5	-	35.0	39.5	46.0	-	
	β-picoline	-	-	23.5	-	33.5	39.0	48.0	-	
Heptox.H	Et_2PhP	-	-	-	-	31.0	40.5	45.0	-	
	Bu_2PhP	-	-	-	-	31.0	41.0	46.0	-	
	Ph_2EtP	-	-	-	29.5	-	41.0	46.0	-	
	NO_2	-	-	-	28.6	35.1	40.0	-	-	5
	CN	-	-	-	30.5	36.0	40.0	-	-	
Niox.H	NCSe	-	20.0	26.0	-	33.0	40.0	-	-	

Diox.H	L or X	$\overline{\nu}_A$	$\overline{\nu}_B$	$\overline{\nu}_X$	$\overline{\nu}_\Delta$	$\overline{\nu}_E$	$\overline{\nu}_\Phi$	$\overline{\nu}_\Gamma$	$\overline{\nu}_H$	Ref.
	N_3	15.8	19.0	-	30.5	-	40.0	42.5	-	
	S_2O_3	-	-	-	29.5	-	39.5	48.0	-	9
Cpdox.H	NO_2	-	-	24.4	29.9	34.2	39.2	-	-	
Heptox.H	N_3	15.5	19.0	-	30.5	-	40.0	43.0	-	
Octox.H	N_3	15.7	19.2	-	30.5	-	40.5	43.0	-	

Table 2.

Absorption bands of the $[Co(Niox.H)_2XY]$ type complexes.

Ξ	Ψ	$\overline{\nu}_A$	$\overline{\nu}_B$	$\overline{\nu}_X$	$\overline{\nu}_\Delta$	$\overline{\nu}_E$	$\overline{\nu}_\Phi$	$\overline{\nu}_\Gamma$	$\overline{\nu}_H$	Ρεφ.
	pyridine	-	-	-	29.5	33.5	39.7	44.8	48.8	10
	β-picoline	-	-	-	28.5	34.0	39.2	45.0	48.4	10
	NH_3	-	-	-	28.0	33.5	39.5	-	48.3	10
	o-ethyl-aniline	-	-	-	29.2	33.1	38.9	-	48.5	10
	m-xylidine	-	-	-	28.1	33.2	39.8	-	47.6	10
NO_2	o-anisidine	-	-	-	27.8	33.4	39.3	45.5	48.1	10
	p-anisidine	-	-	-	26.8	32.5	39.5	45.2	48.6	10
	p-phenetidine	-	-	-	27.5	33.0	39.2	-	48.7	10
	p-Cl-aniline	-	-	-	29.5	33.2	39.5	-	48.5	10
	p-Br-aniline	-	-	-	29.5	33.5	39.6	-	48.5	10
	thiourea	-	-	-	30.0	36.0	40.8	-	49.0	10
	p-anisidine	-	-	25.6	-	31.9	39.1	-	-	6
	m-toluidine	-	-	25.0	28.9	32.3	39.2	-	-	6
	o-phenetidine	-	-	26.0	-	32.7	38.6	-	-	6
I	p-Cl-aniline	-	-	24.1	28.9	32.1	39.4	-	-	6
	p-toluidine	-	-	-	30.6	-	39.4	-	-	6
	aniline	-	-	26.7	30.3	33.3	39.5	-	-	6
	α-naphtyl-amine	-	-	23.7	30.8	32.3	39.1	-	-	6
NCS	aniline	-	-	-	30.7	-	39.1	-	-	6
N_3	NO_2	-	21.0	-	31.0	-	41.0	-	-	
	allil-thiourea	-	-	27.0	30.0	-	40.0	-	48.0	9
	p-toluidine	-	-	-	33.0	35.0	40.0	-	47.0	9
SO_3	p-I-aniline	-	-	-	-	32.0	39.8	-	49.0	9
	β-picoline	-	-	-	-	32.0	40.5	-	-	9
	aniline	-	-	-	-	32.0	40.0	-	-	9
S_2O_3	pyridine	-	-	-	-	32.0	39.2	-	48.0	9

Band C is situated at the limit of the visible region and it might imply also a ligand field transition, but the high molar extinction coefficient values indicate a CT transition, which masks the crystal field transition if there is such one.

Bands D, E, F, G, H are presumed to imply CT transitions. Band F is present in all spectra investigated and this is in agreement with Ablov's hypothesis, that this band is due to the $Co(Diox.H)_2$ moiety.

In order to clear up the nature of the transitions implied in the appearance of the CT bands, mean values of the wave numbers ($\overline{\nu}$) have been calculated and presented in Table 3.

Table 3.

Mean values of the wave numbers in kK.

Ligand	$\overline{\nu}_B$	$\overline{\nu}_X$	$\overline{\nu}_\Delta$	$\overline{\nu}_E$	$\overline{\nu}_\Phi$	$\overline{\nu}_\Gamma$	$\overline{\nu}_H$
Niox.H	19.86	24.96	29.83	32.77	39.79	44.60	48.30
Heptox.H	19.00	23.50	30.00	32.62	40.17	45.67	-
X = Y = amine	20.02	24.25	27.20	32.45	40.16	47.00	-
X = Y = phosphine	-	-	29.50	31.00	40.83	45.67	-
X = Y = amine + phosphine	20.02	24.25	27.78	32.24	40.29	46.20	-
X = Y = anion	19.30	25.20	29.92	34.57	39.90	42.83	-
X = Y (D_{4h})	19.84	24.39	29.16	32.76	40.18	44.94	-
X = NO_2; Y = amine	-	-	28.58	33.54	39.55	45.12	48.45
X = I; Y = amine	-	25.22	29.90	32.43	39.17	-	-
X = SO_3; Y = amine	-	27.00	(33.00)	32.60	39.17	-	48.00
X ≠ Y (L) (C_{4h})	21.00	25.52	29.40	33.02	39.58	-	48.30
General mean	19.89	24.75	29.32	32.91	39.82	45.00	48.30

With respect to band B, one may observe that in the case of diamino-derivatives (X = Y = amine), the wave number $\overline{\nu}_B$ is higher than with the diacido-complexes, with ligands situated at the beginning of the spectrochemical series. This phenomenon pleads for the importance of the cristal field strength, i. e. for the cristal field transition character of band B.

Band C may be presumed to imply a Co → X charge transfer transition. As seen from Table 3, $\overline{\nu}_C$ is 24.25 for diamino- and 25.2 for the diacido-derivatives, in perfect agreement with the above assignment, since the negative charge of the acido X ligand requires a higher energy for this transition. Further, one can observe that $\overline{\nu}_C$ is higher for the polar acido- amino-complexes of C_{4h} simmetry, as compared to the D_{4h} type diamino ones. This also agrees with the above assignment of the transition.

In the case of band D the relatively high difference in $\overline{\nu}_D$ between the phosphine and amine derivatives, and between the iodo- and nitro-nonelectrolytes, respectively suggests the idea that also Co → X CT transition occurs.

Bands E and F seem to imply transition in the $Co(Diox.H)_2$ moiety. Practically the axial ligands X and Y have no influence upon $\overline{\nu}_F$ and also $\overline{\nu}_E$ [15] are very close to the general mean values indicated in Table 3.

On the contrary, with the bis-diphenylglyoximato-Co(III) complexes an important shift of band E and especially of band F is observed [14]. The corresponding mean wave numbers are the following: $\overline{\nu}_E$ = 31 kK, $\overline{\nu}_F$ = 37.7 kK [15]. Since this shift is due to the electron withdrawing effect of the phenyl groups, the transition may be presumed to consist of Co → Diox.H charge transfer.

Bands G and H are situated at the boundary of the spectral region investigated, where the absorption is very high. Therefore their determination is rather difficult. This is why for the majority of the complexes these bands are not reported in Table 1 and 2.

Up to now we discussed only the crystal field transitions and the CT transitions, but in the electronic spectra absorption bands may be due also to electronic transitions in the co-ordinated ligands. The chelating agents, i. e. the dioximes and the amino (phosphine) ligands have several absorption bands in the UV region comprized between 25 and 50 kK. Therefore the above discussed bands may have a complex character, i. e. the overlap of CT and ligand transition bands may occur.

Thus, the free dimethylglyoxime has two absorption bands at 31.5 and at 37.7 kK, respectively [16] and the pure α-diphenylglyoxime absorbs at 28.5 and 34.5 kK [17]. One cannot exclude the possibility, that bands E and F of the bis-dioximino-Co(III)-complexes are due to the same electron transitions occurring in the co-ordinated dioxime. Both wave numbers are shifted towards higher values, as compared to the free dioximes, which might be due to the relatively strong covalent character of the Co–N bonds.

REFERENCES

1. A. V. Ablov, M. P. Filippov, Zhur. neorg. Khim., **3**, 1565 (1958).; **4**, 2204, 2213 (1959).
2. C. Matsumoto, T. Kato, K. Shinra, Nippon Kagaku Zasshi, **86**, 1266 (1965)., C.A. **65**, 13 027 (1966).
3. J. Jamano, J. Masuda, K. Shinra, Inorg. Nucl. Chem. Letters, **4**, 581 (1968).
4. J. Masuda, M. Sakano, K. Shinra, Bull. Chem. Soc. Japan, **42**, 2296 (1969).
5. J. Zsakó, J. Sata, Cs. Várhelyi, Rev. Roumaine Chim., **18**, 1759 (1973).; Idem, Stud. Univ. Babeş-Bolyai, Ser. Chem., **18**, (1), 37 (1973).
6. R. Ripan, Cs. Várhelyi, L. Szotyori, Stud. Univ. Babeş-Bolyai, Ser. Chem., **11**, (1), 33 (1966).
7. Cs. Várhelyi, L. Szotyori, J. Edler, Rev. Roumaine Chim., **11**, 497 (1966).
8. R. Ripan, Cs. Várhelyi, L. Szotyori, Stud. Univ. Babeş-Bolyai, Ser. Chem., **12**, (2), 133 (1967).
9. R. Ripan, Cs. Várhelyi, L Szotyori, Z. anorg. allg. Chem., **357**, 149 (1968).
10. R. Ripan, Cs. Várhelyi, L. Szotyori, Stud. Univ. Babeş-Bolyai, Ser. Chem., **13**, (2), 79 (1968).
11. Cs. Várhelyi, A. Benk✱, M. Somay, A. Koch, Acta Chim. Acad. Sci. Hung., **97**, 167(1978).
12. Cs. Várhelyi, J. Zsakó, Cs. Várhelyi jr., G Liptay, Periodica Polytechnica, Ser. Chem. Eng., **36**, (1), 43 (1992).
13. R. Ripan, I. Soos, Cs. Várhelyi, Stud. Univ. Babeş-Bolyai, Ser. Chem., **10**, (2), 49(1965).

14. R. Ripan, Cs. Várhelyi, B. Böhm, Stud. Univ. Babeş-Bolyai, Ser. Chem., **10**, (1), 87(1965); Anal. Univ. Al. I. Cuza, Iaşi, **11**, (1), 15 (1965).
15. Cs. Várhelyi, M. Somay, A. Koch, E. Grünwald, Monatsh. Chem., **109**, 1311 (1978).
16. G. Kortüm, Z. physik. Chem. B, **43**, 271 (1939).

J. Meisenheimer, O. Dorner, Liebigs Ann. Chem., **502**, 156 (1933).

STUDIA UNIVERSITATIS BABEŞ-BOLYAI, CHEMIA, XLIII, 1-2, 1998

THERMORHEOLOGICAL BEHAVIOUR OF SILICONE OIL (AK 10^6)

ADINA GHIRIAN* and B. HOCHSTEIN**

ABSTRACT. The rheological measurements have been made to determine the behaviour of silicone oil AK 10^6. It was determined the viscoelastic temperature dependence properties. A value of 43 kJ/mol for the energy of activation has been determined.

INTRODUCTION

Rheological measurements are carried out on materials having industrial interest for one of the following reasons: quality control of raw materials, ingredients and final product; to study the influence of recipe ingredients or modifications on rheological properties and to supplement the information provided by the product behaviour during practical use. The motivation for any rheological study is often the hope that observed behaviour in industrial situations can be correlated with same easily measured rheometrical function. The conditions under which the measurements are carried out depend on the information which is required.

Two different methods are available for determining the rheological behaviour of silicone oil that was tested in our experiment: static and dynamic [1].

Static tests involve the imposition of a step change in stress (or strain) and the observation of the subsequent development in time of the strain (or stress).

In the rheological context the term "dynamic measurement" refers to an experiment in which either the stress or the strain (and usually both) varies harmonically with time. The dynamic tests are: oscillatory strain, wave propagation by using high frequency studies and stady flow.

Compared to steady shear experiments, dynamic tests generally are performed at small strain amplitudes so that they result in only a slight or neglijable disruption of the material microstructure. This feature of oscillatory measurements is on particular advantageous when studying multi-phase materials.

The use of oscillatory methods increased considerably with the development of comercial rheometers. The avantage of oscillatory tests is that a single instrument can cover a very wide frequency range.

MEASUREMENT PRINCIPLES

When dynamic tests are to be carried out on viscoelastic fluids, like silicone oil, the material is usually confined between cylinders, cones or plates as in steady rotational rheometry (Figure 1).

Torsional rheometers (like Cone-Plate and Plate-Plate are used for oscillatory measurements in dynamic experiments for high viscosity fluids and suspensions.

* *"Babeş-Bolyai" University Cluj-Napoca, Department of Chemical Engineering.*
** *University of Karlsruhe, Institut fur Mechanische Verfahrenstechnik und Mechanik.*

Two parameters have to be selected for an oscillation measurement: frequency and stress. The frequency values can be selected. The selected range depends on the sample and the properties which are studied.

A common deformation made for investigating linear viscoelastic behaviour of viscoelastic materials is oscillatory frequency sweep. For oscillatory measurements the sample is subjected to a sinusoidal deformation $\gamma(t)$ with an amplitude at an angular frequency $\omega = 2\pi f$ (Equation (1)), where f is the frequency of oscillation, [2], and the response is sinusoidal too, but with a difference $\delta(\omega t)$ (Figure.2), (Equation (2)).

The ***Oscillatory Frequency Sweep*** program has been used to analyse the thermodynamic of rheological behaviour of silicone oil AK 10^6.

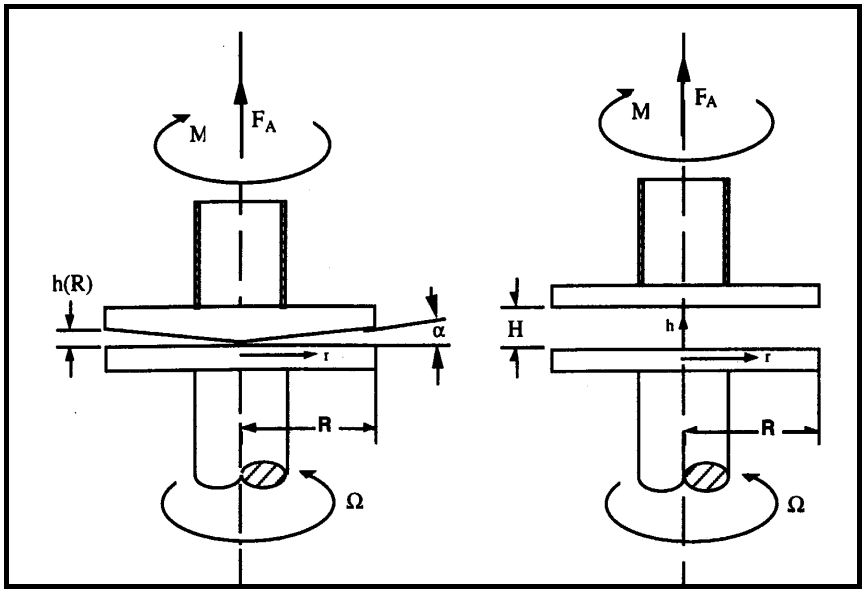

Fig.1. Schematic representations of two rotational viscometers (a. Cone - Plate; b. Plate - Plate).

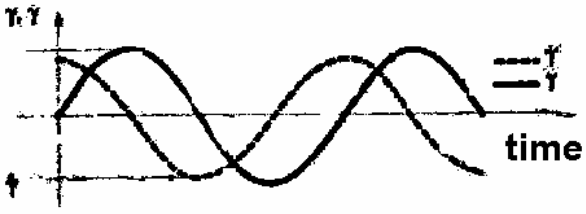

$$\gamma(t) = \gamma \bullet \sin(\omega t) \qquad (1)$$

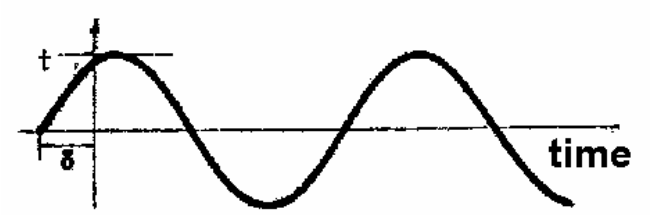

$$\tau(t) = \tau \bullet \sin(\omega t + \delta) \qquad \textbf{(2)}$$

Fig.2. Strain, shear rate and shear stress during a dynamic experiment.

The calculated values in oscillatory tests are dynamic viscosity, phase shift, storage, loss and complex modulus. They can be measured as a function of frequency, time and temperature. This type of measurement gives information about a sample's structure and elasticity or behaviour at gelation or crystallisation.

It is a convention to plot results of oscillatory tests in terms of the dynamic viscosity **η'** and dynamic rigidity **G'**.

For more understanding of the oscillatory method which have been used to discuss the response of viscoelastic material the following terms have been considered:

- the "complex shear modulus" **G*(ω)** (Equation (3)):

$$\left|G^*(\omega)\right| = \frac{\tau(\omega)}{\gamma} \qquad \textbf{(3)}$$

The complex shear modulus **G*(ω)** can be separated in to two component material functions, the "storage modulus" **G'(ω)** and the "loss modulus" **G''(ω)** [3]. The "storage modulus" **G'(ω)** is a measure of the elasticity energy stored by the material, while the "loss modulus" **G"(ω)** is proportional to the energy dissipated (i.e. the viscous portion). The "complex shear" modulus can be calculated from the storage and loss moduli, (Equation (4)).

$$\left|G^*(\omega)\right| = \sqrt{G'(\omega)^2 + G''(\omega)^2} \qquad \textbf{(4)}$$

- the "complex viscosity" **η*(ω)** has been determined by frequency sweep method, at a constant strain amplitude (Equation 5)):

$$\left|\eta^*(\omega)\right| = \frac{\left|G^*(\omega)\right|}{\omega} \qquad \textbf{(5)}$$

The thermorheological measurements suggest that we should give attention to the temperature as an inherent rheological variable.

The effect of temperature on the rheological properties (in particular on the viscosity) has been used to characterize the rheological behaviour of silicone oil AK 10^6 [4].

A new relation has been introduced, relation of Arrhenius (Equation (6)). It has the following form for two different temperatures:

$$\eta_o(T) = \eta_o(T_o)\exp\left[\frac{E_o}{R}\left(\frac{1}{T}-\frac{1}{T_o}\right)\right] \qquad \textbf{(6)}$$

where $\boldsymbol{\eta_o}$ is the viscosity at the zero shear rate.

In this relation the specific parameter which can characterize the material behaviour is the activation energy $\mathbf{E_o}$ (kJ/mol). R is the gas constant (R = 8.314 10^{-3} kJ/mol.K) and T is absolute temperature.

The proportional representation of null viscosity introduces a new constant called "factor of the displacement with the temperature" or "shift factor" [5] and noted $\mathbf{a_T}$ (Equation (7)).

$$a_T = \frac{\eta_o(T)}{\eta_o(T_o)} \qquad \textbf{(7)}$$

The value of $\mathbf{a_T}$ may be found empirically by shifting the curve for temperature T sideways until the overlopping part matches to T_o curve (reference temperature).

Ferry [5] discusses a particular very widely used empirical expression for $\mathbf{a_T}$, the WLF equation introduced by Williams, Landel and Ferry [6] (Equation (8)).

$$\log a_T = -\frac{C1(T-To)}{C2+T-To} \qquad \textbf{(8)}$$

where the constants C1 and C2 depend on the choise of reference temperature To.

The validity of Equation (6) draws to a Arrhenius curve in semilogarithmic scale, where the coefficient a_T is represented against the reciprocal of absolute temperature (1/T). The straight line plot has the slope s. The activation energy of the flow, (Equation (9)) is proportional with the slope s:

$$Eo = R \bullet s \bullet \ln 10 \qquad \textbf{(9)}$$

EXPERIMENTAL

We have determined the rheological behaviour of silicone oil AK 10^6 using a Haake RheoStress RS 150 with a cone-plate system.

The test material has been contained between the cone and the plate with an angle of 4^o (Type: C35/4H). The bottom member, the plate, (the imput) undergoes forced harmonic oscillations about its axis and this motion is transmitted through the test material to the top member, the cone, (the output) the motion of which is contrained by a torsion bar. Since both members move, the shear rate is proportional to tha relative velocity between them.

The Hakee rheometer RS 150 is used in combination with a computer working with a MS - Windous software. The software is used to send the measurement conditions to the instrument and calculate and present the received data. The following parts complete the apparatus: air filter (with max 4 bar), regulator power box, monotor cooler and an external temperature regulator.

RESULTS AND DISCUSSION

The experimental data have been presented in forms of graphs.

To illustrate the using of the time dependence we have plotted the values of storage modulus **G'** and loss modulus **G''** against ω on a logarithmic scale, and the values of complex viscosity η^* against the ω (rad/s).

Figure 3 shows the storage modulus **G'** and loss modulus **G''** versus frequencies for silicone oil AK 10^6 at 20^oC at two different stresses. (50 Pa, OSC-1RMD and 250 Pa, OSC-2RMD, noted in graph). The curves are similar that meaning that for the same range of frequencies the deformation of the sample for the two different stresses is insignificant.

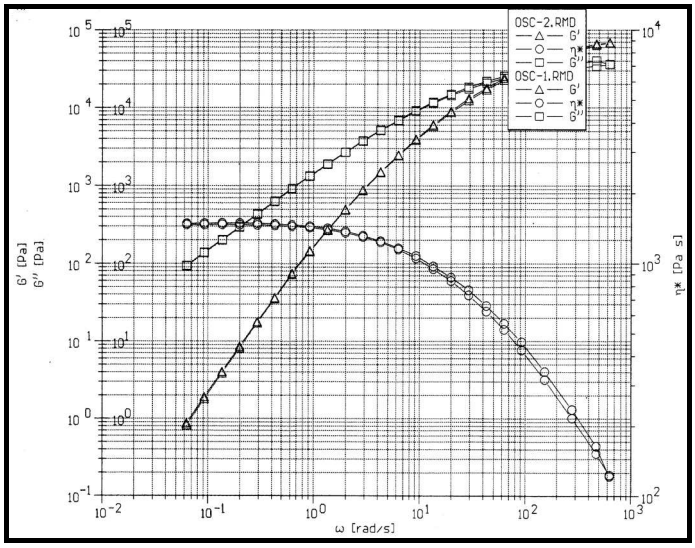

Fig.3. Dependence of the storage, loss moduli and complex viscosity on angular frequency ω (rad/s^{-1}).

To obtained the thermodynamic parameters a_T and **Eo** which can show us the behaviour of the silicone oil tested the complex shear modulus **G*** was presented as a function of various angular frequencies ω (Figure 4) at different temperatures (5^oC, 10^oC, 20^oC, 40^oC, 60^oC and 80^oC). Each temperature determination gives a different curve (Figure 4).

At a constant value of the complex shear modulus (i.e. **G*** 4 10^4 Pa) we have read the ω_i values, which corresponds to different curves. With these values and with ω_0 for the standard temperature (20^oC) we have calculated the "shift factor" a_T and then have plotted these values against 1/T (with T-absolute temperature) (Figure 5)

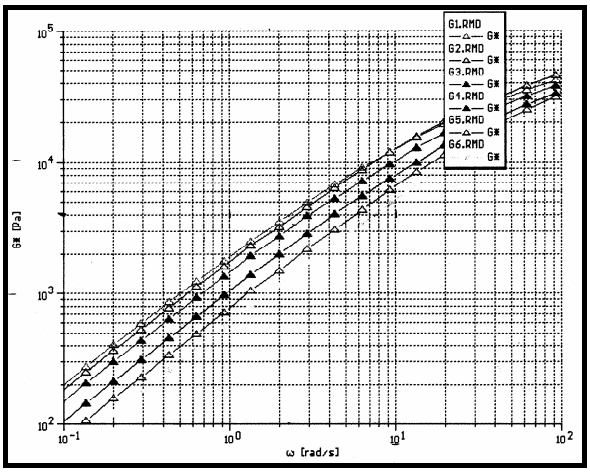

Fig.4. Dependence of the complex modulus on angular frequency ω(rad/s^{-1})

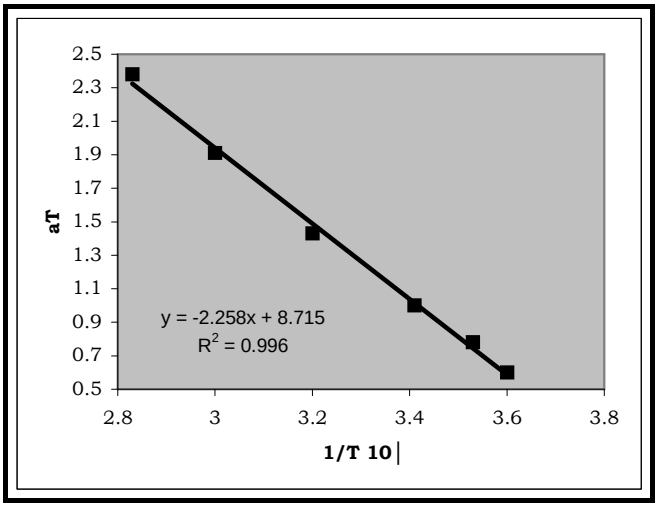

Fig.5. Determination of the activation energy (dependence of a_T on temperature 1/T)

The linear dependence shows a linear viscoelasticity behaviour of the silicone oil AK 10^6 tested (simple fluid). This line can be esed to determine the value of the "shift factor" or coefficient for another temperature (e.g., we calculated 50^0C the value of $\mathbf{a_T}$ = 1.75 and $\omega_i = 5.25 s^{-1}$).

The value Eo calculated by equation (9) is:

Eo = R s ln 10 = 8.314 10^{-3} 10^3 2.258 ln 10 = 43.2 kJ/mol.

REFERENCES

1. H. A. Barnes, J. F. Hutton and K. Walters, *An Introduction to Rheology*, Edn. Elsevier, 1989.
2. B. Hochstein and W. Gleissle, *Rheology 95*, 1995, 72-79.
3. M. Pahl, W. Gleissle and H. Martin Laun, *Praktishe Rheologie der Kunststoffe und Elastomere*, VDI-Verlang Gmblt, Dusseldorf, 1991.
4. Harry H. Hull, *An Approach to Rheology Through Multi-Variable Thermodynamics*, Cold-Comp. , Pittsburg, PA 15222, 1981.
5. J.D.Ferry, *Viscoelastic Properties of Polymers*, 2nd Edn.John Wiley & Sons, 1970.
6. M. L. Williams, R. F. Landel and J. D. Ferry, *J.Amer.Chem.Soc*., 1955, 77, 3781.

STUDIA UNIVERSITATIS BABEŞ-BOLYAI, CHEMIA, XLIII, 1-2, 1998

LIPOPHILICITY CHARACTERIZATION OF A LARGE NUMBER OF DIOXANES AND SPIRANS BY REVERSED-PHASE THIN-LAYER CHROMATOGRAPHY

GABRIELA CÎMPAN*, SIMION GOCAN, NELI OLAH, ION GROSU, SORIN MAGER

ABSTRACT. The lipophilicity of over 70 compounds, dioxanes and spirans, was studied by reversed phase thin layer chromatography, on silica-C18 plates, and methanol-water or acetone-water as mobile phase. The R_{Mw} values were obtained by extrapolation to 100% water as mobile phase and these are a measure of the compounds lipophilicity. The partition coefficient between n-octanol and water, CLogP, was obtained from Pomona College database (Claremont, CA, USA). Linear correlations have been obtained between the R_{Mw} values and the calculated LogP values.

INTRODUCTION

The lipophilicity of substances can be expressed by the partition coefficient between n-octanol and water, $P_{o/w}$ [1-3]. The $LogP_{o/w}$ values can be measured experimentally by the shake-flask method or can be calculated by using different calculation procedures. The direct measurement of $LogP_{o/w}$ values by equilibration between n-octanol and water faces some difficulties as the necessary high purity of the substance that must be available in an adequate quantity. In addition, this method is time consuming and can be applied only in a limited range on the lipophilicity scale. The difficulties can be overcame by using Reversed Phase Liquid Chromatography (RPLC), and these methods have been applied for some years [4-7]. The chromatographic methods show distinct advantages as speed of determination, better reproducibility, only small amounts of sample are necessary, and high purity of the sample is not a condition. Among liquid chromatographic methods, Reversed Phase Thin-Layer Chromatography (RP-TLC) is an alternative technique that can correlate the lipophilicity of compounds with the retention parameters [8, 9]. Martin and Synge [10] and Consden *et al.* [11] derived a relationship between the partition coefficient *P* and R_f values in partition chromatography. Bate-Smith and Westall [12] introduced the term $R_M = \log(1/R_f-1)$. Boyce and Milborrow [13] suggested the use of this value in order to avoid the practical difficulties that often arise in the direct determination of the partition coefficient. The R_M value measured by RP-TLC has been used as a reliable alternative to the classical LogP in order to express the lipophilic character of a substance [14-16].

* *Faculty of Chemistry and Chemical Engineering, "Babeş-Bolyai" University, 11 Arany Janos street, 3400, Cluj-Napoca, Romania.*

The aim of the present study is to find a linear correlation between the R_M values obtained for a large number of dioxanes and spirans by RP-TLC and the calculated LogP values. Similar studies on a few numbers of the same compounds were successful and encouraged to increase the number of compounds on the same structures [17]. Methanol-water and acetone-water was used as a binary mobile phase on silica gel C18 as non-polar stationary phase. The LogP values were obtained from the Pomona College database (Claremont, CA, USA).

EXPERIMENTAL

The structures of the studied compounds are shown in Figure 1. The RPTLC experiments were performed on silica gel C18 plates, which have fluorescence indicator for 254 nm, obtained from Macherey-Nagel (Germany). The plate dimensions were 10x20 cm and the layer width was 0.25 mm. The samples were prepared as 0.1 mg/ml solutions in methanol-chloroform (1:1, v/v). Mixtures of methanol-water and acetone-water were used as polar mobile phase. The concentration of organic modifier was modified in the range 95-70%. The samples were applied onto the plates as spots by using an automated applicator Desaga AS-30, 1.5 cm from the bottom edge. The plates were developed in normal chambers, previously equilibrated for 30 minutes. The migration distance was 8 cm in all cases. After development, the plates were dried in a gentle air stream. The visualisation was performed in UV light, in the cases were this was possible, or in VIS after spraying with a mixture of vanillin (1% in ethanol) and sulphuric acid (20% in ethanol) in equal parts, followed by heating at 110^0C for 5 minutes. The derivatisation reaction leads to coloured spots, from light pink, purple, to dark green. The R_f values were measured with a Shimadzu CS-9000 dual-wavelength flying spot scanner, in reflection mode at a suitable wavelength according to the visualisation method.

RESULTS AND DISCUSSION

The studied compounds were synthesised at Organic Chemistry Department (Faculty of Chemistry and Chemical Engineering, "Babe¿-Bolyai" University, Cluj-Napoca, Romania) [18-29].

The R_M values, $R_M = \log(1/R_f-1)$, were measured for both elution systems, methanol-water and acetone-water, for the concentrations 70/30, 75/25, 80/20, 85/15 and 90/10 (v/v). The corresponding values are shown in Tables 1 and 2. Between the R_M values and the concentration of organic modifier in the mobile phase, a linear correlation can be established (equation 1):

$$R_M = a_0 + a_1X \qquad (1)$$

where X is the molar fraction of methanol or acetone in the eluent. The a_0 values are the intercept, R_{Mw} values, for 100% water as mobile phase, taking into account that the linearity of equation 1 is maintained even at low concentration of organic solvent in the eluent. The R_{Mw} values for both eluent systems, methanol-water and acetone-water, are presented in Table 1 and 2. Usually, the correlation coefficient,

r, is very good (r>0.99). The few exemptions are due to experimental errors, because the front line was no always straight. We assumed that the non-polar stationary phase, silica-C18 (from Macherey-Nagel) has a high degree of free silanol groups, which induce secondary interactions between the compounds, mobile phase and stationary phase. In order to check this hypothesis, a standard mixture test of lipophilic coloured substances: Sudan red, bromophenol blue and alizarin yellow, from Merck (Darmstadt, Germany) was separated by thin-layer chromatography on plates with silica and silica-C18 layers, both from Macherey-Nagel (Germany). The mobile phase was benzene in both cases. The elution order of the three dyes was the same in both cases, although the partition mechanism should be different. Surprisingly, the R_f values differ by only 3% for the two plates. These observations confirm that the secondary interactions are very strong on the used plates and the linearity of the correlation (1) can not be very good.

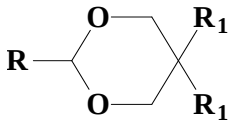

R = *m*-O_2N-C_6H_4-, R_1 = $COOC_2H_5$ **D_1**
R = *o*-O_2N-C_6H_4-, R_1 = $COOC_2H_5$ **D_2**
R = *p*-O_2N-C_6H_4-, R_1 = $COOC_2H_5$ **D_3**
R = β-$C_{10}H_7$-, R_1 = CH_3 **D_{45}**
R = *i*-C_3H_7, R_1 = CH_3 **D_{56}**
R = *p*-$(CH_3)_2N$-C_6H_4, R_1 = CH_3 **D_{37}**

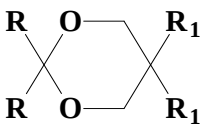

R = C_6H_5-CH(Br)-, R_1 = $COOC_2H_5$ **D_9**
R = C_6H_5-CH_2-, R_1 = $COOC_2H_5$ **D_{11}**
R = C_6H_5-, R_1 = $COOC_2H_5$ **D_{13}**
R = C_2H_5-CH(Br)-, R_1 = CH_3 **D_{48}**
R = CH_2(Br), R_1 = CH_3 **D_{72}**

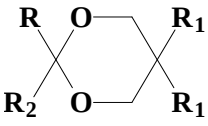

R = CH_3, R_2 = C_6H_5-, R_1 = $COOC_2H_5$ **D_5**
R = CH_3, R_2 = C_6H_5-, R_1 = $COOCH_3$ **D_6**
R = CH_2-Br, R_2 = C_6H_5, R_1 = $COOC_2H_5$ **D_{12}**
R = C_6H_5-CH(OOC-CH_3)-, R_2 = C_6H_5, R_1 = CH_3 **D_{38}**
R = C_6H_5-CH(OH)-, R_2 = C_6H_5, R_1 = CH_3 **D_{40}**

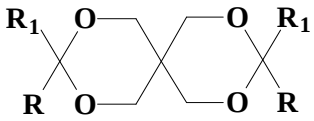

R = C_6H_5, R_1 = CH_3 **D_7**
R = *i*-C_3H_7, R_1 = CH_3 **D_8**
R =CH_2(Br), R_1= CH(Br)-CH_3 **D_{10}**
R = R_1 = CH_2(Br) **D_{14}**
R = R_2 = C_6H_5, **D_{15}**
R = *p*-O_2N-C_6H_4-, R_2 = CH_2Br **D_{23}**
R = $(CH_3)_2C$ (Br)-, R_1 = H **D_{41}**
R = CH_2(Br), R_1 = H **D_{47}**
R = C_6H_5-, R_2 = CH_2Br **D_{44}**

Figure 1. The structures of studied dioxanes and spirans

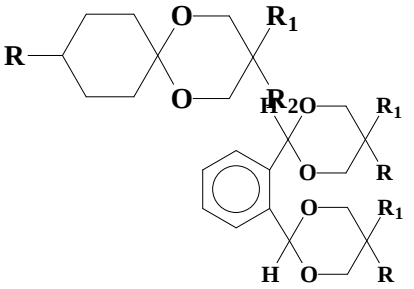

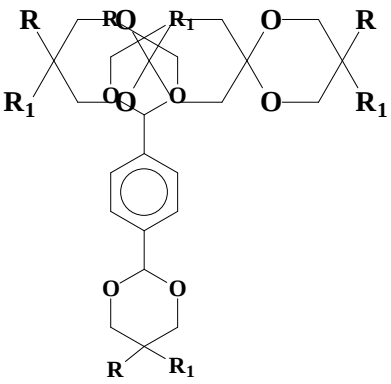

$R = R_1 = COOC_2H_5$ **D_4**
$R = C_2H_5$, $R_1 = CH_3$ **D_{21}**
$R = H$, $R_1 = CH_3$ **D_{27}**
$R = R_1 = COOCH_3$ **D_{28}**

$R = C_2H_5$, $R_1 = CH_3$ **D_{18}**
$R = R_1 = COOC_2H_5$ **D_{26}**

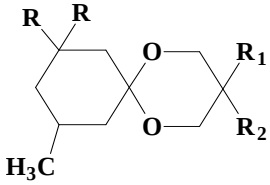

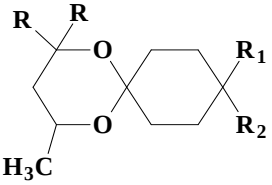

$R = R_1 = R_2 = H$ **D_{51}**
$R = CH_3$, $R_1 = R_2 = COOC_2H_5$ **D_{52}**
$R = R_1 = R_2 = CH_3$ **D_{55}**
$R = R_1 = H$, $R_2 = CH_3$ **D_{64}**

$R = R_1 = H$, $R_2 = t\text{-}C_4H_9$- **D_{57}**
$R = CH_3$, $R_1 = R_2 = H$ **D_{59}**
$R = R_1 = H$, $R_2 = CH_3$ **D_{61}**
$R = R_1 = R_2 = H$ **D_{67}**
$R = R_1 = CH_3$, $R_2 = H$ **D_{68}**

D_{20} **D_{29}** **D_{62}**
$R = C_6H_5$-, $R_1 = R_2 = COOC_2H_5$ **D_{19}**
$R = t\text{-}C_4H_9$-, $R_1 = R_2 = COOC_2H_5$ **D_{22}**

$R = R_1 = COOC_2H_5$ **D_{17}**
$R = CH_3$, $R_1 = C_2H_5$ **D_{25}**

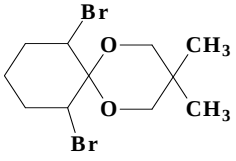

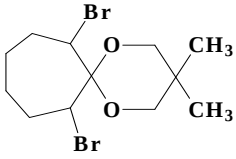

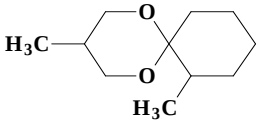

$R = CH_3$, $R_1 = CH_3$, $R_2 = C_2H_5$ **D_{70}**
$R = t\text{-}C_4H_9$-, $R_1 = H$, $R_2 = CH_3$ **D_{36}**
$R = CH_3$, $R_1 = R_2 = COOCH_3$ **D_{35}**

$R = H$, $R_1 = CH_3$ **D_{32}**
$R = R_1 = H$ **D_{33}**
$R = R_1 = C_6H_5$ **D_{46}**

Figure 1. The structures of studied dioxanes and spirans (continuation).

$R = C_6H_5$-, $R_1 = R_2 = CH_3$ **D_{42}**
$R = C_2H_5$-, $R_1 = R_2 = COOC_2H_5$ **D_{50}**
$R = H$-, $R_1 = R_2 = COOC_2H_5$ **D_{54}**

$R = CH_3$, $R_1 = R_2 = H$ **D_{58}**

R = CH_3, R_1 = CH_3, R_2 = H	**D_{63}**
R = *t*-C_4H_9-, R_1 = R_2 = H	**D_{65}**
R = H, R_1 = CH_3, R_2 = C_2H_5	**D_{66}**
R = H, R_1 = CH_3, R_2 = H	**D_{69}**

R = $COOC_2H_5$	**D_{53}**	**D_{71}**
R = CH_3	**D_{60}**	

R = C_2H_5	**D_{16}**
R = C_6H_5	**D_{30}**
R = *t*-C_4H_9	**D_{31}**
R = CH_3	**D_{43}**
R = H	**D_{49}**
	D_{39}

Figure 1. The structures of the studied dioxanes and spirans (continuation).

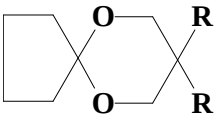

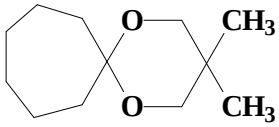

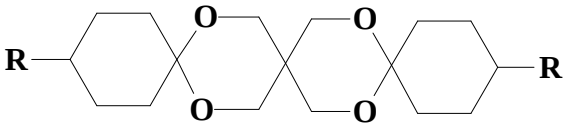

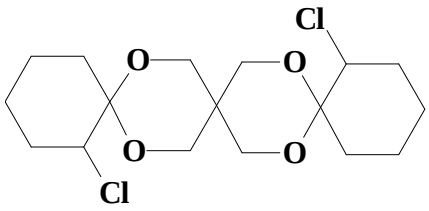

Table 1.

The dependence of R_M values on the acetone molar fraction, X, in the binary mobile phase, acetone-water. The corresponding concentrations are 70/30, 75/25, 80/20, 85/15, 90/10 (v/v). R_{Mw} is the extrapolated value to 100% water as eluent, a_1 is the slope of equation (1), r is the correlation coefficient for 95% confidence limits.

Compound	R_M X/(1-X)					$R_M = R_{Mw} + a_1 X$		
	0.364/0.636	0.424/0.576	0.495/0.505	0.582/0.418	0.688/0.312	R_{Mw}	a_1	r
D1	0.309	0.070	-0.131	-0.257	-0.676	1.319	-2.851	0.989
D2	0.313	0.068	-0.138	-0.265	-0.621	1.258	-2.716	0.990
D3	0.368	0.121	-0.105	-0.246	-0.572	1.324	-2.763	0.991
D4	0.532	0.252	-0.084	-0.261	-0.635	1.744	-3.492	0.991
D5	0.389	0.089	-0.057	-0.203	-0.578	1.331	-2.749	0.985
D6	0.115	0.005	-0.205	-0.445	-0.730	1.109	-2.665	0.998
D7	0.886	0.658	0.345	0.033	-0.304	2.216	-3.705	0.998
D8	0.692	0.508	0.218	-0.068	-0.443	1.984	-3.530	0.999
D9	0.999	0.399	0.333	0.038	-0.317	2.152	-3.648	0.960
D10	0.841	0.515	0.112	-0.126	-0.489	1.160	-2.251	0.790
D11	0.717	0.470	0.160	-0.119	-0.395	1.927	-3.448	0.994
D12	0.387	0.140	-0.075	-0.327	-0.573	1.406	-2.928	0.995
D13	0.607	0.372	0.047	-0.203	-0.503	1.815	-3.429	0.994
D14	0.660	0.403	0.147	-0.165	-0.387	1.715	-3.257	0.992
D15	0.466	0.160	-0.057	-0.229	-0.557	1.481	-2.985	0.989
D16	1.592	1.235	1.061	0.736	0.061	3.214	-4.460	0.988
D17	0.767	0.484	0.192	-0.029	-0.434	2.030	-3.593	0.996
D18	1.032	0.624	0.304	-0.158	-0.480	2.643	-4.658	0.991
D19	0.658	0.372	0.077	-0.080	-0.432	1.766	-3.225	0.989
D20	0.921	0.621	0.391	0.242	-0.389	2.271	-3.748	0.982
D21	0.849	0.550	0.261	0.071	-0.430	2.180	-3.759	0.993
D22	1.005	0.670	0.472	0.296	-0.235	2.252	-3.545	0.987
D23	1.005	0.586	0.276	0.036	-0.360	2.355	-4.007	0.987
D25	0.865	0.575	0.419	0.209	-0.239	2.000	-3.201	0.991
D26	0.463	0.183	-0.098	-0.244	-0.682	1.636	-3.352	0.991
D27	0.261	0.082	-0.115	-0.225	-0.535	1.093	-2.348	0.993
D28	0.042	-0.158	-0.382	-0.441	-0.723	0.802	-2.222	0.981
D29	1.195	0.630	0.209	-0.085	-0.443	2.766	-4.827	0.973
D30	1.317	0.849	0.530	0.254	-0.162	2.773	-4.338	0.986
D31	1.798	1.541	1.369	0.931	0.583	3.173	-3.776	0.996
D32	0.319	0.108	0.016	-0.077	-0.515	1.159	-2.328	0.968
D33	-0.142	-0.202	-0.294	-0.358	-0.673	0.458	-1.551	0.961
D35	0.406	0.169	0.070	-0.064	-0.555	1.388	-2.709	0.973
D36	0.912	0.632	0.484	0.286	-0.163	2.017	-3.107	0.990
D37	-0.115	-0.254	-0.393	-0.427	-0.723	0.500	-1.729	0.977
D38	0.707	0.428	0.163	-0.022	-0.370	1.814	-3.198	0.993
D39	0.720	0.463	0.089	-0.180	-0.499	2.046	-3.775	0.993
D40	0.510	0.257	0.033	-0.117	-0.459	1.498	-2.847	0.992
D42	0.778	0.575	0.288	0.045	-0.271	1.937	-3.240	0.998
D43	1.180	0.785	0.583	0.335	-0.105	2.455	-3.720	0.990
D44	0.979	0.743	0.358	0.056	-0.294	2.398	-3.976	0.995
D45	0.575	0.436	0.149	-0.089	-0.374	1.669	-2.995	0.997
D47	0.016	-0.129	-0.552	-1.005	-1.015	1.282	-3.562	0.953

Compound	R_M X/(1-X)					$R_M = R_{Mw} + a_1 X$		
	0.364/0.636	0.424/0.576	0.495/0.505	0.582/0.418	0.688/0.312	R_{Mw}	a_1	r
D48	1.067	0.727	0.282	-0.064	-0.417	2.665	-4.594	0.991
D49	0.810	0.515	0.383	0.182	-0.252	1.887	-3.055	0.989
D50	0.849	0.523	0.374	0.181	-0.341	2.049	-3.391	0.985
D51	0.432	0.237	0.181	0.036	-0.343	1.221	-2.183	0.975
D52	0.837	0.583	0.412	0.171	-0.313	2.069	-3.388	0.993
D53	0.389	0.140	0.043	-0.091	-0.555	1.341	-2.656	0.995
D54	0.542	0.304	0.192	0.017	-0.461	1.588	-2.877	0.982
D55	1.091	0.796	0.650	0.376	-0.045	2.282	-3.345	0.994
D56	0.242	0.047	0.009	-0.149	-0.661	1.198	-2.547	0.955
D57	0.949	0.727	0.550	0.323	-0.092	2.074	-3.099	0.996
D58	0.423	0.269	0.162	0.014	-0.356	1.266	-2.279	0.985
D59	0.969	0.736	0.552	0.378	-0.017	2.001	-2.894	0.994
D60	0.430	0.271	0.178	-0.017	-0.358	1.296	-2.340	0.990
D61	0.468	0.341	0.174	-0.029	-0.189	1.212	-2.074	0.996
D62	0.397	0.261	0.145	-0.078	-0.207	1.076	-1.905	0.993
D63	0.450	0.252	0.176	-0.052	-0.218	1.153	-2.020	0.991
D64	0.452	0.294	0.180	-0.061	-0.216	1.194	-2.085	0.994
D65	0.679	0.430	0.317	0.040	-0.143	1.539	-2.496	0.990
D66	0.661	0.447	0.319	0.054	-0.153	1.537	-2.490	0.995
D67	0.532	0.137	0.292	0.031	-0.302	1.269	-2.215	0.917
D69	0.327	0.137	0.050	-0.182	-0.302	0.993	-1.932	0.987
D70	0.841	0.583	0.425	0.145	-0.056	1.784	-2.735	0.992
D71	0.621	0.395	0.305	0.010	-0.146	1.441	-2.358	0.986

Table 2.

The dependence of R_M values on the methanol molar fraction, X, in the binary mobile phase, methanol-water. The corresponding concentrations are 70/30, 75/25, 80/20, 85/15, 90/10 (v/v). R_{Mw} is the extrapolated value to 100% water as eluent, a_1 is the slope of equation (1), r is the correlation coefficient for 95% confidence limits.

Compound	R_M X/(1-X)					$R_M = R_{Mw} + a_1 X$		
	0.800/0.200	0.716/0.284	0.640/0.360	0.572/0.428	0.509/0.491	R_{Mw}	a_1	r
D1	-0.386	0.008	0.194	0.442	0.665	2.451	-3.501	0.996
D2	-0.351	0.017	0.159	0.442	0.620	2.291	-3.266	0.994
D3	-0.325	0.028	0.192	0.480	0.717	2.477	-3.489	0.996
D4	-0.146	0.221	0.530	0.870	1.120	3.354	-4.380	0.999
D5	-0.105	0.150	0.281	0.591	0.826	2.389	-3.152	0.990
D6	-0.392	-0.035	0.086	0.299	0.571	2.119	-3.109	0.990
D7	-0.461	-0.219	0.841	1.247	1.753	5.874	-8.097	0.982
D9	0.259	0.945	1.127	1.605	2.102	5.075	-5.973	0.988
D11	0.135	0.709	0.888	1.415	1.720	4.426	-5.333	0.991
D12	-0.186	0.266	0.523	0.787	1.073	3.208	-4.195	0.997
D13	-0.089	0.397	0.593	1.044	1.392	3.876	-4.956	0.993
D15	-0.194	0.122	0.203	0.498	0.651	2.097	-2.843	0.988
D16	0.765	1.303	1.418	1.845	2.115	4.380	-4.466	0.987
D17	-0.506	-0.300	-0.050	0.331	0.641	2.607	-3.991	0.986
D18	-0.176	0.583	0.711	1.313	1.655	4.736	-6.054	0.984

Compound	R_M X/(1-X)					$R_M = R_{Mw} + a_1 X$		
	0.800/0.200	0.716/0.284	0.640/0.360	0.572/0.428	0.509/0.491	R_{Mw}	a_1	r
D19	0.017	0.462	0.633	1.110	1.135	3.446	-4.255	0.987
D20	0.549	1.242	1.626	1.814	2.010	4.606	-4.879	0.972
D21	0.052	0.500	0.659	1.127	1.249	3.416	-4.169	0.987
D22	0.287	0.635	0.940	1.224	1.643	3.875	-4.524	0.995
D25	0.293	0.590	0.738	0.997	1.332	2.991	-3.340	0.988
D26	-0.410	0.014	0.215	0.738	0.894	3.259	-4.587	0.989
D27	-0.347	-0.021	0.145	0.360	0.464	1.917	-2.776	0.992
D28	-0.788	-0.413	-0.296	-0.010	0.136	1.739	-3.110	0.990
D29	0.143	0.655	0.965	1.311	1.580	4.088	-4.876	0.997
D30	0.602	1.058	1.422	1.780	2.110	4.727	-5.149	0.999
D31	1.016	1.556	1.826	2.217	2.551	5.162	-5.142	0.997
D32	-0.045	0.129	0.134	0.394	0.544	1.504	-1.967	0.963
D33	-0.261	-0.124	-0.053	0.103	0.180	0.956	-1.524	0.993
D35	-0.133	0.134	0.241	0.502	0.856	2.391	-3.199	0.976
D36	0.334	0.671	0.961	0.997	1.332	2.935	-3.207	0.982
D37	-0.501	-0.218	-0.137	0.249	0.350	1.878	-2.980	0.980
D38	-0.017	0.408	0.615	1.025	1.263	3.489	-4.372	0.995
D40	-0.176	0.174	0.366	0.826	0.976	3.065	-4.065	0.990
D42	0.179	0.561	0.747	1.140	1.423	3.535	-4.209	0.994
D43	0.443	0.776	1.055	1.326	1.643	3.672	-4.053	0.998
D44	0.242	0.739	0.952	1.710	1.835	4.796	-5.716	0.980
D45	-0.270	0.085	0.155	0.423	0.581	2.017	-2.814	0.986
D47	0.097	0.619	0.799	1.580	1.653	4.579	-5.607	0.974
D48	0.318	0.727	0.895	1.505	1.886	4.527	-5.340	0.982
D49	0.258	0.535	0.710	0.961	1.230	2.843	-3.250	0.995
D50	0.148	0.461	0.705	0.961	1.332	3.265	-3.929	0.994
D51	0.008	0.240	0.297	0.526	0.639	1.720	-2.129	0.987
D52	0.158	0.486	0.705	0.982	1.332	3.256	-3.898	0.994
D53	-0.201	0.046	0.123	0.422	0.608	1.967	-2.730	0.985
D54	-0.052	0.227	0.326	0.645	0.903	2.471	-3.184	0.985
D55	0.394	0.695	0.817	1.224	1.643	3.622	-4.121	0.974
D56	0.456	0.704	0.887	1.247	1.643	3.559	-3.973	0.979
D57	0.389	0.695	0.940	1.272	1.643	3.720	-4.221	0.992
D58	0.072	0.240	0.450	0.998	1.332	3.501	-4.452	0.966
D59	-0.524	0.070	0.316	0.572	1.332	4.086	-5.766	0.973
D60	-0.454	0.112	0.235	0.572	1.332	3.919	-5.499	0.961
D61	0.021	0.375	0.713	0.751	0.851	2.387	-2.850	0.958
D62	0.021	0.375	0.713	0.751	0.851	2.387	-2.850	0.958
D63	0.021	0.375	0.713	0.751	0.851	2.387	-2.850	0.958
D64	0.023	0.268	0.491	0.680	0.877	2.358	-2.919	0.999
D65	0.211	0.607	0.825	1.089	1.182	2.961	-3.365	0.989
D66	-0.096	0.607	0.693	0.974	1.097	3.144	-3.846	0.951
D67	-0.065	0.243	0.385	0.518	0.691	1.955	-2.473	0.991
D68	0.429	0.807	0.947	1.237	1.440	3.160	-3.380	0.993
D69	-0.060	0.398	0.478	0.587	0.851	2.255	-2.788	0.963
D70	0.248	0.653	0.720	1.040	1.415	3.226	-3.724	0.977
D71	0.103	0.510	0.677	1.097	1.415	3.611	-4.403	0.991

Table 3.

The CLogP values for the studied dioxanes and spirans.

Compound	CLogP	Compound	CLogP	Compound	ClogP	Compound	CLogP
D1	2.576	D20	3.256	D39	2.147	D58	2.091
D2	2.496	D21	4.688	D40	3.690	D59	3.129
D3	2.576	D22	4.626	D41	1.099	D60	2.051
D4	3.474	D23	3.313	D42	4.018	D61	2.610
D5	3.352	D24	5.929	D43	2.819	D62	2.610
D6	2.294	D25	2.924	D44	3.827	D63	2.610
D7	3.421	D26	3.524	D45	4.085	D64	2.610
D8	2.529	D27	2.592	D46	2.606	D65	3.418
D9	5.929	D28	1.358	D47	-0.757	D66	3.139
D10	1.745	D29	3.815	D48	4.179	D67	2.091
D11	4.663	D30	4.597	D49	1.781	D68	3.129
D12	3.555	D31	5.473	D50	3.828	D69	2.091
D13	4.391	D32	0.828	D51	2.091	D70	3.658
D14	0.687	D33	-0.210	D52	4.337	D71	3.169
D15	2.383	D34	4.188	D53	2.221		
D16	3.877	D35	2.241	D54	2.780		
D17	2.206	D36	3.937	D55	4.167		
D18	4.738	D37	3.106	D56	2.066		
D19	4.188	D38	4.527	D57	3.937		

The relationship between the R_{Mw} values obtained in acetone-water system and the calculated CLogP values is shown in equation 2:

$$R_{Mw}(X) = 0.801(\pm 0.286) + 0.298(\pm 0.085)\ CLogP \quad (2)$$
$$s = 0.441,\ F = 49,\ r = 0.653,\ n = 68$$

where s is the fit standard error, F is the statistic parameter for F test, n is the number of compounds and r is the correlation coefficient for 95% confidence limits.

In order to improve the linearity of equation 2, only the compounds, which have two dioxanic cycles, were included in equation 3.

$$R_{Mw}(X) = 1.044(\pm 0.325) + 0.390(\pm 0.113)\ CLogP \quad (3)$$
$$s = 0.352,\ F = 53,\ r = 0.878,\ n = 18$$

The similar correlations with equations 2 and 3 but for methanol-water as eluent are shown in equations 4 and 5. Equation 4 takes into account all the compounds and equation 5 only the compounds with two dioxanic cycles in the structures, except D7 and D47, which were eliminated as outliers.

$$R_{Mw}(X) = 1.605(\pm 0.588) + 0.507(\pm 0.171)\ CLogP \quad (4)$$
$$s = 0.846,\ F = 35,\ r = 0.601,\ n = 64$$
$$R_{Mw}(X) = 0.981(\pm 0.626) + 0.818(\pm 0.196)\ CLogP \quad (5)$$
$$s = 0.452,\ F = 89,\ r = 0.953,\ n = 11$$

In literature, the R_{Mw} values are arbitrarily correlated with X, the molar fraction of organic modifier in the mobile phase, or φ, the same concentration, but expressed as volumetric percent. No improvement in the linearity of relationships 2 and 3 was found by replacing X with φ. No significant rules were found between the R_{Mw} values obtained for acetone-water and methanol-water as mobile phase. Theoretically, these data should have the same value. This fact was observed in the literature and was

attributed to the role of organic modifier in the compound partition between the stationary and the mobile phase and to secondary interactions.

REFERENCES

1. T. Fujita, J. Iwasa, C. Hansch, *J. Am. Chem. Soc*., 1964, **86,** 5175.
2. C. Hansch, S. M. Anderson, *J. Org. Chem*., 1967, **32,** 2583.
3. R. N. Smith, C. Hansch, M. A. Ames, *J. Pharm. Sci*., 1975, **64,** 65.
4. Th. Braumann, *J. Chromatogr*., 1986, **373,** 1981.
5. L. G. Danielson, Yu-Hui Zhang, *Trends Anal. Chem*., 1996, **15,** 188.
6. R. Kaliszan, *Anal. Chem*., 1992, **64,** 619A.
7. R. J. E. Grouls, E. W. Ackerman, H. H. M. Korsten, D. D. Breimer, *J. Chromatogr. B*, 1997, **694,** 421.
8. K. P. Dross, R. Mannhold, R. F. Rekker, *Quant. Struct.-Act. Relat*., 1992, **11,** 36.
9. K. Dross, C. Sonntag, R. Mannhold, *J. Chromatogr. A*, 1994, **673,** 113.
10. A. J. P. Martin, R. L. M. Synge, *Biochem. J*., 1941, **35,** 1358.
11. R. Consden, A. H. Gordon, A. J. P. Martin, *Biochem. J*., 1944, **38**, 224.
12. E. C. Bate-Smith, R. G. Westall, *Biochim. Biophys. Acta*, 1950, **4**, 427.
13. C. B. C. Boyce, B. V. Milborrow, *Nature*, 1965, **208**, 537.
14. G. L. Biagi, A. M. Barbaro, A. Sapone, M. Recanatini, *J. Chromatogr. A*, 1994, **662**, 341.
15. G. L. Biagi, A. M. Barbaro, A. Sapone, M. Recanatini, *J. Chromatogr. A*, 1994, **669**, 246.
16. G. L. Biagi, A. M. Barbaro, M. Recanatini, *J. Chromatogr. A*, 1994, **678**, 127.
17. S. Gocan, Gabriela Cimpan, I. Fromondi, I. Grosu, *Proceedings of the Conference of Chemistry and Chemical Engineering*, Bucharest, 1995, 433.
18. S. Mager, M. Horn, I. Grosu, M. Bogdan, *Monatsh. Chem*., 1989, **120**, 735.
19. I. Grosu, S. Mager, G. Plé, M. Horn, *J. Chem. Soc. Chem. Commun*., 1995, 167.
20. I. Grosu, G. Plé, S. Mager, *Tetrahedron*, 1995, **52**, 2659.
21. I. Grosu, S. Mager, G. Plé, *J. Chem. Soc. Perkin Trans. 2*, 1995, 1351.
22. I. Grosu, S. Mager, G. Plé, R. Martinez, M. Horn, R. R. Gavino, *Monasth. Chem*., 1995, **126**, 1021.
23. I. Grosu, S. Mager, G. Plé, E. Mesaros, *Tetrahedron*, 1996, **52**, 12783.
24. I. Grosu, S. Mager, G. Plé, L. Muntean, I. Schirger, *Heterocyclic Communications*, 1996, **2**, 423.
25. I. Grosu, B. C. Camacho, A. Toscano, G. Plé, S. Mager, R. Martinez, R. R. Gavino, *J. Chem. Soc. Perkin Trans. 1*, 1997, 775.
26. I. Grosu, G. Plé, S. Mager, R. Martinez, C. Mesaros, B. C. Camacho, *Tetrahedron*, 1997, **53**, 6215.
27. S. Mager, I. Grosu, M. Horn, I. Hopârtean, M. Darabantu, C. Puscas, D. Kovacs, G. Plé, *Romanian Quatery Reviews*, 1995, **3**, 221.
28. S. Mager, I. Hopârtean, M. Horn, I. Grosu, *Studia Univ. "Babes-Bolyai", Chemia*, 1979, **24**, 32.
29. S. Mager, I. Grosu, *Studia Univ. "Babes-Bolyai", Chemia*, 1988, **33**, 47.

STUDIA UNIVERSITATIS BABEŞ-BOLYAI, CHEMIA, XLIII, 1-2, 1998

SYNTHESIS AND STEREOCHEMISTRY OF SOME SPIRO-1,3-OXATHIANE DERIVATIVES

LUMINIÞA MUNTEAN, ION GROSU, SORIN MAGER, ALEXANDRINA NAN

ABSTRACT. The synthesis and the stereochemistry of two new spiro-1,3-oxathianes are discussed. NMR and IR investigations revealed flexible and semi-flexible structures.

INTRODUCTION

In the last years, alkyl 1,3-oxathiane derivatives are strongly used as chiral auxiliaries in asymetric synthesis [1-6].

In this context it was considered of interest to develop investigations on the structure and stereochemistry of some new spiro-1,3-oxathianes bearing a hydroxy group in position 3 of the heterocycle (Scheme 1):

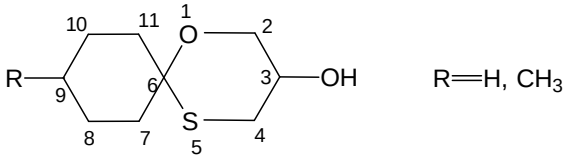

Scheme 1

RESULT AND DISCUSSION

3-Hydroxy-1-oxa-3-thia-spiro[5.5]undecane ***1*** and his 9-methyl derivative ***2*** are obtained by a condensation reaction between the appropiate cyclohexanone and 3-mercapto-1,2-propanediol, in acidic conditions (*para*-toluenesulfonic acid - PTSA) with the azeotropic removal of the resulted water (Scheme 2):

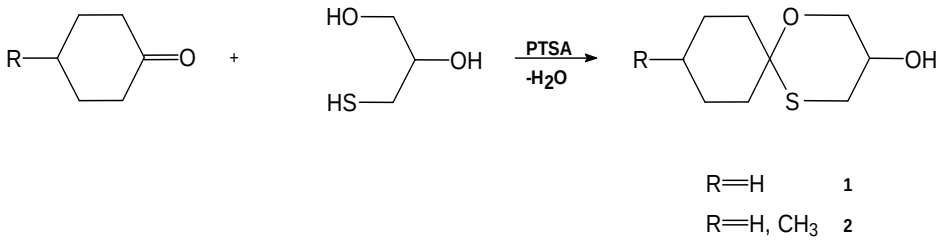

Scheme 2

To avoid the formation of the pentacyclic isomers, the reaction was performed under thermodynamic control (the reaction time was quite long, 48-72 hours, the presence of four compounds (the starting ketome, two pentacyclic isomers and the desired product); at the end of the reaction, there were only two (the starting ketone and the 1,3-oxathiane).

Compounds ***1*** and ***2*** exhibit two diastereisomers: one with the sulfur atom (considered as a substituent of the cyclohexane ring) of the heterocycle in axial position of the ciyclohexane ring (A), the other one with the sulfur equatorial (B). In the case of compound ***1*** because of the small difference between the conformational free enthalpies of a SR group and of an OR [7] group the cyclohexane ring has a flipping structure, which induces a conformational equilibrium between structures A and B (Scheme 3):

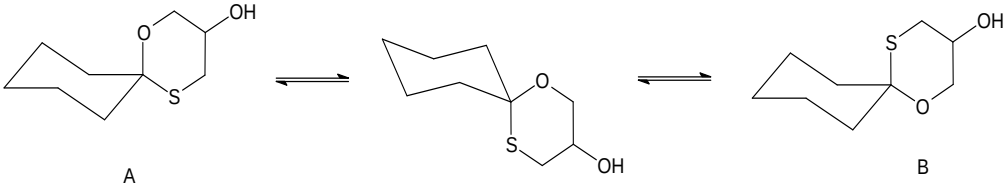

Scheme 3

Compound ***1*** is investigated by ^{1}H- and ^{13}C-NMR spectroscopy, IR spectroscopy and mas-spectrometry. These investigations revealed the flexible structure of this compound.

The positions 2 and 4 of the spirane are different. The ^{1}H-NMR spectrum, exhibits for the protons of 2-position, two doublets of doublets (an AB system, with a further splitting of the signals due to the vicinal coupling with the proton of position 3), (Figure 1). For the protons of 4-position a similar group of signals are obtained but with significantly lower difference of chemical shifts. The peaks are overlapped and an assigment was not possible.

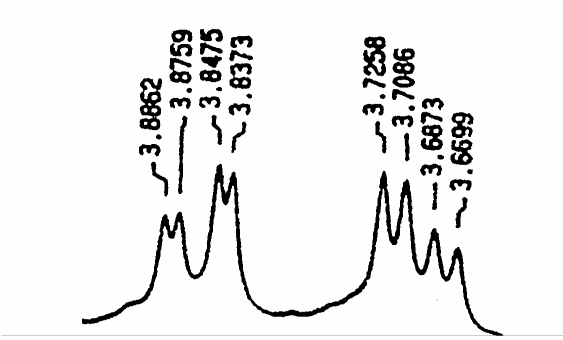

Figure 1

For the anancomeric 1,3-oxathianes, literature date [8-10] indicate a difference between chemical shifts similar to that of 1,3-dioxanes ($\Delta\delta$=0.4-1.0 ppm) for the axial and equatorial protons attached to the carbon atom of the heterocycle placed near the oxygen. A smaller difference ($\Delta\delta$=0.12-0.42 ppm) is predicted for the protons of the axial and equatorial positions of the carbon closer to the sulfur atom.

Despite the fact that for compound ***1***, the geminal protons of positions 2 and 4 exhibit different signals, the small differences between chemical shifts ($\Delta\delta$=0.16 ppm, respectively overlapped peaks) indicate a flexible structure.

IR investigations aprove this conclusion. The IR spectra, recorded at different values of concentration, in benzene, show for the OH group two bands: at 3580 cm^{-1} (hydrogen-bonded OH) and 3667 cm^{-1} (monomeric OH). The increase of the concentrations of the solution led to a higher band for the hydrogen-bonded OH (the other band is almost disappeared) Figure 2).

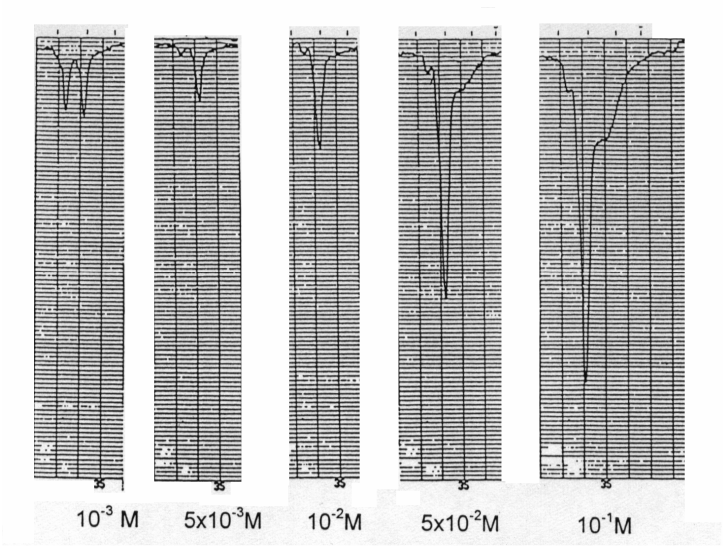

Figure 2

As a consequence, the H-bounds are intermolecular, proving the flipping structure of the compound.

The mass spectra of the compound ***1*** is illustrated in Figure 3; the main fragmentation pattern is shown in Scheme 4:

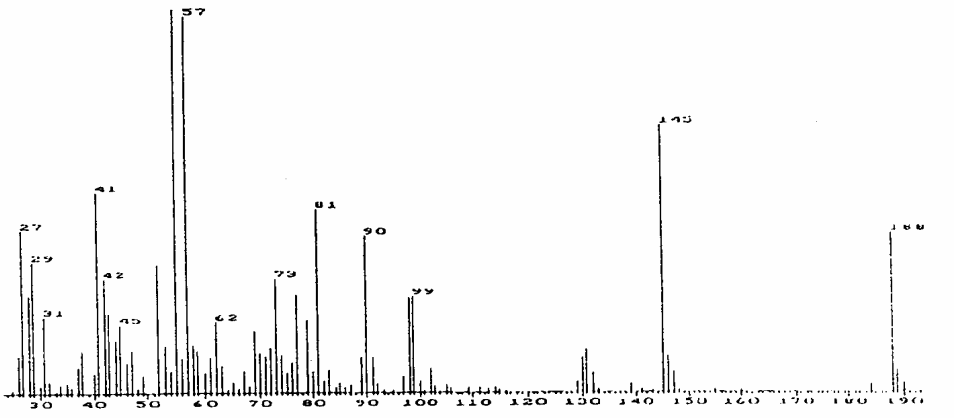

Figure 3

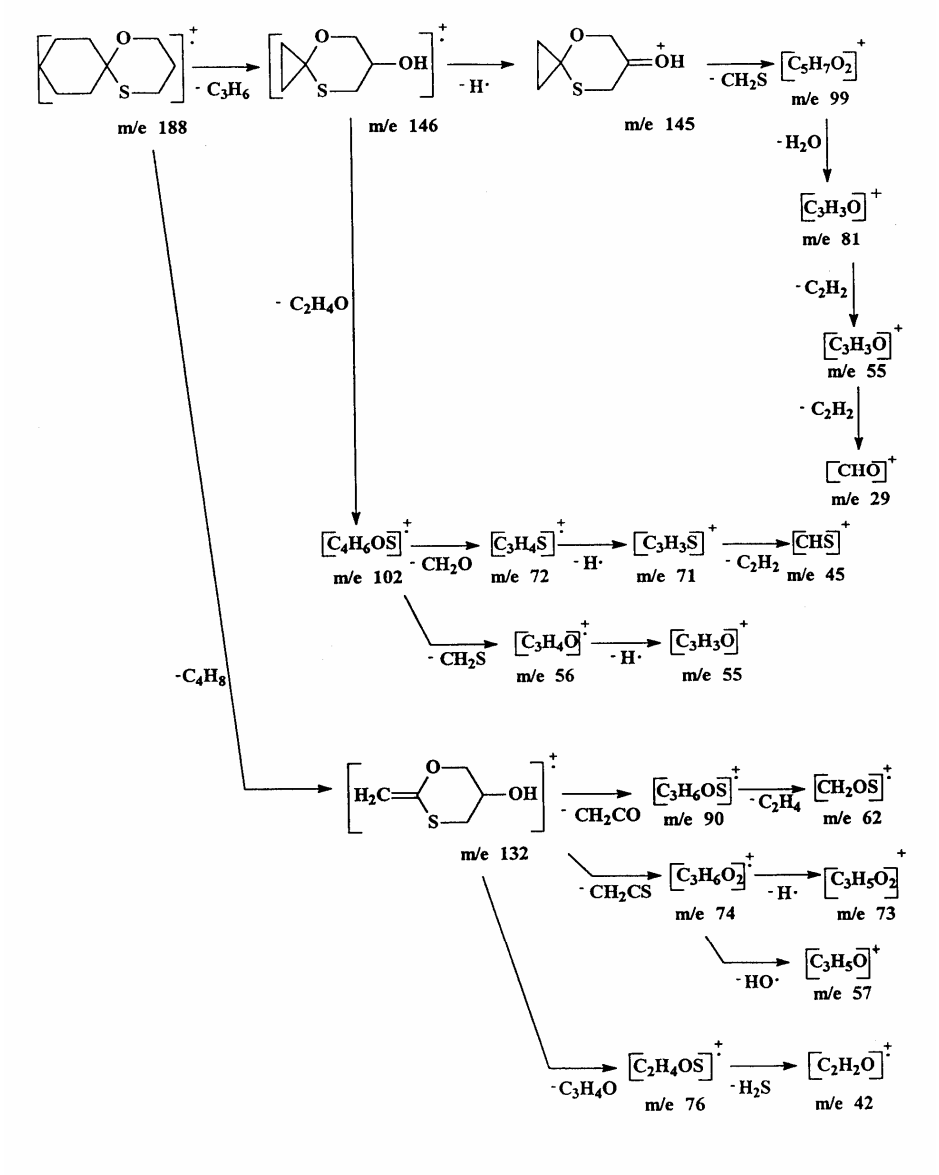

Scheme 4

For compound ***2***, with a rigid cyclohexane ring ("holding" methyl group) the changing of one diastereoisomer into the other can occur only by a ring-opening step.

The ^{1}H-NMR spectrum revealed the presence of two diastereoisomers. Two AB systems (doublets of doublets - the further splitting being due to the vicinal coupling with 3-position proton) could be identified (peaks 1,2,3,4,5,6,7,8 and 9,10,11,12,13,14,15,16) (Figure 4):

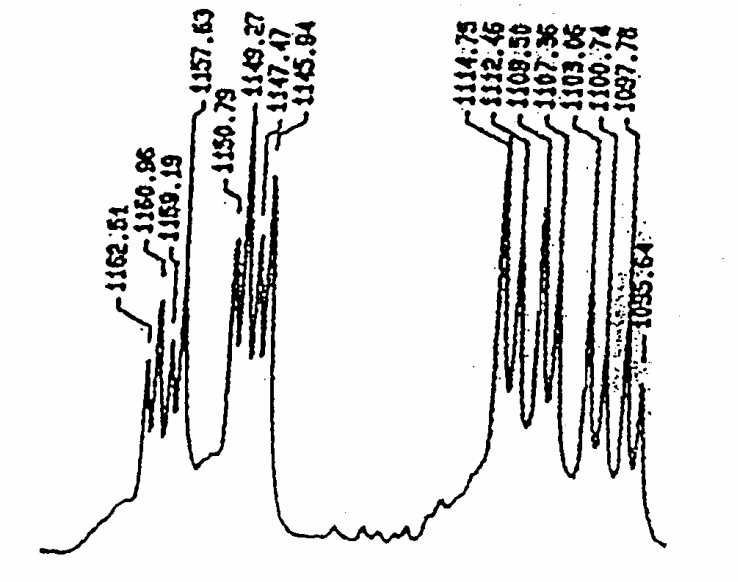

Figure 4

EXPERIMENTAL

General

NMR spectra have been run on a VarianGemini spectrometer, operating at 300 MHz fr protons and 75 MHz for carbon atoms, using $CDCl_3$ as solvent, in 5 mm tubes. The IR spectra were recorded on a SPECORD 75 IR spectrometer. The EI mass spectra have been recorded at 70 eV with a MAT 311 mass spectrometer.

Compounds 1 and 2, general procedure

Stoichiometric amounts of 3-mercapto-1,2-propanediol and carbonyl compound (0.05 mol) with catalytic amounts of *p*-toluenesulfonic acid (0.1 g) were refluxed in 100 ml benzene and the resulted water was removed using a DeanStark trap. After the reaction carried out (48-72 hours, chromatographic control), the catalyst was neutralized after cooling at room temperature (0.1 g KOH, stirring for 0.5 h). The reaction mixture was washed twice with 50 ml water. After drying (Na_2SO_4) the benzene was removed and the spiro-1,3-oxathianes were purified by low pressure distillation.

3-Hydroxy-1-oxa-5-thia-spiro[5.5]undecane ***1***
Yield: 60%; bp: 102-104^{0}C/0.05 mm; $C_9H_{16}O_2S$ (188.13); calc: 57.45 C, 8.98 H, 15.97 S
found: 57.28 C, 8.67 H, 15.77 S

^{1}H-NMR ($CDCl_3$): δ = 4.32 - 4.41 (m, 1H, CH), 3.86, 3.70 (ddd, 2H, AB system, J = 11.6 Hz, J' = 3.1 Hz, J'' = 5.2 Hz), 2.92 - 3.01 (m, 2H, overlapped peaks), 1.27 - 2.10 (m, 11H, overlapped peaks, cyclohexane ring and OH).
^{13}C-NMR ($CDCl_3$): 128.36 (C^6), 81.55 (C^2), 63.70 (C^3), 40.47; 40.11 (C^7, C^{11}), 33.36 (C^4), 25.41: 25.08 (C^8, C^{10}), 24.32 (C^9).

3-Hydroxy-9-methyl-1-oxa-5-thia-spiro[5.5]undecane ***2***
Yield: 58%; bp: 110^0C/ 0.05 mm; $C_{10}H_{18}O_2S$ (202.14); calc: 59.41 C, 8.90 H, 15.86 S
found: 59.21 C, 8.69 H, 15.67 S
^{1}H-NMR ($CDCl_3$, mixture of two diastereoisomers): 4.24 - 4.40 (m, 1H, overlapped peaks, CH), 3.84 - 3.68 (ddd, 2H, AB system, overlapped peaks, J = 11.7 Hz, J' = 3.3 Hz, J'' = 5.1 Hz, J'' = 5.3 Hz), 2.88 - 3.01 (m, 2H, overlapped peaks), 2.35 (s, 1H, OH), 1.00 - 2.20 (m, 8H, overlapped peaks, cyclohexane ring), 0.91 (dd, 3H, overlapped peaks, J - 6.0 Hz, J = 6.4 Hz).
^{13}C-NMR ($CDCl_3$, mixture of two diastereoisomers): 81.76, 81.53 (C^2); 63.70 (C^3); 40.13, 39.82, 39.51, 38.91 (C^7, C^{11}); 34.28, 33.52, 33.26, 32.85, 32.38, 32.07 (C^4, C^8, C^{10}); 31.68, 30.72 (C^9); 21.73, 21.57 (CH_3).

REFERENCES

1. E.L. Eliel, J.K. Koshimies, B. Lohri, *J.Am.Chem.Soc.*, 1978, ***100***, 1614.
2. E.L. Eliel, S. Morris-Natschke, *J.Am.Chem.Soc.*, 1984, ***106***, 2937.
3. J.E. Lynch, E.L. Eliel, *J.Am.Chem.Soc.*, 1984, ***106***, 2943.
4. H. Xu-Chang, E.L. Eliel,, *Chem.Lett.*, 1987, 41.
5. S.V. Frye, E.L. Eliel, *J.Org.Chem.*, 1985, ***50***, 3402.
6. S.V. Frye, E.L. Eliel, *J.Am.Chem.Soc.*, 1988, ***110***, 484.
7. E.L. Eliel, *Angew.Chem.internat.Edit.*, 1965, ***4***, 761.
8. H.R. Buys, *Recueil*, 1970, ***89***, 1244.
9. N. de Wolf, H.R. Buys, *Tetrahedron Letters*, 1970, ***30***, 551.
10. E. Juaristi, G. Cuevaras, *Tetrahedron*, 1992, ***33***, 1847.

STUDIA UNIVERSITATIS BABEŞ-BOLYAI, CHEMIA, XLIII, 1-2, 1998

^{1}H AND ^{13}C NMR SPECTROSCOPY AS A SUITABLE METHOD FOR THE CHARACTERIZATION OF PHENYLANTIMONY CHLORIDES

ANCA SILVESTRU, CRISTIAN SILVESTRU*

ABSTRACT. ^{1}H and ^{13}C NMR spectra have been recorded for $CDCl_3$ solutions of triphenylantimony, Ph_3Sb, phenylantimony(III) chlorides, Ph_2SbCl and $PhSbCl_2$, and phenylantimony(V) chlorides, Ph_3SbCl_2 and $Ph_2SbCl_3H_2O$, respectively, as well as for solutions containing mixtures of them. A possibility to establish the composition of mixtures containing the above mentioned compounds or to detect the impurities due to the synthetic methods usedd to prepare phenylantimony halides, using ^{1}H and ^{13}C NMR data, is presented.

INTRODUCTION

Phenylantimony(III) chlorides, $PhSbCl_2$ and $PhSbCl_3$, and phenylantimoniu(V) chlorides, Ph_3SbCl_2 and Ph_2SbCl_3, are useful to starting materials in syntheses of organoantimony compounds with different inorganic or organic ligands. The NMR studies in solution give a suitable method to identify them in mixtures, or to prove their purity. It has been reported before [1] about the possibilities to appreciate quantitatively the content of such compounds in reaction mixture using the ^{1}H NMR spectroscopy. Although the ^{1}H NMR spectra are very useful, in some cases, due to the presence of different phenyl groups bond to antimony and the proton – proton coupling phenomena, the overlap of signals is possible and the spectra appear very complicate. The ^{13}C NMR spectra seem to be more useful to characterize the phenylantimony chlorides and to identify the composition of reaction mixtures containing them, due to the clear separation between typical ^{13}C resonance signals for Ph_nSbCl_{3-n} derivatives. The ^{13}C NMR signals don't overlap each other and could be used certainly to identify the organoantimony impurities present in the phenylantimony chlorides used as starting materials in chemical synthesis.

EXPERIMENTAL

Triphenylantimony and all other starting materials were commercially available. $SbCl_3$ was freshly sublimed before use. ^{1}H and ^{13}C NMR spectra were recorded as $CDCl_3$ solutions on a VARIAN GEMINI 300 instrument operating at 299.5 and 75.4 MHz, respectively. The chemical shifts were referenced to the internal chloroform peak (d = 7.26 ppm and d = 77.0 ppm for ^{1}H and ^{13}C, respectively).

All the phenylantimony halides have been prepared according to literature methods. Ph_2SbCl and $PhSbCl_2$ obtained by redistribution reactions between

* *Faculty of Chemistry and Chemical Engineering, "Babe¿-Bolyai" University, 11 Arany Janos Str., 3400, Cluj-Napoca, Romania.*

Ph_3Sb and $SbCl_3$ in stoichiometric molar ratio in the absence of a solvent, were used without further purification [2]. The redistribution reaction between Ph_4Sn and $SbCl_5$ in CCl_4, followed by crystallisation from a 5N HCl solution led to $Ph_2SbCl_3.H_2O$ [3], while the oxidation reaction of Ph_3Sb with SO_2Cl_2 gave the corresponding triphenylantimony dichloride (recrystallized from CCl_4) [4].

All mixtures of phenylantimony compounds investigated by means of NMR spectroscopy were prepared directly in NMR tubes.

RESULTS AND DISCUSSIONS

1. Syntheses of $PhSbCl_2$, Ph_2SbCl, Ph_3SbCl_2 and $Ph_2SbCl_3.H_2O$

Phenylantimony(III) chlorides have been obtained by shaking for 24 hr reaction mixtures obtained from triphenylantimony and antimony(III) chloride, in stoichiometric ratio and in absence of solvent [2]:

$$2\ Ph_3Sb + SbCl_3 \longrightarrow 3\ Ph_2SbCl$$

$$Ph_3Sb + 2\ SbCl_3 \longrightarrow 3\ Ph_2SbCl_2$$

These methods of synthesis afford the possibility to obtain mixtures of organoantimony compounds due to an equilibrium or other processes, *e.g.* oxidation to antimony(V). Therefore, phenylantimony(V) chlorides were also prepared. Diphenylantimony(V) trichloride was obtained by reacting tetraphenyltin and antimony pentachloride, and recrystallisation from a solution of 5N HCl affords its isolation as white crystals of $Ph_2SbCl_3.H_2O$ [3]:

$$Ph_4Sn + SbCl_5 \longrightarrow Ph_2SbCl_3 + Ph_2SnCl_2$$

Triphenylantimony(V) dichloride was prepared by oxidation of triphenylantimony with sulfuryl chloride [4]:

$$Ph_3Sb + SO_2Cl_2 \longrightarrow Ph_3SbCl_2 + SO_2$$

Since phenylantimony(III) chlorides are important starting materials for other organoantimony compounds, it is important to check their purity and a NMR spectroscopy is a very useful method for this purpose.

2. NMR spectra

^{1}H and ^{13}C NMR data recorded for the phenylantimony halides and Ph_3Sb are given in Tables 1 and 2.

As it was previously noted [1] the resonance signals of the *ortho*-protons of the discussed compounds are very useful to calculate the quantitative composition of a mixture or the purity of each phenylantimony compound, if they don't overlap with other signals. However, the proton NMR spectra for mixtures of organoantimony compounds containing phenyl groups are always complicated due to the proton-proton coupling phenomena.

The phenylantimony(III) chlorides, $PhSbCl_2$ and Ph_2SbCl are conveniently obtained by redistribution between Ph_3Sb and $SbCl_3$ in 1:2 and 2:1 molar ratio, respectively [2], but the use of this method might result in an impure product if the

reaction is not completed. The ^{1}H NMR spectrum for Ph_2SbCl (Fig. 1, a) presents a doublet of dublets at δ = 7.70 ppm (*ortho* – protons) and a multiplet signal at δ = 7.47 ppm (*meta* + *para* – protons). In additon, two groups of very low intensity signals, *i.e.* a doublet of doublets at δ = 8.32 ppm and a multiplet at δ = 7.60 ppm, are also present. According to the synthetic route, it was reasonable to suppose that these signals of low field (δ =8.32 ppm), but complicated very much the space at 7.3 -–7.5 ppm, where the signals due to the *meta* + *para* – protons in Ph_2SbCl and those due to the Ph_3Sb protons overlap each other (Fig. 1, b). This behavior suggests the low field resonance at δ = 8.32 ppm observed for the reaction product is due to an other phenylantimony compound.

As a consequence of the size and inductive effects of the substituents, in mixtures containing $PhSbCl_2$, Ph_2SbCl, Ph_3Sb, Ph_3SbCl_2 and Ph_2SbCl_3, the ^{13}C NMR signals do not overlap each other and it is easier to identify the composition of such reaction mixtures (Table 2).

The ^{13}C NMR spectrum of Ph_2SbCl (crude product) confirms the presence of an impurity, *i.e.* eight resonance signals (four of them of very low intensity) were observed, which could be assigned to two different phenyl groups in the mixture (Fig. 2, a, Table 2). The addition of the excess of Ph_3Sb resulted in four new signals, characteristic for the four nonequivalent carbon atoms of a new type of phenyl group (Fig. 2, b). None of the 12 signals overlap each other.

The comparison of the ^{13}C NMR spectra of Ph_2SbCl (crude product) and Ph_3SbCl_2 suggests the impurity to be this phenylantimony(V) chloride, probably formed in the reaction between Ph_3Sb and traces of HCl present in $SbCl_3$, although the later was freshly sublimed. This was confirmed by ^{1}H and ^{13}C NMR spectra. Indeed, the ^{13}Cresonance signals corresponding to the impurity increase in intensity when pure Ph_3SbCl_2 was added to the Ph_2SbCl (crude product) (Fig. 2, c).

The ^{13}C NMR spectra were also used to prove their utility to establish undoubtfully the composition of mixtures of phenylantimony compounds. Thus, ($PhSbCl_2$ + Ph_3Sb), ($PhSbCl_2$ + Ph_2SbCl) and ($PhSbCl_2$ + Ph_2SbCl +Ph_3Sb), as well as ($PhSbCl_2$ + Ph_3Sb) mixtures were prepared and their spectra show that in each case the resonances are very well separated and can be easily assigned to a particular phenylantimony compound. Even when four components are present in the mixture, *i.e.* $PhSbCl_2$ + Ph_2SbCl + Ph_3Sb + Ph_3SbCl_2, the sixteen expected ^{13}C resonances are not overlapped.

In case of the triphenylantimony(V) dichloride, the ^{1}H NMR spectra are not very suggestive. If the compound contains some Ph_3Sb, and this is possible taking into account the syntheses method, in the ^{1}H NMR spectra three groups of multiplets signals are present (Table 1). The signal at the lowest field corresponds to the *ortho* – protons in Ph_3SbCl_2 (greater deshielding), while the signal at the highest field corresponds to the overlap of the signals given by the *ortho* – protons in Ph_3Sb and those given by the *meta* and *para* – protons in Ph_3Sb (the lowest deshielding).

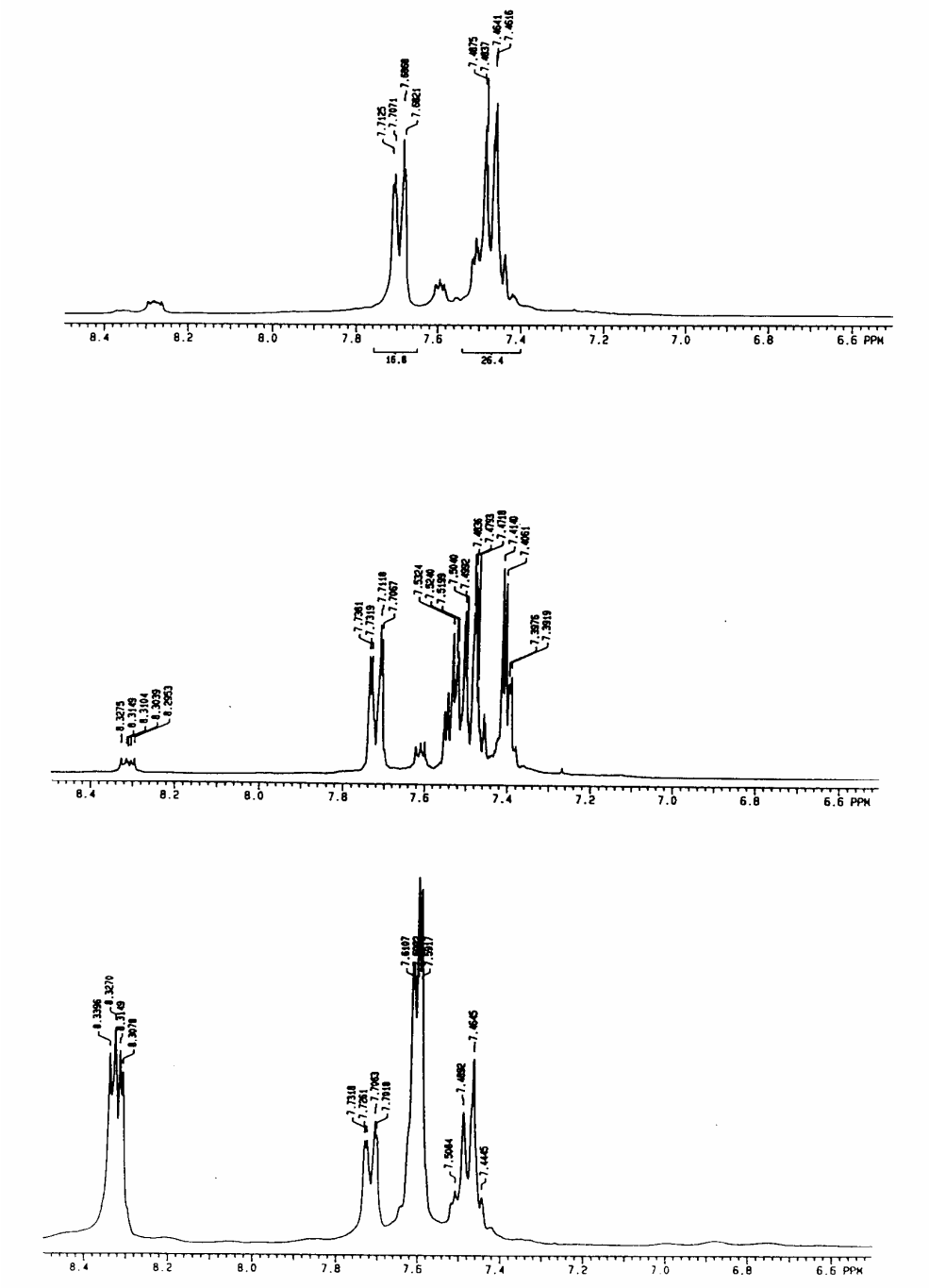

Figure 1. ^{1}H – NMR spectra for (a) Ph_2SbCl, (b) $Ph_2SbCl + Ph_3Sb$ and (c) $Ph_2SbCl + Ph_3SbCl_2$

Table 1.

^{1}H NMR data (δ, ppm and J, Hz) for phenylantimony(III)- and phenylantimony(V) chlorides, Ph_3Sb and mixtures of these compounds

Compound / mixture	Chemical shifts (δ, ppm) and coupling constants proton – proton ($^{n}J_{HH}$, Hz)	
	H - *ortho*	H – *meta* + *para*
Ph_2SbCl (Ph_3SbCl_2 as impurity)	[8.28dd ($^{3}J_{HH}$ = 7.1; $^{4}J_{HH}$ = 3.8)] 7.70dd ($^{3}J_{HH}$ = 7.6; $^{4}J_{HH}$ = 1.5)	[7.60m] (Ph_3SbCl_2) 7.47m (Ph_2SbCl)
Ph_3Sb	7.55dd ($^{3}J_{HH}$ = 6.5; $^{4}J_{HH}$ = 3.0)	7.41m
(Ph_2SbCl + Ph_3Sb) (also Ph_3SbCl_2 as impurity)	[8.31dd ($^{3}J_{HH}$ = 7.1; $^{4}J_{HH}$ = 3.8)] 7.72dd ($^{3}J_{HH}$ = 7.7; $^{4}J_{HH}$ = 1.7) 7.50m[a]	[7.61m] (Ph_3SbCl_2) (Ph_2SbCl) 7.44m (Ph_3Sb)
(Ph_2SbCl + Ph_3SbCl_2 + Ph_3Sb)	8.38dd ($^{3}J_{HH}$ = 6.4; $^{4}J_{HH}$ = 2.9) 7.76dd ($^{3}J_{HH}$ = 7.2; $^{4}J_{HH}$ = 1.2) 7.54m[b]	(Ph_3SbCl_2) (Ph_2SbCl)
(Ph_2SbCl + Ph_3SbCl_2)	8.32dd ($^{3}J_{HH}$ = 6.6; $^{4}J_{HH}$ = 3.0) 7.72dd ($^{3}J_{HH}$ = 7.5; $^{4}J_{HH}$ = 1.5)	7.60m (Ph_3SbCl_2) (Ph_2SbCl) 7.48m (Ph_3Sb)
Ph_3SbCl_2	8.27dd ($^{3}J_{HH}$ = 6.6; $^{4}J_{HH}$ = 3.0)	7.57m
$PhSbCl_2$	7.87d ($^{3}J_{HH}$ = 7.7)	7.59dd[c] (*meta*) 7.51t[d] (*para*)
($PhSbCl_2$ + Ph_3Sb)	7.93d ($^{3}J_{HH}$ = 6.9) 7.63m[e]	(Ph_3SbCl_2) 7.46m (Ph_3Sb)
($PhSbCl_2$ + Ph_2SbCl + Ph_3Sb) (also Ph_3SbCl_2 as impurity)	[8.36dd ($^{3}J_{HH}$ = 6.6; $^{4}J_{HH}$ = 3.0)] 7.93d($^{3}J_{HH}$ = 6.8) 7.79dd ($^{3}J_{HH}$ = 7.2; $^{4}J_{HH}$ = 1.4) 7.56m[f]	(Ph_3SbCl_2) ($PhSbCl_2$) (Ph_2SbCl)
($PhSbCl_2$ + Ph_2SbCl) (also Ph_3SbCl_2 as impurity)	[8.24dd ($^{3}J_{HH}$ = 6.6; $^{4}J_{HH}$ = 3.0)] 7.88d($^{3}J_{HH}$ = 6.8) 7.70dd ($^{3}J_{HH}$ = 7.4; $^{4}J_{HH}$ = 1.6) 7.54m[g]	(Ph_3SbCl_2) ($PhSbCl_2$) (Ph_2SbCl)
$Ph_2SbCl_3.H_2O$[h]	8.32dd ($^{3}J_{HH}$ = 6.4; $^{4}J_{HH}$ = 3.1)	7.63m
(Ph_3SbCl_2 + Ph_2Sb)	8.38dd ($^{3}J_{HH}$ = 7.1; $^{4}J_{HH}$ = 2.3) 7.61m[i]	(Ph_3SbCl_2) 7.44m (Ph_2SbCl)

[a](Ph_2SbCl – *meta* + *para*, Ph_3Sb – *ortho*); [b]Ph_2SbCl – *meta* + *para*, Ph_3SbCl_2 – *meta* + *para*, Ph_3Sb – *ortho* + *meta* + *para*; [c3]$^{3}J_{HH}$ = 7.1; [d3]$^{3}J_{HH}$ = 6.9; [e]($PhSbCl_2$ - *meta* + *para*, Ph_3Sb – *ortho*); [f] Ph_2SbCl – *meta* + *para*, $PhSbCl_2$ - *meta* + *para*, Ph_3Sb – *ortho* + *meta* + *para*, Ph_3SbCl_2 – *meta* + *para*; [g]Ph_2SbCl – *meta* + *para*, $PhSbCl_2$ - *meta* + *para*, Ph_3SbCl_2 – *meta* + *para*; [h]The signal due to the protons in water molecule appears at δ = 2.18 ppm (singlet); [1] Ph_3Sb – *ortho*, Ph_3SbCl_2 – *meta* + *para*.

The central signal is due to the overlap of the signals given by the *ortho* – protons in Ph_3Sb and those given by the *meta* and *para* – protons in Ph_3SbCl_2. In the ^{13}C NMR spectra of the same mixture it is easier to distinguish the two components because the signals are very well separated (Figure 3).

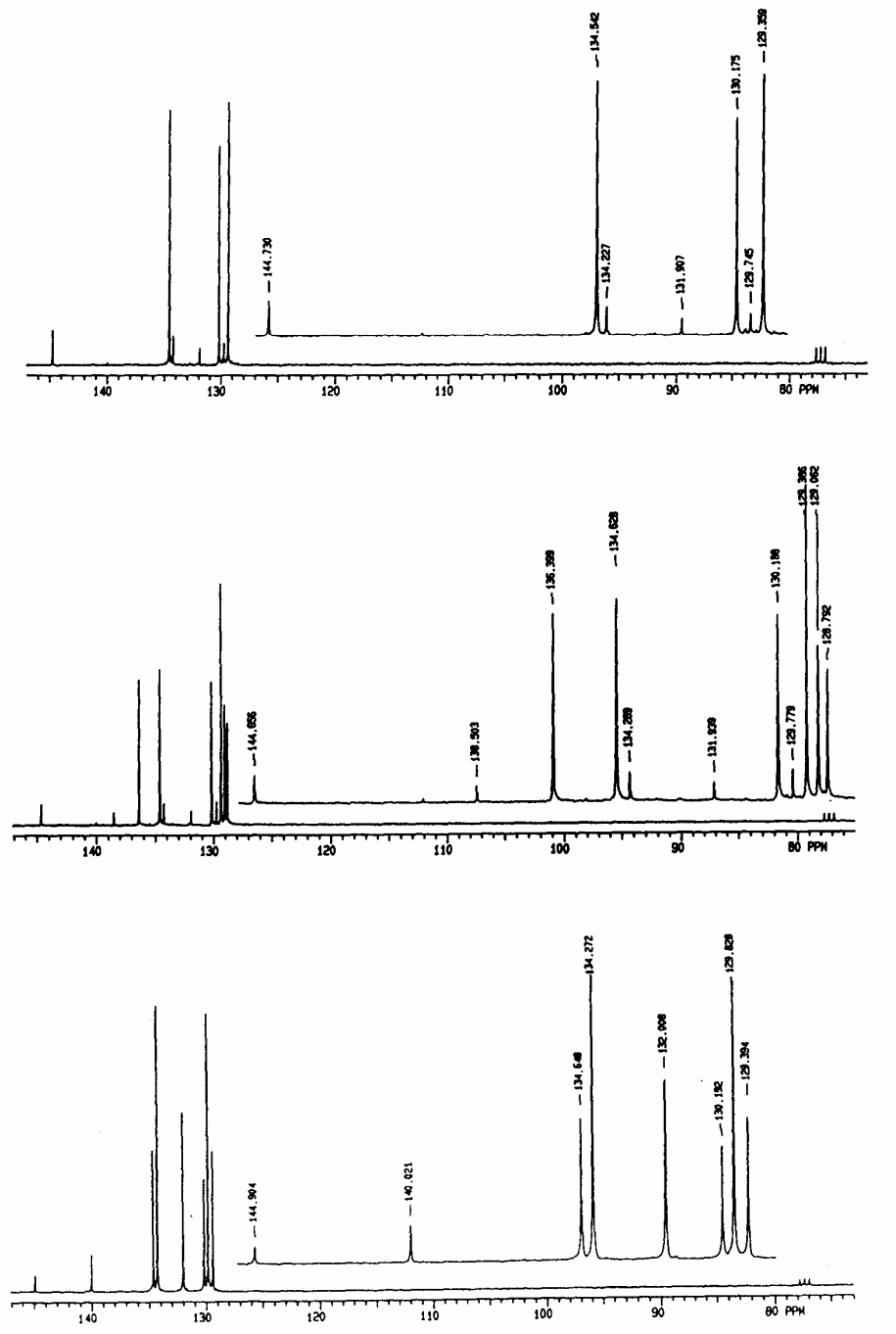

Figure 2. ^{13}C – NMR spectra for (a) Ph_2SbCl, (b) $Ph_2SbCl + Ph_3Sb$ and (c) $Ph_2SbCl + Ph_3SbCl_2$

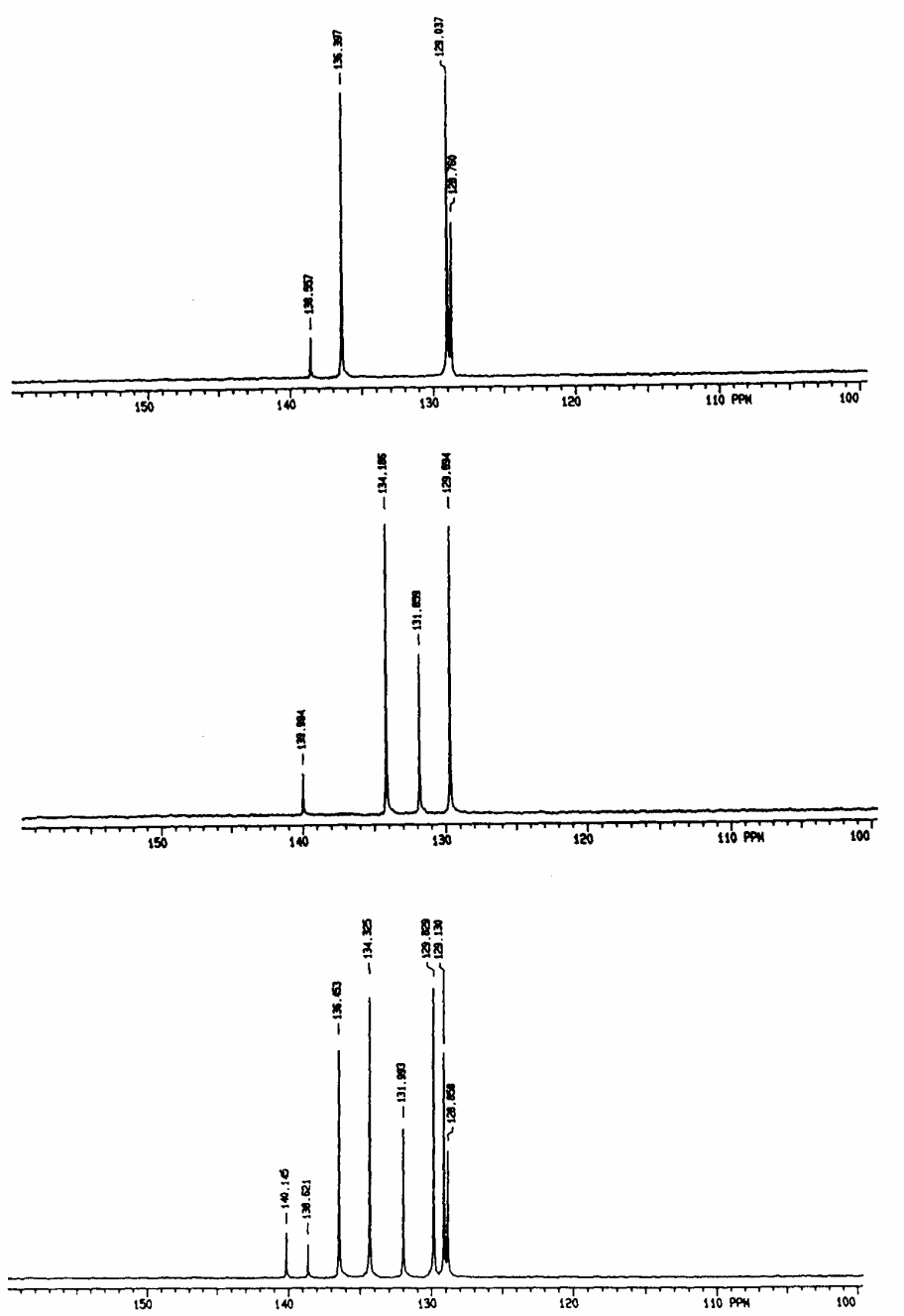

Figure 3. ^{13}C – NMR spectra for (a) Ph_3Sb, (b) Ph_3SbCl_2 and (c) Ph_3Sb + Ph_3SbCl_2

ACKNOWLEDGEMENTS

This work was supported by the Roumanian Academy. The financial support provided by OLTCHIM S.A. (C.Roibu – General Manager) for the service of the Varian NMR equipment ("Babes – Bolyai" University) is also greatly acknowledged.

REFERENCES

1. G.Alonzo, H.J.Breunig, M.Denker,K.H.Ebert, W.Offermann, *J.Organomet.Chem.*, 522 (1996), 237.
2. M.Nunn, D.B.Sowerby, D.M.Wesolek, *J.Organomet.Chem.*, 251 (1983), C45.
3. I.Haiduc, C.Silvestru, *Inorg. Synth.*, 23 (1985), 194.
4. A.J.Banister, L.F.Moore, *J.Chem.Soc.A,* (1968), 1137.